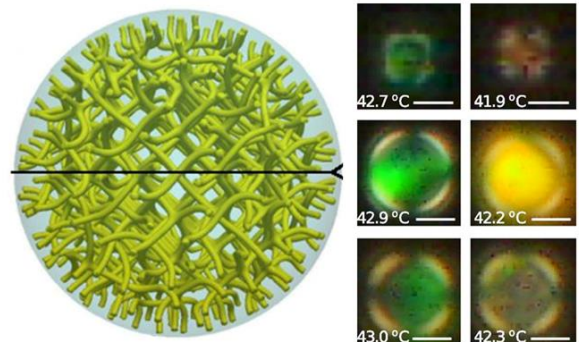
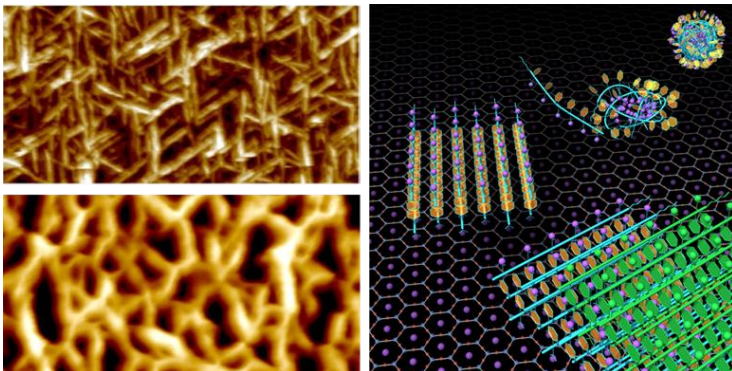
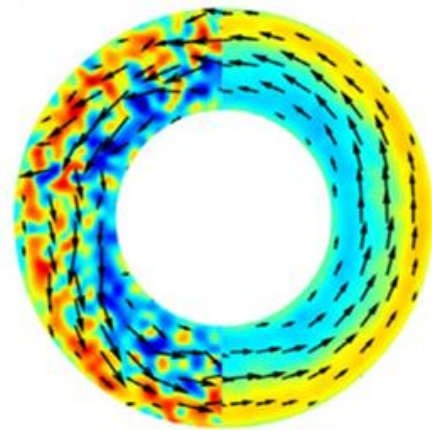
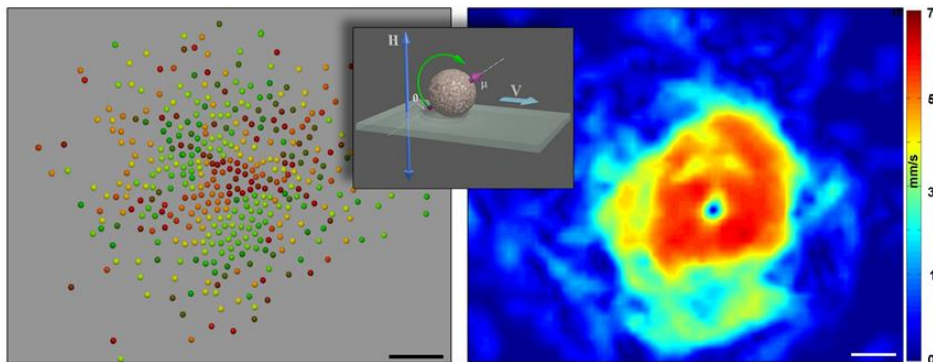
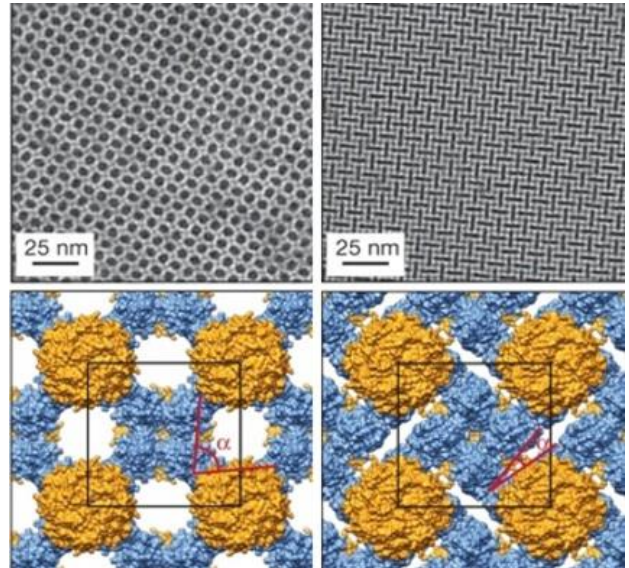
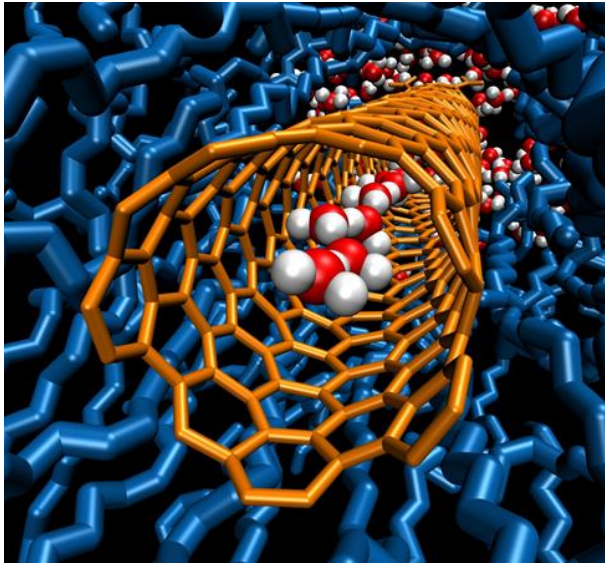


# Biomolecular Materials Principal Investigators' Meeting—2017

August 15–17, 2017

Gaithersburg Marriott Washingtonian Center, Gaithersburg, MD



U.S. DEPARTMENT OF  
**ENERGY**

Office of  
Science

Office of Basic Energy Sciences  
Materials Sciences and Engineering Division

## On the Cover

- Top Left:** Computer model showing sub-1nm carbon nanotube porin (orange) embedded in the lipid membrane (dark blue) with a single chain of hydrogen-bonded water molecules inside the nanotube cavity. This configuration boosts proton transport rates by an order of magnitude over bulk values. *Courtesy: Lawrence Livermore National Laboratory (Tunuguntla, et. al., Nature Nanotechnology 11, 639, 10.1038/NNANO.2016.43, (2016))*
- Top Right:** Electron microscopy views (top) of open and closed conformations of flat, 2-D sheets of porous square protein crystals linked at the corners by precisely positioned disulfide bonds. Pores go (reversibly) from open to closed as the flexible crystal is stretched. In the bottom panels, the top and bottom halves of the protein lattice are colored orange and blue, respectively, to highlight relative molecular orientations in each state. *Courtesy: F. Akif Tezcan, University of California, San Diego (Suzuki, et. al., Nature 533, 369-373, DOI: 10.1038/nature17633, (2016))*
- Middle Left:** Inset: Concept of a magnetic roller in a uniaxial alternating magnetic field. Left: Snapshot of magnetic rollers with color-coded velocity directions; Right: self-assembled global vortex of rollers with the color changes indicating differences of particle velocity. *Courtesy: Argonne National Laboratory (Kaiser, et. al., Science Advances 3, e1601469 (2017))*
- Middle Right:** Flow map demonstrates long-ranged coherent flows of a confined active fluid in toroidal donut-shaped “pipe.” Left and right half-plane of each figure illustrate instantaneous and time-averaged motion of the self-organized flows; color tones on left half represent localized counter-clockwise (blue) and clockwise vortex-like movement (red). *Courtesy: Zvonimir Dogic, Brandeis University (Wu, et. al, Science, 10.1126/science.aal1979, (2017))*
- Bottom Left:** Top Left: In situ AFM image collected during assembly of porous network from peptoids with alternating hydrophilic and hydrophobic monomers and a hydrophobic tail via a two-step nucleation and growth process, showing 5 nm wide linear structures, 3.3 nm in height, that grew outwards to form vertically oriented 2-D sheets aligned along three directions, each separated by 120°. Bottom Left: Ex situ AFM image of final self-assembled 3-D network. Right: Depiction of two-step process for the formation of three-fold arrays of 2D crystals via disordered clusters. *Courtesy: Pacific Northwest National Laboratory (Ma, et al., Nature Materials, 10.1038/NMAT4891, (2017))*
- Bottom Right:** Simulated defect structure of a blue phase in a liquid droplet. Defects arrange themselves into a highly ordered lattice whose geometrical characteristics can be controlled by manipulating the droplet’s size and temperature. Panels on right show experimentally observed blue-phase droplets, where color is altered by temperature changes of a fraction of a degree. *Courtesy: Nicholas Abbott, University of Wisconsin-Madison & Juan de Pablo, University of Chicago (Martinez-Gonzalez et al., PNAS, 112, 13195–13200, 10.1073/pnas.1514251112, (2015))*

---

This document was produced under contract number DE-SC0014664 between the U.S. Department of Energy and Oak Ridge Associated Universities.

The research grants and contracts described in this document are supported by the U.S. DOE Office of Science, Office of Basic Energy Sciences, Materials Sciences and Engineering Division.

## Foreword

This volume comprises the scientific content of the 2017 Biomolecular Materials Principal Investigators' Meeting sponsored by the Materials Sciences and Engineering (MSE) Division in the Office of Basic Energy Sciences (BES) of the U. S. Department of Energy (DOE). The meeting, held on August 15–17, 2017, at the Gaithersburg Marriott Washingtonian Center in Gaithersburg, Maryland, is the seventh such meeting on this topic conducted by BES. The meeting's focus is on the development of predictive and scalable assembly incorporating error correcting and defect-managing mechanisms based on the principles and concepts of biology to achieve spatial and temporal control of energy-efficient pathways for synthesizing beyond-equilibrium multicomponent hierarchical materials. The agenda at this year's meeting is representative of many of the major scientific areas supported by the Biomolecular Materials program to achieve this goal. This meeting will provide an opportunity to consider how this program may continue to evolve to support DOE's mission and to help MSE in assessing the state of the program, identifying new research directions and recognizing programmatic needs. It also provides participants the opportunity to see the entire research program, learn about the latest advances, develop new ideas, and forge new collaborations.

The Biomolecular Materials Core Research Activity was initiated following the recommendations of a Basic Energy Sciences Advisory Committee (BESAC) workshop in 2002. Recent BES workshop reports including Synthesis Science-Research to Enable Transformative Discoveries and Innovation for Energy, and Challenges at the Frontiers of Matter and Energy: Transformative Opportunities for Discovery Science have clearly identified biology's blueprint for translating atomic and nanoscale phenomena into mesoscale materials that display complex yet well-coordinated collective behavior as an inspiration for developing the knowledge base to create materials with the precise control of complexity and totally new properties needed for next-generation energy technologies. To address these goals, the Biomolecular Materials program supports fundamental research in the design and scalable creation of robust energy-relevant materials and systems that rival or exceed biology's extraordinary effectiveness for controlling matter, energy, and information. Areas of supported research include bioinspired synthesis and assembly approaches with control of mechanisms and kinetics to form resilient, adaptive materials that display novel, unexpected properties that are far from equilibrium and possess self-regulating and -repair capabilities. Many projects combine theory and experiment to develop new design ideas and accelerate discovery.

I look forward to the active participation of the attendees at this meeting and hope that the collective sharing of their ideas and new research results will bring fresh insights for the continued development of this field and its value to DOE, as has been the case at past BES Principal Investigators' Meetings. The advice and help of Meeting Chairs Nicholas Abbott and Christine Keating in organizing this meeting are deeply appreciated. My sincere thanks go to Teresa Crockett in MSE and Linda Severs at the Oak Ridge Institute for Science and Education (ORISE) for their outstanding work in taking care of all the logistical aspects of the meeting.

Mike Markowitz,  
Program Manager, Biomolecular Materials  
MSE, BES, Office of Science  
U.S. Department of Energy



# *Agenda*



**2017 Biomolecular Materials  
Principal Investigators' Meeting Agenda**

**Meeting Chairs: Christine Keating** (Penn State University) and **Nicholas Abbott** (University of Wisconsin-Madison)

**Tuesday, August 15, 2017**

7:00 – 8:00 **Breakfast** (also presentation and poster set-up. Copies of all presentations for Monday need to be given to Teresa Crockett prior to the end of the meeting on Tuesday.)

**Session 1: Actively Managing Synthesis and Repair**  
Chair: **Nick Abbott**, University of Wisconsin-Madison

8:00 – 8:30 **Rebecca Schulman**, Johns Hopkins University  
*Resilient Hydrogels from the Nanoscale to the Macroscale*

8:30 – 8:40 *Discussion*

8:40 – 9:10 **Anna Balazs**, University of Pittsburgh  
*Designing Bio-Inspired, Adaptive Gels with Controllable 3D Structures*

9:10 – 9:20 *Discussion*

9:20 – 9:50 **Timothy Scott**, University of Michigan  
*Fabrication and Assembly of Robust, Water-Soluble Molecular Interconnects via Encoded Hybridization*

9:50 – 10:00 *Discussion*

10:00 – 10:30 **Break**

10:30 – 11:00 **Paul Chaikin**, New York University  
*Self-Assembly and Self-Replication of Novel Materials from Particles with Specific Recognition*

11:00 – 11:10 *Discussion*

11:10 – 11:40 **Michael Strano**, MIT  
*Materials Exhibiting Biomimetic Carbon Fixation and Self Repair: Theory and Experimental Synthesis*

11:40 – 11:50 *Discussion*

- 11:50 – 12:30 **Poster Introductions (Posters 1–17)**
- 12:30 – 1:30 **Working lunch with continued discussions; Introductory remarks by Helen Kerch, Acting Team Lead for Materials Discovery, Design and Synthesis; CRA Updates by Mike Markowitz, Program Manager, Biomolecular Materials CRA**
- 1:30 – 3:00 **Poster Session 1 and Discussions**
- Session 2: Actively Managing Synthesis and Repair, continued**  
Chair: **Jessica Winter**, Ohio State University
- 3:00 – 3:30 **Omar Saleh**, University of California, Santa Barbara  
*Strain Distributions and Structural Changes in Motor-Driven Gels*
- 3:30 – 3:40 *Discussion*
- 3:40 – 4:10 **George Whitesides**, Harvard University  
*Dynamic, Adaptive, Systems and Materials: Complex, Simple, and Emergent Behaviors*
- 4:10 – 4:20 *Discussion*
- 4:20 – 4:50 **Break**
- 4:50 – 5:20 **Uli Weisner**, Cornell University  
*Basic Research Needs for Synthesis Science for Energy Technologies Workshop*
- 5:20 – 5:30 *Discussion*
- 5:30 – 7:00 **Poster Session 1, continued**
- 7:00 – 8:30 **Working Dinner: General discussion on new opportunities, collaborative exchanges**

## Wednesday, August 16, 2017

7:00 – 8:00 **Breakfast** (Also presentation and poster set-up. Copies of all presentations for Tuesday need to be given to Teresa Crockett prior to the end of the meeting on Wednesday.)

### **Session 3: Accounting for Imperfections When Assembling Colloids**

Chair: **F. Akif Tezcan**, University of California, San Diego

8:00 – 8:30 **Alexey Snezhko**, Argonne National Laboratory  
*Dynamics of Active Self-Assembled Materials*

8:30 – 8:40 *Discussion*

8:40 – 9:10 **Mike Solomon**, University of Michigan  
*Self-Assembly for Colloidal Crystallization and Biomimetic Structural Color*

9:10 – 9:20 *Discussion*

9:20 – 9:50 **Sanat Kumar**, Columbia University  
*Guiding Nanoparticle Assemblies through the Use of DNA Nanocages*

9:50 – 10:00 *Discussion*

10:00 – 10:25 **Break**

### **Session 3, continued:**

10:25 – 10:55 **Jeetain Mittal**, Lehigh University  
*Biomolecular Assembly Processes in the Design of Novel Functional Materials*

10:55 – 11:05 *Discussion*

11:05 – 11:35 **Juan de Pablo**, Argonne National Laboratory/University of Chicago  
*Computational Materials Science: Midwest Integrated Center for Computational Materials*

11:35 – 11:45 *Discussion*

11:45 – 12:25 **Poster Introductions (Posters 18–32)**

12:25 – 1:25 **Working Lunch with continued discussions on potential impact of Computational Materials Science Centers for Soft Materials**

1:25 – 2:55 **Poster Session 2**

- Session 4: Errors: Avoidance or Repair**  
Chair: **Joanna Aizenberg**, Harvard University
- 2:55 – 3:25 **Zhibin Guan**, University of California, Irvine  
*Bioinspired Design of Multifunctional Dynamic Materials*
- 3:25 – 3:35 *Discussion*
- 3:35 – 4:05 **F. Akif Tezcan**, University of California, San Diego  
*Protein Self-Assembly by Rational Chemical Design*
- 4:05 – 4:15 *Discussion*
- 4:15 – 4:40 **Break**
- 4:40 – 5:10 **Hao Yan**, Arizona State University  
*DNA Nanostructure Directed Designer Excitonic Networks*
- 5:10 – 5:20 *Discussion*
- 5:20 – 5:50 **Surya Mallapragada**, Ames Laboratory  
*Bioinspired Materials*
- 5:50 – 6:00 *Discussion*
- 6:00 – 7:00 **Poster Session 2, continued**
- 7:00 – 8:30 **Working Dinner: General discussion on new opportunities, collaborative exchanges**

## Thursday, August 17, 2017

- 7:00 – 8:00 **Breakfast** (Also presentation & poster set-up. Copies of all presentations for Thursday need to be given to Teresa Crockett prior to the end of the meeting.)
- Session 5: Managing Synthesis and Assembly at Interfaces**  
Chair: **Christine Keating**, Penn State University
- 8:00 – 8:30 **John Evans**, New York University  
*Material lessons of biology: Proteomic based nanoporous materials at the mesoscale*
- 8:30 – 8:40 *Discussion*

- 8:40 – 9:10 **Uli Wiesner**, Cornell University  
*Early Formation Stages and Pathway Complexity in Functional Bio-Hybrid Nanomaterials*
- 9:10 – 9:20 *Discussion*
- 9:20 – 9:50 **Tom Russell**, Lawrence Berkeley National Laboratory  
*Adaptive Interfacial Assemblies towards Structuring Liquids*
- 9:50 – 10:00 *Discussion*
- 10:00 – 10:30 **Break**
- 10:30 – 11:00 **Dan Hammer**, University of Pennsylvania  
*Designing Smart, Responsive Communicating Microcapsules from Polymersomes*
- 11:00 – 11:10 *Discussion*
- 11:10 – 11:40 **Trevor Douglas**, Indiana University  
*Self-Assembly of Virus Particle Based Materials for Hydrogen Catalysis*
- 11:40 – 11:50 *Discussion*
- 11:50 – 12:00 *Remarks, Concluding Comments*  
**Christine Keating** and **Nicholas Abbott**, Meeting Chairs  
**Mike Markowitz**, Program Manager, Biomolecular Materials
- 12:00 **Adjourn**



# *Table of Contents*



## Table of Contents

<b>Foreword</b> .....	i
<b>Agenda</b> .....	v
 <b>Laboratory Projects</b>	
<i>Active Assembly of Dynamic and Adaptable Materials</i>	
<b>George D. Bachand, Erik Spoerke, Mark Stevens, and Darryl Sasaki</b> .....	3
<i>Precision Synthesis and Assembly of Ionic and Liquid Crystalline Polymers</i>	
<b>Juan J. de Pablo, Wei Chen, Seth Darling, Paul Nealey, and Matt Tirrell</b> .....	7
<i>Bioinspired Materials</i>	
<b>Surya Mallapragada, Andrew Hillier, Marit Nilsen-Hamilton, Tanya Prozorov, Alex Travesset, David Vaknin, and Wenjie Wang</b> .....	18
<i>Directed Organization of Functional Materials at Inorganic-Macromolecular Interfaces</i>	
<b>Aleksandr Noy, Anthony van Burren, James J. De Yoreo, Chun-Long Chen, and Marcel Bayer</b> .....	24
<i>Adaptive Interfacial Assemblies Towards Structuring Liquids</i>	
<b>Thomas P. Russell, Brett Helms, Paul Ashby, Alex Zettl, and Philip Geissler</b> .....	29
<i>Dynamics of Active Self-Assembled Materials</i>	
<b>Alexey Snezhko, Andrey Sokolov, Igor Aronson, and Andreas Glatz</b> .....	34
 <b>University Grant Projects</b>	
<i>Bioinspired Hierarchical Design of Chiral Mesoscale Liquid Crystalline Assemblies</i>	
<b>Nicholas L. Abbott and Juan J. de Pablo</b> .....	41
<i>Energy Transductions in Multimodal Stimuli-Responsive Reconfigurable Systems with Information Encoding Capabilities</i>	
<b>Joanna Aizenberg and Anna Balazs</b> .....	46
<i>Biomimetic Templated Self-Assembly of Light Harvesting Nanostructures</i>	
<b>Alfredo Alexander-Katz</b> .....	50

<i>Design and Synthesis of Structurally Tailored and Engineered Macromolecular (STEM) Gels</i> <b>Anna C. Balazs and Krzysztof Matyjaszewski</b> .....	54
<i>Designing Dual-functionalized Gels that Move, Morph, and Self-organize in Light</i> <b>Anna C. Balazs</b> .....	60
<i>Self-Assembly and Self-Replication of Novel Materials from Particles with Specific Recognition</i> <b>Paul M. Chaikin, Nadrian C. Seeman, David Pine, and Marcus Weck</b> .....	64
<i>Large-Scale Self-Organization and Spontaneous Flows in Microtubule Based Soft Active Matter</i> <b>Zvonimir Dogic</b> .....	69
<i>Self-Assembly of Virus Particle Based Materials for Hydrogen Catalysis</i> <b>Trevor Douglas</b> .....	73
<i>Control of Charge Transfer and Light-Driven Reactions in Nanocrystal-Enzyme Complexes</i> <b>Gordana Dukovic</b> .....	77
<i>Functional Droplets and Particles: Recognition, Repair, and Transport</i> <b>Todd Emrick</b> .....	81
<i>Early Formation Stages and Pathway Complexity in Functional Bio-Hybrid Nanomaterials</i> <b>Lara A. Estroff and Ulrich Wiesner</b> .....	85
<i>Material Lessons of Biology: Proteomic Based Nanoporous Materials at the Mesoscale</i> <b>John Spencer Evans</b> .....	90
<i>Programmable Dynamic Self-Assembly of DNA Nanotubes</i> <b>Elisa Franco</b> .....	95
<i>Bioinspired Design of Multifunctional Dynamic Materials</i> <b>Zhibin Guan</b> .....	99
<i>Development of Smart, Responsive Communicating and Motile Microcapsules</i> <b>Daniel A. Hammer and Daeyeon Lee</b> .....	104
<i>Surface Mechanical Properties of Bioinspired Architectures</i> <b>Chung-Yuen Hui and Anand Jagota</b> .....	109
<i>Surface Mechanical Properties of Bioinspired Architectures</i> <b>Anand Jagota and Chung-Yuen Hui</b> .....	114
<i>Bioinspired Mineralizing Microenvironments Generated by Liquid-Liquid Phase Coexistence</i> <b>Christine D. Keating</b> .....	119

<i>Guiding Nanoparticle Assemblies through the Use of DNA Nanocages</i> <b>Sanat K. Kumar, Oleg Gang, and Shawn Douglas</b> .....	123
<i>Controlled Synthesis and Ordered Assembly of Co<sub>3</sub>O<sub>4</sub> Nanowires using Genetically Engineered Bacterial Flagella as Biotemplates</i> <b>Chuanbin Mao and Chunlong Chen</b> .....	128
<i>Biomolecular Assembly Processes in the Design of Novel Functional Materials</i> <b>Jeetain Mittal</b> .....	132
<i>Neutralization of a Distributed Coulombic Switch Tunes Reflectin Assembly and Biophotonics</i> <b>Daniel E. Morse and Robert Levenson</b> .....	137
<i>Electrostatic Driven Self-Assembly Design of Functional Nanostructures</i> <b>Monica Olvera de la Cruz and Michael J. Bedzyk</b> .....	141
<i>Exploration of Chemically-Tailored, Hierarchically-Patterned 3-D Biogenic and Biomimetic Structures for Control of Infrared Radiation</i> <b>Joseph W. Perry and Kenneth H. Sandhage</b> .....	146
<i>Miniaturized Hybrid Materials Inspired by Nature: Directed Assembly in Dissipative Charged Biomolecular Materials Systems</i> <b>C. R. Safinya, Y. Li, and K. Ewert</b> .....	152
<i>Measuring Transport Characteristics of Water Confined in Biological Materials</i> <b>Ozgur Sahin</b> .....	157
<i>Strain Distributions and Structural Changes in Motor-Driven Gels</i> <b>Omar A. Saleh, Deborah K. Fygenson, and Robert M. McMeeking</b> .....	161
<i>Programmable Dynamic Self-Assembly of DNA Nanostructures</i> <b>Rebecca Schulman</b> .....	165
<i>Resilient Hydrogels from the Nanoscale to the Macroscale</i> <b>Rebecca Schulman</b> .....	169
<i>Fabrication and Assembly of Robust, Water-Soluble Molecular Interconnects via Encoded Hybridization</i> <b>Timothy F. Scott</b> .....	173
<i>Self-Assembly for Colloidal Crystallization and Biomimetic Structural Color</i> <b>Michael J. Solomon and Sharon C. Glotzer</b> .....	177
<i>Self-Assembly and Self-Repair of Novel Photovoltaic Complexes: Synthetic Analogs to Natural Processes</i> <b>Michael S. Strano</b> .....	182

<i>New Functions Emerging from Dynamics in Supramolecular Biomolecular Materials</i> <b>Samuel I. Stupp</b> .....	186
<i>Protein Self-Assembly by Rational Chemical Design</i> <b>F. Akif Tezcan</b> .....	191
<i>Dynamic, Adaptive, Systems and Materials: Complex, Simple, and Emergent Behaviors</i> <b>George M. Whitesides</b> .....	196
<i>Exploring Fundamental Properties of Dynamic DNA Origami –Nanoparticle Composites</i> <b>Jessica Winter, Carlos Castro, Michael Poirier, and Ezekiel Johnston-Halperin</b> .....	200
<i>DNA Nanostructure Directed Designer Excitonic Networks</i> <b>Hao Yan, Neal Woodbury, Yan Liu, Mark Bathe, and David Whitten</b> .....	205
<b>Poster Listing</b> .....	211
<b>Author Index</b> .....	217
<b>Participant List</b> .....	221

***LABORATORY  
PROJECTS***



## Active Assembly of Dynamic and Adaptable Materials

**Principal Investigator:** George D. Bachand

**Co-Investigators:** Erik Spoerke, Mark Stevens, and Darryl Sasaki

**Mailing Address:** Sandia National Laboratories, PO Box 5800, MS 1303, Albuquerque, NM

**Email:** gdbacha@sandia.gov

### Program Scope

The *Active Assembly of Dynamic and Adaptable Materials* project examines fundamental materials science issues at the intersection of biology, nanomaterials, and hybrid interfaces. The overall goal is to understand and apply key principles and strategies by which biomolecular and biomimetic assembly processes may be used to develop materials whose assembly, configuration, organization, and disassembly can be programmed or self-directed in *ex vivo* environments. More specifically, we aim to adapt biomolecular transport and assembly processes from nature to achieve hierarchical, dynamic structures for transformative information/energy systems. Recently, we have focused on two general areas: (i) exploring the active assembly and organization of novel hybrid and composite nanomaterials based on kinesin-microtubule transport;<sup>1</sup> and (ii) understanding the design principles underlying the controlled assembly of synthetic nanostructures that mimic the structure and dynamics of microtubule filaments (MTs).<sup>2</sup> MTs are hollow filaments composed of  $\alpha\beta$  tubulin dimers whose energy-dissipative assembly is used to push, pull, or rearrange the cell's cytoskeleton. MTs also serve as "train tracks" for the bidirectional transport of organelles by the motor proteins through the conversion of chemical energy into mechanical work. Living organisms use the concerted and dynamic interactions between motors and MTs for physiological processes ranging from chromosomal segregation at the cellular level to macroscopic color changing behaviors at the organismal level. Thus, learning to exploit, mimic, and/or translate the role of these active proteins and emergent biological behaviors represents an opportunity to dramatically advance nanomaterials assembly.

### Recent Progress

#### *Role of defects in the active assembly of nanocomposite rings*

Several research groups have shown that the collective action of kinesin molecular machines acting on MT shuttles carrying "sticky" cargo (e.g., streptavidin-coated Qdots) can drive their active self-assembly into nanocomposite rings.<sup>3</sup> We recently described three distinct mechanisms involved in the active assembly of MT rings based on the real-time observation of nucleation events.<sup>4</sup> Our prior work also noted that ring structures are topologically and morphologically diverse, including twisted/kinked domains and in- and out-of-plane loops,<sup>5</sup> which raises questions as to the role of such "defects" in the assembly and dynamic nature of these metastable structures. To address this issue, we generated "defective" MT building blocks that contained varying ratios of biotinylated (blue) and non-biotinylated segments (Fig. 1, left) using a directed head-

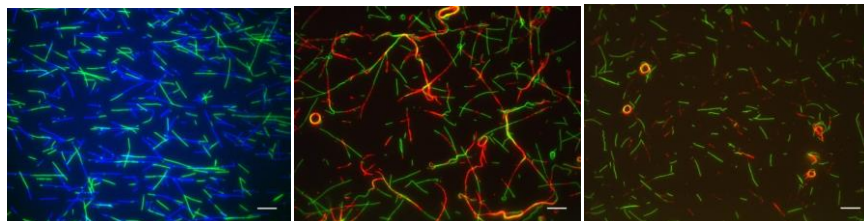


**Fig. 1.** Fluorescent photomicrographs of MTs with 50% defects before (left), upon addition of quantum dots (middle) and 30 min post-assembly (right). Bar = 10  $\mu\text{m}$ .

to-tail assembly process. Here, the biotinylated segments represent “compliant” building blocks, while the non-biotinylated segments serve as “defects” based on their inability to form biotin-streptavidin bonds and offset the strain energy associated with highly bent MTs. Assembly of ring structures from these MTs suggest that micron-scale defects significantly affect the assembly process (Fig. 1, middle & right). Specifically, we observed that “defective” segments were selectively removed from rings during the assembly process. Our data suggest that this selective removal of defects is both a consequence of their inability to offset the bending energy associated with the ring morphology, as well as the mechanical shearing by the kinesin motors. This system provides a novel perspective in terms of achieving low-defect nanocomposite materials based on energy-dissipative assembly.

### Modeling MT Depolymerization

Depolymerization of MTs is related to the dephosphorylation of GTP-tubulin to GDP-tubulin, which is also accompanied by an allosteric compaction in the  $\alpha$ -tubulin. One hypothesis suggests that this shape change generates sufficient mechanical strain in the MT to drive catastrophic depolymerization in the absence of a GTP cap.<sup>6</sup> To investigate this hypothesis, molecular dynamics simulations were performed with MTs assembled from coarse-grained  $\alpha\beta$ -tubulin dimers, based on a model that we previously developed.<sup>7,8</sup> We mimicked tubulin compaction by changing the angle of the bottom surfaces of  $\alpha$ -subunits (Fig. 2a). Our previous simulations showed that uncompacted ( $\theta=0$ ) monomers self-assemble into tubules for a range of lateral and vertical interaction strengths. In the present work, the interaction strengths and the compaction angle were varied to evaluate dependencies among these parameters and the stability of a tubule. These simulations show that this shape transformation does indeed induce catastrophic MT depolymerization *via* the well-known “rams’ horns” pathway (Fig. 2b). Catastrophic events were observed only around compaction angles resembling the “bent” dimer conformation experimentally measured in bulk solution, and at subunit attraction strengths consistent with recent experimental estimates. We also show that compacted MTs can be stabilized *via* short non-compacted (i.e., GTP-tubulin) end caps. Overall, this work supports the hypothesis that mechanical strain due to the shape change in tubulin has the ability to induce catastrophic depolymerization.

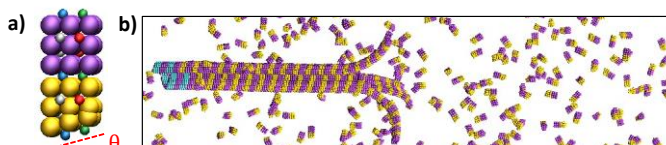


**Fig. 2.** a) Image of model  $\alpha\beta$  tubulin dimer with  $\alpha$  tubulin (yellow) compacted by angle  $\theta$ . Small spheres on the vertical and lateral sides show the location of the attractive sites. b) Snapshot of depolymerization with the left end (cyan) fixed and the right end showing rams horn after disassociation of tubulin dimers.

### Conformational Destabilization of Synthetic Peptide Nanostructures

Here we explored the use of shape changes in synthetic molecular building blocks to regulate their self-assembly, attempting to mimic the structural destabilization and depolymerization observed in MTs. We studied a synthetic peptide building block comprised of a self-assembling

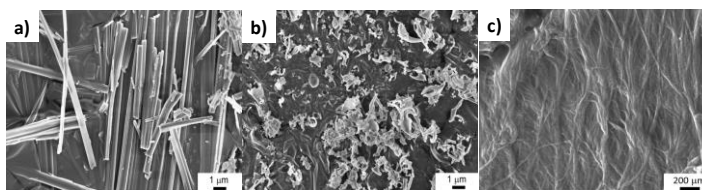


**Fig. 3.** SEM images of AzbFF as a) assembled nanotubes, b) disordered peptide after UV-triggered molecular conformation change, and c) re-assembled nanofibers after relaxation.

dipeptide, (di(phenylalanine)) (FF),<sup>9</sup> modified with an azobenzene (Azb) derivative. Azobenzene undergoes a UV-excited *trans* to *cis* photo-isomerization, followed by a thermal relaxation back to a predominantly *trans* conformation. We demonstrated the molecular assembly of AzbFF building blocks (in the extended, predominantly *trans* state), forming tubular nanostructures (Fig. 3a) with extended  $\beta$ -sheet character. Upon UV-stimulated photoisomerization of the Azb derivative, the tubular nanostructures disassembled (Fig. 3b) and the  $\beta$ -sheet content was lost. Upon relaxation of the Azb back to the *trans* state, the AzbFF building blocks reassembled, forming nanofibers (Fig. 3c) with strong  $\beta$ -sheet character, demonstrating that the shape change and assembly could be reversibly cycled. This work is a key demonstration of how, as with MTs, changes the molecular conformation of a synthetic building block can be used to regulate dynamic assembly of a supramolecular structure.

## Future Plans

Continuing work on this project will be focused on two general themes: (i) enhanced understanding the role of molecular shape change, structural instability, and assembly dynamics in natural and synthetic systems, and (ii) exploring the emergence of actively assembled structures using stabilizers to temporally regulate metastability. Relevant to the first theme, we will continue studying the MT polymerization-depolymerization cycle with a focus on tuning the coarse-grained model for tubulin. Experimental work will continue exploring the use of azobenzene and other shape-changing functionalities with a goal of reversing the influence of the conformation change on assembly in order to more closely mimic natural MT dynamics. With regard to the second theme, we are currently exploring the ability to chemically encode assembly instructions into the structure of the MT building blocks as a means of regulating the dynamic assembly of nanocomposites. We are also exploring the use of surface patterned ligands (molecular rewards) that can temporally and spatially stabilize lipid and polymer nanotube networks that result from the action of kinesin motor-assembly.

## Acknowledgments

Support provided by the Department of Energy, Office of Basic Energy Sciences, Division of Materials Sciences and Engineering, Project KC0203010. This work was performed, in part, at the Center for Integrated Nanotechnologies, an Office of Science User Facility operated for the U.S. Department of Energy (DOE) Office of Science. Sandia National Laboratories is a multi-mission laboratory managed and operated by National Technology and Engineering Solutions of Sandia, LLC., a wholly owned subsidiary of Honeywell International, Inc., for the U.S. Department of Energy's National Nuclear Security Administration under contract DE-NA-0003525.

## Abstract References

- (1) Bachand, G. D.; Bouxsein, N. F.; VanDelinder, V.; Bachand, M. Biomolecular Motors in Nanoscale Materials, Devices, and Systems. *Wiley Interdiscip. Rev. Nanomedicine Nanobiotechnology* **2014**, *6*, 163–177.
- (2) Bachand, G. D.; Spoerke, E. D.; Stevens, M. J. Microtubule-Based Nanomaterials: Exploiting Nature's Dynamic Biopolymers. *Biotechnol. Bioeng.* **2015**.
- (3) Aoyama, S.; Shimoike, M.; Hiratsuka, Y. Self-Organized Optical Device Driven by Motor Proteins. *Proc. Natl. Acad. Sci.* **2013**, *110*, 16408–16413.
- (4) VanDelinder, V.; Brener, S.; Bachand, G. D. Mechanisms Underlying the Active Self-

- Assembly of Microtubule Rings and Spools. *Biomacromolecules* **2016**, acs.biomac.5b01684.
- (5) Liu, H. Q.; Spoerke, E. D.; Bachand, M.; Koch, S. J.; Bunker, B. C.; Bachand, G. D. Biomolecular Motor-Powered Self-Assembly of Dissipative Nanocomposite Rings. *Adv. Mater.* **2008**, *20*, 4476–4481.
  - (6) Alushin, G. M.; Lander, G. C.; Kellogg, E. H.; Zhang, R.; Baker, D.; Nogales, E. High-Resolution Microtubule Structures Reveal the Structural Transitions in  $\alpha\beta$ -Tubulin upon GTP Hydrolysis. *Cell* **2014**, *157*, 1117–1129.
  - (7) Cheng, S.; Stevens, M. J. Self-Assembly of Chiral Tubules. *Soft Matter* **2014**, *10*, 510.
  - (8) Cheng, S.; Aggarwal, A.; Stevens, M. J. Self-Assembly of Artificial Microtubules. *Soft Matter* **2012**, *8*, 5666–5678.
  - (9) Jones, B. H.; Martinez, A. M.; Wheeler, J. S.; McKenzie, B. B.; Miller, L. L.; Wheeler, D. R.; Spoerke, E. D. A Multi-Stimuli Responsive, Self-Assembling, Boronic Acid Dipeptide. *Chem Commun* **2015**, *51*, 14532–14535.

### DOE-Sponsored Publications (2016-2017)

- VanDelinder, V, Brener, S, Bachand, GD (2016) Mechanisms underlying the active self-assembly of microtubule rings and spools. *Biomacromolecules* **17**, 1048-1056.
- Greene, AC, Sasaki, DY, and Bachand GD (2016) Forming giant-sized polymersomes using gel-assisted rehydration. *J. Vis Exp* (111), e54051-1-7.
- Greene, AC, Henderson, IM, Gomez, A, Paxton, WF, VanDelinder, V, Bachand GD (2016) The role of membrane fluidization in the gel-assisted formation of giant polymersomes. *PLoS ONE* **11**(7), e0158729.
- Lam, AT, VanDelinder, V, Kabir, AMR, Bachand, GD, Hess, H, and Kakugo, A (2015) Cytoskeletal motor-driven active self-assembly. *Soft Matter* **12**(4), 988-997 (*invited review*).
- Bordovsky, S., Wong, C.S., Bachand, G.D., Stachowiak, J.C., and Sasaki, D.Y. (2016). Engineering lipid structure for recognition of the liquid ordered membrane phase. *Langmuir* **32**(47): 12527-12533.
- Hanson, JM, Gettel, DL, Tabaei, SR, Jackman, J, Kim, MC, Sasaki, DY, Liedberg, B, Cho, N-J, and Parikh, AN (2016) Cholesterol-enriched microdomain formation induced by viral-encoded membrane active amphipathic peptide. *Biophys. J.* **110**, 176-187.
- Zeno, WF, Johnson, KE, Sasaki, DY, Risbud, SH, and Longo, ML (2016) Crowding-induced mixing behavior of lipid bilayers: Examination of mixing energy, phase, packing geometry, and reversibility. *Langmuir* **32**(18), 4688-4697.
- VanDelinder, V., Adams, P., and Bachand, G.D. (2016) Mechanical splitting of microtubules into protofilament sheets by surface-bound kinesin-1. *Sci. Rep.*, **6**, 39408-1-10.
- Greene, A.C., Bachand, M., Gomez, A., Stevens, M.J., and Bachand, G.D. (2017) Interactions regulating the end-to-end directed assembly of biological Janus rods. *Chem. Commun.*, **53**, 4493-4496.
- Stevens, M.J. (2017) The long persistence length of model tubules. *J. Chem. Phys.* (*in press*).
- Mahajan, K., Cui, Y., Dorcena, C.J., Bouxsein, N.F., Bachand, G.D., Chalmers, J., and Winter, J.O. (2017). Magnetic quantum dots for evaluating microtubule properties. *Biotechnol. J.* (*in revision*).
- Martinez, A.M, Jones, B.H. McGrath, D.V., Hernandez, E., Wheeler, J.S., and Spoerke, E.D. Azobenzene-mediated dynamic peptide assembly. *Macromolecules* (*in review*).

## **Precision synthesis and assembly of ionic and liquid crystalline polymers**

**Juan J. de Pablo<sup>(1)</sup> (PI)**

**Wei Chen<sup>(1)</sup>, Seth Darling<sup>(2)</sup>, Paul Nealey<sup>(1)</sup>, Matthew Tirrell<sup>(1)</sup> (co-PIs)**

**Institute for Molecular Engineering, Materials Sciences Division<sup>(1)</sup>, and Nanoscale Science and Technology Division<sup>(2)</sup>, Argonne National Laboratory**

### **Program Scope**

Past efforts to understand charged polymeric and liquid crystalline materials have largely focused on homopolymers and their properties in the bulk. In this FWP, entitled Precision Synthesis and Assembly of Ionic and Liquid Crystalline Polymers, we are investigating (1) the role of charge sequence on the behavior of polymeric molecules, (2) the role of patterned surfaces in directing the assembly of charged block polymer electrolytes, and the concomitant transport properties, and (3) the use of polymer-brush patterned substrates in controlling the 3D assembly of chiral liquid crystalline materials. The program relies on the synergistic use of synthesis, characterization, theory and computation to make progress on these three fronts. The overall aim of the research is to elucidate fundamental principles that will impact a wide array of energy technologies, ranging from antifouling coatings for separation membranes, to solid electrolytes for energy storage applications.

### **Recent Progress**

Building on our previous work, which was focused on homo-charged polyelectrolytes, and multi-valent interactions among them, we have recently started to explore new ground in macromolecules bearing both positive and negative charges. Though special cases of hetero-charged polymers have been explored in the past, there is actually a continuum of possible charge distributions that constitutes a progression from randomness to increasing degrees and scales of order in charge sequences. The diverse possibilities suggested by Figure 1, and our ability in the Argonne Polymer Foundry to synthesize many such structures with precision by living anionic polymerization, controlled free radical polymerization and, with amino acid monomers, solid phase peptide synthesis, serve to highlight the bio-inspired character of this work, bringing to synthetic polymers a similar diversity of interactions as in biological macromolecules and, in some cases, going beyond. We know that in biology such a diversity of primary sequences in proteins dictates larger scale structures, ranging from highly ordered to intrinsically disordered, each evolved to carry out particular functions.

Our recent studies have been directed toward synthesis and characterization of hetero-charged polymers in solution, as surface-grafted brushes, and as thin films. The science that is being developed will provide new insights and tools for a wide variety of potential applications, ranging from surface treatments to reduce biofilm formation and increase biocompatibility, to development of electro-active devices.

An example of our efforts is illustrated in Figure 2, where coarse-grained molecular dynamics enhanced by free-energy sampling methods was used to examine the roles of solvophobicity and multivalent salts on polyelectrolyte brush collapse. Specifically, we demonstrated that while ostensibly similar, solvophobic collapsed brushes and multivalent-ion collapsed brushes exhibit distinct mechanistic and structural features. Notably, we found that multivalent-induced heterogeneous brush collapse is observed under good solvent polymer backbone conditions, demonstrating that the mechanism of multivalent collapse is not contingent upon a solvophobic backbone. The potential of mean-force (PMF) between two individual brush strands confirms this analysis, revealing starkly different PMFs under solvophobic and multivalent conditions, suggesting the role of multivalent “bridging” as the discriminating feature in trivalent collapse. Structurally, multivalent ions show a propensity for nucleating order within collapsed brushes, whereas poor-solvent collapsed brushes are more disordered; this difference is traced to the existence of a metastable PMF minimum for poor solvent conditions, and a global PMF minimum for trivalent systems, under experimentally relevant conditions.

Another major theme of research during the past year was solvent annealing of block copolymer material systems to enable precise control over their three-dimensional nanostructure under non-equilibrium

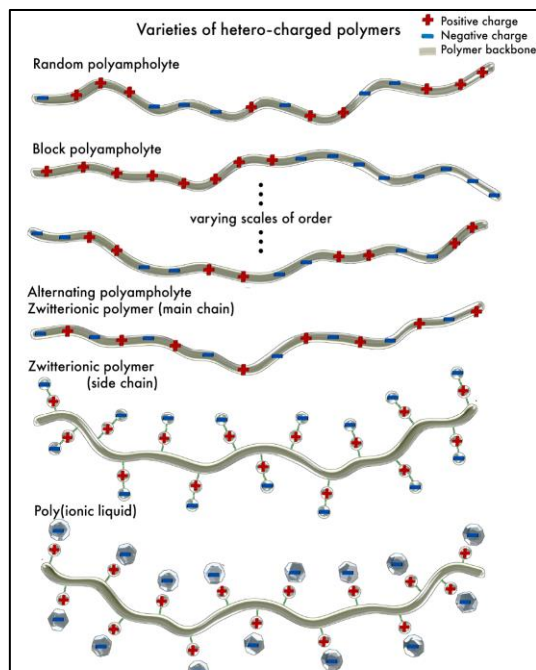


Figure 1 - Varieties of hetero-charged polymers shown schematically with differing degrees and arrangements of positive and negative charges. In addition to the specific structures illustrated here, one can envision (a) block copolymers with either neutral or homo- or hetero-charged blocks, (b) incorporation of additional types of interactions (hydrophobic, hydrogen bonding, mesogenic, for example) and, of course, (c) poly(ionic liquids) with the positive and negative charges positionally exchanged.

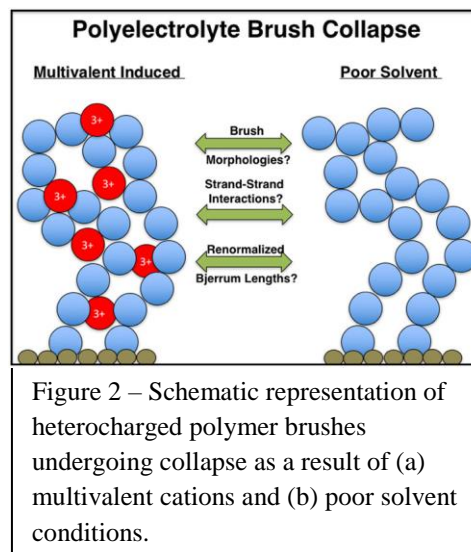


Figure 2 – Schematic representation of heterocharged polymer brushes undergoing collapse as a result of (a) multivalent cations and (b) poor solvent conditions.

conditions. During the solvent annealing process, we typically operate at room temperature, expose the polymer film to an environment with constant partial pressure of solvent in nitrogen, hold the film for a period of time at constant volume fraction solvent (swelling ratio), and then remove the solvent from the environment causing the solvent to evaporate from the film. One of the highlights of the FWP was to demonstrate that achieving high levels of perfection in DSA via solvent-annealing requires control over the volume fraction of solvent in the film during annealing in such a manner that: 1) the solvated polymer film remains in the micro-phase separated state (not disordered), 2) the solvated domains retain wetting differences to respond to the chemical patterns, and 3) the mobility of the polymer is high. Using the PS-P2VP system, a combined experimental and theoretical approach was used to delineate the relationships between solvent quality with respect to the blocks of the copolymer, solvent selectivity, evaporation rates, molecular weight, microstructure (e.g. diblock versus triblock), volume fraction solvent, and annealing time. Figure 3 shows several examples of perfectly assembled structures with very high resolution (8 nm features), high aspect ratio (>20), and non-bulk morphologies.

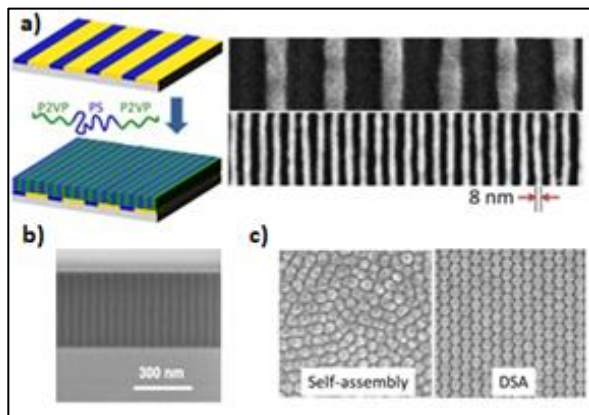


Figure 3 – DSA via solvent annealing of a (a) triblock copolymer with 8 nm features. b) High aspect ratio structures for potential membrane applications and c) non-equilibrium non-bulk copolymer morphologies.

Building on that discovery, the solvent annealed PS-P2VP system was used to develop an experimental platform to investigate block copolymer electrolytes. Connecting structure and morphology to bulk transport properties, such as ionic conductivity, in nanostructured polymer electrolyte materials is a difficult proposition because of the challenge of precisely and accurately controlling order and the orientation of ionic domains in such polymeric films. In particular, poly(styrene-

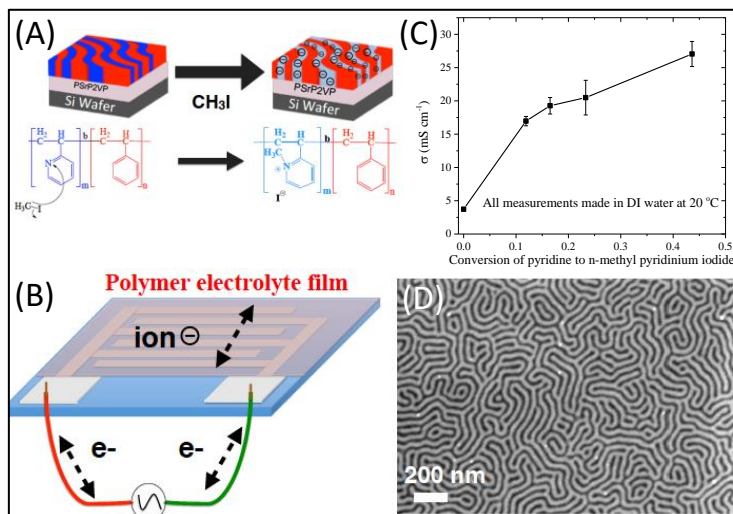


Figure 4 – (A) Schematic representation of the post-assembly vapor reaction that introduces ionic species into the P2VP domains. (B) Experimental design for electrochemical characterization using interdigitated electrodes with large cross-sectional area for high statistical significance. (C) Conductivity of the film as a function of degree of functionalization, showing conductivity comparable to that of commercial devices. (D) Experimental SEM image showing the film after the MeI vapor reaction with the preserved nano-domain architecture.

block-2-vinyl pyridine) (PSbP2VP) block copolymers were assembled perpendicularly to a substrate surface over large areas through chemical surface modification at the substrate and utilizing solvent vapor annealing. After block copolymer assembly, a novel chemical vapor infiltration reaction (CVIR) technique was developed to selectively convert the 2-vinyl pyridine block to 2-vinyl n-methyl pyridinium (NMP<sup>+</sup> X<sup>-</sup>) groups – which are anion charge carriers (Figure 4). The block copolymer electrolytes maintained their orientation and ordered nanostructure upon the selective introduction of ion moieties into the P2VP block and post ion-exchange to other counter-ion forms (X<sup>-</sup> = chloride, hydroxide, etc.).

A significant focus of our FWP has also sought to guide the assembly of chiral liquid crystalline materials by relying on lithographic patterning with liquid-crystalline polymer brushes. Specifically, we have relied on poly(6-(4-methoxy-azobenzene-4'-oxy) hexyl methacrylate) (PMAZO) brushes grafted to sub-lithographically nano-patterned –OH terminated Si surfaces. By controlling molecular weight, concentration, and annealing temperature, we showed that it is possible to manipulate surface coverage and anchoring orientation. Using evolutionary computation, and the knowledge gained from our past work on copolymer DSA, we were then able to create stable, perfectly ordered macroscopic single-crystal specimens of blue phases I and II. Specifically, by designing specific patterns on a substrate, we managed to control the crystallographic plane of the lattice that is presented to the substrate or the interface. Note that the liquid crystal was represented at the level of a Landau-de Gennes theory for the local tensor order parameter. Such a theory, which expresses the free energy as a sum of elastic-energy contributions, enthalpic contributions, and surface energy contributions, provides a quantitative description of the systems of interest to this work. The physical properties that enter the theory

and that we optimized in order to design new materials included thermodynamic quantities that dictate the nematic-isotropic (NI) transition), elastic moduli, the chirality (or pitch) of the materials, and the surface (or anchoring) energies (W) of the materials and polymer-brush patterned surfaces. These properties were reversed engineered, by relying on the dynamic evolutionary computation (DEC) strategies proposed in our recent work, in a manner

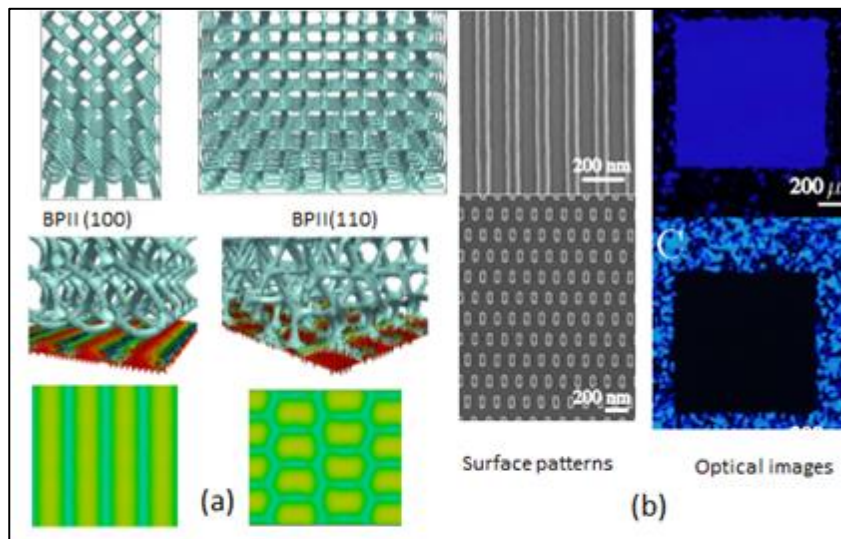


Figure 5 – (a) Defect structure of the BPII with different lattice orientations (100 and 110). Surface pattern designed to promote single-crystal formation along specified orientation. (b) SEM images of two different patterned surfaces and corresponding micrographs of the single-crystal BPII oriented along the 100 and 110 planes.

intended to yield ideal, mono-domain single crystals over macroscopic areas. The fitness function for inverse design with evolutionary computation was given by the difference between an ideal blue phase, with a specified orientation, and that produced by our field-theoretic models. Some of the results of this work are shown in Figure 5, where it is shown that different patterns serve to stabilize different lattice orientations. One can also appreciate from the experimental micrographs in the Figure that it is indeed possible to create blue phase single crystals over macroscopic areas.

## Future Plans

Moving forward, we plan to use atomic force microscopy (AFM), x-ray and neutron scattering, surface forces apparatus (SFA) measurements, and coarse-grained molecular dynamics (MD) simulations to study the structure of polyelectrolyte brushes in a variety of solvent conditions. More specifically, AFM images will provide a direct visualization of lateral inhomogeneities on the surface of polyelectrolyte brushes, collapsed in solutions containing trivalent counterions, whereas x-ray and neutron scattering will yield structural characteristics normal to the surface of the brushes. These results will be interpreted in the context of a coarse-grained molecular model, and corroborated by accompanying interaction-force measurements with the SFA. Our preliminary results confirm that lateral inhomogeneities are absent from polyelectrolyte brush layers, collapsed in a poor solvent without multivalent ions. Importantly, taken together, AFM, SFA, scattering, and our molecular model present a detailed picture in which solvophobic and multivalent-ion induced effects work in concert to drive strong phase separation, with electrostatic bridging of polyelectrolyte chains playing an essential role in the collapsed structure formation.

We also intend to use directed self-assembly (DSA) of block copolymer electrolytes in conjunction with the experimental platform described above to address the most fundamental questions concerning ion transport in charged polymer systems. The aim is to direct the assembly of block copolymer electrolytes using chemoepitaxy strategies into deterministic structures that enable measurements of conductivity and capacitance in specific structural motifs.

Specifically, the DSA process will be modified such that interdigitated electrodes (with bonding pads) are patterned and deposited via a lift-off process on top of the chemically patterned surface and prior to BCP coating and annealing. The samples will be placed in a chamber to control temperature and humidity, and the conductivity and capacitance

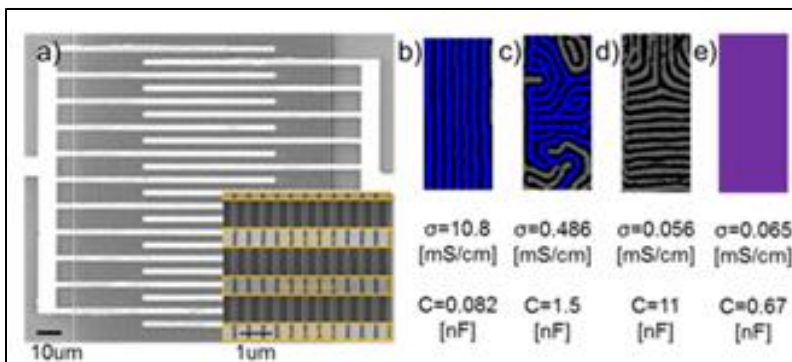


Figure 6 – (a) Interdigitated electrodes with graphoepitaxy guide structures. (b-e) Ion conductivity and capacitance as a function of domain structure in BCE films.

properties of the assembly will be determined using electrochemical impedance spectroscopy. The use of interdigitated electrodes will greatly increase signal to noise in the analysis.

Our preliminary results using the above platform have been encouraging. We have, for example, performed a set of experiments in which we assembled the domains of a lamellae-forming BCE perpendicular to the substrate with: 1) a direct path between the electrodes, 2) a tortuous path between electrodes with fractional connectivity, and 3) orthogonal orientation of alternating insulating and conducting domains with respect to the electrodes. Figure 6 provides representative images of the interdigitated arrays with the graphoepitaxy template, the assembled poly(styrene-block-2vinylpyridine/*n*-methylpyridinium iodide) (PS-P2VP/NMP<sup>+</sup> I<sup>-</sup>) morphologies, and the corresponding results from analyzing the EIS data (taken at 95% relative humidity). Even in these rather rudimentary first experiments with known film structure, several preliminary observations stand out: 1) the conductivity of the directly connected domains (Figure 6b) is approximately half that of the pure P2VP/NMP<sup>+</sup> I<sup>-</sup> homopolymer (data not shown), 2) the conductivity of the directly connected domains is ~250x that of the domains oriented primarily orthogonal to the electrodes (Figure 6d), and 3) the conductivity of the domains with tortuous paths and dead ends (Fig. 6c), is 25x smaller than that of the directly connected domains. These data show that structural connectivity and characterization of vanishingly small numbers of defects is a prerequisite to the understanding and eventual application of these materials.

For patterned liquid crystalline polymer brushes, our immediate plans are to characterize the blue phase single-crystal samples created as outlined above. The resulting optical (e.g. reflectivity, transmission, Kossel microscopy) and scattering measurements will be interpreted by relying on the DEC formalism as outlined in our recent work, implemented this time in the context of scattering as well as optical transmission, and by relying on the field theory mentioned above. An important aspect of this work will seek to characterize the dynamic response of these single crystals. Another direction of our work will seek to determine how the underlying films respond to external fields, including strain and voltage. In the later stages of our research, we will also aim to stabilize and manipulate other phases of LCs (and their corresponding defects), including splayed and bent phases, helical phases, and cholesteric phases of interest for applications. We will also aim to understand the connections that we believe exist between these mesogenic materials and poly(ionic liquids), a point that has been noted previously, but not pursued extensively.

### **Publications (Last two years):**

1. Ramirez-Hernandez, A.; Peters, B. L.; Andreev, M.; Schieber, J. D.; de Pablo, J. J., A multichain polymer slip-spring model with fluctuating number of entanglements for linear and nonlinear rheology. *Journal of Chemical Physics*, 2015, 143 (24).

2. Hernandez-Ortiz, J. P.; de Pablo, J. J., Self-consistent description of electrokinetic phenomena in particle-based simulations. *Journal of Chemical Physics*, 2015, 143 (1).
3. Hur, S. M.; Onses, M. S.; Ramirez-Hernandez, A.; Nealey, P. F.; Rogers, J. A.; de Pablo, J. J., Interplay of Surface Energy and Bulk Thermodynamic Forces in Ordered Block Copolymer Droplets. *Macromolecules*, 2015, 48 (13), 4717-4723.
4. Segal-Peretz, T.; Winterstein, J.; Doxastakis, M.; Ramirez-Hernandez, A.; Biswas, M.; Ren, J. X.; Suh, H. S.; Darling, S. B.; Liddle, J. A.; Elam, J. W.; de Pablo, J. J.; Zaluzec, N. J.; Nealey, P. F., Characterizing the Three-Dimensional Structure of Block Copolymers via Sequential Infiltration Synthesis and Scanning Transmission Electron Tomography. *Acs Nano*, 2015, 9 (5), 5333-5347.
5. Whitmer, J. K.; Fluit, A. M.; Antony, L.; Qin, J.; McGovern, M.; de Pablo, J. J., Sculpting bespoke mountains: Determining free energies with basis expansions. *Journal of Chemical Physics*, 2015, 143 (4).
6. Williamson, L. D.; Nealey, P. F., Macrophase Separation of Blends of Diblock Copolymers in Thin Films. *Macromolecules*, 2015, 48 (12), 3997-4003.
7. Priftis, D.; Leon, L.; Song, Z. Y.; Perry, S. L.; Margossian, K. O.; Tropnikova, A.; Cheng, J. J.; Tirrell, M., Self-Assembly of alpha-Helical Polypeptides Driven by Complex Coacervation. *Angewandte Chemie-International Edition*, 2015, 54 (38), 11128-11132.
8. Farina, R.; Laugel, N.; Yu, J.; Tirrell, M., Reversible Adhesion with Polyelectrolyte rushes Tailored via the Uptake and Release of Trivalent Lanthanum Ions. *Journal of Physical Chemistry C*, 2015, 119 (26), 14805-14814.
9. Mok, J. W.; Lin, Y. H.; Yager, K. G.; Mohite, A. D.; Nie, W. Y.; Darling, S. B.; Lee, Y.; Gomez, E.; Gosztola, D.; Schaller, R. D.; Verduzco, R., Linking Group Influences Charge Separation and Recombination in All-Conjugated Block Copolymer Photovoltaics. *Advanced Functional Materials*, 2015, 25 (35), 5578-5585.
10. Jung, I. H.; Zhao, D. L.; Jang, J.; Chen, W.; Landry, E. S.; Lu, L. Y.; Talapin, D. V.; Yu, L. P., Development and Structure/Property Relationship of New Electron Accepting Polymers Based on Thieno 2',3':4,5 pyrido 2,3-g thieno 3,2-c quinoline-4,10-dione for All-Polymer Solar Cells. *Chemistry of Materials*, 2015, 27 (17), 5941-5948.
11. Lu, L. Y.; Chen, W.; Xu, T.; Yu, L. P., High-performance ternary blend polymer solar cells involving both energy transfer and hole relay processes. *Nature Communications*, 2015, 6, 7327.

12. Das, S.; Keum, J. K.; Browning, J. F.; Gu, G.; Yang, B.; Dyck, O.; Do, C.; Chen, W.; Chen, J. H.; Ivanov, I. N.; Hong, K. L.; Rondinone, A. J.; Joshi, P. C.; Geohegan, D. B.; Duscher, G.; Xiao, K., Correlating high power conversion efficiency of PTB7: PC71 BM inverted organic solar cells with nanoscale structures. *Nanoscale*, 2015, 7 (38), 15576-15583.
13. Kipp, D.; Mok, J.; Strzalka, J.; Darling, S. B.; Ganesan, V.; Verduzco, R., Rational Design of Thermally Stable, Bicontinuous Donor/Acceptor Morphologies with Conjugated Block Copolymer Additives. *ACS Macro Letters*, 2015, 4 (9), 867-871.
14. Arges, C. G.; Kambe, Y.; Suh, H. S.; Ocola, L. E.; Nealey, P. F., Perpendicularly Aligned, Anion Conducting Nanochannels in Block Copolymer Electrolyte Films. *Chemistry of Materials*, 2016, 28, 1377–1389.
15. Suh, H. S.; Chen, X. X.; Rincon-Delgadillo, P. A.; Jiang, Z.; Strzalka, J.; Wang, J.; Chen, W.; Gronheid, R.; de Pablo, J. J.; Ferrier, N.; Doxastakis, M.; Nealey, P. F., Characterization of the shape and line-edge roughness of polymer gratings with grazing incidence small-angle X-ray scattering and atomic force microscopy. *Journal of Applied Crystallography*, 2016, 49, 823-834.
16. Ren, J.; Ocola, L. E.; Divan, R.; Czaplewski, D. A.; Segal-Peretz, T.; Xiong, S.; Kline, R. J.; Arges, C. G.; Nealey, P. F., Post-directed-self-assembly membrane fabrication for in situ analysis of block copolymer structures. *Nanotechnology*, 2016, 27 (43).
17. Yu, J.; Mao, J.; Yuan, G. C.; Satija, S.; Chen, W.; Tirrell, M., The effect of multivalent counterions to the structure of highly dense polystyrene sulfonate brushes. *Polymer*, 2016, 98, 448-453.
18. Yu, J.; Mao, J.; Yuan, G. C.; Satija, S.; Jiang, Z.; Chen, W.; Tirrell, M., Structure of Polyelectrolyte Brushes in the Presence of Multivalent Counterions. *Macromolecules*, 2016, 49 (15), 5609-5617.
19. Brettmann, B. K.; Laugel, N.; Hoffmann, N.; Pincus, P.; Tirrell, M., Bridging Contributions to Polyelectrolyte Brush Collapse in Multivalent Salt Solutions. *Journal of Polymer Science Part a-Polymer Chemistry* 2016, 54 (2), 284-291.
20. Pacalin, N. M.; Leon, L.; Tirrell, M., Directing the phase behavior of polyelectrolyte complexes using chiral patterned peptides. *European Physical Journal-Special Topics*, 2016, 225 (8-9), 1805-1815.
21. Jiang, X. K.; Li, J. Y.; Zhao, X. J.; Qin, J.; Karpeev, D.; Hernandez-Ortiz, J.; de Pablo, J. J.; Heinonen, O., An O(N) and parallel approach to integral problems by a kernel-independent fast multipole method: Application to polarization and magnetization of interacting particles. *Journal of Chemical Physics*, 2016, 145 (6).

22. Qin, J.; de Pablo, J. J., Criticality and Connectivity in Macromolecular Charge Complexation. *Macromolecules*, 2016, 49 (22), 8789-8800.
23. Qin, J.; de Pablo, J. J., Ordering Transition in Salt-Doped Diblock Copolymers. *Macromolecules*, 2016, 49 (9), 3630-3638.
24. Qin, J.; de Pablo, J. J.; Freed, K. F., Image method for induced surface charge from many-body system of dielectric spheres. *Journal of Chemical Physics*, 2016, 145 (12).
25. Qin, J.; Li, J. Y.; Lee, V.; Jaeger, H.; de Pablo, J. J.; Freed, K. F., A theory of interactions between polarizable dielectric spheres. *Journal of Colloid and Interface Science*, 2016, 469, 237-241.
26. Zhang, R.; Roberts, T.; Aranson, I. S.; de Pablo, J. J., Lattice Boltzmann simulation of asymmetric flow in nematic liquid crystals with finite anchoring. *Journal of Chemical Physics*, 2016, 144 (8).
27. Li, X.; Armas-Perez, J. C.; Martinez-Gonzalez, J. A.; Liu, X. Y.; Xie, H. L.; Bishop, C.; Hernandez-Ortiz, J. P.; Zhang, R.; de Pablo, J. J.; Nealey, P. F., Directed self-assembly of nematic liquid crystals on chemically patterned surfaces: morphological states and transitions, *Soft Matter*, 2016, 12 (41), 8595-8605.
28. Ji, S. X.; Wan, L.; Liu, C. C.; Nealey, P. F., Directed self-assembly of block copolymers on chemical patterns: A platform for nanofabrication. *Progress in Polymer Science*, 2016, 54-55, 76-127.
29. Kawaue, A.; Matsumiya, T.; Seo, T.; Maehashi, T.; Seshimo, T.; Yamano, H.; Miyagi, K.; Dazai, T.; Chen, X. X.; Rincon-Delgadillo, P.; Gronheid, R.; Nealey, P. F.; Ohmori, K., Ionic Liquid for Directed Self-Assembly of PS-b-PMMA. *Journal of Photopolymer Science and Technology*, 2016, 29 (5), 667-670.
30. Segal-Peretz, T.; Zhou, C.; Ren, J. X.; Dazai, T.; Ocola, L. E.; Divan, R. N. S.; Nealey, P. F., Three Dimensional Assembly in Directed Self-assembly of Block Copolymers. *Journal of Photopolymer Science and Technology*, 2016, 29 (5), 653-657.
31. Wan, L.; Ji, S. X.; Liu, C. C.; Craig, G. S. W.; Nealey, P. F., Directed self-assembly of solvent-vapor-induced non-bulk block copolymer morphologies on nanopatterned substrates. *Soft Matter*, 2016, 12 (11), 2914-2922.
32. Wu, G. P.; Liu, X. Y.; Chen, X. X.; Suh, H. S.; Li, X.; Ren, J. X.; Arges, C. G.; Li, F. X.; Jiang, Z.; Nealey, P. F., Directed Self-Assembly of Hierarchical Supramolecular Block Copolymer Thin Films on Chemical Patterns. *Advanced Materials Interfaces*, 2016, 3 (13).

33. Xiong, S. S.; Wan, L.; Ishida, Y.; Chapuis, Y. A.; Craig, G. S. W.; Ruiz, R.; Nealey, P. F., Directed Self-Assembly of Triblock Copolymer on Chemical Patterns for Sub-10-nm Nanofabrication via Solvent Annealing. *ACS Nano*, 2016, 10 (8), 7855-7865.
34. Wu, Q. H.; Zhao, D. L.; Schneider, A. M.; Chen, W.; Yu, L. P., Covalently Bound Clusters of Alpha-Substituted PDI-Rival Electron Acceptors to Fullerene for Organic Solar Cells. *Journal of the American Chemical Society*, 2016, 138 (23), 7248-7251.
35. Zhao, D. L.; Wu, Q. H.; Cai, Z. X.; Zheng, T. Y.; Chen, W.; Lu, J.; Yu, L. P., Electron Acceptors Based on alpha-Substituted Perylene Diimide (PDI) for Organic Solar Cells. *Chemistry of Materials*, 2016, 28 (4), 1139-1146.
36. Cai, Z.; Li, L.; Lo, W.-Y.; Zhao, D.; Wu, Q.; Zhang, N.; Su, Y.-A.; Chen, W.; Yu, L., Controlled Self-Assembly of Cyclophane Amphiphiles: From 1D Nanofibers to Ultrathin 2D Topological Structures, *Macromolecules*, 2016, 49, 5172–5178.
37. Ramírez-Hernández, A.; Peters, B. L.; Schneider, L.; Andreev, M.; Schieber, J. D.; Müller, M.; de Pablo, J. J., A multi-chain polymer slip-spring model with fluctuating number of entanglements: Density fluctuations, confinement, and phase separation. *Journal of Chemical Physics*, 2017, 146, 014903.
38. Jackson, N. E.; Brettmann, B. K.; Vishwanath, V.; Tirrell, M.; de Pablo, J. J., Comparing Solvophobic and Multivalent Induced Collapse in Polyelectrolyte Brushes. *ACS Macro Letters* 2017, ASAP, 155–160.
39. Martinez-Gonzalez, J.A.; Li, X. ; Sadati, M ; Zhou, Y. ; Zhang, R. ; Nealey, P.F.; de Pablo, J.J., Directed self-assembly of liquid crystalline blue-phases into ideal single-crystals, *Nature Communications*, 2017, 8, 15854.
40. Xie, H.L. ; Li, X. ; Ren, J.X. ; Bishop, C. ; Arges, C.G. ; Nealey, P.F., Controlling Domain Orientation of Liquid Crystalline Block Copolymer in Thin Films Through Tuning Mesogenic Chemical Structures, *J. Pol. Sci. B*, 2017, 55, 532-541.
41. Kambe, Y. ; Arges, C.G. ; Patel, S.N. ; Stoykovich, M.P. ; Nealey, P.F., Ion Conduction in Microphase-Separated Block Copolymer Electrolytes, *Electrochem. Soc. Int.*, 2017, 26, 61-67.
42. Li, X.; Armas-Pérez J.C.; Hernández-Ortiz J.P.; Arges C.G.; Liu X.; Martínez-González J.A.; Ocola L.E.; Bishop C.; Xie H.; de Pablo, J. J.; Nealey, P.F., Directed Self-Assembly of Colloidal Particles onto Nematic Liquid Crystalline Defects Engineered by Chemically Patterned Surfaces, *ACS Nano*, 2017, 11, 6492–6501.
43. Xiong, SS.; Chapuis, Y.; Wan, L.; Gao, H.; Li, X.; Ruiz, R.; Nealey, P.F., Directed self-assembly of high-chi block copolymer for nano fabrication of bit patterned media via solvent annealing. *Nanotechnology*, 2016, 27, 415601.

44. Segal-Peretz, T.; Ren, J.; Xiong, S.S.; Khaira, G.; Bowen, A.; Ocola, L.E.; Divan, R.; Doxastakis, M.; Ferrier, N.; de Pablo, J.; Nealey, P. F., Quantitative Three-Dimensional Characterization of Block Copolymer Directed Self-Assembly on Combined Chemical and Topographical Prepatterned Templates, *ACS Nano*, 2017, 11, 1307-1319.
45. Arges, C.G.; Kambe, Y.; Dolejsi, M.; Wu, G.P.; Segal-Peretz, T.; Ren, J.X.; Cao, C.; Craig, G.; Nealey P.F., Interconnected ionic domains enhance conductivity in microphase separated block copolymer electrolytes, *Journal of Materials Chemistry A*. 2017, 11, 5619-5629.
46. Mo, D.; Wang, H.; Chen, H.; Qu, S.; Chao, P.; Yang, Z.; Tian, L.; Su, Y.-A.; Gao, Y.; Yang, B.; Chen, W.; He, F.; “Chlorination of Low-Band-Gap Polymers: Toward High-Performance Polymer Solar Cells”, *Chem. Mater.*, 2017, 29, 2819–2830.
47. Hu, Z.; Chen, H.; Qu, J.; Zhong, X.; Chao, P.; Xie, M.; Lu, W.; Liu, A.; Tian, L.; Su, Y.-A.; Chen, W.; He, F.; “Design and Synthesis of Chlorinated Benzothiadiazole-Based Polymers for Efficient Solar Energy Conversion”, *ACS Energy Lett.*, 2017, 2, 753–758.
48. Wu, Q.; Zhao, D.; Yang, J.; Sharapov, V.; Cai, Z.; Li, L.; Zhang, N.; Neshchadin, A.; Chen, W.; Yu, L.; “Propeller-Shaped Acceptors for High-Performance Non-Fullerene Solar Cells: Importance of the Rigidity of Molecular Geometry”, *Chem. Mater.*, 2017, 29, 1127–1133.
49. Liang, X.; Tan, L.; Liu, Z.; Ma, Y.; Zhang, G.; Wang, L.; Li, S.; Dong, L.; Li, J.; Chen, W.; “Poly(naphthalene diimide) vinylene: solid state red emission and semiconducting properties for transistors”, *Chem. Commun.*, 2017, 53, 4934-4937.

## Bioinspired Materials

**PIs:** Surya Mallapragada, Andrew Hillier, Marit Nilsen-Hamilton, Tanya Prozorov, Alex Travesset, David Vaknin, and Wenjie Wang, Ames Laboratory

**Mailing Address:** Division of Materials Sci. and Eng., Ames Laboratory, Ames, IA 50011

**Email:** [suryakm@iastate.edu](mailto:suryakm@iastate.edu)

**Program Scope:** The objective of the Bioinspired Materials FWP is to explore biomimetic mechanisms and routes for the growth of hierarchically self-assembled functional materials with fundamental new properties for a variety of energy applications. Our approach uses coupled organic and biological macromolecules seen in nature to template and control the growth of inorganic/metallic phases. Our interdisciplinary FWP team has successfully demonstrated the value of this integrated experimental approach guided by computational work for room temperature synthesis of a variety of bioinspired nanocomposites, including hydroxyapatite, zirconia and complex magnetic nanocrystals. Our current and future efforts are focused on moving “beyond” nature by using bioinspired approaches and biological templates to synthesize systems not seen in living organisms. We are developing bioinspired “bottom-up synthesis” approaches where biological macromolecules and their synthetic analogs serve as templates for metallization to create nanoscale structures and to provide options for higher-level 2-D and 3-D mesoscale organization and alignment. Using this approach, we are working towards creating “use-inspired” functional tailored metamaterials to illustrate targeting specific functions and to directly address DOE’s Grand Challenge #3, which is to orchestrate atomic and electronic constituents to control material properties. This controlled bottom-up approach for materials design aligns well with DOE’s priorities laid out in the Synthesis workshop report for the synthesis of complex nanostructures and multi-scale assemblies of potential energy relevance.

**Recent Progress:** The two main goals of the work in the Bioinspired Materials FWP are to 1) develop the underlying science needed to design, synthesize and characterize individual nanostructures, and 2) extend this knowledge to assembling these individual nanostructures into 2D and 3D mesoscale superstructures, in the context of targeting function and creating bioinspired metamaterials. While metamaterials provide an ideal use-inspired focus, the bioinspired multi-scale synthesis approaches developed here can be broadly used for targeting other functional structures as well. Our interdisciplinary approach integrates synthesis with theory and computation as well as detailed characterization, primarily involving scattering studies (at the DOE User facilities at Argonne) as well as electron and atomic force microscopy to achieve our goals. Progress towards these goals is summarized below.

**Goal 1: Creation of individual nanostructures using bottom-up approaches:** We are investigating the creation of metamaterial resonator designs such as split-ring resonators using bioinspired bottom-up approaches

***Creation and testing DNA circles and protein-DNA binding for establishing the split rings:*** DNA circles were created using a tiling approach that employed oligonucleotides of varying lengths as shown in the cartoon (**Fig. 1A**). Two longer oligonucleotides with complementary ends were used to create the circles and shorter tiles were hybridized to make the circle double stranded. One of the two overlapping segments of the larger oligonucleotides contained two adjacent sequences of an E-Box sequence that binds to the transcription factor MAX. To establish that the circles were created by mixing the identified oligonucleotides, the samples

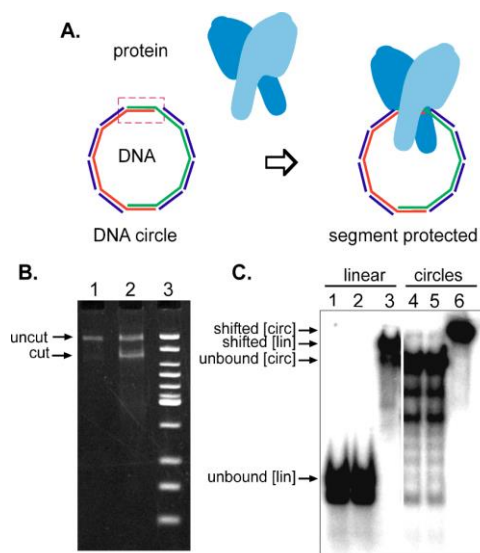


**Fig. 1** Creating and testing DNA circles and protein interactions. **A)** design of the circles, which are constructed by two oligonucleotides with complementary ends (orange and green) and shorter tiles (purple) to create double stranded circles with one or more protein binding domains (red dashed square). The addition of a protein that binds the circle results in a region of the circle being protected, which will then prevent local metallization, thus resulting in a split ring resonator. **B)** The circles were designed with a restriction digestion site in the protein binding site. If the circles are created then they will be cut by Bfa1: 1) control, 2) Bfa1-treated, 3) molecular weight standards. **C)** EMSA test of MAX binding to linear double-stranded oligonucleotides and circles shows that, in the absence of MAX (1,4) or in the presence of albumin (2,5) there is no shift of the radiolabeled circles. The shift of radiolabeled DNA occurs only in the presence of MAX (3,6).

were resolved by polyacrylamide gel electrophoresis after incubation with or without the restriction endonuclease, Bfa1. The Bfa1 site exists only in the E-Box region and thus, a single cut is expected if the circles have been created. The results (**Fig. 1B**) show that the circles were cut in a single location. To create a split ring resonator from DNA circles it is necessary to

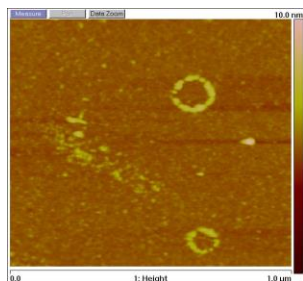


**Fig. 2.** Tapping mode AFM height images showing DNA-templated silver rings on mica. The rings are formed by photo-induced reduction of DNA-Ag<sup>+</sup> complex. The 365-nm wavelength UV light was used as the light source. 14.43ng/μl of circular DNA was mixed with 0.1mM of AgNO<sub>3</sub>. The solution was then exposed to UV irradiation for 30 min. Under the UV exposure the Ag<sup>+</sup> is reduced to metal Ag and bound to the DNA backbone. The height of the Ag anchored DNA was found to be about 3nm. The thickness and the coverage of Ag on the DNA template can be tailored by the successive reduction processes.

protect a portion of the DNA from silver or gold deposition. This was done with a protein that binds the E-box. Recombinant MAX was used in these studies. Radiolabeled circles and linear oligonucleotides with the E-box sequence were incubated in the presence or absence of MAX or in the presence of albumin, the latter as a control for the specificity of the MAX-DNA interaction. These samples were resolved through a polyacrylamide gel following an EMSA (Electrophoretic Mobility Shift Assay) protocol (**Fig. 1C**). The results show that MAX binds both the linear DNA and the circles (shifted). The difference in rate of travel of the unbound linear DNA and circles in this gel, which is due to their different Stokes radii and structures, also demonstrates that circles have been formed.

**Metallization of DNA rings:** These DNA circles were metallized using a photochemical silver reduction process that led to the formation of silver nanoparticle seeds on the circular DNA, as confirmed by UV-Vis spectra (data not shown) and by atomic force microscopy (**Fig. 2**).

**Goal 2: Self-assembled mesoscale 2D and 3D structures:** Here we focus on the fabrication of the desired metamaterials that are characteristic of crystalline super-structures employing existing building blocks and individual nanostructures described in Goal 1. We are interested in existing building blocks and individual nanostructures described in Goal 1. We are interested particularly in the templated and hierarchical self-assembly of nanoscale motifs into 2D or 3D mesoscale crystalline super-lattices whose regularity is directly associated with the environment of the motifs. Our strategy for mesoscale structures involves creating DNA as well as synthetic

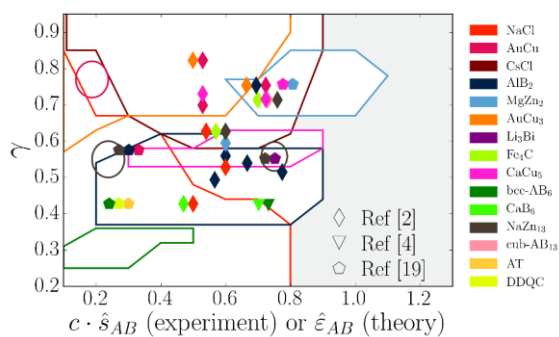


**Fig. 3.** Solid lines define the phase boundaries computed, the symbols are the results of 36 experiments. The correlation between experiment and theory is almost perfect.<sup>17</sup>

synthetic block copolymer templates that form 2D and 3D structures to template the formation and/or assembly of gold nanoparticles. To characterize the structures formed, we are employing a host of scattering techniques such as small- and wide-angle scattering (SAXS and WAXS, respectively), reflectivity, grazing incidence small- and wide-angle scattering, and spectroscopic techniques including XANES, XNTRF, and anomalous diffraction. Studying super-structure of 2D systems provides the basis for fabricating more complicated 3D architectures and structurally tuning 2D array of nanoscale objects that can be metamaterials. These

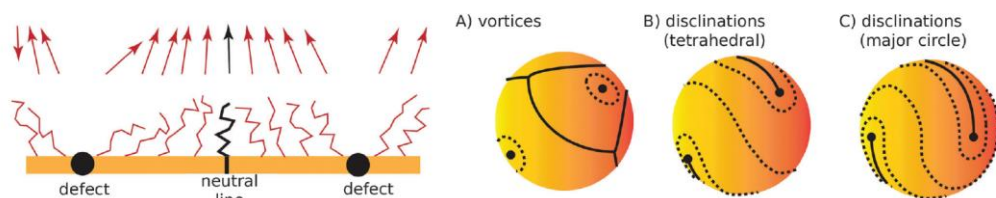


**Fig. 4.** Orbifold topological model for nanoparticle assemblies.<sup>3</sup>

studies are also crucial to understanding control of assembly processes in reduced and confined dimensions.

We have developed a model to predict the phase diagram of nanoparticles with hydrocarbon capping ligands and with DNA programmable self-assembly, using the HOODLT software, developed by the FWP. The results provide a general framework to predict observed crystalline phases formed while building nanomaterial assemblies (**Fig. 3**), and can help the rapid development of tunable nanomaterial structures and provides fundamental insights into nanoparticle interactions. In subsequent work, a new model, the Orbifold Topological model (OTM) has been presented, (**Fig. 4**), which successfully predicts the structure, density, lattice constant, etc. of any nanoparticle superlattice. Using these predictions to guide the experiments, we have demonstrated self-assembly of DNA-functionalized gold nanoparticles at the air-water

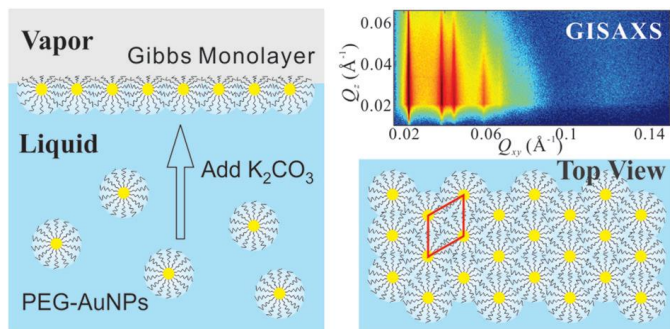


**Fig. 5** Salt-induced 2D hexagonal superlattices of polymer-gold nanoparticles at the air-water interface.<sup>4</sup>

interface by manipulating salt concentrations. Grazing incidence small-angle X-ray scattering and X-ray reflectivity showed that noncomplementary ssDNA-AuNPs dispersed in aqueous solutions spontaneously accumulate at the vapor-liquid interface in the form of a single layer by increasing  $MgCl_2$  or  $CaCl_2$  concentrations. Furthermore, the monolayer undergoes a transformation from short- to long-range (hexagonal) order above a threshold salt-

concentration. Quantitative analysis reveals that divalent cations screen the charge of ssDNA, and that the hydrophobic hexyl-thiol group, commonly used to functionalize the ssDNA for capping the AuNPs, is likely the driving force for the accumulation of the NPs at the interface.

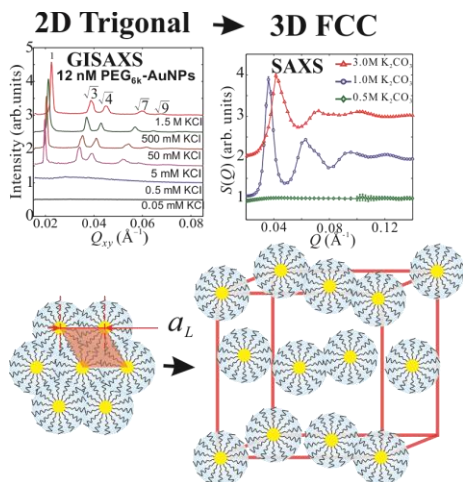


**Fig. 6** Transition from 2D order to short range 3D crystallization of PEG-Au nanoparticles with  $K_2CO_3$  as extracted from the structure factor  $S(Q)$  from SAXS.<sup>2</sup>

compatible with the Hofmeister series.

Using combined experimental evidence and theoretical analysis we have pursued similar strategies to lead to 3D formation of ordered nanoparticle structures. Our small-angle X-ray scattering (SAXS) study reveals the spontaneous formation of PEG-AuNPs assemblies in high-concentration salt solutions that exhibit short-range 3D order with fcc symmetry (**Fig. 6**). We argue that the assembly into fcc crystals is driven by the partnering nearest-neighbors to minimize an effective surface-tension gradient at the boundary between the polymer shell and the high-salt media. SAXS and other results of PEG-AuNPs of various Au core diameters in the range of 10 to 50 nm were analyzed in the framework of brush-polymer theory revealing that the grafting density of PEG systematically decreases with the diameter of the AuNPs.

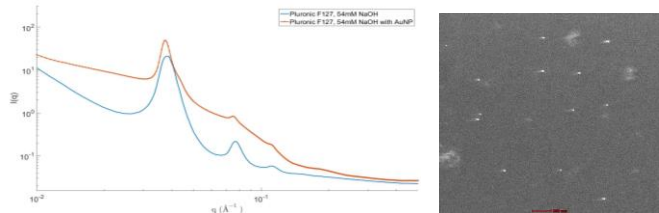


**Fig. 7(a)** 3D Pluronic gels with lamellar structure in the absence and presence of gold nanoparticles (b) fluid cell direct TEM imaging of gold nanoparticles in Pluronic gels

Using aqueous solutions of block copolymers such as Pluronics, and using gold salts to grow the nanoparticles in situ while the polymer forms 3D gels, we can access not just bcc and fcc structures, but also lamellar structures as shown in **Fig. 7a**. Techniques are being developed using a TEM fluid cell to directly image Au nanoparticles and their spatial arrangement in the polymer gels (**Fig. 7b**). TEM shows fairly uniform Au nanoparticles dispersed in the polymeric matrix.

**Future Plans:** Long a unique strength of Ames Laboratory, metamaterials provide an ideal use-inspired focus and targeting of function for the multi-scale bioinspired synthesis approaches that are a focus of this FWP. The complex architectures required for functional metamaterials are at the length scales ideally suited to bioinspired approaches, and are difficult to achieve using conventional top-down methods. We will build on the approaches described to create hierarchically self-assembled 2D and 3D mesoscale that demonstrate the existence of the desired resonances characteristic for functional metamaterials.

## Publications (Aug 2015–Aug 2017)

1. H. Zhang, W. Wang, M. Akinc, S.K. Mallapragada, A. Travesset, D. Vaknin, "Ion-Specific Interfacial Crystallization of Polymer-Grafted Nanoparticles", *J. Phys. Chem. C* (in press).
2. H. Zhang, W. Wang, M. Akinc, S.K. Mallapragada, A. Travesset, D. Vaknin, "Assembling and ordering Polymer-Grafted Nanoparticles in Three Dimensions", *Nanoscale*, **9**, 8710 (2017). DOI:10.1039/c7nr00787F
3. A. Travesset, "Topological Structure Prediction in Binary Nanoparticle Superlattices, *Soft Matter*, **13**, 147 (2017). DOI: 10.1039/c6sm00713a
4. H. Zhang, W. Wang, S.K. Mallapragada, A. Travesset, and D. Vaknin, "Macroscopic and Tunable Nanoparticle Superlattices," *Nanoscale*, **9**, 164 (2017). 10.1039/c6nr07136h
5. H. Zhang, V. Malik, S.K. Mallapragada, and M.A. Akinc, "Synthesis and Characterization of Gd-Doped Magnetite Nanoparticles", *J. Magn. Magnetic Mater.*, **423**, 386 (2017).
6. W. J. Wang, H. H. Zhang, I. Kuzmenko, S.K. Mallapragada, and D. Vaknin, "Assembling Bare Au Nanoparticles at Positively Charged Templates," *Scientific Reports*, **6**, 26462 (2016). 10.1038/srep26462
7. S. Nayak, H. H. Zhang, X. P. Liu, S. R. Feng, P. Palo, M. Nilsen-Hamilton, M. Akinc, and S.K. Mallapragada, "Protein Patterns Template Arrays of Magnetic Nanoparticles," *RSC Advances*, **6**, S7048-S7056 (2016). 10.1039/c6ra07662a
8. M. Elshobaki, R. S. Gebhardt, J. A. Carr, W. R. Lindemann, W. Wang, E. M. Grieser, S. Venkatesan, E. Ngo, U. Bhattacharjee, J. Strzalka, Z. Jiang, Q. Qiao, J. W. Petrich, D. Vaknin, S. Chaudhary. Tailoring Nanoscale Morphology of Polymer: Fullerene Blends Using Electrostatic Field. *ACS Appl. Mater. Interfaces* **9**, 2678–2685 (2016).
9. C. Calero, C. Knorowski and A. Travesset, "Determination of the Anharmonic Free Energy Contributions: Low Temperature Phases of the Lennard-Jones Systems" *J. Chem. Phys.* **144**, 124102 (2016); <http://dx.doi.org/10.1063/1.4944069>
10. H. Zhang, W. Wang, N.Hagen, I. Kuzmenko, M. Akinc, A. Travesset, S. K. Mallapragada, and D. Vaknin, "Self- Assembly of DNA Functionalized Gold Nanoparticles at the Liquid-Vapor Interface", *Advanced Materials Interfaces*, **3**, 1600180 (2016).
11. W. Wang, H. Zhang, S. Feng, J. San Emeterio, S.K. Mallapragada, D. Vaknin, "Iron Ion and Iron Hydroxide Adsorption to Charge- Neutral Phosphatidylcholine Templates", *Langmuir*, **32**, 7664-7670 (2016).
12. N. Horst and A. Travesset, "Prediction of Binary Nanoparticle Superlattices from Soft Potentials," *J. Chemical Physics*, **144**, 014502 (2016). [10.1063/1.4939238](https://doi.org/10.1063/1.4939238)
13. G. Tulli, W. J. Wang, V. Rullaud, W. R. Lindemann, I. Kuzmenko, D. Vaknin, and P. Shahgaldian, "Binding of Calixarene-Based Langmuir Monolayers to Mercury Chloride Is Dependent on the Amphiphile Structure," *RSC Advances*, **6**, 9278-9285 (2016). 10.1039/c5ra25470a
14. Z. Avazbaeva, W. Sung, J. Lee, M. D. Phan, K. Shin, D. Vaknin, and D. Kim, "Origin of the Instability of Octadecylamine Langmuir Monolayer at Low Ph," *Langmuir*, **31**, 13753-13758 (2015). 10.1021/acs.langmuir.5b03947
15. Z. T. Graber, W. Wang, G. Singh, I. Kuzmenko, D. Vaknin, and E. E. Kooijman, "Competitive Cation Binding to Phosphatidylinositol-4,5-Bisphosphate Domains Revealed by X-Ray Fluorescence," *RSC Advances*, **5**, 106536-106542 (2015). 10.1039/c5ra19023a
16. W. R. Lindemann, R. L. Philip, D. W. W. Chan, C. T. Ayers, E. M. Perez, S. P. Beckman, J. Strzalka, S. Chaudhary, and D. Vaknin, "Oriented Polyvinylidene Fluoride-Trifluoroethylene (P(VDF-TrFE)) Films by Langmuir-Blodgett Deposition: A Synchrotron X-Ray Diffraction

Study," *Physical Chemistry Chemical Physics*, **17**, 29335-29339 (2015).

10.1039/c5cp04307g

17. A. Travasset, "Binary Nanoparticle Superlattices of Soft Particle Systems", *PNAS*, **112**, 9563 (2015).
18. X. P. Liu, H. Zhang, S. Feng, G. Parada, J. Anderegg, M. Nilsen-Hamilton, M. Akinc, and S.K. Mallapragada, "The Role of Surface Hydrophobicity on the Function of the Biomineralization Protein Mms6 in Facilitating Magnetite Nanocrystal Formation", *I&EC Res.*, **54**, 10284 (2015). Invited article.

## Directed Organization of Functional Materials at Inorganic-Macromolecular Interfaces

Aleksandr Noy, Anthony van Burren (LLNL), James J. De Yoreo, Chun-Long Chen,  
Marcel Bayer (PNNL)

### Program Scope

This project is building a quantitative physical picture of macromolecular organization and its relationship to function, and uses macromolecular organization to derive new functionality with biological levels of control over molecular transport and separations. We have approached this problem from two converging directions. In the first, we created artificial membrane nanopores using carbon nanotube scaffolds [1], assembled them into 2D biological membrane environments [2], and studied their transport characteristics [3,4]. These structures allowed us to investigate the fundamental role of molecular confinement in biological transport mechanisms and exploit them to create artificial transporters with efficiency rivaling or exceeding their natural analogs. In the second, we created a new type of self-reparable membrane-mimetic 2D nanomaterials from lipid-like sequence-defined biopolymers—peptoids, and investigated the repair kinetics by tuning substrate chemistry and peptoid sequences [5,6]. We demonstrated that peptoid membranes can be used for nanoscale patterning of functional objects, assembly of hexagonally-patterned nanoribbons on mica surfaces, and studies of nucleation pathways [7,8].

Taking lessons from those studies and using the natural biological structures as an inspiration, we are continuing to develop synthetic macromolecular systems that mimic the hierarchical organization and fine-tuned functionality of biological membranes. 2-D peptoid assemblies either serve as scaffolds for assembly of carbon nanotube pores, or directly self-assemble into porous networks in which the pores size and chemistry is controlled by the peptoid sequence. Several complementary characterization efforts cut across all tasks: atomic-scale characterization using small-angle x-ray scattering (SAXS) x-ray diffraction (XRD), x-ray imaging (STXM), and high-speed AFM imaging.

### Recent Progress

#### Role of molecular confinement in biomimetic transport mechanisms in carbon nanotube porins.

Carbon nanotube porins (CNTPs) reproduce structural characteristics of membrane proteins in a simplified pore

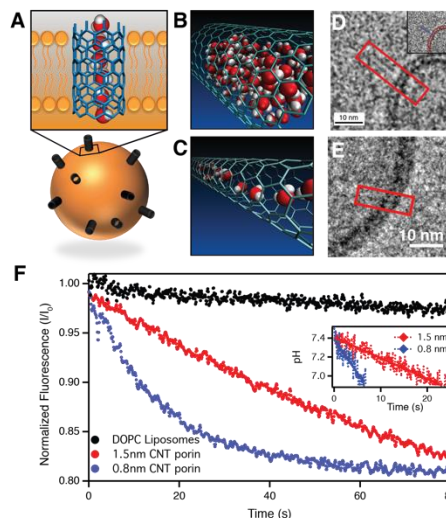


**Figure 1. Carbon nanotube porins (CNTPs) and proton transport through them.** (A) CNTPs in a lipid vesicle. (B,C) Snapshots from computer simulations of CNTPs of two different diameters, showing different arrangement of water molecules inside the nanotube pores. (D, E) Cryogenic TEM images of 1,5 nm (D) and 0.8 nm (E) diameter CNTP (red frames). F. Kinetics of proton transport in nCNTPs and wCNTPs. Inset shows a zoom-in for the initial region of the pH change kinetics. Data from [3].

geometry [1], including their ability to insert spontaneously into lipid membranes (Fig. 1). This platform also allows us to create and manipulate molecular confinement. In particular, we compared two CNTPs of different diameters, 1.5 nm (wCNTPs) and 0.8 nm (nCNTPs), which have nearly identical structure and configuration in the lipid bilayer (Fig. 1D,E), yet feature different arrangement of water molecules: wCNTPs pores preserve an almost bulk-like arrangement, nCNTPs squeeze water down to single hydrogen-bonded chain of molecules [2,3].

**Proton transport through nanotube porins.** Proton transport in biological systems and CNTPs proceeds through a “hopping” Grotthuss mechanism, where proton is transported by quick rearrangement of hydrogen bonds between water molecules. CNTP presence in vesicle walls led to significantly faster proton transport between the vesicle lumen and bulk solution, indicating that CNTPs act as fast proton conductors. The central result of this study [3] was the observation of a *much faster* proton transport rates in *much narrower* nCNTPs (10× of bulk value!) (Figure 1F), as 1D water arrangement in nCNTPs creates a perfect relay chain for Grotthuss transport. Indeed, our measured proton permeability closely matched the value predicted for the ideal proton transport conditions in carbon nanotubes. In contrast, proton diffusion coefficient in wCNTP barely exceeds the bulk value, due to bulk-like arrangement of water in wCNTPs [3].

### Water transport and ion rejection in CNTPs.

Both nCNTPs and wCNTPs supported fast water transport in response to an osmotic gradient (Fig. 2) [4]. Remarkably, the nCNTP water permeability was an order of magnitude higher than the permeability of wCNTPs, indicating that confinement provided the critical ingredient for fast transport. nCNT permeability also exceeded that of biological water channel, aquaporin-1 (AQP1) by 5× [4]!

Single CNTP conductance and reversal potential measurements showed that negatively-charged COO<sup>-</sup> groups at nCNTPs rims make them highly selective cation conductors (Fig. 2C) over a range of ion concentrations up to 2M. Rim charges are also responsible for an unusual nCNTP

conductance characteristics at pH 7, where temporary ion binding to rim COO<sup>-</sup> groups leads to conductance saturation at higher salt concentrations (Fig. 2D) [4]. Overall, a unique combination of high water permeability and strong ion selectivity in nCNTPs shows promise for energy-efficient water desalination.

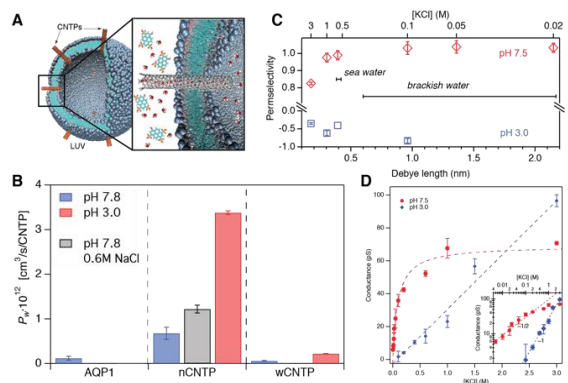


**Figure 2. Water transport in CNTPs.** (A) Schematics of the osmotic transport measurement. (B). Water permeability of CNTPs at different solution pH. Gray bar shows water permeability using seawater-level NaCl solution as a draw. (C) Permeability of nCNTPs measured at different KCl concentrations and pH values. (D) Ionic conductance of nCNTPs as a function of KCl concentration. From [4].

**Assembly of self-repairable membrane-mimetic 2D materials from lipid-like peptoids.** By taking advantage of the hydrogen bond formation between polar monomers and the formation of strong hydrophobic interactions between  $N_4$ -Clpe monomers, we demonstrated that peptoids containing six Nce and six  $N_4$ -Clpe groups assemble into highly crystalline 2D nanomembranes (Fig. 3) through a solvent-induced, spontaneous crystallization process [5]. Based on the AFM, TEM and XRD data, we built a model of the Pep-1 nanomembrane (Fig. 3D) and used it for molecular dynamic simulations (Fig. 3E). The simulated XRD spectrum (Fig. 3C) matched three major peaks of the experimental data, confirming the accuracy of the newly developed force fields. Both *in-situ* and *ex-situ* AFM studies show these 2D nanomembranes are highly stable in pure organic solvents (e.g.,  $CH_3CN$ ). These nanomembranes exhibit a number of properties associated with cell membranes, including thicknesses in the 3.5 - 5.6 nm range and the ability to self-repair. Self-repair occurs on both negatively and positively charged substrates and even in the absence of an underlying surface [6]. Following dissection of pre-assembled peptoid membranes and upon introduction of a peptoid monomer solution, peptoid membranes self-repair anisotropically. Moreover, the ability to self-repair enables synthesis of nanoscale-patterns of distinct functional groups within membranes [5,6].

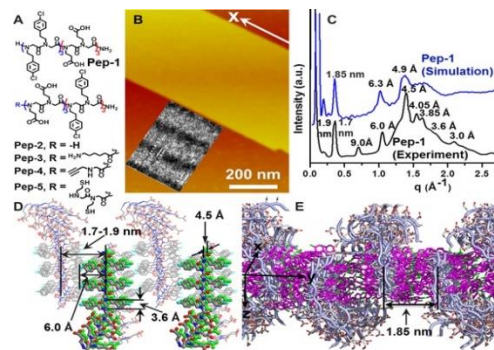


**Figure 3. Assembly of peptoid membranes.** (A) Structures of **Pep-1 - Pep-5**. (B) AFM image showing **Pep-5** membrane; inset is a HR-TEM image showing well-aligned strips within the membrane along x-direction. (C) Experimental and simulated XRD data of **Pep-1** membranes. (D) Proposed model of **Pep-1** membrane based on AFM, TEM and XRD data. (E) **Pep-1** membrane model generated from MD simulations showing well-aligned polar groups. Data from [5].

**Understanding peptoid assembly pathways and their relationship to sequence.** While sequence-defined polymers hold great promise to mimic proteins and peptides for functions, their controlled assembly on surfaces still remains underdeveloped as does an ability to rationally design sequences based on rules for achieving a desired structure and function. We demonstrated the assembly of 12-mer peptoids containing alternating acidic and aromatic residues into networks of hexagonally-patterned nanoribbons on mica surfaces [7]. Here,  $Ca^{2+}$ -carboxylate coordination creates peptoid-peptoid and peptoid-mica interactions that control self-assembly. *In-situ* AFM showed that peptoids first assembled into discrete nanoparticles, these particles then transformed into hexagonally-patterned nanoribbons on mica surfaces. AFM-based dynamic force spectroscopy studies show that peptoid-mica interactions are much

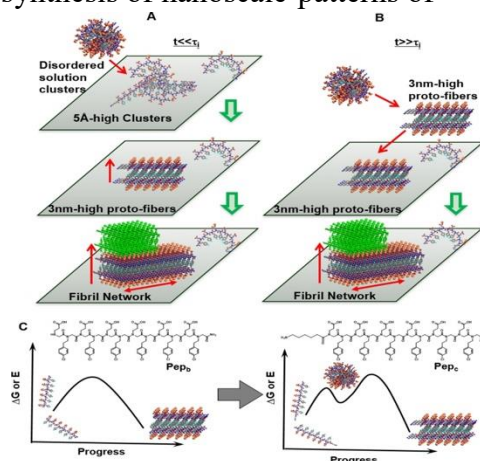


**Figure 4.** Peptoid crystallization pathways and energy landscapes derived from assembly dynamics. (A, B)  $Pep_c$  assembly process at early (A) and late (B) stages showing effect of hydrophobic region on cluster formation. (C) Alteration in pathway from a single step for  $Pep_b$  to a two-step process for  $Pep_c$  and corresponding energy barriers associated with the addition hydrophobic region to  $Pep_b$ . Data from [8].

stronger than peptoid-peptoid interactions, illuminating the driving forces for surface-directed peptoid assembly [7].

Using *in situ* AFM to directly observe crystallization of peptoids, we showed that crystallization pathways are sequence dependent. When a short hydrophobic region is added to the sequence that directly forms crystalline particles, crystallization follows a two-step pathway that begins with creation of disordered clusters of 10-20 molecules and is characterized by highly non-linear crystallization kinetics in which clusters transform into ordered structures that then enter the growth phase (Fig. 4). The results shed new light on non-classical crystallization mechanisms and have implications for design of self-assembling polymers [8].

## Future Plans

Our future plans center on integrating CNTPs into peptoid membranes, understanding the atomic level structure and dynamics of these assemblies, and understanding and manipulating the interface water structure and mechanisms for transport and molecular selectivity.

## References

1. J. Geng, K. Kim, J. Zhang, R. Tunuguntla, L. R. Comolli, F. I. Allen, K. R. Cho, D. Munoz, Y. M. Wang, C. P. Grigoropoulos, C. M. Ajo-Franklin & A. Noy *Stochastic Transport and Gating in Carbon Nanotube Porins in Lipid Membranes*, **Nature**, **514**, 612-615 (2014).
2. R. H. Tunuguntla, A. Escalada, V. Frolov & A. Noy *Synthesis, lipid membrane incorporation, and ion permeability testing of carbon nanotube porins*, **Nature Prot.**, **11**, 2029 (2016)
3. R. H. Tunuguntla, F. I. Allen, K. Kim, A. Belliveau & A. Noy *Ultra-Fast Proton Transport in Sub-1-nm Diameter Carbon Nanotube Porins*, **Nature Nano.**, **11**, 639 (2016).
4. R. Tunuguntla, R. Henley, Y.-C. Yao, T.A. Pham, M. Wanunu & A. Noy *Enhanced water permeability and tunable ion selectivity in sub-1-nm carbon nanotube porins*, **Science**, accepted. (2017).
5. H. B. Jin, F. Jiao, M. D. Daily, Y. L. Chen, F. Yan, Y.-H. Ding, X. Zhang, E. J. Robertson, M. D. Baer & C. L. Chen, *Highly stable and self-repairing membrane-mimetic 2D nanomaterials assembled from lipid-like peptoids*. **Nature Comm.**, **7**, 12252 (2016)
6. F. Jiao, Y. L. Chen, H. B. Jin, P. G. He, C. L. Chen & J. J. DeYoreo, *Self-repair and patterning of 2D membrane-like peptoid materials*. **Adv. Funct. Mater.**, **26**, 8960 (2016).
7. C. L. Chen, R. N. Zuckermann & J. J. De Yoreo, *Surface-directed assembly of sequence-defined synthetic polymers into networks of hexagonally-patterned nanoribbons with controllable functionalities*. **ACS Nano**, **10**, 5314 (2016).
8. X. Ma, S. Zhang, F. Jiao, C. J. Newcomb, Y. Zhang, A. Prakash, Z. Liao, M. D. Baer, C. J. Mundy, J. Pfaendtner, A. Noy, C. L. Chen & J. J. De Yoreo, *Tuning crystallization pathways through sequence engineering of biomimetic polymers*. **Nature Mater.** **16**, 767 (2017).

### **Publications for the past 2 years.**

- R. H. Tunuguntla, A. Escalada, V. Frolov, A. Noy *Synthesis, lipid membrane incorporation, and ion permeability testing of carbon nanotube porins*, **Nature Prot.**, *11*, 2029 (2016)
- M.D. Daily, M.D. Baer and C.J. Mundy, “Divalent Ion Parameterization Strongly Affects Conformation and Interactions of an Anionic Biomimetic Polymer” **J. Phys. Chem. B**, , *120*, 2198 (2016).
- I.C. Tran, R. H. Tunuguntla, K. Kim, T. Willey, J.R.I. Lee, T. Weiss, A. Noy, T. van Buuren *Structure of Carbon Nanotube Porins in Lipid Bilayers: an In-Situ Small-Angle X-ray Scattering (SAXS) Study*, **Nano Letters**, *16*, 4019 (2016)
- R. H. Tunuguntla, F. I. Allen, K. Kim, A. Belliveau, A. Noy *Ultra-Fast Proton Transport in Sub-1-nm Diameter Carbon Nanotube Porins*, **Nature Nanotechnology**, *11*, 639 (2016).
- C. L. Chen, R. N. Zuckermann & J. J. De Yoreo, *Surface-directed assembly of sequence-defined synthetic polymers into networks of hexagonally-patterned nanoribbons with controllable functionalities*. **ACS Nano**, *10*, 5314 (2016).
- H. B. Jin, F. Jiao, M. D. Daily, Y. L. Chen, F. Yan, Y.-H. Ding, X. Zhang, E. J. Robertson, M. D. Baer & C. L. Chen, *Highly stable and self-repairing membrane-mimetic 2D nanomaterials assembled from lipid-like peptoids*. **Nature Comm.**, *7*, 12252 (2016)
- F. Jiao, Y. L. Chen, H. B. Jin, P. G. He, C. L. Chen & J. J. DeYoreo, *Self-repair and patterning of 2D membrane-like peptoid materials*. **Adv. Funct. Mater.**, *26*, 8960 (2016).
- R.H. Tunuguntla, A. Belliveau, X. Chen, A. Noy *High-Yield Synthesis and Optical Characterization of Carbon Nanotube Porins*, **J. Phys. Chem. C**, *121*, 3117 (2017)
- Y. Zhang, R.H. Tunuguntla, P-O. Choi, A. Noy *Real-time dynamics of carbon nanotube porins in supported lipid membranes visualized by high-speed AFM*, **Phil. Trans. Roy. Soc. B.**, *372*, 20160226 (2017).
- X. Ma, S. Zhang, F. Jiao, C. J. Newcomb, Y. Zhang, A. Prakash, Z. Liao, M. D. Baer, C. J. Mundy, J. Pfaendtner, A. Noy, C. L. Chen & J. J. De Yoreo, *Tuning crystallization pathways through sequence engineering of biomimetic polymers*. **Nature Mater.** *16*, 767 (2017).
- R. Tunuguntla, R. Henley, Y.-C. Yao, T.A. Pham, M. Wanunu, A. Noy *Enhanced water permeability and tunable ion selectivity in sub-1-nm carbon nanotube porins*, **Science**, accepted. (2017).

## **Adaptive Interfacial Assemblies Towards Structuring Liquids (DE-AC02-05-CH11231)**

**Thomas P. Russell**, Materials Sciences Division, Lawrence Berkeley National Laboratory; **Brett Helms** and **Paul Ashby**, Molecular Foundry, Lawrence Berkeley National Laboratory, Berkeley, CA; **Alex Zettl**, Department of Physics, and **Philip Geissler**, Department of Chemistry, University of California at Berkeley, Berkeley, CA

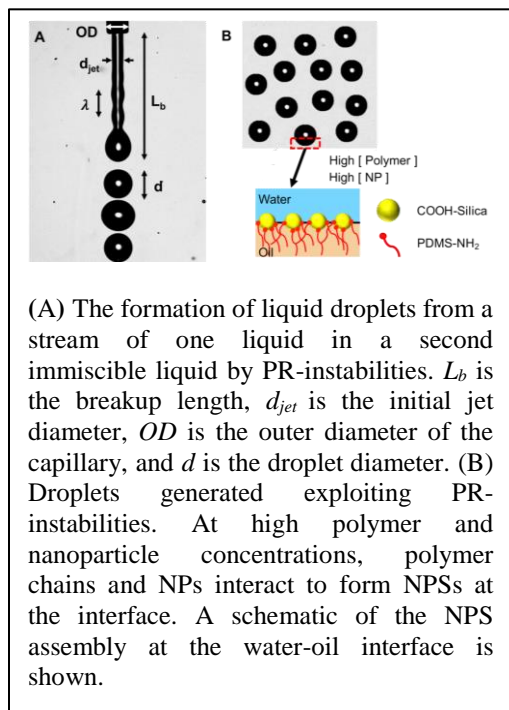
### **Program Scope**

This Seed Program aims to develop a new concept in materials –*Adaptive Interfacial Assemblies Towards Structuring Liquids*– based on the jamming of interfacial assemblies of NP-surfactants (NPSs)<sup>1</sup>. The spatial and temporal characteristics of structured liquids span from the nanoscopic to macroscopic, over orders of magnitude in time, making these systems mesoscopic in space and time. We address questions in translating control over individual nanoparticle chemistries and their assembly and dynamics at interfaces, cascading events on the nanoscopic level to the macroscopic level. We will quantitatively characterize the interfacial assemblies of NPSs, their dynamics, and their response to external stimuli. Chemistries will be developed to tailor the responsiveness of the assemblies. From these studies a new family of adaptive materials will emerge having the desirable characteristics of fluids—rapid transport of energy carriers and controlled dissipation of mechanical energy—and the structural stability of a solid. We will establish a foundation for generating all-liquid, energy-relevant systems that can be re-structured upon demand. This leads to new concepts and design strategies for directing energy flow in materials, and materials with an unprecedented dynamic range of properties.

The objectives of the Seed Program are two-fold: **I. Understanding of the basic principles underpinning the structuring of liquids:** By quantifying the kinetics of formation of NPS assemblies at interfaces and their interfacial dynamics and jamming, by systematically controlling the size and shape of the NPs and polymer NPS interactions, we will be able to shape and re-shape macroscopic liquid constructs. **II. Structured liquids that adapt and respond:** By configuring responsive chemical functionality on the NPSs we can switch between attractive and repulsive interactions in a manner that is independent of but compatible with the NPS interactions pinning the NPSs to the interface, we will be able (i) to generate structured liquids that can be reconfigured *on-demand* and (ii) to tailor the optical and mechanical properties of the NPS assemblies

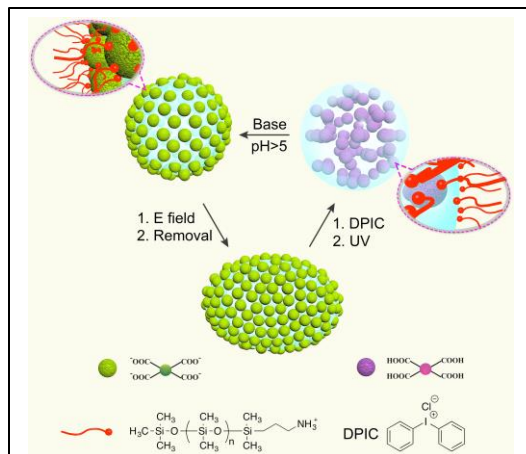
### **Recent Progress**

**Effect of Nanoparticle Surfactants on Plateau-Rayleigh Instabilities<sup>2</sup>:** Structured liquids, whose 3-D morphology can adapt and respond to external stimuli, represent a revolutionary materials platform for next-generation energy technologies, such as batteries, photovoltaics, and thermoelectrics. Structured liquids can be crafted by the jamming of interfacial assemblies of NPSs. Due to the interactions between functional groups on nanoparticles dispersed in one liquid and polymers having complementary end-functionality dissolved in a second immiscible fluid,



the anchoring of a well-defined number of polymer chains onto the NPs leads to the formation of NP-surfactants that assemble at the interface and reduce the interfacial energy. Microfluidic techniques provide a simple and versatile route to produce one liquid phase in a second where the shape of the dispersed liquid phase can range from droplets to tubules depending on the flow conditions and the interfacial energies. In this study, the effect of NP-surfactants on Plateau-Rayleigh (PR) instabilities of a free-falling jet of an aqueous dispersion of carboxylic acid functionalized silica NPs into a toluene phase containing amine-terminated polydimethylsiloxane (PDMS-NH<sub>2</sub>), is investigated. NP-surfactants were found to significantly affect the breakup of laminar liquid jets, resulting in longer jet breakup lengths and dripping to jetting flow transitions.

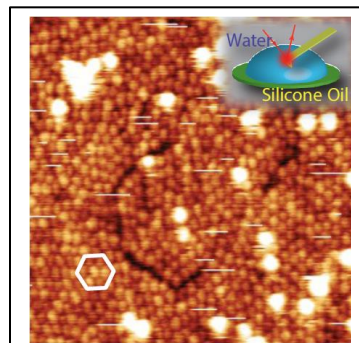
**Structured Liquids with pH-Triggered Reconfigurability<sup>3</sup>:** Structured liquids can be produced in biphasic liquid media when NPs assemble at the interface between the two fluids. This can also be achieved using non-covalent interactions between polymers dissolved in one medium and NPs dispersed in the second provided the polymer and NPs bear complementary functionality (e.g., complementary electrostatics), forming NPSs. Assemblies of NPSs are disordered yet dynamic, in that there is a well-regulated number of polymer chains in dynamic association with the NP surface. An external field can be used to deform the spherical shape of the liquid domains, increasing the interfacial area between the two fluids allowing additional NPSs to assemble at the interface. Upon release of the deforming field, the interfacial area decreases causing the assembly of NPSs to jam, locking-in non-equilibrium shapes of the fluids. We show that it is now possible to reconfigure such structured liquids back into their equilibrium spherical shapes remotely using a water-soluble photoacid generator, which can be triggered by light to disrupt the dynamic complementarity between the polymers and NPs in their jammed state. We rationalize the observed



Through pH-tuning of electrostatic interactions between polymer ligands and nanoparticles at structured-liquid interfaces, liquid droplets could be directed between a jammed non-equilibrium state and a dynamic reconfigurable state. The nanoparticle-surfactant dynamics highly depends on the pH, so that the liquids can be structured using an external field and under variation of pH, or alternatively being realized by a remote-photo-tuning.

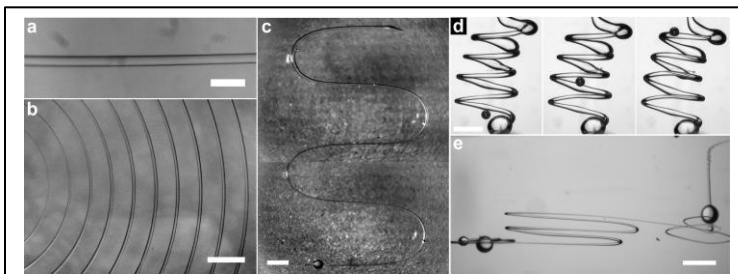
behavior by carrying out detailed analysis of NPS dynamics as a function of pH. Our results indicate that molecular engineering can be used to initiate and guide the kinetic trajectory between non-equilibrium and equilibrium states of matter using dynamic materials chemistry.

**Fine tuning the nanoparticles packing at water-oil interfaces through ionic strength:** We have demonstrated the use of ionic strength to tune the interfacial packing of NPSs at the water-oil interface. As the ionic strength increases, the rate of formation and assembly of NPSs at and oil-water interface can be markedly enhanced. Both the interfacial tension and high-speed image analysis experiments were performed at the water-oil interface. In addition, the first *in situ* AFM images of NPSs at the water-oil interface are shown the provide a real-space image of the packing of the NPSs assembled at the interface.



*In situ* AFM image of NPs assembled at the water- toluene interface with 100 mM NaCl, where the white hexagon shows the hexagonal packing of Nanoparticles and the inset shows the schematic diagram of the experimental setup.

**3D Printing of Adaptive, Structured Liquids:** Liquids lack the structure required to impart complex, spatial functionality. Interfacial assemblies of colloids and nanoparticles have mechanical properties that, despite their negligible thickness, can be used to structure liquids into an extremely broad array of shapes and structures<sup>4-6</sup>. A method that fully exploits the structure, functionality, and reconfigurability offered by all-liquid systems would open an entirely new platform for energy storage, biphasic reaction media, soft electronic devices and biomimetic soft robotic devices. We have demonstrated the 3D printing of water in oil, in which the structure is locked-in by the interfacial jamming of nanoparticle surfactants, NPSs. The jamming of the NPSs leads to elastic interfaces, resulting in macroscopic, extended, bicontinuous liquid systems that adapt to external stresses and stimuli. These systems can be readily functionalized by a wide range of nanoparticles and functional polymers, as the binding of the particles depends solely on the complementarity of the surface functionalities of the components comprising the assemblies<sup>3,4-7</sup>. We envisage dynamic, reconfigurable constructs that can be regulated and altered by external stimuli.



**Two- and three-dimensional printed, all-liquid systems.** **a**, An aqueous thread in oil, diameter 100  $\mu\text{m}$ . Scale bar, 0.4 mm. **b**, High magnification image of a 40 cm-long spiral. Scale bar, 1 mm. **c**, Composite micrograph of an extended, sigmoidal structure. Scale bar, 2 mm. **d**, Time series of a 3D printed coil, after (l-r) 0, 4, and 16 min. Scale bar = 0.5 mm. **e**, An interconnected, fully three-dimensional system. Scale bar, 2 mm.

## Future Plans

The very promising imaging results of the NPS assemblies at fluid-fluid interfaces will be pursued to determine the spatial location and dynamics of all NPSs in the assemblies, fully characterizing the state of order (or disorder) as the assemblies are compressed from the liquid to glassy state. We will focus on the heterogeneous nature of the assemblies and the development of percolated pathways to support in-plane load in the jammed state. These studies will be augmented by theoretical studies on disordered assemblies taking the ligand into specific account.

We have demonstrated the ability to shape and 3D print liquids. However, the mechanical properties of the structures are not known and will be determined. We have developed a cell to deform structures using an air bubble that will allow determination of the storage and loss moduli. 3D printed constructs will be used to perform simple tensile testing to examine relaxation processes in the assemblies that will be augmented with fluorescence recovery pattern photo-bleaching to evaluate in-plane diffusion of the NPS assemblies.

We will configure specific chemistries in the NP coatings to selectively manipulate NP-NP interactions, independent of the NP-polymer interactions, upon application of a chemical or physical stimulus. These are critical new capabilities that will allow us to evolve the mesostructure of the interfacial NP assemblies in a controlled manner and on demand.

## References

1. Cui, M., Emrick, T. & Russell, T. P. Stabilizing liquid drops in nonequilibrium shapes by the interfacial jamming of nanoparticles. *Science* (80-. ). **342**, 460–464 (2013).
2. Huang, C. *et al.* Structured Liquids with pH-Trigged Reconfigurability. *Adv. Mater.* **28**, 6612–6618 (2016).
3. Toor, A., Helms, B. A. , and Russell, T. P. , “Effect of Nanoparticle Surfactants on the Break-Up of Free-Falling Water Jets During Continuous Processing of Reconfigurable Structured Liquid Droplets”, *Nano Letters*, 17.5 (2017): 3119-3125.
4. Clegg, P. S. *et al.* Emulsification of partially miscible liquids using colloidal particles: Nonspherical and extended domain structures. *Langmuir* **23**, 5984–5994 (2007).
5. Subramaniam, A. B., Abkarian, M., Mahadevan, L. & Stone, H. a. Colloid science: non-spherical bubbles. *Nature* **438**, 930 (2005).
6. Erni, P., Jerri, H. A., Wong, K. & Parker, A. Interfacial viscoelasticity controls buckling, wrinkling and arrest in emulsion drops undergoing mass transfer. *Soft Matter* **8**, 6958–6967 (2012).
7. Sun, Z., Feng, T. & Russell, T. P. Assembly of graphene oxide at water/oil interfaces: Tessellated nanotiles. *Langmuir* **29**, 13407–13413 (2013).
8. Feng, T., Hoagland, D. A. & Russell, T. P. Assembly of Acid-Functionalized Single-Walled Carbon Nanotubes at Oil/Water Interface. *Langmuir* **30**, 1072–1079 (2014).
9. Toor, A., Feng, T. & Russell, T. P. Self-assembly of nanomaterials at fluid interfaces. *Eur. Phys. J. E* **39**, (2016).

## Publications

1. C. Hang, Z. Sun, M. Cui, F. Liu, B.A.Helms and T. P. Russell, “Structured Liquids with pH-Triggered Reconfigurability”, *Advanced Materials* 2016, 28, 6612–6618.
2. A. Toor, T. Feng and T.P. Russell, “Self-assembly of nanomaterials at fluid interfaces”, *Eur. Phys. J. E***39**, 57 (2016), DOI 10.1140/epje/i2016-16057-x
3. A. Toor, B. A. Helms, and T. P. Russell. 2017. “Effect of Nanoparticle Surfactants on the Break-Up of Free-Falling Water Jets During Continuous Processing of Reconfigurable Structured Liquid Droplets”, *Nano Letters*, 17.5 (2017): 3119-3125.
4. C. Huang, M. Cui, Z. Sun, F. Liu, B. A. Helms, and T. P. Russell, “Self-Regulated Nanoparticle Assembly at Liquid/Liquid Interfaces: A Route to Adaptive Structuring of Liquids”, *Langmuir*, revision submitted.
5. C. Huang, J. Forth, W. Wang, K. Hong, G. S. Smith, B. A. Helms, and T. P. Russell., “Bicontinuous structured liquids with sub-micron domains using nanoparticle surfactants”, *Nature Nanotechnology*, revision resubmitted.
6. J. Forth, X. Liu, A. Toor, S. Shi, B. A. Helms and Thomas P. Russell, "3D Printing of Adaptive, Structured Liquids", *Nature*, under review.
7. R. Li, Y. Chai, Y. Jiang, P. D. Ashby, A. Toor and T. P. Russell, “Carboxylated Fullerene at the Oil/Water Interface”, *ACS Applied Materials and interfaces*. Revision submitted to *ACS Applied Materials & Interfaces*, accepted, in press.

## **Dynamics of Active Self-Assembled Materials**

**PI: Alexey Snezhko, Co-Investigators: Andrey Sokolov, Igor Aranson, Andreas Glatz**

**Materials Science Division, Argonne National Laboratory, 9700 South Cass Avenue,  
Argonne, IL60439**

### **Program Scope**

Self-assembly, a natural tendency of simple building blocks to organize into complex architectures, is a unique opportunity for materials science. The in-depth understanding of self-assembly paves the way for the design of tailored smart materials for emerging energy technologies, such as materials that can self-heal, regulate porosity, strength, water or air resistance, viscosity, or conductivity. However, self-assembled materials pose a formidable challenge: they are intrinsically complex, with often-hierarchical organization occurring on many nested length and time scales.

The program is focused on the fundamental aspects of out-of-equilibrium dynamics and self-assembly of bio-inspired materials. The main research direction focuses on the design of novel smart materials that can arise from a fundamental understanding of dynamic self-assembly and organization far from equilibrium. The major challenges here are: understanding fundamental mechanisms that lead to collective behavior from the interactions between simple constituents and designing new functional active self-assembled materials.

In the past two years our program yielded discoveries of reconfigurable wires and self-assembled dynamic spinners emerging in out-of-equilibrium magnetic suspensions at liquid interfaces, novel methods of manipulation and control of active suspensions of swimmers by vertical flows. All of these structures and phenomena are generally not available through thermodynamics and accessible only out of equilibrium. For all these systems we have developed theoretical understanding leading to prediction and control of the emergent self-assembled structures. In the next three years we will explore new approaches to synthesis and discovery of novel self-assembled active materials stemming from recent advances of our program: a synthetic system of active (actively spinning) colloids energized by electromagnetic fields, and bio-mimetic suspensions of active swimmers (bacteria and synthetic swimmers) in anisotropic fluids .

The program synergistically combines experiment, theory, and simulations, and focuses on the fundamental issues at the forefront of contemporary materials science. Our long-term goals are to develop a fundamental understanding of out-of-equilibrium self-assembly in active systems as it relates to the BES missions in Biomolecular Materials and Mesoscale Science.

## Recent Progress

Active self-assembled spinner materials. Dissipative colloidal materials use energy to generate and maintain structural complexity. The energy injection rate, and properties of the environment are important parameters that control the outcome of dynamic self-assembly. We conducted studies of ferromagnetic colloidal dispersion confined at liquid-air interface and energized by uniaxial in-plane alternating magnetic field. The system exhibits a remarkable diversity of dynamic self-assembled structures when driven out of equilibrium. Complex collective motion and hierarchical ordering in this out-of-equilibrium system reflects the balance between many

types of interactions among particles, ranging from short-range steric to long-range hydrodynamic and electromagnetic ones. Loose clusters extended along the ac magnetic field are formed at low frequencies. The clusters exhibit periodic changes in shape (pulsations). At elevated frequencies of the applied field, the clusters transform into a cloud of continuously rearranging short chains. In striking contrast with loose clusters, the cloud switches the axis of elongation and extends perpendicular to the ac field. Further increase in the frequency yields a new dynamic phase: spinners (see Fig. 1a). In this phase the particles self-assemble into short chains, and rotate in the plane of the interface in either direction at the frequency of the applied ac magnetic field.

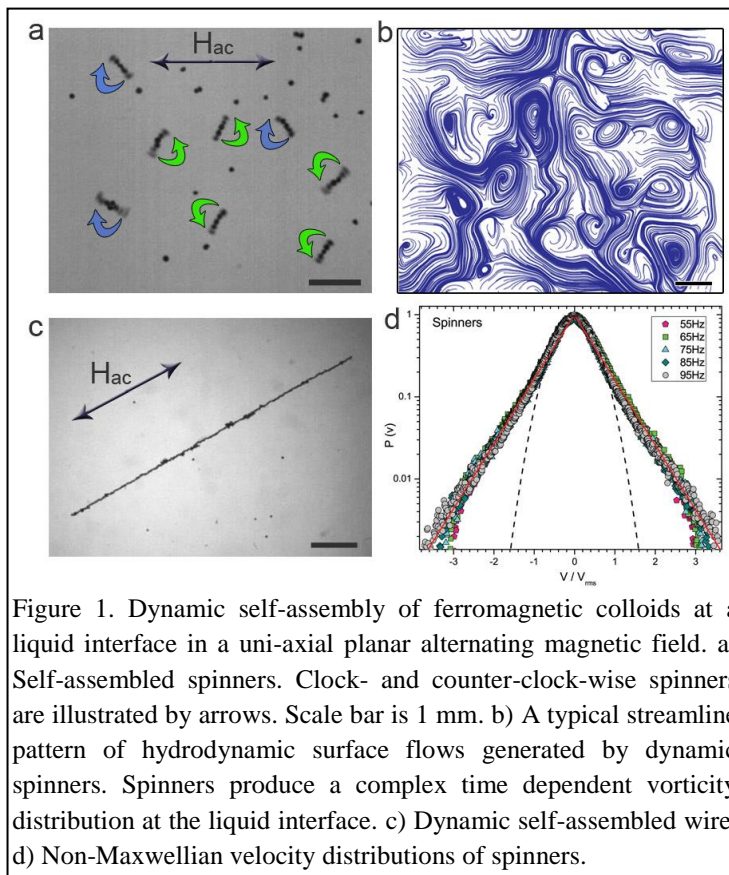


Figure 1. Dynamic self-assembly of ferromagnetic colloids at a liquid interface in a uni-axial planar alternating magnetic field. a) Self-assembled spinners. Clock- and counter-clock-wise spinners are illustrated by arrows. Scale bar is 1 mm. b) A typical streamline pattern of hydrodynamic surface flows generated by dynamic spinners. Spinners produce a complex time dependent vorticity distribution at the liquid interface. c) Dynamic self-assembled wire. d) Non-Maxwellian velocity distributions of spinners.

*The spinners emerge via spontaneous breaking of the uniaxial symmetry of the energizing magnetic field.* Rotations of the spinners create strong vortical hydrodynamic flows, Fig. 1b, and promote active transport. At higher frequencies the spinners give way to dynamic wires (see Fig. 1c). On the basis of controlled experiments we demonstrated that the velocity distributions for spinners is strongly non-Maxwellian, with nearly exponential high energy tails (see Fig. 1d). All discovered phases are reversible and their behavior is controlled by the applied ac magnetic field parameters. Our findings provide experimental access to large ensembles of spinners enabling studies of active spinner materials.

Rapid expulsion of microswimmers by vortical flows. Biosynthetic materials, exemplified by suspensions of micro-swimmers in isotropic and anisotropic liquids (e.g. liquid crystals) are an

emerging class of engineered composite soft materials with the ability to reconfigure their structure and properties in response to external stimuli. This functionality is critical for a variety of applications, from self-healing materials to self-assembled hierarchical structures and micro-robots. However, interactions of micro-swimmers with their fluid environment are complex.

Macroscopic shear flow alters swimming trajectories in a highly nontrivial way and results in dramatic reduction of viscosity and heterogeneous bacterial distributions.

We discovered rapid expulsion of microswimmers, such as motile bacteria, by a

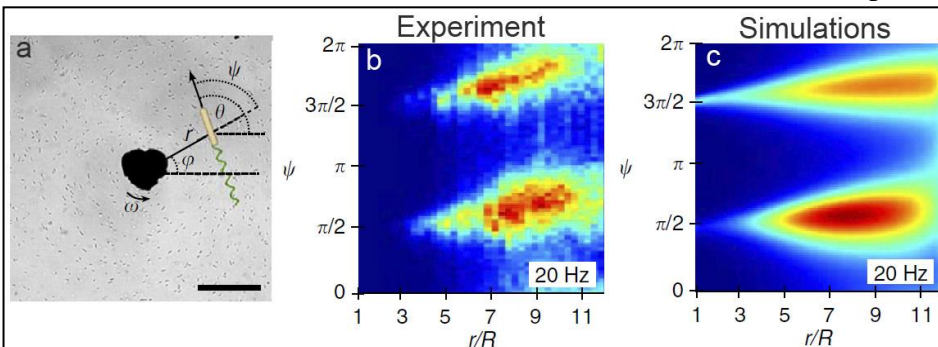


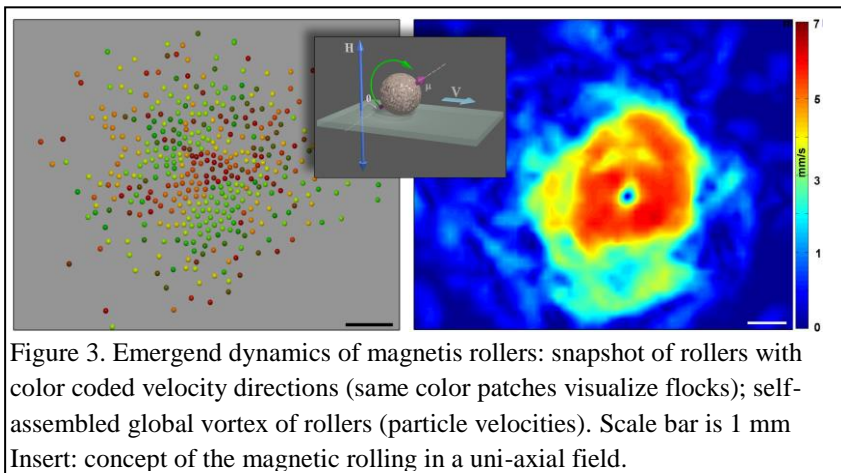
Figure 2. Expulsion of micro-swimmers by a vortical flow created by a spinning microparticle. Comparison of experimental (b) and theoretical (c) probability distributions  $P(r, \psi)$  to find a bacterium at the distance  $r$  from the center of origin and with orientation  $\psi$ .

vortical flow created by a rotating microparticle. We observe the formation of a macroscopic depletion area in a high-shear region, in the vicinity of a microparticle. *Centrifugal force is negligible*: non-motile bacteria remain uniformly distributed. The rapid migration of bacteria from the shear-rich area is caused by a vortical structure of the flow rather than intrinsic random fluctuations of bacteria orientations, in stark contrast to planar shear flow. We also discovered that a small fraction of bacteria is trapped by a rotation particle and released after cessation of rotation. Our mathematical model reveals that expulsion is a combined effect of motility and alignment by a vortical flow, see Fig. 2. We calculated the distribution functions for position and orientation of bacteria  $P(r, \psi)$ . Our theoretical results match well with the experimental data. Our findings offer a novel approach for manipulation of motile particles and shed light on microswimmer–flow interactions.

## Future Plans

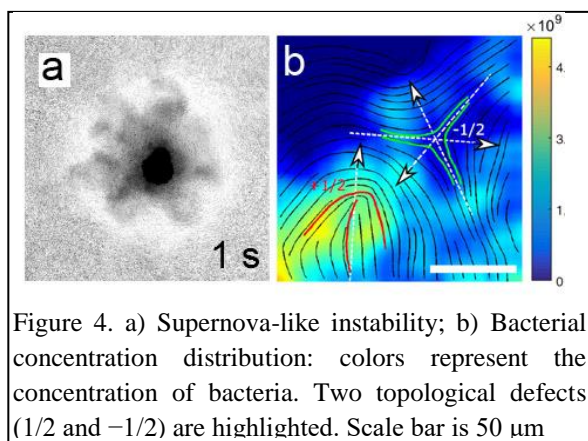
Emergent dynamics of magnetic colloidal rollers. This research direction focuses on a new concept of magnetic colloidal rollers. A colloidal roller couples both rotational and translational motion of the active particle. Recently, the magnetic colloidal rollers have been experimentally realized for the first time in our lab. The rolling motion in our system appears due to a spontaneous symmetry breaking of the clockwise/ counterclockwise rotation experienced by a magnetic sphere in a uniaxial field, see Fig. 3. We have direct access and control over dominant interactions in the magnetic rollers ensemble through parameters of the driving magnetic field. The system also allows selective tuning of the hydrodynamic interactions since the magnetic rollers do not rely on the presence of a liquid. We envision comprehensive studies, both experimental and computational, of complex emergent dynamics of magnetic colloidal rollers. Preliminary results are very promising. The system exhibits a rich variety of dynamic phases.

Gas-like states transform into flocks of rollers as a function of the energizing magnetic field frequency: groups of particles start to move coherently and form well-defined flocks reminiscent of bird flocks, Fig 3. In a certain range of excitation parameters, a continuously rotating vortex, often spanning the entire system,



emerges, Fig. 3 (right panel). The primary goals of this research are (i) understanding of the fundamental mechanisms governing active self-assembly and transport in colloidal rollers systems with long-ranged interactions; (ii) exploration of design concepts of various active tunable dynamic phases and directed transport at the microscale.

Dynamics of active composite materials. We plan to address the intriguing question of the evolution of dense bacterial droplet and motility induced phase separation. Our preliminary experiments produced a surprising discovery of a supernova-like explosion of dense bacterial droplets concentrated by vortical flows: the cessation of the particle rotation results in a violent explosion of the bacterial droplet, see Fig. 4a. We plan to explore in detail the onset of instability as a function of rotational rates and swimmer concentrations. We will combine our expertise in dynamics of liquid crystals, swimming bacteria, and magnetically driven colloids to start a new synergetic research direction on active materials by design. These composite materials are formed by inanimate but highly structured liquid crystals doped by an active component. The active component will be formed either by synthetic swimmers or driven functionalized colloids.



We envision that these materials will have unique mechanical and optical properties not available in their passive counterparts. Our preliminary findings show that microswimmers behave differently around positive and negative topological defects, Fig. 4b. A self-organized increase in the swimmer concentration in the defect cores highly increases the sensitivity of these materials to external stimuli, such as light, magnetic field or chemical signals. We plan to investigate the role of defects on spatio-temporal

response of active nematics. Success in this area will open a new avenue for the design of active bio-composite materials and greatly extend our scope of tools to control microscopic objects in active matter.

## Publications (DOE supported 2016-2017)

1. A. Kaiser, A. Snezhko, I. Aranson, Flocking ferromagnetic colloids, *Science Advances* **3**, e1601469 (2017).
2. M. Genkin, A. Sokolov, O. Lavrentovich, I. Aranson, Topological defects in a Living Nematic Ensnare swimming bacteria, *Phys. Rev. X* **7**, 011029 (2017)
3. G. Kemmel, A. Glatz, I.S. Aranson, Phase slips in superconducting weak links, *Phys. Rev. B* **95**, 014518 (2017).
4. F. Ziebert, I. S. Aranson, Computational approaches to substrate-based cell motility, *Nature Computational Materials* **2**, 16019 (2016).
5. A. Snezhko, Complex collective dynamics of active torque-driven colloids at interfaces. *Current Opinion in Colloid and Interface Science* **21**, 65 (2016).
6. A. Sokolov, I.S. Aranson, Rapid expulsion of microswimmers by a vortical flow, *Nature Communications* **7**, 11114 (2016).
7. B. Winkler, I. Aranson, F. Ziebert, Membrane tension feedback on shape and motility of eukaryotic cells, *Physica D - Nonlinear Phenomena* **318**, 26-33 (2016).
8. T. Mohoric, G. Kokot, N. Osterman, A. Snezhko, A. Vilfan, D. Babic, J. Dobnikar, Dynamic Assembly of Magnetic Colloidal Vortices. *Langmuir* **32**, 5094 (2016).
9. J. Loeber, F. Ziebert, I. Aranson, Macroscopic Model of Substrate-Based Cell Motility, PHYSICAL MODELS OF CELL MOTILITY. Book Series edited by I.S. Aranson, pages: 1-67 (2016).
10. Y.-L. Wang, Z. Xiao, A. Snezhko, J. Xu, L. E. Ocola, R. Divan, J. E. Pearson, G. W. Crabtree, W.-K. Kwok, Rewritable artificial magnetic charge ice, *Science* **352**, 962 (2016).
11. M. Smylie, M. Leroux, V. Mishra, L. Fang, K. Taddei, O. Chmaissem, H. Claus, A Kayani, A. Snezhko, U. Welp, W. K. Kwok, Effect of proton irradiation on superconductivity in optimally doped  $\text{BaFe}_2(\text{As}_{1-x}\text{P}_x)_2$  single crystals, *Physical Review B* **93**, 115119 (2016)
12. F. Ziebert, I. Aranson, Nonlinear Models in Molecular and Cell Biology: Editorial, *Physica D-Nonlinear Phenomena* **318**, 1-2 (2016).
13. M. Smylie, H. Claus, U. Welp, W.-K. Kwok, Y. Qiu, Y. S. Hor, and A. Snezhko, Evidence of nodes in the order parameter of the superconducting doped topological insulator  $\text{NbxBi}_2\text{Se}_3$  via penetration depth measurements, *Physical Review B* **94**, 180510(R) (2016).
14. R. Zhang, T. Roberts, I. Aranson, J. de Pablo, Lattice Boltzmann simulation of asymmetric flow in nematic liquid crystals with finite anchoring, *Journal of Chemical Physics* **144**, 084905 (2016).
15. I. Aranson, Microrobotics: Swimmers by design, *Nature* **531**, 312-313 (2016).

***UNIVERSITY GRANT  
PROJECTS***



## Bioinspired Hierarchical Design of Chiral Mesoscale Liquid Crystalline Assemblies

Nicholas L. Abbott, University of Wisconsin-Madison (Principal Investigator) and Juan J. de Pablo, University of Chicago (Co-Investigator)

### Program Scope

Biology uses elastic stresses, defects, chirality and hierarchical design strategies to create a range of functional materials. This hierarchical organization serves as an amplifier that allows highly localized, molecular events to propagate into the mesoscale, resulting in dynamic functional properties of biological systems that have not yet been fully realized in synthetic material designs. We are pursuing a program of research in which we seek to recreate such principles using synthetic liquid crystals (LC) as a versatile platform. We are elucidating new hierarchical design strategies that heavily leverage chirality and topological defects to realize equilibrium and non-equilibrium, dynamic mesoscale phenomena in the context of nano- and micrometer-sized LC droplets containing nanoparticles. Specifically, we are unmasking how equilibrium and dynamical phenomena emerge from hierarchical organizations in responsive, chiral liquid crystalline assemblies. Overall, this research is advancing new hierarchical designs of meso-scale materials in which biomimetic principles, including the propagation of events or information over multiple temporal and spatial scales, are enacted in a facile manner.

### Recent Progress

We have focused on elucidation of the structure of confined, chiral LC systems, including cholesteric and Blue Phase (BP) liquid crystalline droplets, with particular effort devoted to understanding their topological defects. We have also emphasized elucidation of the role that defects in LCs play in the “positioning” of nanoparticles.

### Internal Structure of Chiral Nematic Droplets

A first set of accomplishments revolve around elucidation of the configurations of confined, cholesteric (Ch) LC phases. The Ch LC phase is the simplest of the chiral nematic phases; the LC

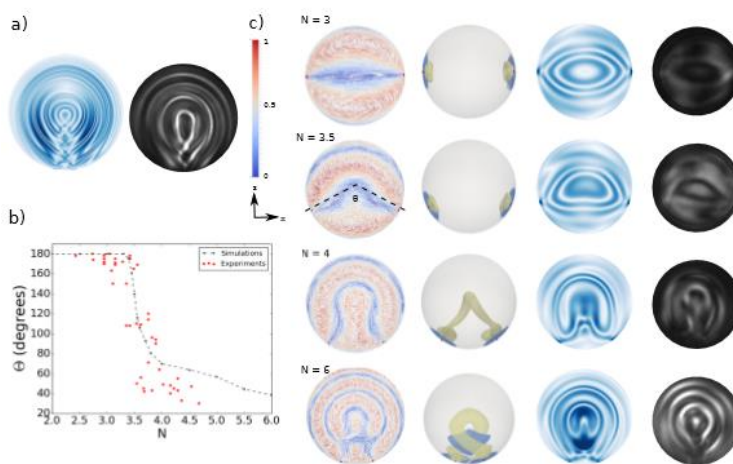


**Figure 1.** a) Simulated polarization micrograph and experimental image for RSS droplet ( $N = 10$ ). b) Dependence of  $\theta$  on  $N$ . c) The four rows show results corresponding to  $N = 3, 3.5, 4$  and  $6$ , respectively. Column 1: director fields of Ch LC droplets for various values of  $N$ . Point defects are shown in red (isosurface for  $S = 0.5$ ). The director field is colored according to its projection onto the  $y$ -axis. In the image corresponding to  $N = 3.5$ , the dashed lines connect two surface point defects with the center of the droplet. The angle between these two dashed lines is defined as  $\theta$ . Column 2: splay-bend isosurfaces of Ch LC droplets. The splay elastic distortion is shown in black (blue online) ( $S_{SB} > 0.0014$ ) and the bend elastic distortion is shown in grey (yellow online) ( $S_{SB} < -0.0014$ ). Column 3: simulated polarization images obtained for incident light along the  $y$ -axis. Column 4: experimental images for droplets of different chirality.

director exhibits a twist along an axis that is orthogonal to the director. While the bulk properties of cholesteric LC (ChLC) phases are well-understood, their structures when confined within micrometer-sized LC droplets are not. Our experimental observations have revealed that cholesteric LC droplets exhibit three dominant configurations, namely a Radial Spherical Structure (RSS), a Diametrical Spherical Structure (DSS), and a Twisted Bipolar Structure (TBS). These structures differ from each other by the symmetry and morphology of the defects. One of our goals has been to understand the pathway leading to the transition from the TBS to RSS configuration (via an increase in  $N$ ). As shown in Figure 1, with increasing chirality, we found a continuous pathway to connect the TBS and RSS configurations. Specifically, by using simulations (Figure 1c, three left columns), an increasingly bent structure was predicted. Remarkably, when performing experiments (Figure 1c, right column), an almost identical series of transition states were identified. As part of this thrust in the project, we also examined the effects of the anchoring strength on the configurations of the Ch LC droplets. For weak anchoring conditions, Ch LC droplets were found to adopt morphologies similar to those of the equilibrium helical phase observed in the bulk. As the anchoring strength increased, a planar bipolar structure was observed, followed by a morphological transition to the bent structure. Overall, the response of the Ch LC to chirality and surface interactions identified here suggests the existence of a wide range of dynamic templates for directing the organization of nanoparticles (as described below).

### Internal Structure of Confined Blue Phase Liquid Crystal Droplets

A second focus of our research has been directed to nematic phases that contain high concentrations of chiral dopants (so-called Blue Phase (BP) LCs). At high loadings of chiral dopants, well-defined three dimensional networks of double twisted cylinders form (Figure 2). Between the double twisted cylinders, periodic arrays of defects appear. These periodic arrays of defects underlie many properties of BPs, including their optical appearance due to Bragg diffraction. We have conducted a synergistic experimental and computational study of the structure of BPs confined to spherical droplets and thin films. As part of these studies, we investigated the morphology of the BP domain structure within droplets.<sup>3</sup> This series of

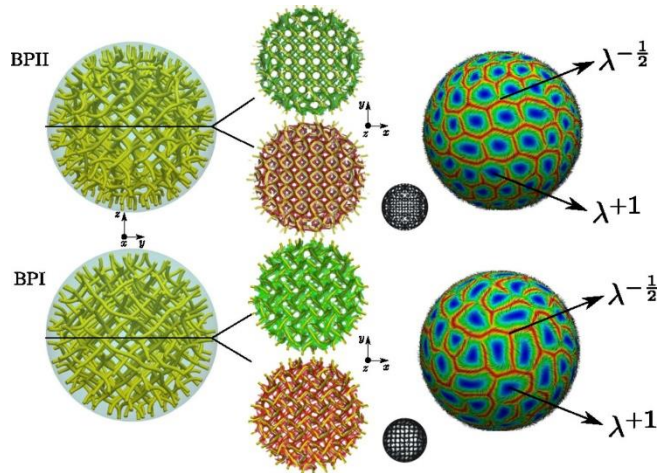


**Figure 2.** Metastable BPII (upper) and BPI (lower) for  $N=10$ . (Left) Nematic order parameter isosurfaces of  $S=0.35$ . (Center) Transverse section showing the splay-bend red ( $SSB=-0.008$ ) and green ( $SSB=0.008$ ) isosurfaces. The disclination lines are bent in the proximity of the droplet interface, where the corresponding cross-polarizer images become dark or diffusive. In the central region, however, the structure is well defined. (Right) Director field in the vicinity of the droplet's surface; the field is characterized by positive and negative lambda defects. The colors correspond to director's orientation: blue when the director has radial direction and red when it is parallel to the surface.

experiments was motivated, in part, by the goal of forming BP *monodomains* within droplets in order to study the effects of confinement on the periodic structure of the BP lattice. In addition to validating the interpretation of our experiments, our computer simulations have revealed insights that are not accessible via experiment. Specifically, our recent computer simulations have revealed a unique feature of BP droplets, namely the way in which the so-called lambda defect cores are distributed across the surface of the droplets. For BPII droplets, either positive or negative defects form a hexagonal array, each having different “lattice” parameters. In contrast, in the case of BPI, the defects do not exhibit a regular structure (Fig. 2). The organization of these defects at surfaces raises intriguing possibilities for controlled localization of nanoparticles. For example, nanoparticles at the interface of BPII droplets could potentially assemble in different arrays, mediated by the positive and negative defects on the BPII droplet and the type of anchoring, homeotropic or planar, of the nanoparticles.

### Hierarchical Positioning of Colloidal Particles using Chiral Liquid Crystal Droplets

A long-term goal of our project is to use the complex LC configurations described above to hierarchically organized nanoparticle systems (using the LC droplets as dynamic templates). Consistent with this goal, over the past year, we have studied the dynamical organization of nanoparticles at the interfaces of Ch LC droplets. For these initial studies, we used Ch LC droplets with TBS and RSS configurations for two reasons. First, they are the two most commonly observed configurations at low ( $N$  less than 4) and high ( $N$  higher than 4) chiralities. Second, the two configurations are clearly distinct in terms of the organization of the LC, and thus we predicted that they would lead to distinct effects on the positioning of colloids. Figure 3 shows the positioning of colloidal particles by the TBS Ch LC configuration. Figure 3A-C show nanoparticles localized at three positions on the Ch droplet;  $\phi = 0^\circ$  (on the defect),  $\phi = 35^\circ$ , and  $\phi = 90^\circ$  (at the equator). To investigate the frequency with which the various positions of the colloids were observed, we measured the probability of a nanoparticle being localized at an angle  $\phi$  with respect to the surface defect. These measurement revealed that 52% of the nanoparticles localized at the defects ( $\phi=0^\circ$ ) and 19% localized at  $\phi=90^\circ$ , as shown in Fig. 3d. From this probability distribution, we calculated the potential of mean force for a nanoparticle at  $\phi=90^\circ$  to be  $-3 k_B T$  (Fig. 3e). Significantly, our simulations also predicted a free energy minimum of comparable depth at

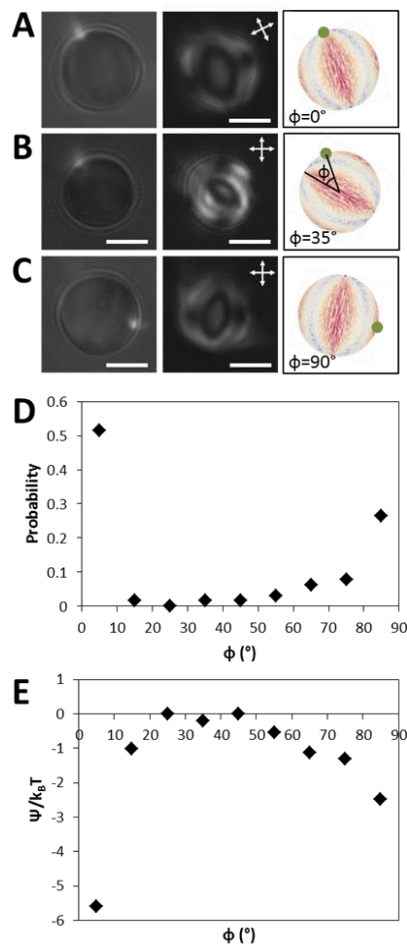


**Figure 3.** Nanoparticle positioning on TBS droplets. Bright field and fluorescence, polarized light micrographs, and corresponding sketches showing polystyrene (PS) colloid localized (A) at one of the surface defects, (B) at an angle with respect to surface defect, (C) at the equator. (D) Angle-dependent probability distribution of PS-colloid localizations on droplets. Probability distribution obtained from 64 droplets. (E) Potential of mean force for the colloids adsorbed on TBS droplets. Scale bars: 5  $\mu\text{m}$ .

the equator, thus providing further support for our experimental conclusions. In addition, we characterized the positions of nanoparticles adsorbed at RSS droplets, revealing that RSS droplets present unusual opportunities for controlling the spacing between pairs of particles (e.g., for controlled energy transfer).

Overall, the results above demonstrate important progress. Specifically, we have characterized the internal structures of micrometer-sized droplets comprised of chiral nematic phases and BP LCs by both experiments and simulations. These are remarkably rich in terms of the range of morphologies and defects that can form within the LC droplets. We have also demonstrated the positioning of colloidal particles at chiral LC interfaces. Such findings are particularly promising in the context of the broader goals of our DOE project, as defects play a central role in mediating the interactions of LCs and nanoparticles. Thus our results support the key concept that chiral LC droplets represent a promising class of templates for directing the organization of nanoparticles.

## Future Plans

Building from the accomplishments described above, and inspired by living systems, in ongoing research, we are exploring the equilibrium and non-equilibrium designs of complex multi-compartment emulsions based on the use of immiscible *structured* oils – oils that have nematic and smectic structures of the type found in biological membranes – to show that these designs can lead to hierarchical organization and function closer to the sophistication of living systems. The scope of these studies includes perfluorocarbon oils that are immiscible with liquid crystals (LCs), and extends into molecular systems that possess chirality, thereby providing access to a class of emulsions that are not accessible with isotropic oils. We are also exploring also how the internal organization of these complex multi-compartment emulsions influences “swimming behaviors” that result from dissipative processes.

## Publications

Wang, X; Zhou, Y; Kim, Y-K; Miller, DS; Zhang, R; Martinez-Gonzalez, JA; Bukusoglu, E; Zhang, B; Brown, TM; de Pablo, JJ; Abbott, NL; Patterned Surface Anchoring of Nematic Droplets at Miscible Liquid—Liquid Interfaces, *Soft Matter*, **2017**, in press.

Bukusoglu, E., Wang, X., Martinez-Gonzalez, J.A., de Pablo, J.J., Abbott, N.L., Strain-Induced Alignment and Phase Behavior of Blue Phase Liquid Crystals in Thin Films, to be submitted to *Soft Matter* prior to September 1, 2017.

Zhou, Y; Bukusoglu, E; Martinez-Gonzalez, JA; Rahimi, M; Roberts, TF; Zhang, R; Wang, XG; Abbott, NL de Pablo, JJ, Structural Transitions in Cholesteric Liquid Crystal Droplets, *ACS NANO*, 10 (7), **2016**, 6484-6490.

Bukusoglu, E; Wang, XG; Zhou, Y; Martinez-Gonzalez, JA; Rahimi, M; Wang, Q; de Pablo, JJ; Abbott, NL., Positioning colloids at the surfaces of cholesteric liquid crystal droplets. *Soft Matter*, 12(42), **2016**, 8781-8789.

Armas-Perez, J.; Londono-Hurtado, A.; Guzman, O.; Hernandez-Ortiz, J.; de Pablo, J. J.,

Theoretically informed Monte Carlo simulation of liquid crystals by sampling of alignment-tensor fields. *J. Chem. Phys.* **2015**, *143*, 0044107.

Martinez-Gonzalez, J. A.; Zhou, Y.; Rahimi, M.; Bukusoglu, E.; Abbott, N. L.; de Pablo, J. J., Blue-phase liquid crystal droplets. *Proc. Nat. Acad. Sci. USA* **2015**, *112*, 13195-13200.

Bukusoglu, E.; Wang, X.; Martinez-Gonzalez, J. A.; de Pablo, J. J.; Abbott, N. L., Stimuli-responsive cubosomes formed from blue phase liquid crystals. *Adv. Mater.* **2015**, *27*, 6892-6898.

Rahimi, M.; Roberts, T. F.; Armas-Pérez, J. C.; Wang, X.; Bukusoglu, E.; Abbott, N. L.; de Pablo, J. J., Nanoparticle Self-assembly at the Interface of Liquid Crystal Droplets *Proc. Nat. Acad. Sci. USA* **2015**, *112*, 5297-5302

Londono-Hurtado, A; Armas-Perez, JC; Hernandez-Ortiz, JP; de Pablo, JJ, “Homeotropic Nanoparticle Assembly on Degenerate Planar Nematic Interfaces: Films and Droplets”, *Soft Matter*, **2015**, *11*(25), 5067-5076.

## **Energy Transductions in Multimodal Stimuli-Responsive Reconfigurable Systems with Information Encoding Capabilities**

**PI: Joanna Aizenberg, Wyss Institute for Biologically Inspired Engineering at Harvard University, Cambridge, MA 02138**

**Co-PI: Anna C. Balazs, University of Pittsburgh, Pittsburgh, PA 15261**

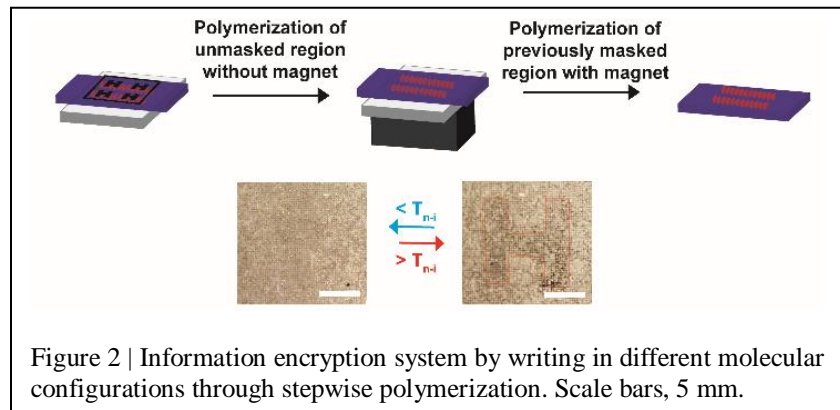
### **Program Scope**

We have proposed to create responsive and dynamically adaptive artificial systems that utilize chemo-mechanical energy transduction to “recognize”, “store”, and “communicate” information about the local environment. These capabilities are enabled through our use of arrays of stimuli-responsive, high-aspect-ratio microstructures. These microstructures form the core of integrated, complex systems that can sense changes in the local environment and respond by reversibly expanding, contracting, bending and tilting, and thus, exhibiting detectable outputs that can be readily read out. The central feature of the proposed systems is their capacity to “encode” and store information about the first stimulus and, through a cascade of energy transductions, to respond in more than an “on-off” mode to complex, non-equilibrium downstream stimuli. Primary stimuli of a chemical or physical nature allow one to access different types of information encoding and energy transduction in our hybrid systems, while the nature, magnitude, directionality, and onset rates of downstream stimuli produce differentially patterned, clearly distinguishable responses.

The active elements of the proposed designs are either stimuli-responsive hydrogels or liquid crystalline elastomers. These two systems can encode, in a precise spatiotemporal fashion, environmental stimuli such as pH, temperature, electromagnetic field, light and others. The modularity of the proposed designs is expected to produce types of energy transductions that have not been available in previous “on-off” systems that relied on the equilibration with the environment in their action. We expect the generated knowledge about the parameter space in these novel systems to be useful in other bioinspired biomolecular systems, including those with built-in self-regulating and autonomic capabilities. We also anticipate that these bioinspired chemo-mechanical systems, in addition to being extremely interesting from the fundamental science perspective, might prove useful in designing next-generation sensors, actuators, optical elements, and highly efficient information storage devices.

In the first phase of the project, we chose liquid crystalline elastomer (LCE) to demonstrate proof-of-concept energy transductions and information encoding capabilities. The anisotropic mechanical responses of LCE with respect to the external field-controlled LC direction form the basis of designing active microstructures. As shown in Fig. 1b, in nematic phase, the interaction among LC functional groups stretches the polymer chains along the direction of the LCs (so-called director), whereas this strain can be released upon heating the system until the transition into isotropic phase (temperature above  $T_{n-i}$ ). As a result, a unidirectional contraction of the elastomer along the director can be achieved. When cooling the system back until the transition into nematic phase takes place (temperature below  $T_{n-i}$ ), the LC constraints recover and the elastomer deforms back to its original size. Thus, the anisotropic nature of LCE transmits the molecular configurations controlled by external fields (e.g. electric or magnetic field) into microscopic deformation behaviors.

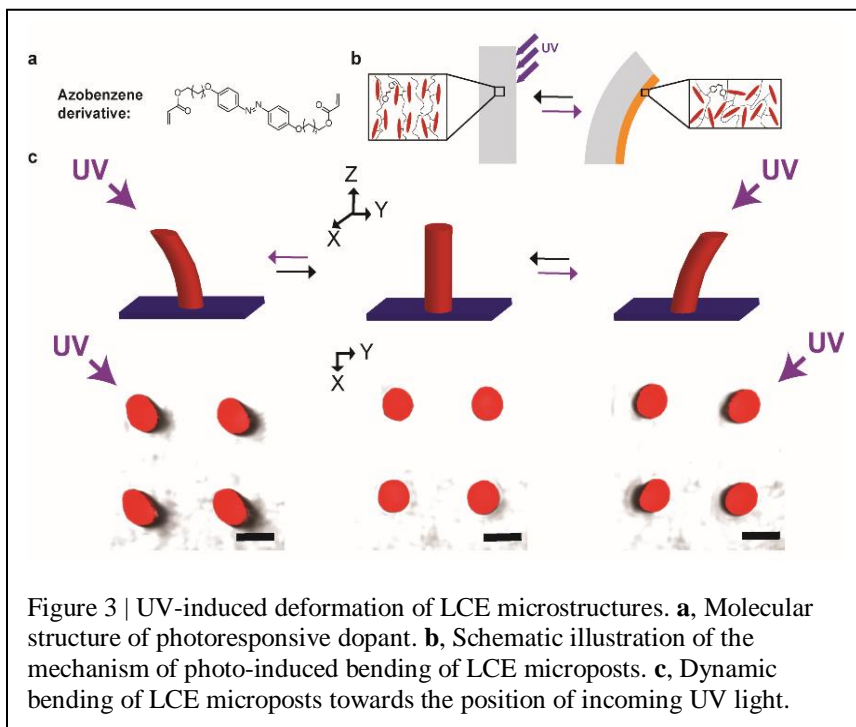




Next, we developed the synthesis of a microstructure array to show the information encryption at a larger scale. Different molecular and structural configurations were encoded in separate regions controlled by photomask during polymerization. Once heated to isotropic phase, the array showed an ‘H’ pattern, due to distinct deformations

in these regions (Fig. 2). The pattern faded away when the system cooled back to nematic phase. This observation leads us to conclude that information can be designed and encrypted in the microstructures via step-wise polymerization, and be sequentially decrypted as a consequence of their thermo-mechanical responsiveness.

In addition to temperature, we incorporated light-responsiveness to the LCE microstructures. By including photosensitive azobenzene-based cross-linkers (Fig. 3a), we can activate the deformation of the LCE microstructures by illumination using UV light. As represented in Fig. 3b, within the penetration depth of UV exposure into microstructure, the trans-cis azobenzene isomerization interrupts the alignment of the LC constituent, leading to a nematic-isotropic phase transition that causes a contraction of the UV-exposed surface of the microstructure.



As a result, we demonstrate in Fig. 3c that the microstructures can manipulate its response to consistently bend towards the position of the UV source, a signature of self-regulation, which senses and responds to the changing external stimulus continuously.

## Future Plans

To further support our proposed interpretation, computer simulations will be performed to deepen our understanding of the relationship between internal configuration of the

microstructure and its deformation. We will explore the parameter space of the energy-transducing transformations using computational modeling, in order to guide experimental optimizations. We also seek to develop an easier one-step method to encode hierarchical information encryption using designed magnet assembly. Besides, the possibility to use temperature and light as orthogonal stimuli to trigger the deformation will be investigated. Moreover, we will explore the application of these responsive and dynamically adaptive artificial systems other than information encryption, such as controlled adhesive systems. In addition to the LCE-based systems, the ones based on stimuli-responsive hydrogels with chemomechanical energy-transducing capabilities will be explored, with the general goal of uncovering and exploiting bioinspired non-equilibrium transformations with information-encoding capabilities.

## References

1. Ohm, C., Brehmer, M., Zentel, R., *Advanced Materials* 22, 3366-3387 (2010).
2. White, T. J., Broer, D. J., *Nature Materials* 14, 1087-1098 (2015).
3. Buguin, A., Li, M., Silberzan, P., Ladoux, B., Keller, P., *Journal of the American Chemical Society* 128, 1088-1089 (2006).
4. Ware, T. H., McConney, M. E., Wie, J. J., Tondiglia, V. P., White, T. J., *Science* 347, 982-984 (2015).
5. Palagi, S., Mark, A. G., Reigh, S. Y., Melde, K., Qiu, T., Zeng, H., Parmeggiani, C., Martella, D., Sanchez-Castillo, A., Kapernaum, N., Giesselmann, F., Wiersma, D. S., Lauga, E., Fischer, P., *Nature Materials* 15, 647-654 (2016).
6. Yu, Y., Nakano, M., Ikeda, T., *Nature* 425, 145 (2003).
7. Camacho-Lopez, M., Finkelmann, H., Palffy-Muhoray, P., Shelley, M., *Nature Materials* 3, 307-310 (2004).
8. van Oosten, C. L., Bastiaansen, C. W. M., Broer, D. J., *Nature Materials* 8, 677-682 (2009).
9. Iamsaard, S., Aßhoff, S. J., Matt, B., Kudernac, T., Cornelissen, J. J. L. M., Fletcher, S. P., Katsonis, N., *Nature Chemistry* 6, 229-235 (2014).

## Publications

1. Cui, J.X., Daniel, D., Grinthal, A., Lin, K.X. & Aizenberg, J. Dynamic polymer systems with self-regulated secretion for the control of surface properties and material healing. *Nature Materials* 14, 790-795 (2015).
2. Liu, Y.; Bhattacharya, A.; Kuksenok, O.; He, X.; Aizenberg, M.; Aizenberg, J.; Balazs, A. C. *Soft Matter* 12, 1374-1384 (2016).
3. Liu, Y.; Kuksenok, O.; He, X.; Aizenberg, M.; Aizenberg, J.; Balazs, A.C. *ACS Applied Materials & Interfaces* 8, 30475-30483 (2016).
4. Liu Y., Yong X., McFarlin I.V.G., Kuksenok O., Aizenberg J., Balazs A.C. Designing a gel-fiber composite to extract nanoparticles from solution. *Soft Matter* 11, 8692-8700 (2015).
5. Shastri, A.; McGregor, L. M.; Liu, Y.; Harris, V.; Nan, H.; Mujica, M.; Vasquez, Y.; Bhattacharya, A.; Ma, Y.; Aizenberg, M.; Kuksenok, O.; Balazs, A. C.; Aizenberg, J.; He, X. *Nature Chemistry* 7, 447-454 (2015).
6. Sutton A., Shirman T., Timonen J.V.I., England G.T., Kim P., Kolle M., Ferrante T., Zarzar L.D., Strong E., Aizenberg J. Photothermally triggered actuation of hybrid materials as a new platform for in vitro cell manipulation. *Nature Communications* 8, 14700 (2017).

## Biomimetic Templated Self-Assembly of Light Harvesting Nanostructures

PI: Alfredo Alexander-Katz, Massachusetts Institute of Technology

**Program Scope:** Nature has utilized multiple routes to assemble nanostructured materials with different functions for multiple purposes. In this project we are interested in studying the self-assembly of supramolecular antenna-like structures with very specific features using block copolymers as templates. This system mimics naturally-occurring ultra-efficient light harvesting antennas found in Green Sulfur Bacteria, so-called Chlorosomes. The complex organization of these antennas, which are composed of small organic chromophores (BacterioChlorophyll C in this case) is dictated by the shape of the mesostructure as well as the internal interactions between the chromophores themselves and the polymer-chromophore interactions. With this in mind, the overall aim of this project is to find which are the design rules using simulations and experimental validation of such systems for creating tailored assemblies. A desired outcome would be to use single

molecules that have already been shown to be functional and incorporate them to block copolymers to obtain the desired enhanced functionality.

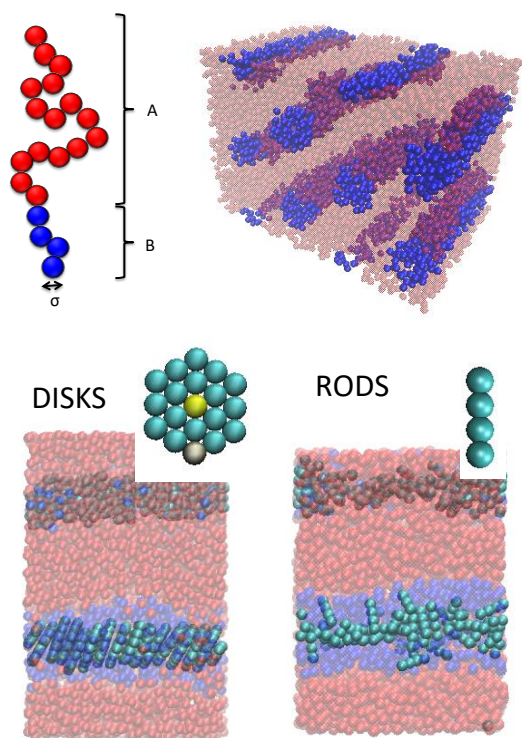


**Figure 1 . Block copolymer self-assembly with disks and rods.** In the upper row we show how a diblock copolymer composed of two distinct chemical groups self-assembles into an ordered meso structure. In this case the volume fraction of B is 0.25 and this yields a cylindrical phase. In the lower row, we show two different systems that can be blended with the aforementioned block copolymer system: rods and disks. As can be seen, disks assemble into an ordered columnar pack while rods do not exhibit a preferred orientation.

**Recent progress:** We have made substantial progress towards the goal of assembling biomimetic antennas in block copolymer matrices. In particular we have developed moved forward in several areas: i) we have developed a particle-based approach for sampling rapidly the conformations of this system using enhanced MC techniques, ii) explored the phase diagram for disks and rods in block copolymer confinement and mapped out the polymer mediated interactions between disks, iii) developed the methods experimentally to probe our simulation findings, and iv) developed ultra efficient Lattice Boltzmann (LB) code originally developed for field-based simulations, and this

code has been very useful for other out-of-equilibrium systems.

More in detail, we have studied the self-assembly of disks and rods in confined geometries composed of cylindrical block copolymers (see Fig. 1). Both of these geometries correspond to different levels of coarse-grained systems. In particular we envision that small chromophoric disk-like molecules as porphyrin will assemble into rods under the right conditions. Such structures have already been reported in the literature and we have already observed their appearance at low pHs in our own studies. In the case that we have disks we find enhance ordering due elastic deformation of the block copolymer domains, and as the concentration increases depletion interactions lead to highly ordered domains of disks. These findings have been recently published in ref. On the other hand, in the case of rods we find a rather counterintuitive phenomenon: the BCP confinement prevents the isotropic to nematic transition at the expected volume fractions. This is due to a subtle interplay of entropies. In particular, the entropy lost by the BCP chains is larger than the entropy gain due to the alignment of the rods. This effectively yields isotropic phases of rods in confined BCP cylinders (see Fig. 2). In a “hard” corresponding confinement, the system does go into a nematic phase, which implies that the chains themselves have an important contribution in the ordering of this system. While we are still speculating about the implications of such a change, one can envision a different mechanism of energy transport depending on the organization of the chromophores inside the BCP domain.

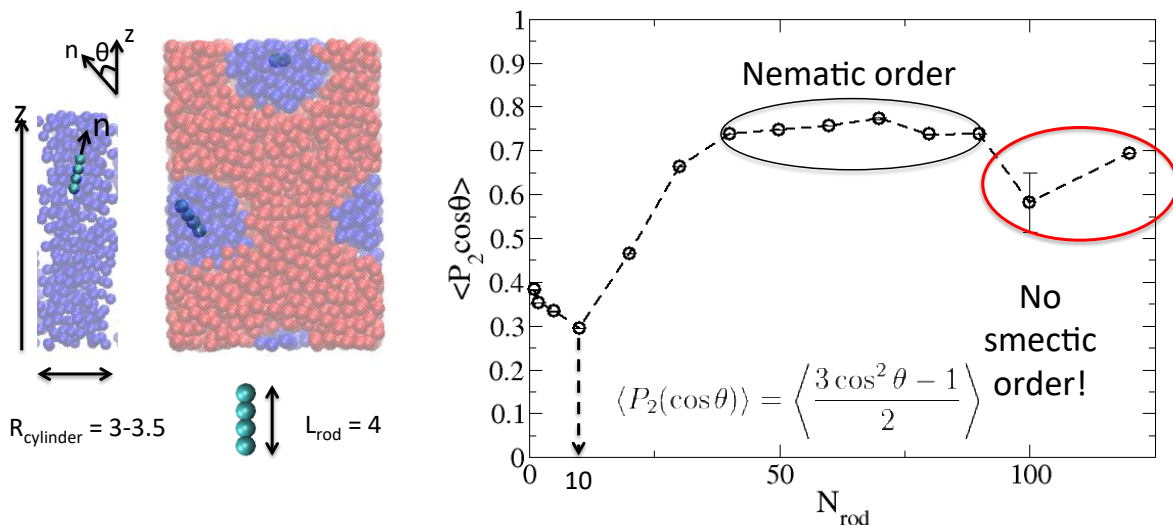


**Figure 2. Self-assembly of rods in BCP confinement.** ( Left) Snapshot of the cylindrical phase containing a rod 4 units long. The angle theta indicates how aligned the rod is with respect to the axis of the cylinder. (Righth) The order parameter for a liquid crystal composed of rods. As can be seen in this plot, increasing the density of rods in the lower density regime reduces the level of alignment. Note that the system never reaches the smectic phase.

To validate our simulation results we have constructed a porphyrin system in the lab. Porphyrins are disk-like molecules and constitute the functional part of chlorophyll. We are using TTPS4 which is the free base form of porphyrin and contains four sulfonate groups to make it soluble. This molecule in acidic conditions forms rod-like aggregates and we want to probe if these aggregate order in the BCP matrix or not. To do this we have

infiltrated PS-P4VP cylindrical BCP systems with a solution containing Porphyrin under different conditions. The first unexpected result is that porphyrin is able to infuse the PVP block rather simply, and we do not need to use strong acids for this to happen. Nevertheless, we probed the system under more or less acidic conditions. We also washed extensively the system to discard any porphyrins that might be left over. We measure reflectance spectrum of the different systems prepared on a silicon wafer. Our preliminary results do in fact agree with the notion that J-aggregates of porphyrin are not preferred inside the BCP domains. This can be seen in the absorption spectrum shown in Fig. 3 where the peak around 700nm has disappeared in the case of porphyrin-bcp mixture in acid. As mentioned above we need to reproduce these results several times, but they clearly demonstrate that confining molecules in BCP environments is more than just confining the system into a cylinder or a box.

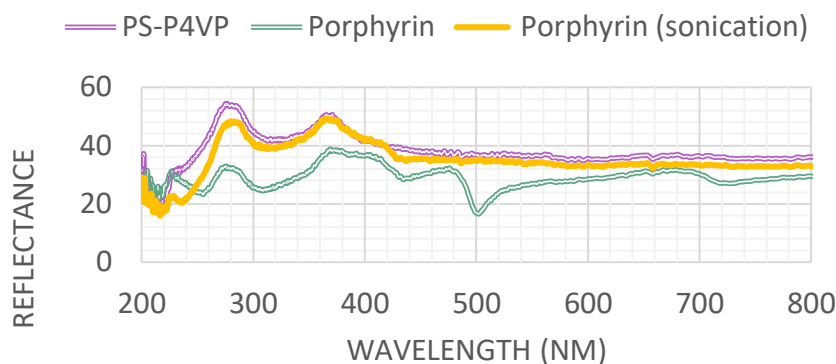


**Figure 3.** UV-Vis reflectance spectrum for PS-b-P4VP, PS-b-P4VP/TPPS before washing and PS-b-P4VP after washing.

In addition to the BCP-porphyrin nanocomposite, we were also interested in looking into other compounds that look like the porphyrin molecule, but could have other functionalities. To this end we were able to put different types of inorganic materials by using the ethylenediaminetetraacetic (EDTA) coordination compounds as precursors. The EDTA salts with negative charge were attracted to the positively charged P4VP block, similar to the transport pathway of TPPS molecules. After etching with oxygen plasma for 5 minutes, the EDTA salts turned to metal (for noble metals) or metal oxide (for other transition metals). Figure 5 demonstrates selected examples of metal and metal oxide mesh structure by inheriting the patterns formed by the P4VP block. This could open interesting possibilities to create nanostructures composites, similar to the ones that biological systems produce, yet with more functional roles. We are currently experimenting with oxides, rare earth oxides, and some noble metals like Pt for catalysis.

As an interesting spin-off project, we have used our optimized Lattice Boltzmann code (originally developed for performing field theoretic simulations of particles in block copolymers) to study active colloids in liquids. We have also performed validating experiments on this system. Our results in this area have demonstrated the emergence of very long-range interaction in such systems that is dependent on the elasticity of the system.

**Future plans:** In the next year we plan to start wrapping up all the leads from this project. We plan to submit several manuscripts on different aspects of the project such as the phase behavior of rods in BCP matrices. We are starting to incorporate “chemistry” into the models, but we are hoping to get a better sense of what are the important interactions from experiment. On the experimental side, we have developed a new route to form confined matrices of porphyrins and will continue exploring this area to understand if we can actually create aggregates inside. So far we only see the signal from single porphyrins. As shown above, we have been successful at inserting other functional compounds and we will pursue this avenue further.

**Publications from this award:**

- 1.- **Artificial tribotactic microscopic walkers: walking based on friction gradients**, J. Steimel, J. L. Aragonés and A. Alexander-Katz, *Phys. Rev. Lett.* **113**, 178101 (2014).  
*(Highlighted also in Physics from the American Physical Society)*
- 2.-**Emergent ultra-long-range interactions between active particles in hybrid active-inactive systems**, J. Steimel, J. L. Aragonés, Helen Hu, Naser Qureshi, and A. Alexander-Katz, *PNAS*. **Vol. 113 (17)** 4652-4657 (2016).
- 3.- **Elasticity-induced force reversal between active spinning particles in dense media**, J. L. Aragonés, J. Steimel, and A. Alexander-Katz, *Nature Commun.* **7:11325** (2016).
- 4.- **Block copolymer templated self-assembly of disk-shaped molecules** J. L. Aragonés, and A. Alexander-Katz, *J. Chem. Phys.* *in press*
- 5.- **Aggregation Dynamics of Active Rotating Particles in Dense Passive Media**, J. Steimel, J. L. Aragonés and A. Alexander-Katz, *under revision*.
- 6.- **Anisotropic nanoparticle distribution in block copolymer model defects**, YongJoo Kim and Alfredo Alexander-Katz, *in revision*.

## **Design and Synthesis of Structurally Tailored and Engineered Macromolecular (STEM) Gels**

**PI: Anna C. Balazs (Univ. of Pittsburgh); Co-PI: Krzysztof Matyjaszewski (Carnegie Mellon University)**

### **Program Scope**

Polymer gels are comprised of crosslinked polymer networks with interstitial space filled by a solvating fluid (water for hydrogels), which can account for 90 % or more of the material's volume. As such, they are often referred to as “soft and wet” materials. Polymer gels can behave as stimuli-responsive materials, capable of responding to temperature, pH, ionic strength, electric fields, and light. Owing to this exceptional versatility, polymer gels are used in a wide range of applications such as drug delivery/release agents, biomimetic materials and tissue engineering scaffolds, protective coating, and actuators. We have been investigating the synthesis and application of covalently crosslinked polymer gels prepared using atom transfer radical polymerizations (ATRP).<sup>1</sup> ATRP offers an effective means to synthesize well-controlled polymeric materials with narrow molecular weight distributions, composition, chain-end functionalities, and macromolecular architectures. Our primary goal has been to take full advantage of controlled/living polymerization techniques to develop a new platform of “living” hierarchical polymer materials with broadly tunable chemical composition, structure, and function. We addressed this challenge by designing and creating Structurally Tailored and Engineered Macromolecular (STEM) gels.

### **Recent Progress**

Through a combination of modeling and experiments, we devised effective routes to form “stackable gels.”<sup>2,3</sup> In this process, a solution of ATRP initiator, monomer, and cross-linkers was introduced on top of a first gel, and these new components then underwent polymerization to form the subsequent layer. This process was simulated using dissipative particle dynamics (DPD). The simulations indicated that the covalent bond formation between the different layers is primarily due to reactive chain-ends. In the complementary experiments, multilayered gels were synthesized using either free radical polymerization (FRP) or ATRP. It was observed that chemically identical materials preserved their structural integrity independent of the polymerization method.

This approach was extended to two gels synthesized separately in two incompatible solvents. The integrity of these materials, however, was poor. This issue was addressed by using poly (n-butyl acrylate)-co-poly((oligo (ethylene glycol) methacrylate) miktoarm star polymers

(MSPs) as molecular/mechanical linkers. **Figure 1** illustrates the results of our collaborative studies on using the MSPs as effective “gluing” agents.

In the next collaborative studies, the combination of FRP and controlled/living ATRP as a route to forming robust “stackable” amphiphilic gels without interfacial agents was examined (**Figure 2**).<sup>3</sup> In the DPD simulations and experiments, the bottom layer of the gel is created first and then a solution of new initiators, monomers and cross-linkers is introduced on top of this first layer. In the simulations, all possible combinations using FRP and ATRP gels were investigated and experiments were performed to capture the macroscopic performance of the stackable amphiphilic gels. The combination of FRP and ATRP yielded single-piece, connected, amphiphilic gels regardless of the order of polymerization and the FRP layer was found to be an effective as a gluing agent for the ATRP layers.

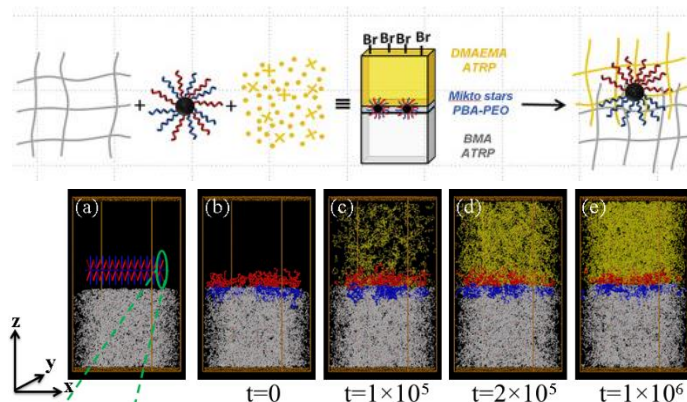


**Fig.1. Top:** Schematic of our process for binding two immiscible gels with MSPs. **Bottom:** Simulation output: (a) Initial configuration of MSPs at top of first gel layer. (b) Equilibrium configuration of MSP at the interface. (c-e) Time evolution of second gel layer in the presence of MSPs.<sup>2</sup>

Moreover, to elucidate gelation by ATRP, Monte Carlo simulations were employed. The effect of intramolecular crosslinking (IC) (cyclization) the gel point for various reagent ratios and dilutions was investigated. It was shown that intramolecular crosslinking did not significantly change the gel point in condensed systems (no solvent or below 10%), but that it significantly increased gel points in diluted systems (40–90% of the solvent).

Notably a new class of nanocomposites was modeled. The fundamental unit in these materials is a polymer grafted nanoparticle (PGN), which encompasses a rigid core and a corona of end-grafted polymers (**Figure 3**).<sup>4</sup> The focus was a concentrated solution of these PGNs. The solution is assumed to be a good solvent for the grafted chains, which are in the semi-dilute regime. Through these studies, the critical parameters (i.e. labile bond energy, fraction of permanent bonds, and strain recovery) that control the mechanical response of rejuvenation of dual cross-linked PGN networks were determined.

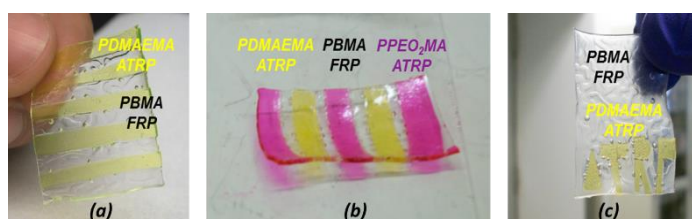


**Fig.2. (a):** Ten-layer gel prepared by connecting ATRP gel using an FRP gel. **(b):** Multi-layer gels obtained by connecting slices different ATRP gels (yellow and purple) with FRP “glue.” **(c):** “ATRP” embedded letter made of an ATRP gel and surrounding matrix made by FRP.<sup>3</sup>

In addition, ATRP gels were used to create novel “living” materials. Well-defined “mother networks” of 2-(2-methoxyethoxy)ethyl methacrylate (poly(MEO<sub>2</sub>MA)) were prepared and subsequently modified using the grafting-from polymerization method to produce “daughter networks” of poly(MEO<sub>2</sub>MA) of various architectures form thermo-responsive hydrogels. It was shown that the  $\alpha$  process assigned to the segmental motions of poly(MEO<sub>2</sub>MA) was independent of the polymer topology and the glass transition temperature,  $T_g$ . In this work, the potential of post-synthesis modifications to introduce new properties into the network was demonstrated.

Other activities included the synthesis of poly(ionic liquid)s (PILs) with low glass transition temperature prepared from a new quaternary ammonium cationic monomer, N-(4-vinylbenzyl)-tris[2-(2-methoxyethoxy) ethyl]ammonium bis(trifluoromethylsulfonyl)imide (VBTA+Tf<sub>2</sub>N). The result was low- $T_g$  PILs that could act as a macromolecular “solvent” to dissolve various polymer systems, separate substances, and serve as a reaction medium for novel synthesis and catalysis. More recently, the surface morphology and organization of PILs, poly[1-(4-vinylbenzyl)-3-butylimidazolium bis(trifluoromethylsulfonyl)imide] have been explored in conjunction with their molecular architecture, adsorption conditions, and post-assembly treatments. It was demonstrated that interplay of capillary forces, macromolecular mobility, and structural relaxation of the polymer chains influenced the dewetting mechanisms in PIL multilayers.

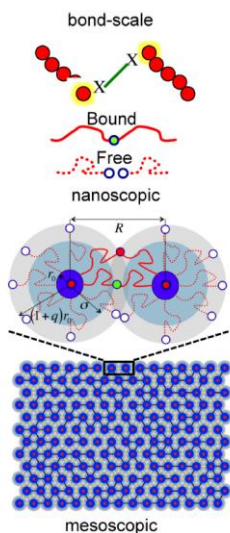


**Fig.3.** Components in our multi-scale model of PGN networks.<sup>4</sup>

As another route to forming STEM gels, polymer networks with three-dimensionally ordered macroporous (3DOM) structures were prepared by colloidal crystal templating. They displayed highly reversible shape memory properties, as confirmed by indirect electron microscopy imaging and direct nanoscale resolution X-ray microscopy imaging of the hydrated gels. Versatile strategies were also developed to further modify the 3DOM gels with organic moieties, polymers, bio(macro)molecules, and inorganic particles to generate materials with new properties (e.g., hydrophobicity, fluorescence, conductivity, and stimuli-responsivity) into the structured gels. Novel composites for (bio)catalysis and separation applications were produced. Modifications of functional groups in the 3DOM gels result in various materials with programmed properties.

The most recent iteration of STEM gels was comprised of a network with latent initiating sites that allow for post-synthesis, spatially-specific modification of the matrix (**Figure 4**).<sup>5</sup> The photo-active STEM gels by FRP of different meth(acrylate) monomers, a crosslinker, and a photo-active dormant initiator (inimer) based on the radical photo-initiator 2-hydroxy-4'-(2-hydroxyethoxy)-2-methylpropiophenone (Irgacure 2959). Infiltration a secondary component was followed by UV-triggered FRP of secondary polymeric chains. Spatial control of Young’s Modulus was realized using photolithography through gradient masks, and single-piece materials combining a range of mechanical properties were obtained.

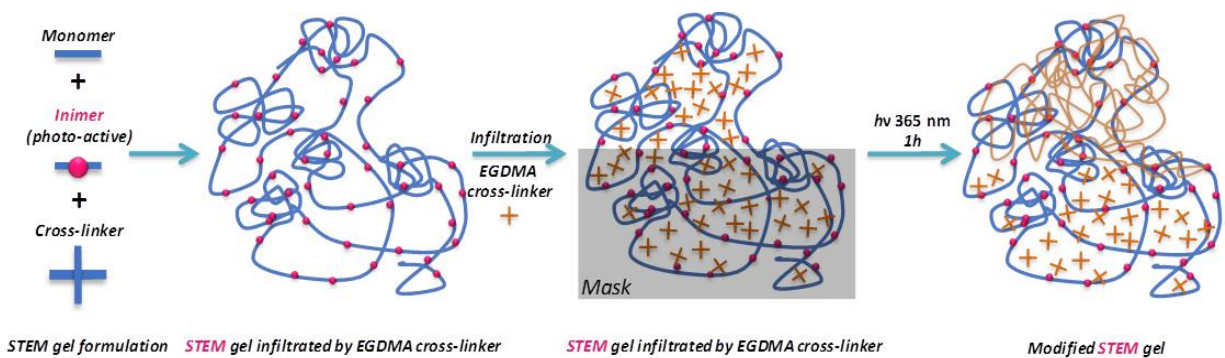


**Fig.4.** Key steps in the formation of the STEM gel network. Assembly of the primary network by FRP (**left**). Infiltration with a secondary bifunctional monomer (**center**). Photo-initiated modifications (**right**).<sup>5</sup>

## Future Plans

Our goal is to design, model, and synthesize precisely tunable polymer networks, thus enabling new macroscopic functionality. We will build on previous results by aiming to develop: **(A)** the additive synthesis of STEM gels by controlled radical polymerizations; **(B)** hierarchical, self-similar STEM gel structures; **(C)** chemistries for spatially selective “imprinting” of 2- and 3-D STEM gel substructures; **(D)** subtractive methods for spatially selective local decomposition of network components for relieving local stresses; and **(E)** introduction of inorganic nanoparticles within the STEM networks. These aims will be pursued through a concerted effort of synthesis, characterization, and multiscale modeling. The unprecedented level of control of supramolecular architecture afforded by the use of spatially selective controlled polymerization will open the door to a better understand into the structure/function relationships of soft materials with a level of complexity approaching biological systems.

## References

- (1) Matyjaszewski, K., Atom Transfer Radical Polymerization (ATRP): Current Status and Future Perspectives, *Macromolecules* 2012, 45, 4015-4039.
- (2) Beziau, A.; Singh, A.; de Menezes, R. N. L.; Ding, H.; Simakova, A.; Kuksenok, O.; Balazs, A. C.; Kowalewski, T.; Matyjaszewski, K., Miktoarm star copolymers as interfacial connectors for stackable amphiphilic gels, *Polymer* 2016, 101, 406-414.
- (3) Beziau, A.; de Menezes, R.; Biswas, S.; Singh, A.; Cuthbert, J.; Balazs, A.; Kowalewski, T.; Matyjaszewski, K., Combining ATRP and FRP Gels: Soft Gluing of Polymeric Materials for the Fabrication of Stackable Gels, *Polymers* 2017, 9, 186.
- (4) Iyer, B. V. S.; Yashin, V. V.; Hamer, M. J.; Kowalewski, T.; Matyjaszewski, K.; Balazs, A. C., Ductility, toughness and strain recovery in self-healing dual cross-linked nanoparticle networks studied by computer simulations, *Progress in Polymer Science* 2015, 40, 121-137.
- (5) Beziau, A.; Fortney, A.; Fu, L.; Nishiura, C.; Wang, H.; Cuthbert, J.; Gottlieb, E.; Balazs, A.; Kowalewski, T.; Matyjaszewski, K. Photoactivated Structurally Tailored and Engineered Macromolecular (STEM) Gels as Precursors for Materials with Spatially Differentiated Mechanical Properties, *Polymer* 2017, Submitted.

## Publications

- (1) Yong, X.; Simakova, A.; Averick, S.; Gutierrez, J.; Kuksenok, O.; Balazs, A. C.; Matyjaszewski, K., Stackable, Covalently Fused Gels: Repair and Composite Formation, *Macromolecules* 2015, 48, 1169-1178.
- (2) Beziau, A.; Singh, A.; de Menezes, R. N. L.; Ding, H.; Simakova, A.; Kuksenok, O.; Balazs, A. C.; Kowalewski, T.; Matyjaszewski, K., Miktoarm star copolymers as interfacial connectors for stackable amphiphilic gels, *Polymer* 2016, 101, 406-414.
- (3) Biswas, S.; Singh, A.; Beziau, A.; Kowalewski, T.; Matyjaszewski, K.; Balazs, A. C., Modeling the formation of layered, amphiphilic gels, *Polymer* 2017, 111, 214-221.
- (4) Polanowski, P.; Jeszka, J. K.; Krysiak, K.; Matyjaszewski, K., Influence of intramolecular crosslinking on gelation in living copolymerization of monomer and divinyl cross-linker. Monte Carlo simulation studies, *Polymer* 2015, 79, 171-178.
- (5) Iyer, B. V. S.; Yashin, V. V.; Hamer, M. J.; Kowalewski, T.; Matyjaszewski, K.; Balazs, A. C., Ductility, toughness and strain recovery in self-healing dual cross-linked nanoparticle networks studied by computer simulations, *Progress in Polymer Science* 2015, 40, 121-137.
- (6) Beziau, A.; de Menezes, R.; Biswas, S.; Singh, A.; Cuthbert, J.; Balazs, A.; Kowalewski, T.; Matyjaszewski, K., Combining ATRP and FRP Gels: Soft Gluing of Polymeric Materials for the Fabrication of Stackable Gels, *Polymers* 2017, 9, 186.
- (7) He, H.; Chung, H.; Roth, E.; Luebke, D.; Hopkinson, D.; Nulwala, H.; Matyjaszewski, K., Low glass transition temperature poly(ionic liquid) prepared from a new quaternary ammonium cationic monomer, *Polymers for Advanced Technologies* 2015, 26, 823-828.
- (8) He, H.; Averick, S.; Mandal, P.; Ding, H.; Li, S.; Gelb, J.; Kotwal, N.; Merkle, A.; Litster, S.; Matyjaszewski, K., Multifunctional Hydrogels with Reversible 3D Ordered Macroporous Structures, *Advanced Science* 2015, 2, 1500069.
- (9) Kozanecki, M.; Pastorczak, M.; Okrasa, L.; Ulanski, J.; Yoon, J. A.; Kowalewski, T.; Matyjaszewski, K.; Koynov, K., Evolution of high-temperature molecular relaxations in poly(2-(2-methoxyethoxy)ethyl methacrylate) upon network formation, *Colloid and Polymer Science* 2015, 293, 1357-1367.
- (10) Erwin, A. J.; Xu, W.; He, H.; Matyjaszewski, K.; Tsukruk, V. V., Linear and Star Poly(ionic liquid) Assemblies: Surface Monolayers and Multilayers, *Langmuir* 2017, 33, 3187-3199.
- (11) Gao, H.; Chan, N.; Oh, J. K.; Matyjaszewski, K. *In-Situ Gelling Polymers*; 1 ed.; Loh, X. J., Ed.; Springer Science: Singapore, 2015; pp 69-105.

(12) Matyjaszewski, K.; Spanswick, J. In Reference Module in Materials Science and Materials Engineering; 1st ed.; Hashmi, M. S. J., Ed.; Elsevier: Oxford, 2016; pp 1-76.

(13) Beziau, A.; Fortney, A.; Fu, L.; Nishiura, C.; Wang, H.; Cuthbert, J.; Gottlieb, E.; Balazs, A.; Kowalewski, T.; Matyjaszewski, K. Photoactivated Structurally Tailored and Engineered Macromolecular (STEM) Gels as Precursors for Materials with Spatially Differentiated Mechanical Properties, Polymer 2017, Submitted.

# Designing Dual-functionalized Gels that Move, Morph, and Self-organize in Light

Anna C. Balazs, University of Pittsburgh, Pittsburgh, PA 15261

## Program Scope

The goal is to design synthetic gels and gel composites exhibiting unprecedented biomimetic behavior that can be controlled by external stimuli. We focus on systems that integrate two modes of chemical functionalization to produce a material with completely new properties, which could not be achieved with just the individual components alone. The dual-functionalization can also permit external cues to be used as orthogonal stimuli, yielding one material that exhibits distinctly different behavior in the presence of the different stimuli. One of the specific goals is to isolate scenarios where the materials can undergo controllable, well-defined motion that mimics the self-propelled movement of biological organisms.

## Recent Progress

Using computational modeling, we designed new, physically-realizable composites that integrate functionalized, photo-responsive fibers with thermo-responsive gels. If the fibers were passive elements, the materials would already exhibit valuable attributes, with the strong fibers acting as a skeleton that reinforces the “muscle” provided by the responsive, active gel. The complexity and potential functionality of the material is, however, increased when the fibers are also stimuli-responsive and thus, constitute active elements. Via our model, we uncovered the cooperative interactions that control the reorganization of the responsive fibers and the morphological changes of the gel in the presence of light, heat and the combination of the two stimuli. These studies provide insight into the complex mechanisms by which multiple stimuli interact with an adaptive material to produce different forms of reconfiguration and actuation. The findings thus reveal the distinct advantage offered by these hybrid materials: a single composite yields access to a range of dynamic responses and structures. On a conceptual level, our results provide guidelines for combining different types of stimuli-responsive components to create adaptive materials that can be controllably and repeatedly actuated to display new dynamic behavior and large-scale motion. Below, we describe three particular examples of this work.<sup>1-3</sup>

### *Embedding flexible fibers into responsive gels to create composites with controllable dexterity*

Using computational modeling, we designed a composite that encompasses a thermo-responsive gel and photo-responsive fibers that extend from the surface of the gel.<sup>1,2</sup> By simulating the effect of light and heat on the sample, we isolated scenarios where these stimuli enable the gel to actuate



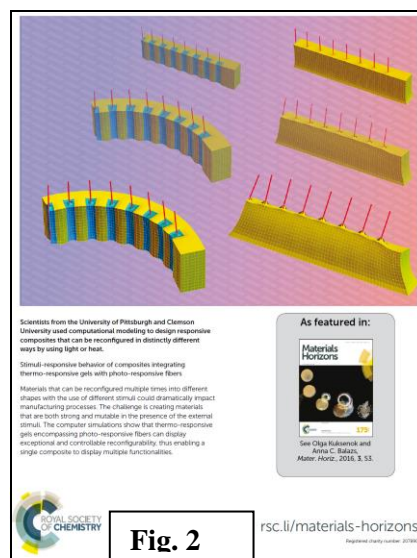
and direct the “finger-like” motion of the embedded fibers. To achieve this distinctive behavior, we considered a gel formed from poly-N-isopropylacrylamide (pNIPAAm), which shrinks when heated above the lower critical solution temperature (LCST). The fibers are functionalized with light-sensitive spirobenzopyran (SP) moieties that extend a finite region into the polymer network. The application of heat causes the entire gel to shrink, while the application of light causes the regions around the functionalized fibers to collapse. With the fibers arranged in a square or circular pattern in the center of the gel, heating the non-illuminated samples drives the fibers to move apart as they bend outward (away from the center). With the application of light, the tips of fibers come together as the fibers bend inward (see **Fig. 1**). In this configuration, the fibers could act as grippers that bind objects in the presence of light. With the illumination turned off, the grippers could controllably release the objects. By placing the fibers closer to the edge of the sample, the combination of heat and light could be harnessed to bind and release larger objects. We also showed that by illuminating the fibers separately, we can manipulate the motion of the individual finger-like objects, and thus, potentially expand the utility of the system. Overall, our findings provide guidelines for controllably reconfiguring the shape of soft materials and thus, tailoring the material to display different functionalities in different environments.

### *Stimuli-responsive behavior of composites integrating thermo-responsive gels with photo-responsive fibers*

When the gel-fiber sample is detached from the surface, then the composites shrink like an accordion when heated and bend like a caterpillar when illuminated (bottom left image in **Fig. 2**).<sup>2</sup> Common to both the tethered and untethered samples, one material displays a distinct response to the different stimuli. Hence, our findings indicate how a given sample can be fashioned into different shapes through the use of separate stimuli. Overall, our results point to a robust method for controllably reconfiguring the morphology of compliant composites and amplifying the effects of external environmental cues (light or temperature) on the behavior of these systems.

### *Modeling gels that morph to move in light*

Human motion is enabled by the concerted expansion and contraction of interconnected muscles that are powered by inherent biochemical reactions. One of the challenges in the field of biomimicry is eliciting this form of motion from purely synthetic materials, which typically do not generate internalized reactions to drive mechanical action. Moreover, for practical applications, this bio-inspired motion must be readily controllable. We developed a computational model to design a new class of polymer gels where structural reconfigurations and internalized reactions are intimately linked to produce autonomous motion, which can be directed with light.<sup>3</sup> These gels contain both spirobenzopyran (SP) chromophores and the ruthenium catalysts that drive the oscillatory Belousov-Zhabotinsky (BZ) reaction. Importantly, both the SP moieties and the BZ reaction are photosensitive. By exposing the dual-functionalized gels to non-uniform illumination, we showed that the localized contraction of the gel (due to the SP moieties) in the presence of traveling chemical waves (due to the BZ reaction) leads to new forms of spontaneous, self-sustained movement, which cannot be achieved in either gel alone.



## Future Plans

We will now utilize our gel lattice spring model to simulate systems where the fibers are completely localized on the surface of the gel (i.e., at the top, bottom, or both of these layers). In this manner, we can exploit the full length of the fibers to regulate the movement of the polymer network. Building on the findings shown in **Figs. 3** and **4**, we will determine how to arrange the fibers in the outer layer(s) to achieve new structural transitions that could not be readily achieved through other means. Consequently, we will be designing new forms that enable new functionality.

Consider the image in **Fig. 3**, which depicts the graphical output from our simulations on the behavior of a LCST gel that contains a specific arrangement of four fibers (drawn in red in **Fig. 3a**) in the top, outermost layer. The

material is equilibrated at low temperature ( $20^{\circ}\text{C}$ ) and assumes the swollen structure in **Fig. 3a** (see color bar, which indicates the local polymer volume fraction). The temperature is increased to  $32^{\circ}\text{C}$  and the gel shrinks and equilibrates to the structure in **Fig. 3b**. As the temperature was increased; the stiff fibers inhibit the neighboring gel from shrinking to the same degree as the fiber-free regions. Due to this difference in the local shrinkage, the original 2D layer is spontaneously transformed into the 3D structure seen in **Fig. 3b**.

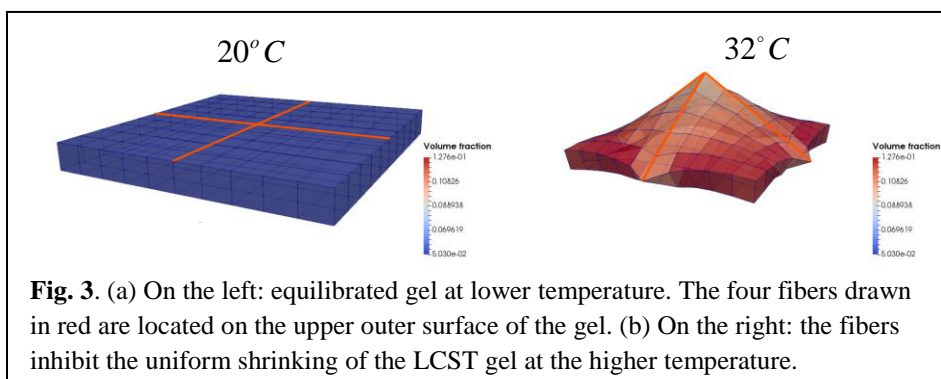


**Fig. 3.** (a) On the left: equilibrated gel at lower temperature. The four fibers drawn in red are located on the upper outer surface of the gel. (b) On the right: the fibers inhibit the uniform shrinking of the LCST gel at the higher temperature.

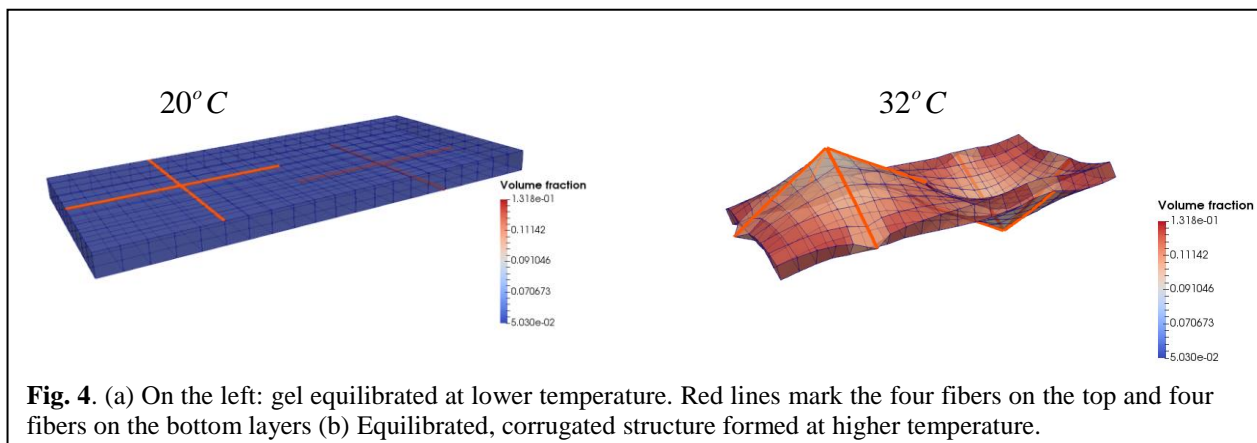


**Fig. 4.** (a) On the left: gel equilibrated at lower temperature. Red lines mark the four fibers on the top and four fibers on the bottom layers (b) Equilibrated, corrugated structure formed at higher temperature.

If the same pattern of fibers is also placed in the lower layer of the neighboring gel, this portion of the gel bulges “downward” (see **Fig. 4**). Hence, the material can dynamically and reversibly switch between a planar and corrugated geometry. There remains a huge parameter space to analyze and thus establish guidelines for harnessing synergistic interactions between stiff fibers and thermo-responsive gels to achieve the desired forms of self-organization.

## References

1. Singh, A., Kuksenok, O. and Balazs, A. C., “Embedding flexible fibers into responsive gels to create composites with controllable dexterity”, *Soft Matter* **12** (2016) 9170-9184. DOI: 10.1039/c6sm02006b
2. Kuksenok, O. and Balazs, A. C., “Stimuli-responsive behavior of composites integrating thermo-responsive gels with photo-responsive fibers”, *Mater. Horizons* **3** (2016) 53-62. DOI: 10.1039/C5MH00212E
3. Kuksenok, O. and Balazs, A. C., “Designing dual-functionalized gels for self-reconfiguration and autonomous motion”, *Scientific Reports* **5** (2015) 9569 (7 pages).

### Publications: 1-3 above and the ones listed below

4. Chen, M., Gu, Y., Singh, A., Zhong, M., Jordan, A. M., Biswas, S., Korley, L. T. J., Balazs, A. C. and Johnson, J. A., “Living additive manufacturing: transformation of parent gels into diversely functionalized daughter gels made possible by visible light photo-redox catalysis”, *ACS Central Science* **3** (2017) 124–134.
5. Singh, A., Kuksenok, O., Johnson, J. A. and Balazs, A. C., “Photo-regeneration of Severed Gel with Iniferter-mediated Photo-Growth”, *Soft Matter* **13** (2017) 1978-1987.
6. Singh, A. Kuksenok, O., Johnson, J. A. and Balazs, A. C., “Tailoring the Structure of Polymer Networks with Iniferter-Mediated Photo-Growth”, *Polymer Chemistry*, **7** (2016) 2955-2964.
7. Li, J., Shklyae, O., Li, T., Liu, W., Shum, H., Rozen, I., Balazs, A. C. and Wang, J., “Self-Propelled Nanomotors Autonomously Seek and Repair Cracks”, *Nano Letts.* **15** (2015) 7077–7085.
8. Yashin, V. V., Kolmakov, G. V., Shum, H. and Balazs, A. C., “Designing Synthetic Microcapsules that Undergo Biomimetic Communication and Autonomous Motion”, *Langmuir* **31** (2015) 11951-11963.
9. Nikolov, S., Shum, H., Balazs, A. C. and Alexeev, A., “Computational Design of Microscopic Swimmers and Capsules: From Directed Motion to Collective Behavior”, *Current Opinion in Colloid and Interface Science* **21** (2015) 44-56.
10. Das, S., Shklyae, O. E., Altemose, A., Shum, H., Ortiz-Rivera, I., Valdez, L., Mallouk, T. E., Balazs, A. C. and Sen, A., “Harnessing Catalytic Pumps for Controllable Delivery of Microparticles in Microchambers”, *Nature Communications* **8** (2017) 14384 (10 pages).
11. Valdez, L., Shum, H., Ortiz-Rivera, I., Balazs, A. C. and Sen, A., “Solatal and Thermal Buoyancy Effects in Self-Powered Phosphatase Micropumps”, *Soft Matter* **13** (2017) 2800-2807.
12. Yong, X., Crabb, E. J., Moellers, N. M., Salib, I., McFarlin IV, G. T., Kuksenok, O. and Balazs, A. C., “Harnessing Self-healing Vesicles to Pick up, Transport and Drop off Janus Particles”, in Self-Assembly: From Surfactants to Nanoparticles, Ramanathan Nagarajan, Ed., Wiley, 2015.
13. Yong, X., Snow, S. C., Kuksenok, O. and Balazs, A. C., “Developing Hybrid Modeling Methods to Simulate Self-Assembly in Polymer Nanocomposites”, in Self-Assembling Systems, Li-Tang Yan, Ed., Wiley, 2017, Chapter 2.
14. Shklyae, O. E., Shum, H., Yashin, V. V. and Balazs, A. C., “Convective self-sustained motion in mixtures of chemically active and passive particles”, *Langmuir*, submitted.

# Self-Assembly and Self-Replication of Novel Materials from Particles with Specific Recognition.

Paul M. Chaikin (PI), Dept. of Physics, New York University.

Nadrian C. Seeman (co-PI), Dept. of Chemistry, New York University.

David Pine (co-PI), Dept. of Physics, New York University.

Marcus Weck (co-PI), Dept. of Chemistry, New York University.

DE-SC0007991

## Program Scope

This program seeks to extend the use of DNA recognition from the nanoscale to the micron scale. This DNA-mediated effort ranges from the exponential growth and selection of nanoscale objects (DNA origami rafts) to the ability to produce specifically assembled colloidal particles with specific chiralities. Achievements and goals include selection of the fittest materials for a given specific environment, control of colloidal assembly order, both initially and dynamically, and using the self-replication system to emulate the origin of life.

## Recent Progress

As part of our program to control the assembly of colloids, we have developed DNA origami belts whose mechanical properties allow them to fit snugly on the surface of a colloid, and through their

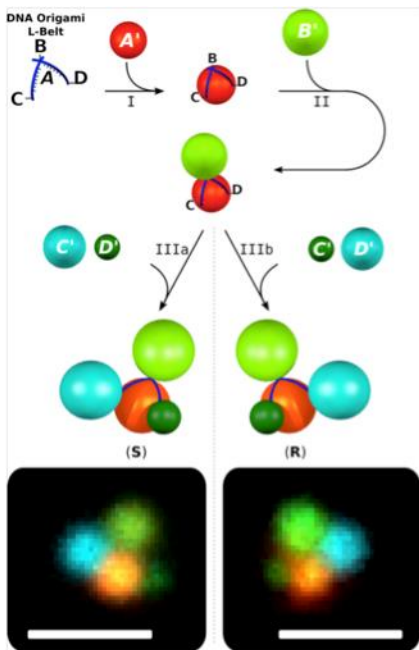


**Figure 1.** Use of a DNA Origami L-Belt to assemble chiral colloids. Differently colored particles bind in an R or S fashion to the red particle.

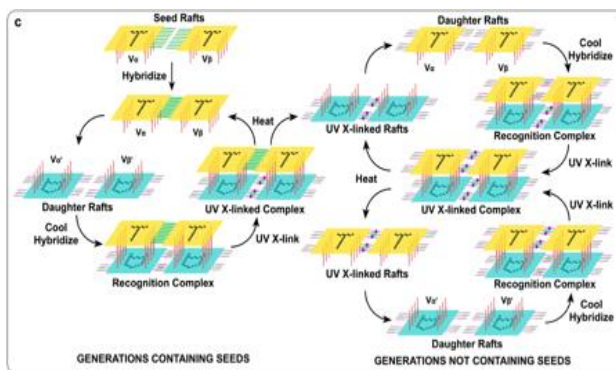


**Figure 2.** Self-Replication of Origami Rafts. Starting with the seed at the upper left, recognition, crosslinking and heating cycles produce replication that has been followed for 24 cycles.

other surface, they can bind another colloid particle. Since the belts can be joined through another DNA origami construct to form an L-shaped arrangement, we can bind several colloid particles to a central particle. In particular we have been able to produce in quantity uniquely left handed or uniquely right-handed colloidal clusters. This is shown in Figure 1.

A central goal of this program has been to develop self-replicating species. We have been remarkably successful at this endeavor, because we have been able to use origami raft tiles with markings on them to behave as species that can replicate in an exponential fashion. A seed dimer of origami rafts is added to a bath of monomers. These bind to it, but not to each other, because their linkage is too weak. The presence of the seed enables them to abut each other, and they can be crosslinked by exposure to UV light to form daughters. Following crosslinking, the system is heated and there are now two sets of seed dimers. The notion is shown in Figure 2.

Self-replication is an important capability. However, its true importance in the production of new materials is that it can be used in a competition for ideal materials in an assortment of environments. As a test of this capability, we have demonstrated that replication predicated on the formation of triplex DNA will outcompete systems that rely on duplex formation at low pH. By contrast, we show that the triplex system is completely overshadowed when the system is shifted to a higher pH environment.

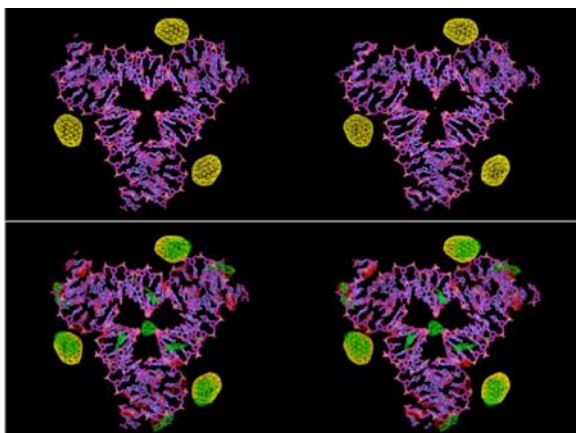


**Figure 3.** *Gold Nanoparticles Incorporated Specifically into a 3D Self-Assembled Rhombohedral Crystal.* Upper panel is anomalous signal, lower is difference electron density superimposed on the anomalous signal.

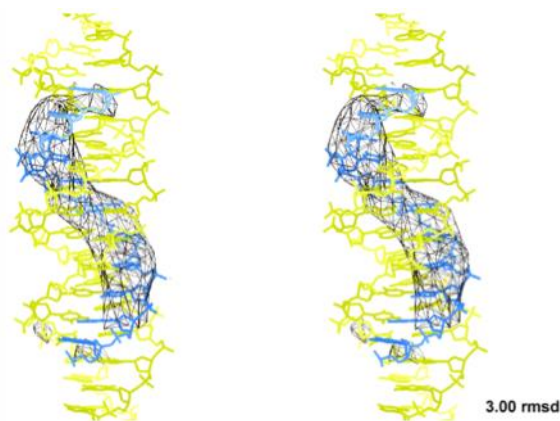


**Figure 4.** *Triplex Electron Density within a 3D Self-Assembled Crystal.* The edge of a three-turn tensegrity triangle (yellow) binds a triplex molecule (blue), in its major groove, with the electron density shown in black.

Much of the work that has been performed and will be performed in this program entails the use of DNA in numerous forms. Thus, we have devoted energy to stabilizing it in 3D self-assembled crystals<sup>1</sup> and to manipulating it there. We have added gold nanoparticles to the crystals, as shown in Figure 3, as well as adding triplex DNA to the crystal, as shown in Figure 4. We have shown that we can deliberately displace the triplex molecules, so that we can build walkers and other machines within a 3D crystal. Thus, we can control the structure of matter in 3D in a dynamic fashion in crystals containing  $\sim 10^{14}$  unit cells.

We have developed a second self-replicating system based on cross-tile origami rafts,<sup>2</sup> shown in Figure 5. Here the available binding regions are the four protruding edges on the cross as well as the topside and underside of the structures. This will allow us to make more complex two dimensional structures and replicate them. It also allows more flexibility in the self-replication process. For example, whereas our original templated replication produced ~ one offspring per cycle or generation, with the cross-tile system we have been able to repeatedly produce seven or more offspring per generation, as illustrated in Figure 5 d-e. This is accomplished by using the parent template as the nucleus of a one dimensional crystal Figure 5 c), permanently fixing the dimer daughters and then melting the crystal so that only the daughters and parent remain. The cross-tile replication process has also been used to demonstrate self-replication literally outside, using the diurnal cycle; a temperature swing from day to night to reversibly hybridize the daughter monomers to the parent dimer template, UV from sunlight at dawn to permanently fix the monomers and then the heat of the day to release the daughters from the parents. Further we have used the cross-tile system toward optimization of the original self-replication cycle reducing the doubling time from 30 hours to 1.5 hours (with replication rate of 1.7). Before with 30 hours we double the population. Now in 30 hours we can multiply by 40,000.

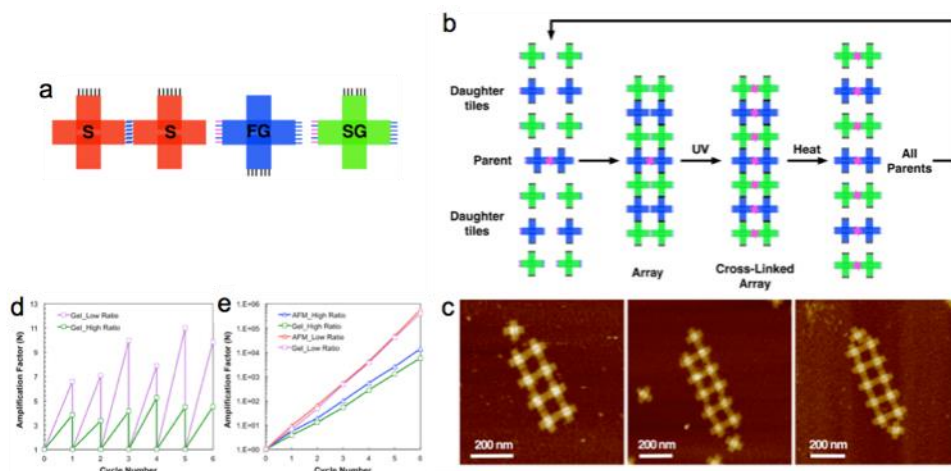


**Figure 5.** a) A set of cross-tile origami rafts that replicate in plane b) and with functionalization on top and bottom can be cycled to produce more than one offspring per parent. c) AFM of parent and future daughters in intermediate array before cross linking. d) the size of “litters” for two different monomer concentrations and e) the exponential growth of the dimers.

Cross-tile origami are also useful in our self-assembly projects with colloids and emulsion droplets. They were used in the preparation of the chiral colloids described above and play a central role in our ability to make emulsion droplets of perfectly controlled valence and specificity. For the emulsions we preform a fixed number of specific adhesion patches on each droplet. This is accomplished by adding to the droplet surface “active” cross-tile origamis with adhesive sticky ends protruding outward. We then use “shepherding” origami rafts to collect all of the active tiles into a patch. The patch can bind specifically to a complementary patch on another droplet. For each patch we use a different set of active and shepherding origami. Figure 6 shows a valence three droplet with the three distinct patches. With only valence one droplets we get dimers. With valence two we get long flexible polymer-like chains. The chains can subsequently be joined and released at their ends or folded in a manner mimicking protein folding.

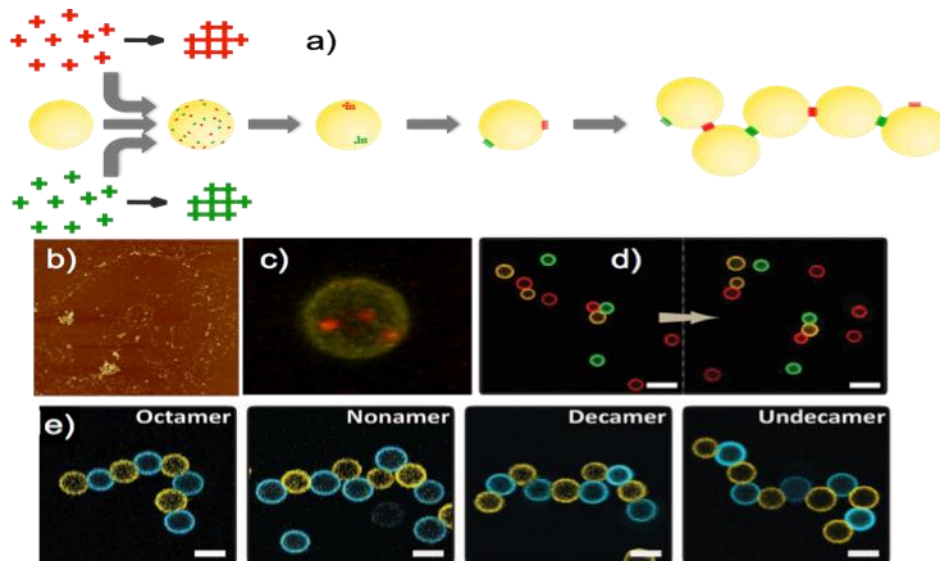


**Figure 6** a) Protocol for making droplets of defined valence. Mobile “active” origami with protruding sticky ends are attached to the surface of a droplet. “Shepherding” origami are next added in excess and collect the active origami into a patch. A different set of active and shepherding origami are added for each patch, here shown for valence two. b) AFM image of a droplet collapsed on a mica surface showing the two patches. c) Confocal micrograph of a droplet of valence three. d) A designed valence two chain with specified color sequence and end to end association is shown after closing the ends and then opening them. e) Valence two produces long flexible chains.

## Future Plans

Evolution to toward larger more complex self-replicating structures.

Introduction of mutations to the self-replication process.

Folding of droplet chains into two and three dimensional structures.

Activation of colloids, emulsions and origami motifs to enable macroscopic motility.

## References

1. J. Zheng, J.J. Birktoft, Y. Chen, T. Wang, R. Sha, P.E. Constantinou, S.L. Ginell, C. Mao, & N.C. Seeman, From Molecular to Macroscopic *via* the Rational Design of a Self-Assembled 3D DNA Crystal, *Nature* **461**, 74-77 (2009).
2. W. Liu, H. Zhong, R. Wang & N.C. Seeman, Crystalline Two-Dimensional DNA Origami Arrays, *Angew. Chemie* **50**, 264-267 (2011).

## Publications

J. Zhao, A.R. Chandrasekaran, Q. Li, X. Li, R. Sha, N.C. Seeman & C. Mao, Post-Assembly Stabilization of Rationally Designed DNA Crystals, *Angew. Chemie Int. Ed.* **54** 9936-9939 (2015).

- D. Niu, R. Sha, H. Jiang, J.W. Canary & N.C. Seeman, The Unusual and Dynamic Character of PX-DNA, *Nucl. Acids Res.* **43**, 7201-7206 (2015).
- Y. Ohayon, R. Sha, O. Flint, B. Chakraborty, H.K. Subramanian, J. Zheng, A.R. Chandrasekaran, H.O. Abdallah, T. Wang, X. Wang, X. Zhang, N.C. Seeman, Covalent Linkage of One-Dimensional DNA Arrays Bonded by Paranemic Cohesion, *ACS Nano* **9**, 10296-10303 (2015).
- Y. Ohayon, R. Sha, O. Flint, A.R. Chandrasekaran, H.O. Abdallah, T. Wang, X. Wang, X. Zhang, N.C. Seeman, Topological Linkage of DNA Tiles Bonded by Paranemic Cohesion, *ACS Nano* **9**, 10304-10312 (2015).
- H.O. Abdallah, Y.P. Ohayon, A.R. Chandrasekaran, R. Sha, K.R. Fox, T. Brown, D.A. Rusling, C. Mao, N.C. Seeman, Stabilization of Self-Assembled DNA Crystals by Triplex-Directed Photo-Crosslinking, *Chem. Comm.*, **52**, 8014-8017 DOI: 10.1039/c6cc03695c (2016).
- C. Simmons, F. Zhang, J.J. Birktoft, X. Qi, D. Han, Y. Liu, R. Sha, H.O. Abdallah, C. Hernandez, Y. Ohayon, N.C. Seeman, H. Yan, Construction and Structure Determination of a Three-dimensional DNA Crystal, *J. Am. Chem. Soc.* **138**, 10047-10054, DOI: 10.1021/jacs.6b06508 (2016).
- P. Paukstelis, N.C. Seeman, 3D DNA Crystals and Nanotechnology, *Crystals* **6**, 97-110, DOI:10.3390/cryst6080097 (2016).
- J. Melinger, R. Sha, C. Mao, N.C. Seeman, M. Ancona, Fluorescence and Energy Transfer in Dye-Labeled DNA Crystals, *J. Phys. Chem. B.* **120**, 12287-12292 (2016).
- Y. Hao, M. Kristiansen, R. Sha, J.J. Birktoft, C. Hernandez, C. Mao, N.C. Seeman, A Device that Works within a Self-Assembled 3D DNA Crystal, *Nature Chem.*, DOI: 10.1038/NCHEM.2745 (2017).
- X. Wang, R. Sha, M. Kristiansen, C. Hernandez, Y. Hao, C. Mao, J. W. Canary & N.C. Seeman, An Organic Semi-Conductor Organized into 3D DNA Arrays via 'Bottom-Up' Rational Design, *Angew. Chemie* **56**, 6445-6448, DOI: 10.1002/anie.201700462 (2017).
- Y. Zhang, A. McMullen, L.-L. Pontani, X. He, R. Sha, N.C. Seeman & P.M. Chaikin, Sequential Self-Assembly of DNA-Functionalized Drops, *Nature Comm.* **8** (21), DOI: 10.1038/s41467-017-00070-0 (2017).

## **Large-scale self-organization and spontaneous flows in microtubule based soft active matter**

**Principle Investigator: Zvonimir Dogic, Department of Physics, Brandeis University, Waltham, MA 02474.**

### **Program Scope:**

Inspired by diverse biological phenomena ranging from ciliary beating and cellular motility to *Drosophila* cytoplasmic streaming our goal is to develop a new category of materials assembled from animate, energy-consuming building blocks. As elemental units we are using microtubules and associated molecular motors that consume energy from ATP hydrolysis to move along the microtubule backbone. The far-from-equilibrium, internally driven active materials we create and study acquire fundamentally new functionalities that have so far been mainly restricted to living organisms. For example, in contrast to well-studied conventional polymer gels, which remain quiescent unless driven by external forces, we have recently described and quantified a phenomena wherein a microtubule-based active fluid spontaneously flows through a pipe. Such force-producing self-pumping active fluids are just one example of desirable biomimetic functionalities that become possible once the materials are released from the constraints of equilibrium. In long-term our goal is to imbue traditional soft materials with the remarkable functionalities of living organisms, including their ability to regenerate and self-heal, flow through constrictions, crawl on surfaces and swim through suspensions.

Microtubule based active materials we study are hierarchically organized. The goal of this project is to characterize their behavior at all relevant lengthscales, ranging from understanding the properties of individual components, such as filamentous microtubules and ATP consuming molecular motors, to mesoscopic microtubule bundles, to dynamics of bulk macroscopic materials. Only understanding and connecting the behavior of active systems across all length scales and levels of complexity will elucidate the design principles required for the engineering of the next generation soft non-equilibrium materials with biomimetic functionalities. Over the past two years we have made progress in each of these areas and most important highlights are described below.

### **Recent Progress:**

*Mechanics of microtubule filaments:* At the most basic level all of the active materials studied in the project are based on the buckling instability of composite bundles whose elemental constituents are filamentous microtubules. Consequently, understanding the elasticity of isolated microtubules is essential for understanding the behavior of composite extensile bundles. Previous experiments have reported that microtubules have a wide range of elastic moduli. Using our optical microscopy techniques we have comprehensively probed the mechanical response of GMPCPP-stabilized microtubules with contour lengths ranging from  $\sim 3 - 15 \mu\text{m}$ . In these experiments, two optically trapped silica beads are attached at different points along a microtubule, and are used to subject the filament to tensile and compressive forces. In the compression region, an interesting, reproducible behavior is observed beyond some threshold strain: the buckling force saturates (or even decreases) with increasing strain (**Fig. 1**). Such behavior indicates softening of the microtubules, an outcome that cannot be captured by Euler-

Bernoulli or Timoshenko beam models often employed in the literature. In collaboration with Mahadevan lab from Harvard we showed that the softening is due to cross-sectional ovalisation - and eventual buckling, an effect first described by Brazier - and that the mechanical response of microtubules is well-captured by an anisotropic elastic shell model with three parameters (one shear, and two stretching moduli). We also probed the properties of a different biological filament - the bacterial flagellum (*Salmonella typhimurium*, strain SJW166). This served as a control experiment; since flagella are neither hollow shells nor highly anisotropic like microtubules, and are therefore expected to behave like ideal slender rods. These results are being prepared for publication.

Moving to more complex assemblages we have also started examining the mechanical behavior and buckling instability of composite microtubule bundles. In particular, we assembled a two filaments bundle and using optical tweezers we then proceed to buckle the assembled construct, while continuously acquiring the force-displacement data. The filaments initially buckle together, but fray at some critical strain, thus breaking the bundle. They re-bundle when the bending process is reversed, usually at a different, smaller strain. The resultant force-displacement curve displays the hysteresis pattern. We are currently developing a theoretical model that can explain these measurements. These two advances lay the foundation for quantitative understanding of internal buckling that is driven by molecular motors. This is the elemental structural motif that drives the dynamics of diverse microtubule based active materials.

*Self-pumping isotropic active fluids:* At the next level of hierarchy we have recently demonstrated that confinement robustly transform turbulent dynamics of bulk active isotropic fluids into long-ranged coherent flows (**Fig. 2**). Surprisingly, this novel first-order non-equilibrium transition occurs across multiple scales and is correlated with the formation of a self-induced nematic liquid crystal that wets the confining surfaces.

Until now the vast majority of active matter studies have been limited to 2D systems. We examined more challenging 3D active isotropic fluids, finding that system dimensionality plays a fundamental and unexpected role. In particular, previous studies have demonstrated that coherent motion in active matter is only possible for confinements smaller than the inherent system lengthscale, such as the vortex diameter. We demonstrated that this is not the case for 3D systems. In our earlier work we have studied microtubule based active isotropic fluids in unconfined geometries and observed turbulent flows comprised of localized vortices. Following up on these foundational studies we have identified a class of geometrical confinements that robustly transform such turbulent dynamics into long-ranged coherent flows.

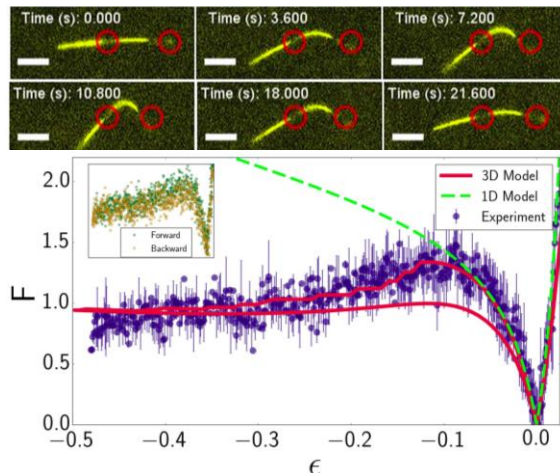


**Fig. 1.** Series of fluorescence images from microtubule compression experiment. The locations of the optical traps are shown in red. Force-strain curve for a microtubule of length  $7.1 \mu\text{m}$  from experiment (blue) and simulation using a 1D model (green, dashed) or a 3D model (red).

Surprisingly, our method work across multiple lengthscales, even for geometries that are orders of magnitude larger than the average vortex size. Somehow the boundaries determine the dynamical state of the system irrespective of its size. Extensive experiments revealed that the transition to coherent flows is controlled by the

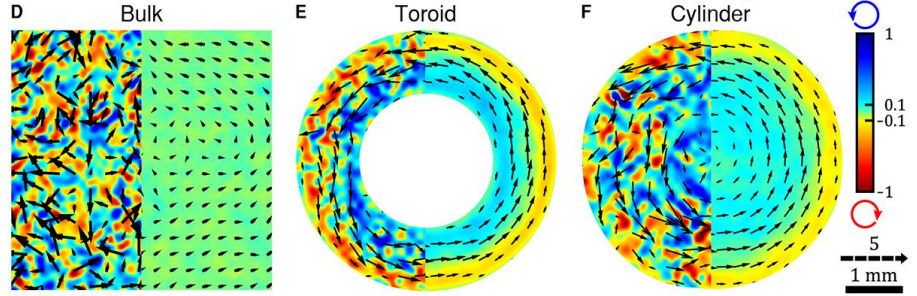


**Fig. 2.** A flow map demonstrates that bulk active fluids exhibit turbulent flows that do not transport material. The vector field indicates the local flow velocity normalized by the mean flow speed. The colormap represents the normalized vorticity distribution, with blue and red tones representing CCW and CW vorticities, respectively. Left and right halves are instant and time averaged plots, respectively.

dimensionless aspect ratio of the channel profile, rather than dimensionful channel size (**Fig. 3**). Our experiments further demonstrate that the transition between turbulent and coherent active flows is an intrinsically 3D effect that is impossible in previously studied systems with reduced dimensionality. An exceedingly simple, yet theoretically unforeseen, criterion predicts the onset of the coherent flows.

We elucidated the microscopic mechanism that drives the coherent flows. Specifically, we demonstrated that the coherent flows are correlated with the transition of a surface bound layer from an isotropic into a nematic liquid crystal. The self-organized nematic layer anchors to the surface at a non-trivial oblique angle. Active stresses generated by this distorted nematic power the macroscopic coherent flows. Our system is remarkably efficient, as active bundles can propel fluid 1000 times their own weight. The self-generated Poiseuille-like flows are highly controllable and robust, persisting at lengthscales ranging from microns to meters. We demonstrate control over the direction, magnitude and lateral profile of the coherent flows. Finally, we show that the coherent flows self-organize in diverse confinements and can even solve a complex fluidic maze. The scale-invariant transition from turbulent to coherent flows is not predicted by current active matter theories, raising fundamental questions in non-equilibrium physics and fluid dynamics. It also paves the way towards engineering novel self-assembled machines that are assembled and powered from machines at smaller lengthscales.

*Dynamics of active 2D nematics:* Motivated by the experimental realization of microtubule based active nematics a number of recent theoretical models have been developed that describe their chaotic dynamics. However, the quantitative comparison between theoretical predictions and experiments is largely still lacking. To facilitate progress in this area we have recently completed a series of experiments whose goal is to quantify the unique dynamics of 2D active nematics. In a first set of experiments we have analyzed the large-scale geometrical and topological features of the fluid flows powered by active nematics. These experimnts were motivated by the recent theoretical model that predicts that the low-Reynolds number turbulence in active nematics is a multiscale phenomenon where, as in inertial turbulence, vortices are created over a range of length scales. Furthermore, the theory predicts that the area of the vortices is exponentially distributed above the active length scale, the scale in which the active stresses are balanced by

spontaneous flow. We have analyzed the self-generated dynamics of two-dimensional active nematics comprised of microtubule filaments and molecule motor kinesin. Quantitative analysis of experimentally measured flows confirms the predicted exponentials scaling, and allows us to extract the active length scale,  $l_a$ . We systematically varied the concentration of ATP, which is the chemical fuel that powers the motion of kinesin motors and determine the dependence of  $l_a$  on the magnitude of active stress.

In another set of experiments we have quantified the dynamics of active nematics at lengthscales below the active length scale,  $l_a$ . At this lengthscales the active stresses are not sufficiently large to distort the nematic director and thus the sample is more or less uniformly aligned, allowing us to study dynamics of monodomain active nematics. By using fluorescent recovery after photobleaching (FRAP) and by tracing single microtubule

we were able to quantify the flows of active nematics on these much smaller lengthscales. These experiments have revealed that the dynamics along the director can be both contractile and extensile, while the dynamics perpendicular to the nematic director exhibit only strongly contractile flows. The results summarizing the flow behavior of active nematics on large and small scales are being prepared for two separate publications.

**Future Plans:** An important future goal will be to quantitatively characterize how geometrical confinement induces transition of chaotic flows of bulk isotropic gels into a different dynamical state characterized by steady-state currents capable of material transport. We will determine the nature of the ensuing transition. In order to accomplish this we have developed a new model system of active isotropic fluids that lasts up to 100 hours, which is an order of magnitude longer than the conventional formulations that have been used so far. Furthermore, our initial work has demonstrated the feasibility of assembling for the first time 3D active nematics. Little is know about dynamics of such materials and we have a unique opportunity to explore this region of phase space. We will also complete our characterization of the flow of 2D active nematics. In another effort, we have demonstrated that confined 2D active nematics behave as tunable oscillators, and we will quantitatively analyze the dynamics of such materials.

**Publications which acknowledge full or partial DOE support:**

1. "Transition from turbulent to coherent flows in confined three-dimensional active fluids" Kunta Wu, Jean Bernard Hishamunda, Daniel. T. N. Chen, Stephen J. DeCamp, Ya-Wen Chang, Alberto Fernandez-Nieves, Seth Fraden, Zvonimir Dogic, *Science*, 355, eaal1979 (2017)
2. "Orientational order of motile defects in active nematics," Stephen J. Decamp, Gabriel S. Redner, Aparna Baskaran, Michael. F. Hagan and Zvonimir Dogic, *Nature Materials*, 14, 1110–1115 (2015).

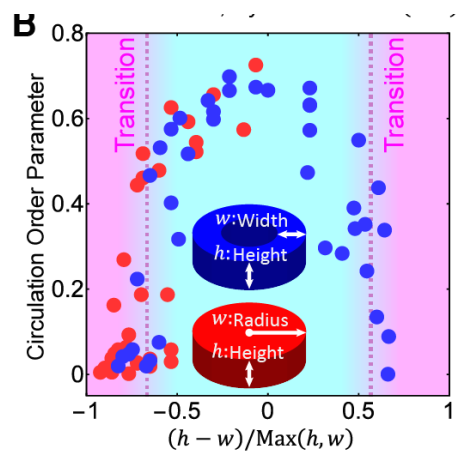


**Fig. 3.** A phase diagram indicating confinement geometries that support circular flows. Circles and dots represent toroidal and cylindrical confinements, respectively.

## Self-Assembly of Virus Particle Based Materials for Hydrogen Catalysis

PI: Trevor Douglas, Department of Chemistry Indiana University

### Program Scope

The overall goal of this project is to design and assemble materials, over multiple length scales, that incorporate active catalysts for hydrogen production. We will examine the encapsulation of enzyme and enzyme mimics within the P22 Virus-like Particle (VLP) through a process of directed self-assembly. Kinetic and structural implications of the encapsulated environment (crowding and spatial arrangement of enzyme subunits) for the heterodimeric [NiFe] hydrogenase, and hydrogenase mimics will be elucidated. Furthermore, we are designing and refining strategies for using the P22 VLP as a nanoscale building block for controlling the higher order assembly of multiple capsids to form hierarchically ordered 3-D superlattice arrays. These directed assembly approaches will be combined to create active P22-based materials that are capable of undertaking complex catalytic reactions.

### Recent Progress

*[NiFe] Hydrogenase encapsulation inside P22 – H<sub>2</sub> nanoreactor.* We previously fused the subunits of the *E. coli* hydrogenase (Hyd-1) to the N-termini of the P22 scaffold proteins and enforced the encapsulation of the *hyaA*: *hyaB* heterodimer through directed self-assembly of the P22 capsid (Fig 1). This resulted in an active nanoparticle where the encapsulated enzymes were >100 times more active than the free enzymes – a direct consequence of enforced encapsulation and dimerization within the P22 capsid.

As an extension of this P22-encapsulated hydrogenase design, we have now integrated an electron mediator (cytochrome b<sub>5</sub>; Cb<sub>5</sub>) and its associated reductase (NADH-dependent cytochrome b<sub>5</sub> reductase; Cb<sub>5</sub>R) with the Hyd-1 and demonstrated their encapsulation and H<sub>2</sub> production activity within the P22 capsid. The monomeric Cb<sub>5</sub>R is an NADH-dependent flavoprotein that naturally catalyzes the reduction of the Cb<sub>5</sub> using NADH. To mimic the orientation and proximity of the natural membrane associated cytochrome b on the C-terminus of Hyd-1 we genetically fused the Cb<sub>5</sub> to the C-terminus of the *hyaA* subunit, by placing the gene for the Cb<sub>5</sub> between the genes for the scaffold protein (SP) and the *hyaA*<sup>1</sup>. The NADH-dependent cytochrome b<sub>5</sub> reductase Cb<sub>5</sub>R, was cloned onto the on the C-terminus of *hyaB*, between the gene for the scaffold protein (SP) and the *hyaB* (Fig. 2). We measured the turnover of the

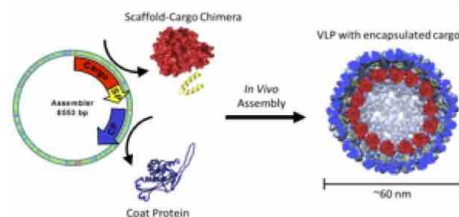


Fig 1. P22 particles assemble using a truncated SP (yellow) fused to an enzyme (red) when expressed together with CP (blue) resulting in virus-like particles with encapsulated enz-SP molecules.

system by introducing NADH and monitoring its oxidation (absorbance at 340nm) while at the same time monitoring the production of Hydrogen using gas chromatography. At pH 5 the efficiency for H<sub>2</sub> production from NADH is 75%. This suggests that there is an efficient electron transfer between the cytochrome b<sub>5</sub> and the active NiFe site of the hydrogenase enzyme (hyaB subunit), mediated through the series of iron-sulfur clusters present in hyaA subunit<sup>2</sup>.

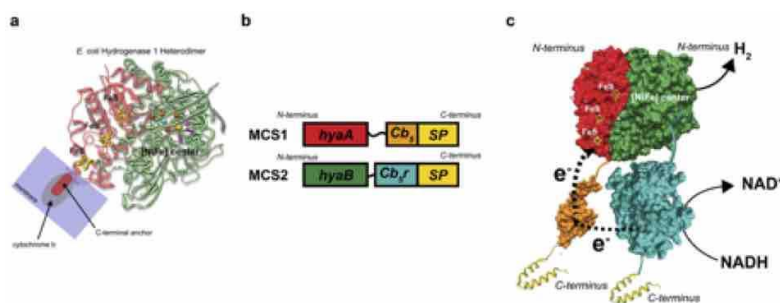


Fig 2. The *E. coli* [NiFe]-hydrogenase 1 (Hyd-1) is a heterodimer (a) built from a large subunit (green) and small subunit (red) with a membrane bound cytochrome b on the C-terminus. (b) Incorporation of a soluble cytochrome b and the cytochrome b reductase between the genes for the scaffold protein (SP) and the hyaA/B facilitated the assembly of the complex hetero-dimer shown in (c) capable of producing H<sub>2</sub> using NADH as reducing agent.

**Dendrimer mediated higher order assembly of P22 VLPs:** We examined the higher order assembly of individual P22 VLP into arrayed materials mediated through electrostatic interactions between P22 and generation 6 polyamide amine (PAMAM) dendrimer (G6). Wild type P22 VLP (wtP22), and three surface modified P22 VLP variants, each displaying a small peptide repeat on the C-terminus<sup>3</sup>, were used as building blocks. The introduced peptides were either net negatively charged (VAALEKE)<sub>2</sub>, neutral (VAALQSQ)<sub>2</sub>, or net positively charged (VAALKEK)<sub>2</sub>, referred to as P22-E2, P22-N2 and P22-K2, respectively. Each VLP was mixed with G6 at pH 7.0 with a range of ionic strength (*I*) and the higher order assembly was initially assessed by the increase in turbidity (Fig. 3a). The P22-E2, P22-N2 and P22-K2 VLP as well as wtP22 all exhibited higher order assembly, however the ionic strength above which assembly does not occur (*I<sub>T</sub>*) was significantly different (Fig. 3a). The trend correlates with differences in the zeta potential of the four constructs (Fig. 3b), namely P22 VLPs with a less negatively charged exterior surface exhibit lower *I<sub>T</sub>* for assembly. Thus the formation of higher order assemblies is strongly affected by the overall surface charge of the VLP, and assembly behavior of VLP can be controlled by

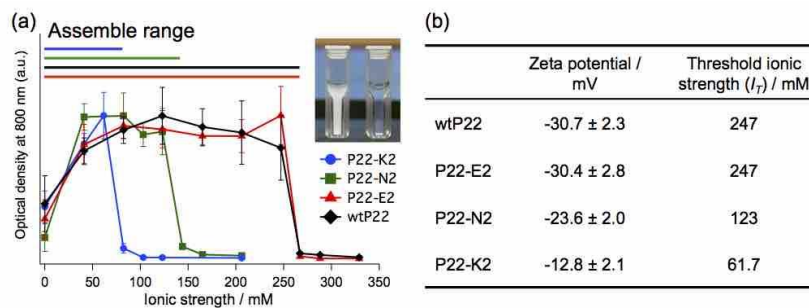


Fig. 3 (a) Assembly of P22 variants under a range of ionic strengths (*I*) was monitored by light scattering at 800 nm. A solution of P22-E2 mixed with G6 in *I* = 206 mM became turbid (inset-left), whereas when mixed in *I* = 329 mM remained clear (right). (b) The zeta potential of each P22 VLP at pH 7.0 and the *I<sub>T</sub>* for assembly with G6. The *I<sub>T</sub>* decreased with decreasing negative surface charge of the VLPs.

manipulating surface charge of VLP.

The assembled structures were analyzed by small angle X-ray scattering (SAXS). For wtP22 samples, broad peaks observed in samples prepared below  $I_T$ , suggested some short-range order (Fig. 4a). The samples prepared from the three variants exhibited sharp SAXS peaks at same  $q$  positions when assembled near their threshold ionic

strength ( $I = 206$  and  $247$  mM for P22-E2,  $123$  mM for P22-N2 and  $61.7$  mM for P22-K2) (Fig 4b). These SAXS profiles best fit with a face centered cubic structure with lattice parameter of  $87.0$  nm. TEM analysis of the assembled samples of P22-E2 and G6 prepared at  $I = 206$  mM showed that the assembled sample has both hexagonal close packed (Fig 4c) and square (Fig 4d) lattices, agreed with the SAXS results.

Taking advantage of the ionic strength threshold differences between the P22 VLP variants shown in Fig 3, we further demonstrated the selective assembly and disassembly of two populations of VLP modules in the arrayed material. When P22-K2, P22-E2 and G6 dendrimer were mixed above  $I_T$  both P22-K2 and P22-E2 modules remained in solution (Fig. 5a and b). When the ionic strength of the mixture was lowered to  $I = 206$  mM, the P22-E2 exclusively assembled into an array while

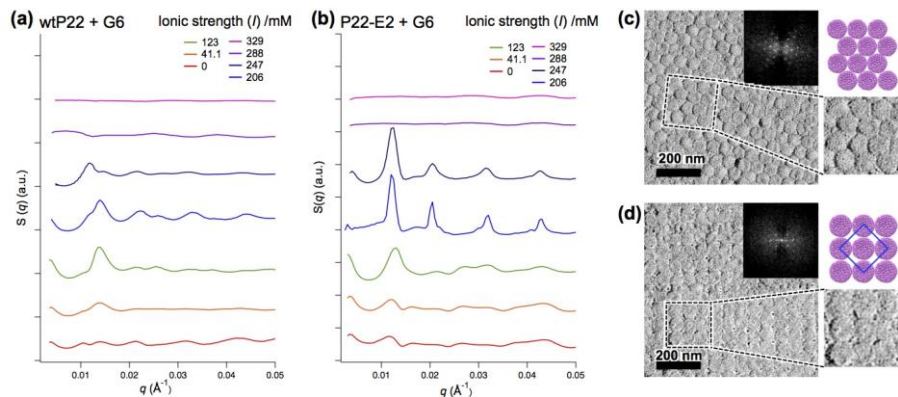


Fig. 4 Structure analysis of P22 VLP assemblies mediated by G6 dendrimer. (a, b) SAXS of (a) wtP22 and (b) P22-E2 - G6 PAMAM assemblies. Structure factor peaks became more prominent with increasing ionic strength up to the threshold ionic strength ( $I_T$ ). (c, d) The structure of the P22-E2 + G6 assembled at  $I = 206$  mM was observed by TEM. showing hexagonal close packing of P22-E2 VLPs (c) and FFT (inset) indicates the inter-row spacing of  $54$  nm (neighbor distance of  $62$  nm), which matches well with the SAXS data. (d) An image of the assembly showing a square lattice arrangement of P22-E2 VLPs with FFT (inset) indicating the center-to-center distance between the nearest neighbor VLPs of  $61$  nm. The blue-line square corresponds to a unit cell on the  $\{100\}$  face.

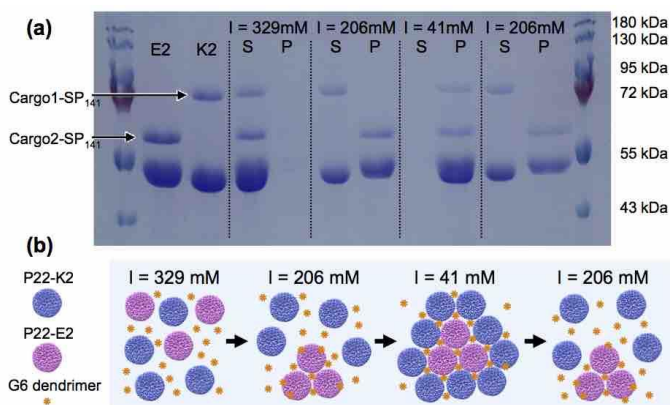


Fig. 5 Selective assembly and disassembly of VLP modules into an arrayed material directed by ionic strength manipulation of the solution. The ionic strength of a solution containing P22-E2 and P22-K2, and G6 dendrimer was varied and the presence of P22-E2 and P22-K2 in solution (S) and in pellet (P) was assessed by SDS-PAGE. (a) The first and last lanes correspond to molecular weight markers. At each ionic strength P22-E2 and P22-K2 showed distinct distribution either in solution or in the pellet. (b) Schematic illustration of selective assembly and disassembly behavior of P22-E2 and P22-K2 VLPs revealed by the electrophoresis analysis.

P22-K2 remained in solution. When the ionic strength was further lowered to  $I = 41$  mM, the P22-K2 assembled into the array leaving no VLPs free in solution. This behavior is consistent with the observed  $I_T$  for assembly of P22-E2 and P22-K2. This process is completely reversible.

## Future Plans

The strategies to design P22 VLP arrays developed here will be applied for constructing P22-Hyd arrays that are responsive to changes in ionic strength, pH, and other environmental triggers. The relation between structure of the arrays and activity will be elucidated. Success of this process will allow us to control the spatial arrangement of different P22 VLPs, which encapsulate different enzymes, as a way to control the functional behavior of these self-assembled systems over multiple length scales. We will work toward optimizing and producing different VLPs containing the hydrogenase and cytochrome/cytochrome reductase and incorporating the enzyme encapsulated P22 VLPs into superlattice arrays, with controlled porosity as a major focus moving forward.

## References

- 1) Patterson D. P., Prevelige P. E., Douglas T., ACS Nano, **2012**, 6, 5000-5009.
- 2) Volbeda A., Amara P., Darnault C., Mouesca J. M., Parkin A., Roessler M. M., Armstrong F. A., Fontecilla-Camps J. C., Proc Natl Acad Sci U S A, **2012**, 109, 5305-5310.
- 3) Servid A., Jordan P., O'Neil A., Prevelige P., Douglas T., Biomacromolecules, **2013**, 14, 2989-2995.

## Publications

1. P.C. Jordan, D.P. Patterson, K.N. Saboda, E.J. Edwards, H.M. Miettinen, G. Basu, M.C. Thielges, T. Douglas “Self-Assembling Biomolecular Catalysts for Hydrogen Production” *Nature Chemistry* (2016) **8**, 179-185. doi: 10.1038/nchem.2416.
2. E. Edwards, R. Roychoudhury, B. Schwarz, P. Jordan, J. Lisher, M. Uchida and T. Douglas, “Co-localization of Catalysts within a Protein Cage Leads to Efficient Photochemical NADH and/or Hydrogen Production” *J. Materials Chemistry B* (2016) **4**, 5375 – 5384.
3. B. Schwarz, M. Uchida, T. Douglas, “Biomedical and Catalytic Opportunities of Virus-Like Particles in Nanotechnology”. *Advances in Virus Research*, (2017) **97**,1-60.
4. Masaki Uchida, Kimberly McCoy, Masafumi Fukuto, Lin Yang, Hideyuki Yoshimura, Heini M. Miettinen, Ben LaFrance, Dustin Patterson, Benjamin Schwarz, Byeongdu Lee, and Trevor Douglas “Self-assembly of active protein cage superlattices catalyzing a two-step coupled synthesis of isobutanol” *Submitted*
5. Kimberly McCoy, Masaki Uchida, Byeongdu Lee and Trevor Douglas “Template driven assembly of an ordered protein framework material from P22 virus-like particles” *in preparation*
6. Aumiller, W.M.; Biner, D.; Miettinen, H.; Douglas, T.”pH-Induced Assembly/Disassembly of P22 Virus-Like Particles:a Biofilm Mimetic” *in preparation*
7. W.M. Aumiller, P.C. Jordan, JC-Y.Wang, E.J. Edwards, H.E. Miettinen, A.L. Le Sueur, M.C. Thielges, A. Zlotnick, T. Douglas “NADH-driven Hydrogen Production via Multienzyme Electron Transfer in a Virus-Like Particle” *in preparation*

## Control of charge transfer and light-driven reactions in nanocrystal-enzyme complexes

Gordana Dukovic, University of Colorado Boulder

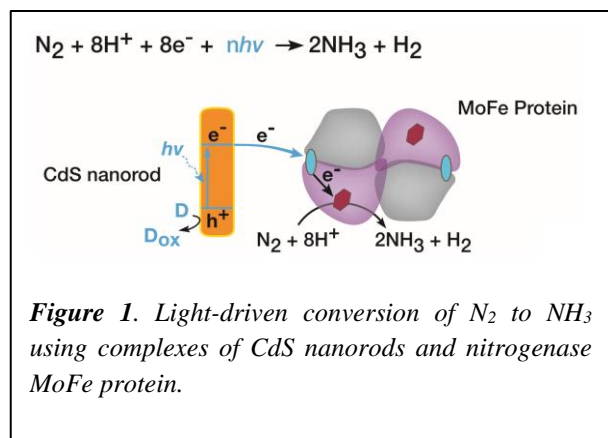
### Program Scope

The overarching long-term goal of this project is to understand how the remarkable light-harvesting properties of semiconductor nanocrystals could be synergistically combined with the outstanding properties of redox enzymes that catalyze complex and useful reactions to enable efficient solar photochemistry. This approach is inspired by photosynthesis, where light absorption is coupled to catalysis via electron transfer steps. Specifically, this project is focused on how the structural properties of semiconductor nanocrystals govern their interactions with natural enzymes, the electron pathways involved, and the final chemistry at the enzyme active site. We aim to provide design principles for *synthetically tailoring* these optimal light absorbers and *integrating* them with enzymatic catalysts in a way that minimizes energy-wasting processes. Furthermore, we aim to understand and control the excited state properties of nanocrystals to enhance their photochemistry.

### Recent Progress

**1. Four redox enzymes photochemically driven by semiconductor nanocrystals.** The bulk of our work on this project has focused on complexes of CdS nanorods and [FeFe]-hydrogenase to photochemically drive H<sub>2</sub> generation, as described below. Additionally, we teamed up with experts in enzyme catalysis to demonstrate that the approach of coupling nanocrystals with redox enzymes to drive photochemical reduction can be adapted to various enzymes. With our NREL collaborators Paul King and Kate Brown, we coupled CdSe quantum dots (QDs) with ferredoxin NADP<sup>+</sup> reductase from *Chlamydomonas reinhardtii*.<sup>1</sup> The resulting complexes were capable of photochemically reducing NADP<sup>+</sup> to NADPH, which then was able to drive alcohol dehydrogenases to convert aldehydes to alcohols.

One is hard pressed to find a more challenging reaction with widespread reach than N<sub>2</sub> reduction to NH<sub>3</sub>. In nature, N<sub>2</sub> fixation is catalyzed by nitrogenases. Because N<sub>2</sub> reduction to NH<sub>3</sub> is an 8-electron process, the enzyme can instead catalyze synthesis of “lower value” products that require fewer electrons, such as H<sub>2</sub>.<sup>2</sup> Using what we had learned about nanocrystal-enzyme interactions, we electrostatically coupled MPA-capped CdS nanorods and CdSe QDs to MoFe protein, a component of nitrogenase from *Azotobacter vinelandii*, and achieve light-driven NH<sub>3</sub> production from N<sub>2</sub> using an enzyme catalyst (**Figure 1**).<sup>3</sup> This work is a result of a collaboration with nitrogenase experts Lance Seefeldt (Utah State) and John Peters (Montana State), as well as our NREL collaborators.



For the purposes of extending our work in the direction of complex chemical reactions, we coupled CdS nanorods and CdSe QDs with 2-oxoglutarate:ferredoxin oxidoreductase (OGOR) from *Magnetococcus marinus* provided by Sean Elliott at Boston University. We are interested in this enzyme because it catalyzes a complex  $CO_2$  reduction reaction that also creates a new carbon-carbon bond. We also have an opportunity to photochemically drive what is in nature a dark reaction. In our work to date, we

have coupled both CdS nanorods and CdSe QDs with OGOR. We used an assay that detects photochemical 2-oxoglutarate generation from  $CO_2$  reduction using a downstream reaction that consumes 2-oxoglutarate and NADH, which has a strong UV-Vis spectroscopic signature with a peak near 340 nm, demonstrating a photochemically driven carbon-carbon formation reaction catalyzed by an enzyme (manuscript in preparation).

**2. Elucidation of ET kinetics in the CdS-hydrogenase system.** The upper limit on the quantum yield of  $H_2$  production in the nanocrystal-hydrogenase system is the quantum efficiency of electron transfer ( $QE_{ET}$ ) because only the photoexcited electrons from the nanocrystal can end up in a  $H_2$  molecule. This is why we placed significant effort on understanding how the dynamics of ET control the overall photochemistry and how these processes can be controlled through rational modifications of the nanocrystal structure. We accomplished this through a combination of transient absorption (TA) spectroscopy, kinetic modeling, and structural modifications of the nanocrystals.

TA spectroscopy allowed us to directly probe the electron injection step from CdS to the enzyme, observed as the shortening of the TA bleach signal that corresponds to the population of excited electrons. Quantifying the rate and efficiency of ET in CdS nanorod-hydrogenase complexes was a challenging task because nanocrystals generally have complicated excited-state decay kinetics.<sup>4</sup> In the case of CdS nanorods, six exponential components are needed to fit the kinetics from 100 femtoseconds to microseconds.<sup>4</sup> Developing physically meaningful kinetic models for such complicated decays remains one of the challenges in nanocrystal spectroscopy. To fit the excited state decay in complexes of CdS nanorods and hydrogenase, we used a kinetic model that accounts for heterogeneities in the number of electron traps and enzymes adsorbed per nanorod to reveal the rate constants for electron-hole recombination ( $k_0$ ), electron trapping ( $k_{tr}$ ), and electron transfer ( $k_{ET}$ ) to the enzyme (**Figure 2**).<sup>5</sup> The model assumes that both the electron traps and the enzymes on the nanorods follow a Poisson distribution, such that the electron population decays as a function of the three rate constants,  $\langle N_{tr} \rangle$ , the average number of electron traps per nanocrystal, and  $\langle N_{enz} \rangle$ , the average number of enzymes per nanorod. We find  $k_0$  to be  $1.5 \times 10^7 \text{ s}^{-1}$ , and  $k_{tr}$  to be 7-fold larger ( $1.1 \times 10^8 \text{ s}^{-1}$ ) with  $\langle N_{tr} \rangle$  of only 0.59 per NR.  $k_{ET}$

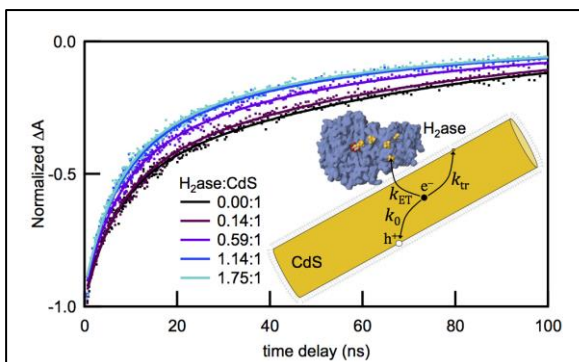


**Figure 2.** Fit of our kinetic model to TA decay of CdS nanorod-hydrogenase samples. Inset shows the electron decay pathways considered in the model.

( $2.4 \times 10^7 \text{ s}^{-1}$ ) is within a factor of two of  $k_0$ , meaning that the two processes are in direct kinetic competition.

A key conclusion from this work is that the quantum yield of  $\text{H}_2$  generation is approximately equal to  $\text{QE}_{\text{ET}}$ , which in turn depends almost entirely on the ratio of  $k_{\text{ET}}$  and  $k_0$ , with electron trapping playing a minor role because of low electron trap density in these nanocrystals. Together with the linear dependence of  $\text{H}_2$  generation on light intensity, this analysis demonstrates that the enzyme is capable of utilizing virtually all the electrons it receives.

This speaks to the remarkable catalytic capabilities of redox enzymes which have evolved to efficiently utilize electrons in an environment of low electron flux. This result also speaks to the biomimetic nature of the CdS-hydrogenase construct, in which the enzyme appears to behave just as it would in nature.

**3. Critical role of surface-capping ligands in nanocrystal-hydrogenase complexes.** In order to manipulate the ratio of  $k_{\text{ET}}$  to  $k_0$  in favor of higher  $\text{QE}_{\text{ET}}$ , we examined the role of nanocrystal surface-capping ligands in the ET process. The binding interaction between CdS nanorods and hydrogenase is electrostatic in nature, with negatively charged 3-mercaptopropionic acid (MPA)

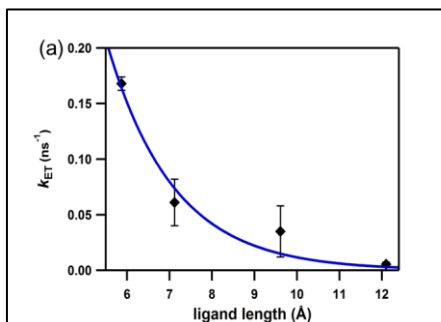


**Figure 3.** Exponential decay of  $k_{\text{ET}}$  in CdS nanorod-hydrogenase complexes as a function of length of the mercaptocarboxylate surface capping ligand.

ligands on the nanocrystal surface binding to the positively charged patch on the enzyme, which is the docking site of the natural electron donor, ferredoxin. The MPA ligands therefore form the interface between the two components and it is natural to expect them to play an important role in determining the value of  $k_{\text{ET}}$ . We measured the value of  $k_{\text{ET}}$ , as well as the  $\text{H}_2$  quantum yield, as a function of the length of the aliphatic chain of the mercaptocarboxylate ligands and found an exponential decay behavior (**Figure 3**) that suggests that the ligand serves as a tunneling barrier for the electron (manuscript in preparation). This result suggests that the value of  $k_{\text{ET}}$  can be manipulated over a wide range by careful selection of surface capping ligands.

**4. Dynamics of trapped holes in CdS and CdSe nanocrystals.** In our efforts to understand the hole scavenging by electron donors in solution, which is inherently necessary in all the nanocrystal-enzyme reduction reactions, we first needed to elucidate the elusive hole dynamics in nanocrystals. In nanoscale CdS and CdSe, hole trapping occurs efficiently on a picosecond timescale, so electrons primarily recombine with trapped, rather than delocalized, holes. We

discovered that the trapped holes on the surface of CdS nanorods are not stationary, as is often assumed, but instead are mobile.<sup>6</sup> Using a combination of TA spectroscopy and theoretical modeling (in collaboration with Joel Eaves), we demonstrated that trapped holes in CdS nanorods are mobile and execute a random walk at room temperature. This phenomenon has important implications for the oxidation photochemistry of CdS nanocrystals as the diffusing holes can sample the nanocrystal surface and find hole acceptors.

## Future Plans

In our future work, we will aim to understand the factors that govern the photochemical carbon-carbon bond formation via CO<sub>2</sub> reduction, catalyzed by nanocrystal complexes with OGOR. These factors include the nanocrystal-enzyme binding interaction, population distribution, driving force (via nanocrystal size), photon flux, etc. We will also work to understand and control the dynamics of hole transfer from nanocrystals to electron donors used for the oxidation half reaction in the nanocrystal-enzyme complexes.

## References

- (1) Brown, K. A.; Wilker, M. B.; Boehm, M.; Hamby, H.; Dukovic, G.; King, P. W. *ACS Catal.* **2016**, *6*, 2201-2204.
- (2) Seefeldt, L. C.; Hoffman, B. M.; Dean, D. R. *Annu. Rev. Biochem.* **2009**, *78*, 701-722.
- (3) Brown, K. A.; Harris, D. F.; Wilker, M. B.; Rasmussen, A.; Khadka, N.; Hamby, H.; Keable, S.; Dukovic, G.; Peters, J. W.; Seefeldt, L. C.; King, P. W. *Science* **2016**, *352*, 448-450.
- (4) Knowles, K. E.; McArthur, E. A.; Weiss, E. A. *ACS Nano* **2011**, *5*, 2026-2035.
- (5) Utterback, J. K.; Wilker, M. B.; Brown, K. A.; King, P. W.; Eaves, J. D.; Dukovic, G. *Phys. Chem. Chem. Phys.* **2015**, *17*, 5538-5542.
- (6) Utterback, J. K.; Grennell, A. N.; Wilker, M. B.; Pearce, O. M.; Eaves, J. D.; Dukovic, G. *Nat Chem* **2016**, *8*, 1061-1066.

## Publications in the last 2 years supported by this award

- J. K. Utterback, A. N. Grennell, M. W. Wilker, O. M. Pearce, J. D. Eaves, G. Dukovic. "Observation of trapped-hole diffusion on the surface of CdS nanorods." *Nature Chemistry*, **2016**, *8*, 1061-1066.
- K. A. Brown, D. F. Harris, M. B. Wilker, A. Rasmussen, N. Khadka, H. Hamby, S. Keable, G. Dukovic, J. W. Peters, L. C. Seefeldt, P. W. King. "Light-driven dinitrogen reduction catalyzed by a CdS:Nitrogenase MoFe protein biohybrid." *Science*, **2016**, *352*, 448-450.
- K. A. Brown, M. B. Wilker, M. Boehm, H. Hamby, A. Dubini, G. Dukovic, P. W. King. "Photocatalytic Regeneration of Nicotinamide Cofactors by Biohybrid Quantum Dot-Enzyme Complexes." *ACS Catalysis*, **2016**, *6*, 2201-2204.
- J. K. Utterback, M. B. Wilker, K. A. Brown, P. W. King, J. D. Eaves, G. Dukovic. "Competition Between Electron Transfer, Trapping, and Recombination in CdS Nanorod-Hydrogenase Complexes." *Physical Chemistry Chemical Physics*, **2015**, *17*, 5538-5542.

## Functional Droplets and Particles: Recognition, Repair, and Transport Todd Emrick

Polymer Science and Engineering Department, University of Massachusetts Amherst

**Program Scope.** This project is examining new synthetic polymers and their interfacial interactions in conjunction with surfaces and nanoscale materials, and specifically probing the preparation of smart, functional droplets that engage in biologically-inspired processes. Pioneering theoretical research inspires our experiments, such as that of Balazs which mimics, by computation, the action of osteoclasts and osteoblasts that controls bone remodeling *in vivo*. Adapting these biological and theoretical designs to experimental materials led to our preparation and use of droplets stabilized by reactive/functional polymers, and ultimately experiments in which ‘smart’ droplets successfully pick up and drop off particles on substrates. Building on this concept, we are studying materials that resemble compositions found in Nature, such as functional polymers that adhere to hydroxyapatite (HA), the principle substituent of bone. This is an ideal test case for examining functional droplets as vehicles for the collection, transport, and deposition of particulates as a mimic of osteoclast/osteoblast behavior. Further adaptation of this concept will connect smart droplets to synthetic materials having the size, shape, and functionality of virus and bacteria, where Nature’s lessons associated with cell adhesion leads to advances in materials associated with the localization, encapsulation, and transportation of these anisotropic nano/mesoscale objects.

**Recent Progress.** Our recent research progress has resulted from focus on the fundamental interactions among polymer-stabilized droplets, nanoparticles, and substrates, in which particles are located, transported, and/or delivered by the droplets to specific regions of substrates. Two major themes are presented in detail: 1) the ability of the original ‘repair-and-go’ concept to restore the mechanical integrity of damaged polymer films (*Advanced Functional Materials* 2016)<sup>1</sup> and 2) a mimicking of biological processes associated with cell recognition and repair (*i.e.*, the action of osteoclasts, osteoblasts, and macrophages) in a materials context in which polymer-stabilized droplets pickup nanoparticles from substrates and transport them to defined locations, either on the same substrate or on different substrate (*Science Advances* 2016).<sup>2</sup>

**1. ‘Repair-and-go’ - achieving mechanical restoration of damaged polymer materials.** Surface microcracking compromises the physical/mechanical properties of polymers and motivates discovery of simple methods that achieve the desired repair and, in the process, conserve the materials used to affect restoration. Realizing such a concept would translate to materials science the specificity and recognition capabilities inherent to biology. Following the pioneering theoretical insight of Balazs and coworkers<sup>3</sup> that described artificial leukocytes in materials repair, we developed microencapsulation methods to realize this concept experimentally. Specifically, we showed that microcapsules, in the form of oil-in-water emulsion droplets, can deposit their nanoparticle contents selectively into damaged regions of the polymer films while leaving the pristine surface essentially devoid of particles.<sup>4</sup> Combining microscopy and mechanical characterization techniques on these substrates, following nanoparticle deposition, confirmed the

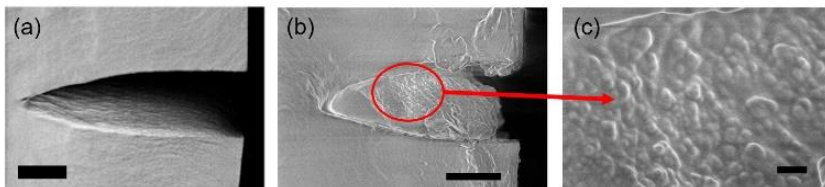


**Figure 1.** Cross-sectional SEM images of (a) a typical crack in the polymer films employed and (b,c) one representative region after SiO<sub>2</sub> NP deposition resulting from ‘repair-and-go’. Scale bars = 2 μm (a, b) and 200 nm (c).

ability of this biomimicry design to deposit significant amounts of nanoparticles into damaged regions of substrates and to effect substantive materials repair.

Scanning electron microscopy (SEM) proved useful for identifying the location of nanoparticles in the polymer film following *repair-and-go* experiments. SEM allowed ‘through-thickness’ visualization of the films and successful probing of the depth of nanoparticle penetration into the cracked regions. SEM samples were prepared by freeze-fracturing the substrate in liquid nitrogen to expose a cross-sectional view. While SEM imaging showed large empty voids in the initially damaged samples (**Figure 1a**, crack width ~ 2 microns; crack depth ~ 8 microns), after *repair-and-go* the presence of nanoparticles in the cracks was evident. For example, **Figure 1b** and **1c** shows spherical objects, representing silica nanoparticles, embedded within the cracks – the dimensions of these features correspond to those of the silica nanoparticles employed in the experiments.

Dynamic mechanical analysis (DMA) was employed to assess the impact of NP deposition on substrate stiffness, with the intention of determining any potential improvement, or other changes, to film mechanics following *repair-and-go* experiments. **Figure 2** plots healing efficiency (or percent recovery of film stiffness) as a function of film thickness, noting that healing efficiency increased as sample thickness decreased, with optimal efficiency reaching 80% and above for the thinner samples. This relationship between healing efficiency and sample thickness is attributed to the larger fractional volume contributed by the nanoparticles to the thinner samples. Importantly, control experiments performed using emulsion droplets containing no encapsulated nanoparticles resulted in no increase in film stiffness, confirming the absence of any solvent or aging effects, and demonstrating the role of nanoparticle deposition in mechanical properties restoration.

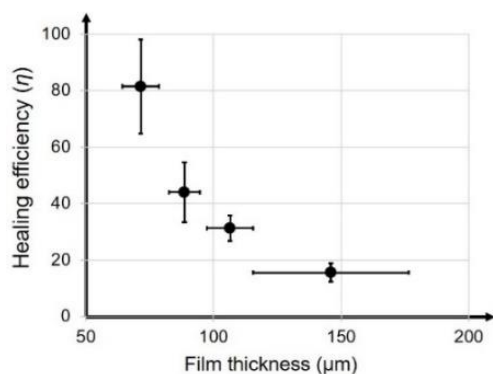


**Fig.2.** Healing efficiency,  $\eta$ , as a function of film thickness.

We sought to augment the beneficial effect of nanoparticle deposition into damaged films with reactive and functional particles amenable to post-deposition curing. For example, *repair-and-go* experiments were performed utilizing a 1:1 weight ratio of epoxy- and amine-functionalized silica nanoparticles, co-encapsulated in oil-in-water emulsion droplets. Post-deposition curing at 90 °C for 4 hours, performed on films containing these reactive nanoparticle healing agents, resulted in essentially full recovery of film stiffness to that of the undamaged film. In another experiment, using only the epoxy-functionalized silica nanoparticles as the crack-filling agent, with a co-encapsulated photo-initiator, UV-triggered post-deposition curing produced films with measured stiffness values that significantly exceeded that of the original polymer film.

**2. Transporting hydroxyapatite nanoparticles (HA NPs) on surfaces.** Experiments inspired by the biological action of osteoclasts and osteoblasts focused on polymer-stabilized emulsion droplets designed to pickup NPs from substrates, carry the NPs for some distance or time period, then deposit the NPs onto a designated surface. The calcium phosphate rich structure of HA NPs,  $(\text{Ca}_5(\text{OH})(\text{PO}_4)_3)$ , reflects the principal materials composition of bone and served as a suitable test case for examining these so-called ‘‘ostedroplets’’ as vehicles for collecting, transporting, and depositing the NPs. A catechol-functionalized zwitterionic polymer surfactant was synthesized for droplet stabilization and to promote electrostatic interactions as well as chelation with  $\text{Ca}^{2+}$  on the NP surface<sup>5</sup> to assist in retrieval and transport. These novel polymers synthesized balance key aspects to enable their

capabilities: 1) suitable amphiphilicity to stabilize the emulsion droplets as they traverse the microfluidic device and come into contact with the substrate; 2) sufficient zwitterionic content to prevent their irreversible adsorption on substrates; and 3) sufficient catechol functionality to promote strong interactions with the HA NPs.

**Figure 3a** shows an optical microscopy image of a silicon substrate which serves as the starting point for these experiments, in which HA NP aggregation produced a visible contrast on the surface by optical microscopy, which was confirmed by SEM to consist of these NPs (in the 50-200 nm range). After the polymer-stabilized droplets traversed the substrate for >100 pulsed intervals, optical microscopy (**Figure 3b**) showed a clean substrate and SEM revealed a complete lack of NPs on the surface, confirming their successful pickup by the catechol-rich droplets. TEM images of dried emulsion droplets after the pickup experiments showed the presence of NPs within the droplet, similar to those of the original HA NP samples (**Figure 3c-d**). Control experiments confirmed the crucial role of using the selected functional polymers in NP pickup. For example, when the pulsed flow was conducted with water only (*i.e.*, no droplets utilized in the flow system), little-to-no NP pickup was observed. In addition, no significant NP pickup occurred when the experiments were conducted with droplets stabilized by polymers lacking catechol functionality. Moreover, NP pickup was modulated by added metal ions, such as  $\text{Ca}^{2+}$  or  $\text{Fe}^{3+}$ , owing to competitive inhibition of the catechol-NP interactions.

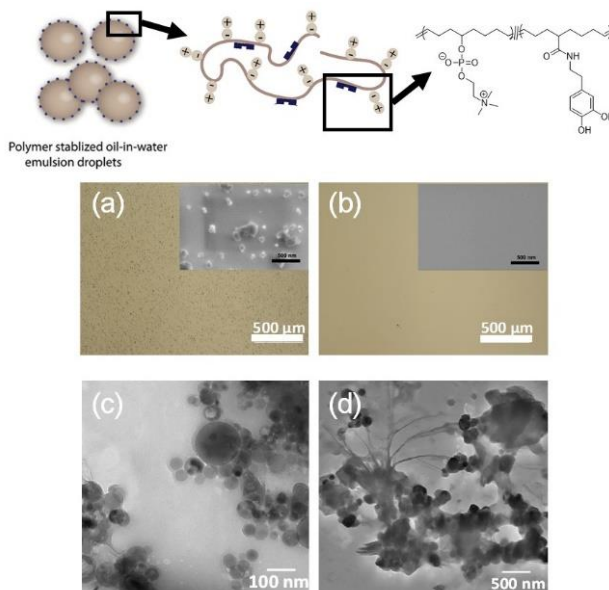


**Figure 3.** (a) Optical and SEM (inset) images of HA NPs coated on Si substrate before attempted NP pickup; (b) optical and SEM (inset) images of the substrate after NP pickup; (c) TEM image of dried HA NPs; (d) TEM image of a portion of a dried droplet showing the presence of HA NPs. Scale bar: 500 nm for insets of (a) and (b).

We also examined the potential for functional droplets to conduct pickup and drop off of NPs in one sequential ‘in-line’ process. For example, experiments were designed to drop off NPs subsequent to the initial pickup event utilizing a polydopamine (PDA)-modified substrate to receive the NPs. As seen in **Figure 4**, HA NP fluorescence was transferred completely from initial silicon substrate (**Figure 4a**) to the PDA-coated substrate (**Figure 4d**). In addition to this fluorescence signature, substrate-to-substrate NP transfer was confirmed by SEM imaging of the HA NPs, as seen in the Figure insets. This experiment represents a key initial step to realizing the concept of *controlled NP relocation* that will be advanced further going forward.

**Future Plans.** The progress described offers rich prospects for future implementation. In one example, substrates containing surface debris resulting from fracture or another damaging event may be healed or repaired using smart

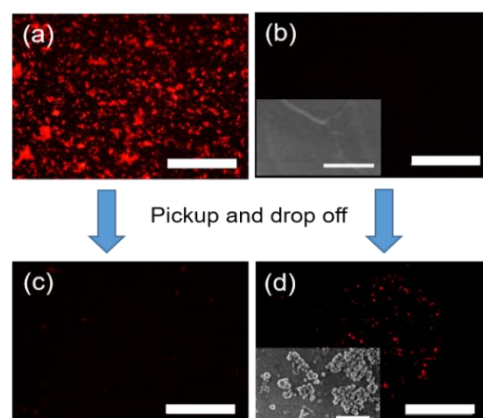


**Figure 4.** Successful pick-up and drop-off of fluorescent HA NPs. Scale bars: 500 nm for the micrographs and 500 nm for the SEM images [insets of (b) and (d)].

droplets tailored with suitable functionality. This offers the potential for *simultaneous cleaning and repairing* of damaged substrates, whereby droplets find debris on the substrates, capture the debris, and transport it to the previously damaged sites for healing. Realizing such concepts would represent a major advance building on our prior work in which nanoparticle-filled droplets were employed to localize filler into damaged regions of substrates. This simultaneous surface cleaning and repair process would simplify self-healing procedures and require minimal outside intervention to accomplish such healing, thus more closely mimicking biological processes associated with cellular capture and release of materials. In a second example of future plans, smart and functional droplets are envisaged for picking up virus- and bacteria-shaped functional materials, focusing on specific interactions between the droplet surface (fluid-fluid interface) and the nano/mesoscale virus/bacteria mimics and comparing the findings to those involving living bacterial microbes or virus particles.

## References

1. Bai, Y.; Chang, C.C.; Zhao, X.; Ribbe, A.; Bolukbasi, I.; Szyndler, M. J.; Crosby, A. J.; Emrick, T., Mechanical restoration of damaged polymer films by “repair-and-go”. *Advanced Functional Materials* 2016, 26(6), 857-863.
2. Bai, Y.; Chang, C.C.; Choudhary, U.; Bolukbasi, I.; Crosby, A. J.; Emrick, T., Functional droplets that recognize, collect, and transport debris on surfaces. *Science Advances* 2016, 2(10), e1601462.
3. Kolmakov, G. V.; Revanur, R.; Tangirala, R.; Emrick, T.; Russell, T. P.; Crosby, A. J.; Balazs, A. C., Using nanoparticle-filled microcapsules for site-specific healing of damaged substrates: creating a ‘repair-and-go’ system. *ACS Nano* 2010, 4, 1115-1123.
4. Kratz, K.; Narasimhan, A.; Tangirala, R.; Moon, S.; Revanur, R.; Kundu, S.; Kim, H.S.; Crosby, A.J.; Russell, T.P.; Emrick, T.; Kolmakov, G.; Balazs, A. C., Probing and repairing damaged surfaces with nanoparticle-containing microcapsules. *Nature Nanotechnology* 2012, 7(2), 87-90.
5. Moriguchi, T.; Yano, K.; Nakagawa, S.; Kaji, F., Elucidation of adsorption mechanism of bone-staining agent alizarin red S on hydroxyapatite by FT-IR microspectroscopy. *Journal of Colloid and Interface Science* 2003, 260(1), 19-25.

## Publications

1. Bai, Y.; Chang, C.C.; Choudhary, U.; Bolukbasi, I.; Crosby, A. J.; Emrick, T., Functional droplets that recognize, collect, and transport debris on surfaces. *Science Advances* 2016, 2(10), e1601462.
2. Bai, Y.; Chang, C.C.; Zhao, X.; Ribbe, A.; Bolukbasi, I.; Szyndler, M. J.; Crosby, A. J.; Emrick, T., Mechanical restoration of damaged polymer films by “repair-and-go”. *Advanced Functional Materials* 2016, 26(6), 857-863.

## EARLY FORMATION STAGES AND PATHWAY COMPLEXITY IN FUNCTIONAL BIO-HYBRID NANOMATERIALS

PI: Lara A. Estroff; Co-PI: Ulrich Wiesner

Department of Materials Science and Engineering, Cornell University, Ithaca, NY 14853

### Program Scope

The focus of this program is on elucidating pathway complexity in interface-driven formation processes of organic-inorganic nanocomposites. We are pursuing two synthetic thrusts and a complementary *in situ* characterization thrust. The two materials systems are chosen to address the role of organic assemblies (System 1) and functionalized, nanopatterned substrates (System 2) in directing the organization of inorganic clusters/particles (amorphous and crystalline) into higher order structures. In System 1 we are investigating the formation of novel 2D silica nanomaterials via a multicomponent organic-inorganic materials assembly process between a structure-directing surfactant, an organic pore expander, and one or more silica precursors. Specifically, we are evaluating the role of different synthesis parameters in determining the nanostructure of never-before seen periodically structured ultrathin 2-D silica sheets. Moving from monolayers to bilayers these sheets may allow, for the first time, observation of the layer-by-layer formation of quasicrystalline structures via interface driven association between inorganic silica clusters and self-assembled organic nanostructures. In System 2 we are using thin films of synthetic block copolymers to direct the growth of inorganic materials. A polystyrene-*block*-poly[(allyl glycidyl ether)-*co*-(ethylene oxide)] (PS-*b*-P(AGE-*co*-EO)) is used to prepare periodically-ordered, reactive thin films. Using thiol-ene click chemistry, the P(AGE-*co*-EO) blocks are selectively modified with a range of organic functional groups, including oligopeptides. These nanostructured substrates are then used to template the solution growth of functional materials such as transition metal oxides. Finally, in a characterization thrust we are applying *in situ* fluid cell atomic force microscopy (AFM) to track interfacial nucleation and growth processes on the nanostructured BCP films with high spatial and temporal resolution. *In situ* AFM will enable mechanistic understanding of the role of the substrate in directing the growth, and in turn will improve our ability to design and control hybrid materials formation. Understanding and controlling formation pathways and organic-inorganic interfaces in hybrid nanomaterials has the potential to be broadly applicable to a range of amorphous and crystalline inorganic materials. Thus results are expected to provide general guidelines and methodologies for the controlled synthesis of hybrid nanomaterials with increasing complexity, offering enormous scientific and technological promise, in areas ranging from energy conversion and storage to catalysis to sensing.

## Recent Progress

### *System 1: Surfactant-directed formation of nanoporous hexagonally ordered 2D silica sheets*

While studying multicomponent organic-inorganic material assembly between a structure directing surfactant (cetyl ammonium bromide, CTAB), an organic pore expander (mesitylene, TMB), and a combination of two types of silanes, tetramethyl-orthosilicate, TMOS, and an amino silane, e.g. aminopropyl trimethoxysilane, APTMS, we observed very thin and periodically structured silica sheets (Fig. 1). Atomic force

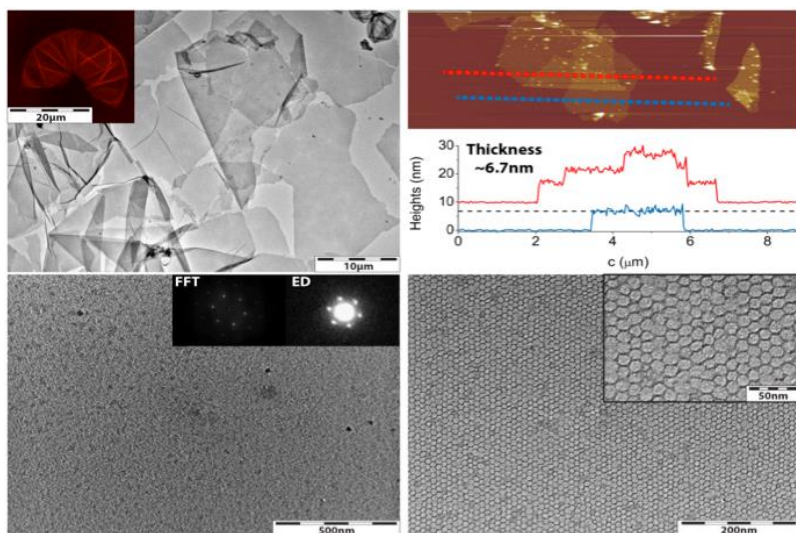


**Fig. 1.** Structural characterization of 2D silica sheets: AFM (upper right), and TEM plus FFT and ED (lower panels).

microscopy (AFM) studies revealed that these silica sheets are 6-7 nm thick (Fig. 1 top) and TEM revealed hexagonally ordered pores (Fig. 1, bottom). Based upon our observations, we propose that these structures form at the TMB-water interface. We hypothesize that the presence of APTMS is key to this association between silica and TMB droplets: At high pH, *i.e.* above the pKa of the amine around 10.6, the aminopropyl group of this silane is not charged and expected to

dive into the hydrophobic TMB droplet, thereby anchoring early silica clusters to the surface.<sup>1,2,3</sup> We further hypothesize that these early silica clusters on the TMB droplet surface electrostatically attract CTAB surfactant micelles to the oil-water interface. The silica sheets can subsequently be isolated and characterized.

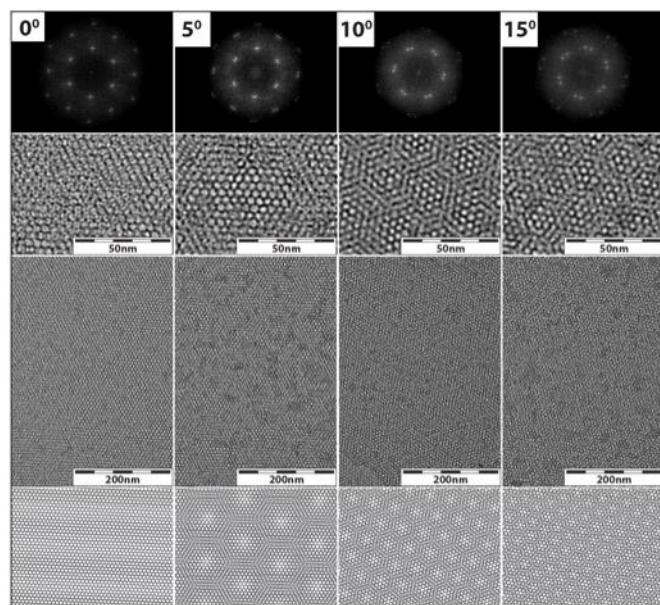


**Fig. 2.** FFTs (top) of a set of TEM images shown at two different magnifications (middle) interpreted in terms of Moiré patterns (bottom) of two hexagonally structured sheets rotated relative to each other.

Under specific reaction conditions, in addition to single layer silica sheets, bilayer formation is observed (Fig. 2). The expected, so called Moiré patterns of such bilayers are shown at the bottom of the figure and are consistent with our TEM observations (middle rows).<sup>4</sup> We therefore are certain that these are bilayer structures.

The fact that the two sets of hexagonal reflexes in the FFT's in Fig. 2 (see 10° and 15° images) are slightly offset suggests that the formation mechanism of these bilayers involves nucleation and growth of a second layer on top of a first one with slightly different periodicity as a result of the changed boundary conditions of growth. Furthermore, often the resulting and fully developed bilayer structures have twelve-fold symmetry and can be tiled by triangles and squares, similar to what we observed for MSNs with dodecagonal quasicrystalline structure.<sup>5</sup> Analysis of details of the associated structure formation processes are ongoing and are complex.

System 2: Block copolymer directed nanostructured surfaces as templates for crystal growth.

We have developed an approach, called *inorganic surface templating on assembled mesostructured polymers* or iSTAMP, to fabricate nanoscale thin film surface structures on the order of 20 nm with the capacity to localize reactions with small molecules and to template the growth of nanostructured, crystalline, transition metal oxides.<sup>6,7</sup> A block copolymer (BCP) of polystyrene-*block*-poly[(allyl glycidyl ether)-*co*-(ethylene oxide)] (PS-*b*-P(AGE-*co*-EO)) was used to prepare a periodically-ordered, reactive thin film (iSTAMP0, Fig. 3). As proof-of-principle demonstrations of the versatility of the chemical functionalization, a small organic molecule, an amino acid, and ultrasmall silica nanoparticles were selectively attached via thiol-ene click chemistry to the exposed P(AGE-*co*-EO) domains of the BCP thin film (iSTAMP1, Fig. 3).<sup>6</sup> The approach employing click chemistry on spatially confined reactive surfaces of BCP thin films overcomes solvent incompatibilities typically encountered when synthetic polymers are functionalized with water-soluble molecules. Moreover, this post-assembly functionalization of a

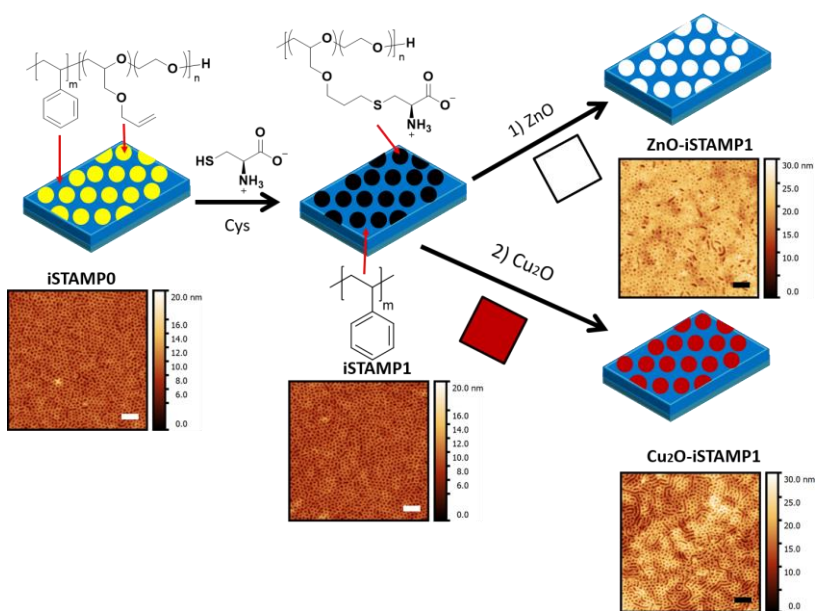


**Fig. 3.** Reaction scheme and representative AFM images of thiol-ene click chemistry performed on nanostructured BCP surfaces followed by selective nucleation and growth of crystalline oxides.<sup>7</sup>

reactive thin film surface preserves the original patterning, reduces the amount of required reactant, and leads to short reaction times.

After functionalization of the hydrophilic domain with the amino acid cysteine, which results in a zwitterionic nanopatterned substrate, we used this template to fabricate crystalline nanostructured inorganics. The functionalized domains template the confined crystallization of copper (I) oxide (Cu<sub>2</sub>O) and zinc oxide (ZnO) with high fidelity,

from aqueous solutions at low temperatures.<sup>7</sup> iSTAMP provides a versatile materials platform to control the growth of nanostructured crystalline materials via the introduction of a plethora of surface functional groups by means of facile thiol-ene click chemistry. The resulting organic substrates can be used to template the growth of multiple different crystalline inorganic materials on surfaces nanostructured via BCP self-assembly.

## Future Plans

For Synthesis System 1, we are systematically varying solution concentrations of the synthesis compounds in order to find out over which synthesis parameter window the 2D sheets are formed and how they vary in structure as a function of solution composition. In addition to the synthesis system consisting of CTAB, TMB, TMOS, APTMS, NH<sub>4</sub>OH, and H<sub>2</sub>O we are exploring other chemical compounds in order to assess (i) whether the silica sheet structures can be systematically modified and (ii) what the limits are of structure formation at the oil-water interface. Finally, we are carefully examining the bilayer structures as a function of reaction time using dry-state as well as cryo-state TEM to elucidate the formation pathway(s) for these intriguing structures.

For Synthesis System 2, we are expanding the diversity of surface functionality introduced into the iSTAMP templates, including carboxylic acid, amino, and alcohol groups. We are assessing how the crystallization changes as a function of surface chemistry, e.g., looking at changes in crystallographic orientation, nanostructure, and selectivity for different oxides. Longer term, we will use the thiol-ene click chemistry to attach peptides to the surfaces to further diversify the chemistry available. We will also change the mesostructure of the polymer thin films by changing the composition of the parent block copolymer.

In parallel with Synthesis System 2, we are preparing to observe, in situ, the nucleation and growth of the oxide materials on the polymer templates using liquid cell AFM. A new AFM was just installed in the PI's lab and we are beginning to characterize the structural changes occurring in the polymer films as a function of pH and ionic strength. In coming months, we will look at the zinc and copper oxide nucleation on these substrates to understand where the first mineral begins to deposit, and how these formation pathway changes as a function of interface chemistry.

## References

1) Suteewong, T.; Sai, H.; Hovden, R.; Muller, D. A.; Bradbury, M.; Gruner, S. M.; Wiesner, U., *Science* **2013**, *340*, 337-341. 2) Ogura, M.; Miyoshi, H.; Naik, S. P.; Okubo, T., *J. Am. Chem. Soc.* **2004**, *126*, 10937-10944. 3) Atluri, R.; Sakamoto, Y.; Garcia-Bennett, A. E., *Langmuir* **2009**, *25*, 3189-3195. 4) MacDonald, A. H.; Bistrizer, R., *Nature* **2011**, *474*, 453-454. 5) Y. Sun, K. Ma, T. Kao, K. A. Spoth, H. Sai, D. Zhang, L. F. Kourkoutis, V. Elser, U. Wiesner, *Nat. Commun.* **2017**, *in press*. 6) Oleske, K. W.; Barteau, K. P.; Turker, M. Z.; Beaucage, P. A.; Estroff, L. A.; Wiesner, U., *Macromolecules* **2017**, *50*, 542-549. 7) Oleske, K.W., Barteau, K.P., Beaucage, P.A., Asenath-Smith, E., Weisner, U., Estroff, L.A. *Cryst. Grow. Des.*, **2017**, *in revision*.

## Publications Supported by BES 2015-2017

- 1) Moore, D.T.; Tan, K.W.; Sai, H.; Barteau, K.P.; Wiesner, U.; Estroff, L.A. “Direct crystallization route to methylammonium lead iodide perovskite from an ionic liquid.” *Chem. Mater.*, **2015**, *27*, 3197.
- 2) Moore, D.T.; Sai, H.; Tan, K.W.; Smilgies, D.M.; Zhang, W.; Snaith, H.J.; Wiesner, U.; Estroff, L.A. “Crystallization kinetics of organic-inorganic trihalide perovskites and the role of the lead anion in crystal growth.” *J. Am. Chem. Soc.*, **2015**, *137*, 2350.
- 3) Zhang, W.; Saliba, M.; Moore, D. T.; Pathak, S.; Horantner, M.; Stergiopoulos, T.; Stranks, S. D.; Eperon, G. E.; Alexander-Webber, J. A.; Abate, A.; Sadhanala, A.; Yao, S.; Chen, Y.; Friend, R. H.; Estroff, L. A.; Wiesner, U.; Snaith, H. J. “Ultra-smooth organic-inorganic perovskite thin-film formation and crystallization for efficient planar heterojunction solar cells.” *Nat. Commun.* **2015**, *6*, 6142.
- 4) Werner, J. G.; Johnson, S. S.; Vijay, V.; Wiesner, U., “Carbon-Sulfur Composites from Cylindrical and Gyroidal Mesoporous Carbons with Tunable Properties in Lithium-Sulfur Batteries.” *Chem. Mater.* **2015**, *27*, 3349-3357.
- 5) Sun, Y.; Sai, H.; Spoth, K. A.; Tan, K. W.; Werner-Zwanziger, U.; Zwanziger, J.; Gruner, S. M.; Kourkoutis, L. F.; Wiesner, U., “Stimuli-Responsive Shapeshifting Mesoporous Silica Nanoparticles.” *Nano Lett.* **2016**, *16*, 651-655.
- 6) Song, R.-Q.; Hoheisel, T. N.; Sai, H.; Li, Z.; Carloni, J. D.; Wang, S.; Youngman, R. E.; Baker, S. P.; Gruner, S. M.; Wiesner, U.; Estroff, L. A., “Formation of Periodically-Ordered Calcium Phosphate Nanostructures by Block Copolymer-Directed Self-Assembly.” *Chem. Mater.* **2016**, *28*, 838-847.
- 7) Susca, E. M.; Beaucage, P. A.; Hanson, M. A.; Werner-Zwanziger, U.; Zwanziger, J. W.; Estroff, L. A.; Wiesner, U., “Self-Assembled Gyroidal Mesoporous Polymer-Derived High Temperature Ceramic Monoliths.” *Chem. Mater.* **2016**, *28*, 2131-2137.
- 8) Oleske, K. W.; Barteau, K. P.; Turker, M. Z.; Beaucage, P. A.; Estroff, L. A.; Wiesner, U., “Block copolymer directed nanostructured surfaces as templates for confined surface reactions.” *Macromolecules*, **2017**, *50*, 542-549.
- 9) Sun, Y.; Ma, K.; Kao, T.; Spoth, K. A.; Sai, H.; Zhang, D.; Kourkoutis, L. F.; Elser, V.; Wiesner, U., “Single particle growth trajectories of mesoporous silica nanoparticles with dodecagonal tiling.” *Nature Commun.* **2017**, *in press*.
- 10) Oleske, K.W., Barteau, K.P., Beaucage, P.A., Asenath-Smith, E., Weisner, U., Estroff, L.A. “Nanopatterning of Crystalline Transition Metal Oxides by Surface Templated Nucleation on Block-Copolymer Mesostructures” *Cryst. Grow. Des.*, **2017**, *in revision*.

## **Material lessons of biology: Proteomic based nanoporous materials at the mesoscale.**

**John Spencer Evans, Department of Craniofacial Medicine and Skeletal Biology, New York University College of Dentistry, New York, NY 10012**

### **Program Scope**

Biological organisms offer many potential models where multiple material properties and construction phenomena intertwine at the mesoscale. A case in point is biomineralization, a process by which organisms employ unique and important assembly mechanisms to create inorganic skeletal elements over different length scales (nano to macro).<sup>1</sup> In some biomineralizing systems, such as the invertebrate mollusk, the shell possesses some very energy-relevant material properties. For example, in mollusk shell nacre mesoscale aragonite tablets possess the properties of fracture-toughness and resistance to crack propagation and these features provide the mollusk with a protective armor that resists pressures (and predators) at underwater depths under high salinity conditions.<sup>2</sup> Once the shell has formed the mollusk retains the ability to repair and regenerate portions of the shell that do experience fracture.<sup>3</sup>

Recent evidence indicates that each single mesocrystal tablet arises from the guided assembly of core-shell spherical nanoparticles or nanograins of calcium carbonate.<sup>2</sup> This assembly process is aided and abetted by numerous protein families or *proteomes* are expressed during shell formation and appear in the mineral matrix.<sup>4</sup> The nacre matrix exists as a hydrogel-like environment,<sup>5</sup> and this environment is formed by the proteomes. A hydrogel environment<sup>6</sup> could easily satisfy three important requirements for nacre mesoscale tablet formation: a) create small limited volume compartmentalization and controlled hydration and ion diffusion which regulates the nucleation kinetics and transformation of mineral nanoparticles; b) allow nanoparticle assembly to occur as the gel phase itself assembles; and c) upon expansion of the mineral phase, portions of the hydrogel phase could become entrapped within the mineral phase and subsequently create organic-containing nanoporosities which serve as regions to prevent crack propagation, induce fracture-resistance, and create a porous material.

### **Recent Progress**

Our previous studies with representative pairs from each nacre protein classification revealed that these disordered, amyloid-like proteins that are strong aggregators and form disordered phases.<sup>A-F</sup> Further, in the aggregated state these proteins can up/down regulate the kinetics and stability of mineral precursors known as pre-nucleation clusters (PNCs) in different ways,<sup>A,D-F</sup> suggesting that it is the protein phase, and not the individual protein molecules, that manipulate the nucleation process *in vitro*.

*a) Hydrogelation.* We investigated 6 nacre-associated proteins and discovered that they exist as mesoscale porous translucent hydrogel particles in solution (**Fig 1**).<sup>A-F</sup> Moreover, biochemical studies confirmed that these porous hydrogel particles are in fact “smart” hydrogels,<sup>6</sup> in that they

morphologically and internally respond to changes in pH and  $\text{Na}^+$ ,  $\text{Ca}^{2+}$ , and  $\text{Mg}^{2+}$  ionic environments (as an example, **Fig 1**),<sup>A,C-F</sup> analogous to the “smart” polymer-based hydrogels described in the literature.<sup>6</sup> The fact that these protein hydrogels nucleate, assemble, and confine mineral nanoparticles *in vitro* within their matrices earmarks them as “composite” hydrogels, i.e., polymeric-based hydrogels that assemble or capture nanoparticles.<sup>6</sup> Hence, the nacre protein hydrogel (*hereafter abbreviated as NPH*) systems are “smart”, “composite” hydrogel systems and thus highly interesting from a nanotechnology and energy materials standpoint.

*b) NPHs affect solvent and solute diffusion.* Recent studies show that hydration plays an important role in the early stages of nucleation (i.e., water removal during ion cluster association) and could affect the stability of pre-nucleation cluster precursors as well as ACC.<sup>7</sup> We postulate that NPHs impact the availability and movement of water,  $\text{Ca(II)}$ , and carbonate/bicarbonate ions, and in doing so, manipulate the kinetics of the nucleation process and possibly the thermodynamic stability of ion clusters, including ACC.

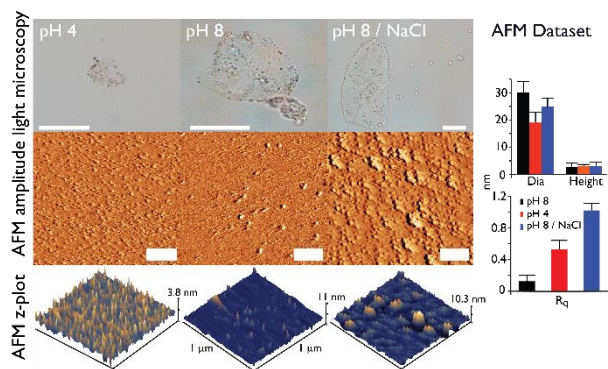


**Fig. 1.** Multiscale imaging of 1.3  $\mu\text{M}$  r-n16.3 protein hydrogels in 8.9 mM  $\text{NaH}_2\text{PO}_4$  (pH 4.0), 10 mM HEPES (pH 8.0), and 30 mM  $\text{NaCl}$ /10 mM HEPES (pH 8 /  $\text{NaCl}$ ). Light microscope images taken at 100x magnification of 30  $\mu\text{M}$  r-n16.3 samples. AFM tapping mode amplitude images are plotted at 1  $\mu\text{m}$  x 1  $\mu\text{m}$ . Scalebars in light microscope images = 10  $\mu\text{m}$ , in AFM = 200 nm.

To test this, we investigated the diffusion of a small anionic tracer,  $\text{Na}_3\text{PO}_4$  at pH 8.0 (equivalent to mineralization pH) in the bulk state and in the presence of 22  $\mu\text{M}$  r-AP7 and r-n16.3 hydrogel solutions using  $^{31}\text{P}$ -NMR DOSY experiments at 25  $^\circ\text{C}$  (DOSY = Diffusion Ordered Spectroscopy). In the DOSY experiment phosphate molecules become spatially labeled, based on their position in the NMR

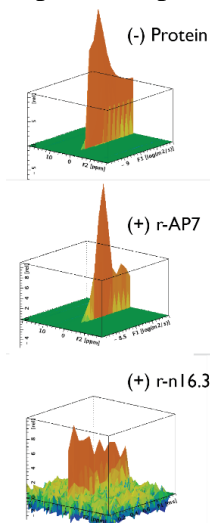


**Fig 2.** 2-D  $^{31}\text{P}$  NMR DOSY experiment of 1 mM  $\text{Na}_3\text{PO}_4$  (pH 8.0) in the absence (-) and presence (+) of 22  $\mu\text{M}$  rAP7 or r-n16.3.  $^{31}\text{P}$  NMR chemical shifts referenced from 85%  $\text{H}_3\text{PO}_4$ . Evans group, unpublished.

tube. If the phosphate molecule moves after the encoding, or ‘labeling’, during the diffusion time ( $\Delta$ ) that follows in the pulse sequence, then its new position can be decoded with a second gradient and a temperature-dependent diffusion coefficient can be calculated. Thus, any phosphate molecules which interact with either hydrogel particle ensemble should exhibit a noticeable change in their diffusion coefficients relative to species in the bulk state (i.e., in the absence of protein). As shown in **Fig 2**, relative to the bulk, protein-free state where only 1 diffusion regime exists (single peak), phosphate molecules in the presence of r-AP7 exist in two different diffusion regimes (x-axis) as indicated

by the two peaks along the y-axis (log diffusion coefficient). Surprisingly, in the presence of r-n16.3, the phosphate diffusion profile is more complex (~5 different peaks), or > 2x that of r-AP7. Thus, we find that NPHs differ in their solute diffusion profiles. This may be relevant to the tasks that each protein performs during the nucleation and crystal modification processes.

c) *Combinatorial proteomics*. Realizing that the nacre layer mineral formation involves the participation of numerous ECM proteins with temporal and spatial considerations<sup>4</sup> we have migrated our research towards the study of nacre protein *ensembles*. The idea here was to analyze protein combinations and their impact on the early and later stages of calcium carbonate nucleation. The novelty here is that we are utilizing defined mole stoichiometries of each protein, testing proportionality and cooperativity, and learning how these factors impact the outcome of in vitro biomineralization. Such information would be extremely powerful: within an in vitro environment we would be more closely approximating what the mollusk does in situ and at the same time provide the energy-based materials community with information on how multiple components and their ratios influence the formation of mesoscale inorganic materials.

Our first test combinatorial case was rAP7 + rPFMG1, two unrelated nacre proteins.<sup>E</sup> They occur in different mollusks (*H. rufescens* versus *P. fucata*) and at different places (shell nacre versus pearl nacre). Initially, we envisioned this pair as a “negative control”, i.e., rAP7 and rPFMG1 would not be expected to exhibit intermolecular interactions or synergistically control nucleation. Contrary to what we expected, both proteins functioned cooperatively and jointly create a hydrogel that resembles a polymer-induced liquid precursor phase, and this phase generates a *second* ACC nucleation event that occurs over a longer time scale and is less stable than the primary event.<sup>E</sup>

Our second test case was taken from the *P. fucata* pearl proteome and featured rPFMG1 + rPFMG2 which are co-expressed during pearl formation<sup>A</sup> and thus represent a “natural” pair unlike the “random” rPFMG1 + rAP7 pairing.<sup>E</sup> Here, we found very different results at 1:1 molar ratios: a) unlike r-AP7 + rPFMG1, rPFMG2 + rPFMG1 co-aggregate in specific molecular ratios to form hybrid hydrogels (**Fig 9**); b) within this hydrogel each protein plays a specific role in the early stages of nucleation. rPFMG2 determines the size of the hydrogel assemblies and regulates the internal structure of the protein films, whereas rPFMG1 enhances the stability of tiny ionic clusters that combine to form calcium carbonate layers of pearl. c) However, once mineral crystals form, PFMG1 and PFMG2 work together and put the finishing touches to the mineral phase by synergistically modifying the mineral crystal surfaces and creating internal porosities. d) The interactions between both proteins is enhanced by Ca(II) ions and may involve Ca(II)-induced interactions between the EF-hand domain of rPFMG1 and the calponin-like domain of rPFMG2. This is the first combinatorial study of the pearl proteome system, and it shows that the role of the PFMG proteins in pearl formation is more complex than we think.

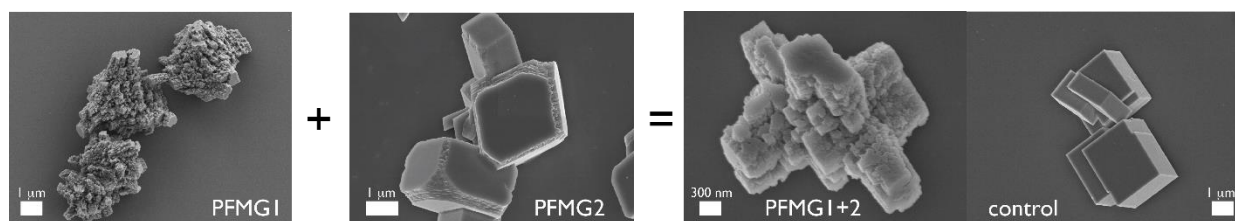


**Fig 3.** SEM images of Si-wafer collected calcite crystals generated in the presence of rPFMG1, rPFMG2, 1:1 rPFMG1:rPFMG2 and protein-deficient control assays (control). Ref 52.

## Future Plans

We will continue to push the boundaries of these fields such that the molecular principles behind protein-mediated nucleation, nano-to-mesoscale assembly, and nanoparticle organization will find their way to energy-related materials development. We will proceed along the following lines of investigation: a) Investigate hydrogel metalation, diffusion effects, and nanoparticle organization within model representatives of each nacre proteome; b) Probe sequence requirements for hydrogelation and mineralization within model representatives of each nacre proteome; c) Perform an *in vitro* study of the pearl proteome: functionality and interactions.

## References

- 1 Wegst, U.G.K., Bai, H., Saiz, E., Tomsia, A.P., Ritchie, R.O. (2015) Bioinspired materials. *Nature Materials* **14**, 23-36.
- 2 Li, X., Chang, W.C., Chao, Y.J., Wang, R., Chang, M. (2004) Nanoscale structural and mechanical characterization of a natural nanocomposite material: The shell of red abalone. *NanoLetters* **4**, 613-617.
- 3 Su, X.W., Zhang, D.M., Heuer, A.H. (2004) Tissue regeneration in the shell of the giant queen conch, *Strombus gigas*. *Chem. Mat.* **16**, 581-593.
- 4 Zhang, G., et al., (2012) The oyster genome reveals stress adaptation and complexity of shell formation. *Nature* **490**, 49-54.
- 5 Nudelman, F., Shimoni, E., Klein, E., Rousseau, M., Bourrat, X., Lopez, E., Addadi, L., Weiner, S. (2008) Forming nacreous layer of the shells of the bivalve *Atrina rigida* and *Pinctada margaritifera*: An environmental and cryo-scanning electron microscopy study. *J. Struct. Biol.* **162**, 290-300.
- 6 Du, X., Shi, J., Xu, B. Supramolecular hydrogelators and hydrogels: From soft matter to molecular biomaterials. *Chem Rev.* **2015**, *115*, 13165-13172.
- 7 Sebastiani, F., Wolf, S.L.P., Born, B., Luong, T.Q., Cölfen, H., Gebauer, D., Havenith, M. (2017) Water dynamics from THz spectroscopy reveal the locus of a liquid-liquid bimodal limit in aqueous calcium carbonate solutions. *Angew. Chem.* **56**, 490-498.

## Publications

A) Jain, G., Pendola, M., Huang, Y.C., Colas, J.J., Gebauer, D., Johnson, S., Evans, J.S. (2017) Exploring the pearl proteome: Functional prioritization and hydrogel regulation phenomena created by a combinatorial pearl-associated 2-protein model system. *Biochemistry*, in press.

B) Evans, J.S. (2017) Polymorphs, proteins, and nucleation theory: A critical analysis. *Minerals* **7**, 62, doi:10.3390/min7040062.

C) Perovic, I., Davidyants, A., Evans, J.S. (2016) Aragonite-associated mollusk shell protein aggregates to form mesoscale “smart” hydrogels. *ACS Omega* **1**, 886-893.

D) Pendola, M., Jain, G., Davidyants, A., Huang, Y.C., Gebauer, D., Evans, J.S. (2016) A nacre protein forms mesoscale hydrogels that “hijack” the biomineralization process within a seawater environment. *Cryst. Eng. Commun.* **18**, 7675-7679.

E) Chang, E.P., Roncal-Herrero, T., Morgan, T., Dunn, K.E., Rao, A., Kunitake, J.A.M.R., Lui, S., Bilton, M., Estroff, L.A., Kröger, R., Johnson, S., Cölfen, H., Evans, J.S. (2016) Synergistic biomineralization phenomena created by a combinatorial nacre protein model system. *Biochemistry* **55**, 2401-2410.

F) Chang, E.P., Perovic, I., Rao, A., Cölfen, H., Evans, J.S. (2016) Insect cell glycosylation and its impact on the functionality of a recombinant intracrystalline nacre protein, AP24. *Biochemistry* **55**, 1024-1035.

## **Programmable dynamic self-assembly of DNA nanostructures**

**PI: Elisa Franco, Mechanical Engineering, University of California at Riverside, Riverside, CA 92521**

**(collaborative project with Rebecca Schulman, Johns Hopkins University)**

### **Program Scope**

The synthesis of novel materials with self-regulation properties akin to those of biological cells is a central challenge in biomolecular materials research. In biological systems, behaviors such as growth, division, and self-repair emerge because molecular self-assembly processes are coupled to and directed by signal transduction and gene expression networks. The goal of this project is to construct synthetic materials with similarly complex structure, where the capacity for adaptive, dynamic responses is achieved by coordinating synthetic self-assembly processes with synthetic molecular circuits and control systems.

### **Recent Progress**

1. We connected dynamic and structural DNA nanotechnology and demonstrated the programmable, dynamic control of self-assembly of DNA nanotubes, a well-known class of micron-sized DNA nanostructures. Control of nanotube assembly is achieved with minimal synthetic gene systems, including an autonomous molecular oscillator. The results are presented in detail in Figure 1. We used a coarse-grained computational model to capture nanotube length distribution dynamics in response to inputs from nucleic acid circuits. Our demonstration opens new avenues for the construction of active nucleic acid materials that can adapt and respond to environmental stimuli, with applications in biomaterials science, nanofabrication, and drug delivery.
2. During the above experiments, we also discovered that RNA polymerases that we use in synthetic genetic circuits destabilize some of the DNA nanostructures. In collaboration with the research group of co-PI Schulman, we characterized the stability of different variants of DNA nanotubes in the presence of different RNA polymerases. We found that certain sequences in sticky-ends of the DNA nanotube monomers (tiles) can resist RNA polymerases better than others. We also found that T7 RNA polymerase (RNAP) can transcribe RNA from the DNA tiles in the nanotube, which suggests a potential mechanism through which the T7 RNAP destabilizes the nanotube.
3. In an attempt to create isothermally assembling nucleic acid nanostructures in presence of a synthetic gene that transcribes one of its components, we designed a hybrid DNA-RNA tile that can assemble into nanotubes. We have demonstrated that such hybrid tiles can form robust nanostructures when annealed. Experiments are in progress to attempt isothermal assembly.

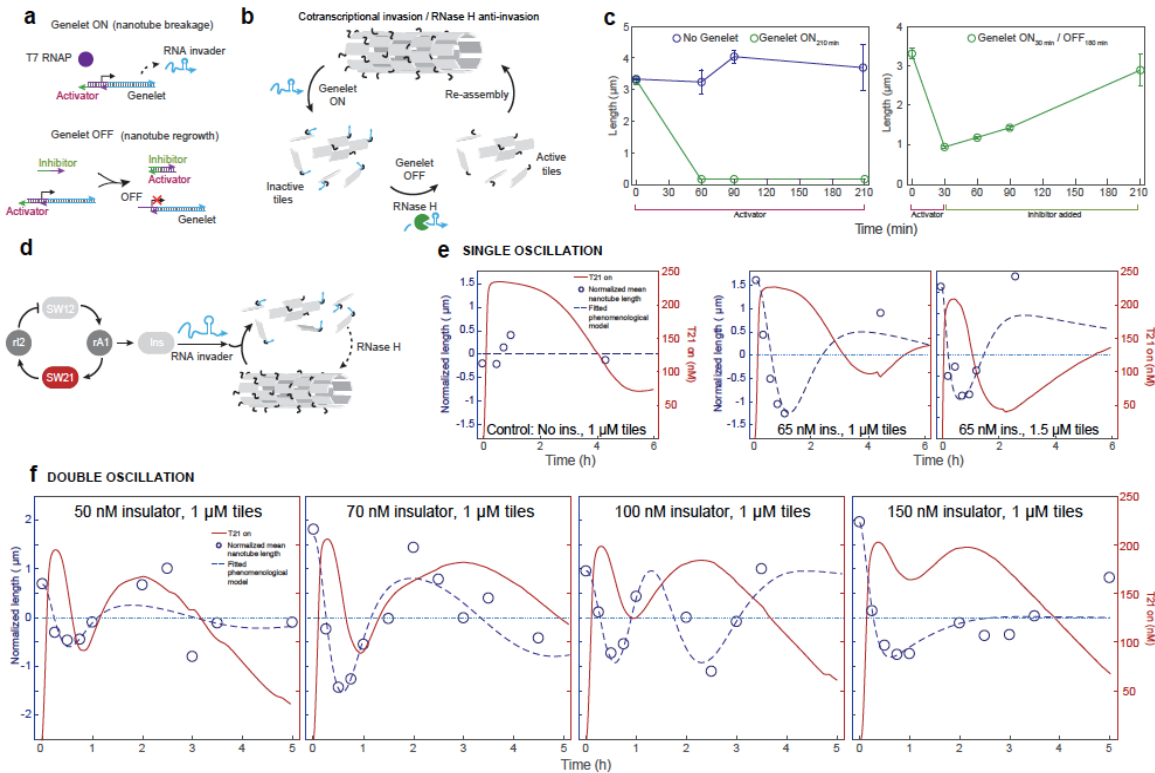


Figure 1: Transcriptional control of nanotube self-assembly. a: A synthetic transcriptional template, or genelet, is ON when the incomplete T7 promoter domain is bound to the activator strand. In the presence of T7 RNA polymerase, RNA invader is produced (top). The genelet is turned off by toehold-mediated displacement of activator by a DNA inhibitor strand (bottom). b: Reaction scheme of cotranscriptional invasion of nanotubes. c: Left: In the absence of genelet, but in the presence of RNAP and RNase H and transcription conditions, the mean nanotube length remains constant (blue). In the presence of genelet ON, nanotubes break and remain disassembled (green). Right: If the genelet is switched off (after 30 minutes from the beginning of the experiment), RNase H degradation dominates the reaction and promotes nanotube regrowth (green). d: Schematic diagram - An insulating genelet is coupled to the oscillator and produces RNA invader; RNase H degradation promotes nanotube regrowth when the invader production rate is low. The insulator genelet is ON when SW21 is ON; thus, the invader production rate reaches its maximum when SW21 is fully active, and nanotubes are expected to break. Fluorimetry experiments report the fraction of active SW21 (red node). e: The concentration of active SW21 concentration is shown in red. We sampled nanotube length at specific time points and we report their normalized mean length (blue circles). A phenomenological fit was used to normalize length as explained in the text. Left: The normalized mean length of nanotubes incubated in the presence of oscillator, but in the absence of insulator genelet, remains constant. Center: In the presence of 65 nM insulator, we varied the total tile concentration. At 1 μM tile concentration, as SW21 becomes active we observe a corresponding decrease of the normalized nanotube mean length; the mean length increases again as SW21 becomes inactive. Right: we observe a similar trend at 1.5 μM tile concentration. The oscillator behavior is affected by the high concentration of tiles, because invader-bound tiles sequester RNase H. f: Keeping the tile concentration fixed at 1 μM tiles, we varied the insulator genelet concentration. At intermediate insulator concentrations (70nM and 100 nM), the nanotube mean length oscillates as it is coupled well with the oscillator circuit.

4. The current design of the dynamic DNA nanotubes requires one activating component (anti-invader, which promotes growth) or deactivating component (invader, which breaks the tube) per tile. And upon activation/deactivation the component is used up permanently and cannot be reused. This is an inefficient system. In biology, many such dynamic tasks are executed efficiently using catalysts. Inspired by biology, we have designed a catalytic activation and deactivation system for our dynamic DNA nanotubes. The catalyst is based on entropy driven strand displacement reactions published by Zhang et al. [1]. We plan to use this catalyst to localize the growth/breakage of nanotubes at specific points in space, by fixing the catalyst at desired locations. Using such spatially controlled dynamics, one could potentially create highly complex motility systems like the one used by *Listeria Monocytogenes* (actin rockets) [2].

5. Biological materials have the capacity for homeostasis and adaptation. For example, cellular scaffolds maintain their size and stiffness in a range of temperatures, and adapt their shape under mechanical stimuli. These behaviors require the presence of feedback. We have identified a simple and general approach for homeostasis in biomolecular networks that relies on ultrasensitive motifs. Computational studies, characterizing the effectiveness of the controllers in the context of single cell gene expression have been recently published in two conference papers.

### **Future Plans**

In the next year we plan to:

A. Complete the characterization of spatial and motility control of nanotube assembly using catalytic circuits (Item 4 above).

B. Build in vitro ultrasensitive motifs for closed loop control using a) RNA aptamers, and b) the CRISPR/Cas9 system. These controllers will be used first to regulate in vitro transcription, and later on to regulate nanotube growth (Item 5 above).

C. Complete and publish our results on the hybrid DNA-RNA nanotubes (Item 3 above).

### **References**

[1] Zhang, D. Y., Turberfield, A. J., Yurke, B., & Winfree, E. (2007). Engineering entropy-driven reactions and networks catalyzed by DNA. *Science*, 318(5853), 1121-1125.

[2] Lambrechts, A., Gevaert, K., Cossart, P., Vandekerckhove, J., & Van Troys, M. (2008). *Listeria* comet tails: the actin-based motility machinery at work. *Trends in cell biology*, 18(5), 220-227.

## **Publications**

Cuba Samaniego, C. and Franco, E. An ultrasensitive biomolecular network for robust feedback control. To appear. 2017 In the Proceedings of the 20th World Congress of the International Federation of Automatic Control, Toulouse, France.

Cuba Samaniego, C. and Franco, E. An ultrasensitive motif for robust closed loop control of biomolecular systems. Accepted. 2017 IEEE Conference on Decision and Control, Melbourne, Australia.

Green, L.N., Subramanian, H.K.K., Mardanlou, V., Kim, J., Hariadi, R.F. and Franco, E., 2017. Autonomous dynamic control of DNA nanostructure self-assembly. Submitted and under peer review at **Nature Chemistry**.

Green, L. N., Amodio, A., Subramanian, H.K.K., Ricci, F., Franco E., 2017. pH-driven reversible self-assembly of micron-scale DNA scaffolds. Submitted to **Nano Letters**.

Mardanlou, V., Green, L.N., Subramanian, H.K.K., Hariadi, R.F., Kim, J. and Franco, E., 2017. A coarse-grained model captures the temporal evolution of DNA nanotube length distributions. Under second round of review with **Natural Computing**.

Mardanlou, V., Green, L.N., Subramanian, H.K.K., Hariadi, R.F., Kim, J. and Franco, E., 2016, September. A Coarse-Grained Model of DNA Nanotube Population Growth. In International Conference on DNA-Based Computers (pp. 135-147). Springer International Publishing.

## **Program Title: Bioinspired Design of Multifunctional Dynamic Materials**

**Principle Investigator: Zhibin Guan, Ph.D.**

**Mailing Address: 1102 Natural Sciences II, Irvine, CA 92697**

**Email: zguan@uci.edu**

### **Program Scope**

The aim of this project is to develop new strategies for designing strong self-healing and dynamic materials for potential energy relevant applications. Several major advances have been made in the last two years toward the design of strong self-healing polymers as well as polymers with unique dynamic properties. In particular, we have demonstrated in several examples the power of using molecular design to dramatically tune the dynamic properties of the bulk materials. Specifically, (1) we established boronic ester exchange as a new dynamic covalent bond for malleable and self-healing polymer design; (2) we demonstrated for the first time the use of Si-O exchange for design dynamic covalent networks (CANs) or vitrimers; and (3) using dynamic metal-ligand interactions, we have created gradient polymer networks having the largest continuous mechanical gradient. Such dynamic and self-healing materials may find important applications in energy production, environmental impact, energy security, and energy saving.

### **Recent Progress**

#### **1. Tune Boronic Ester Exchange Kinetics for Malleable and Self-Healing Polymer Designs**

For many materials applications, the tunability of their dynamic properties is critical. Despite numerous strategies involving dynamic covalent bond exchange for dynamic and self-healing materials, it remains a challenge to be able to tune the malleability and self-healing properties of bulk materials through simple small molecule perturbations. In this study we demonstrated the use of kinetically tunable rates of boronic ester transesterification to effectively tune the malleability and self-healing efficiencies of bulk materials. By placing simple amino substituent at the neighboring group or an aromatic boronic ester, we showed dramatic acceleration of boronic ester exchange in solution, melt and bulk solid. This offers a new tunable dynamic covalent linkage for dynamic material design.

Specifically, we used two telechelic di-boronic ester small molecules (**3** & **4**) with variable transesterification kinetics to dynamically crosslink 1,2-diol-containing polymer backbones (**Figure 1**). We found that the sample crosslinked with fast-exchanging di-boronic ester (**4**) showed enhanced dynamics in solution and gels, which correlates with improved malleability and accelerated healing in bulk compared to the slow-exchanging variant (**3**) under the same conditions. We have successfully demonstrated that the dynamic boronic ester linkage can be used to prepare malleable, self-healing, and reprocessable covalent network polymers. Significantly, tuning the rates of trans-esterification in the crosslinkers varied the malleability and the efficiency of self-healing, demonstrating a direct link between small molecule kinetics and rate of self-healing. This work shows the possibility of bottom-up rational design of dynamic materials with tunable dynamic properties through simple perturbations of small molecule structure and kinetics, which may give rise to materials with a variety of applications, ranging from robust self-healing elastomers to processable thermosets.

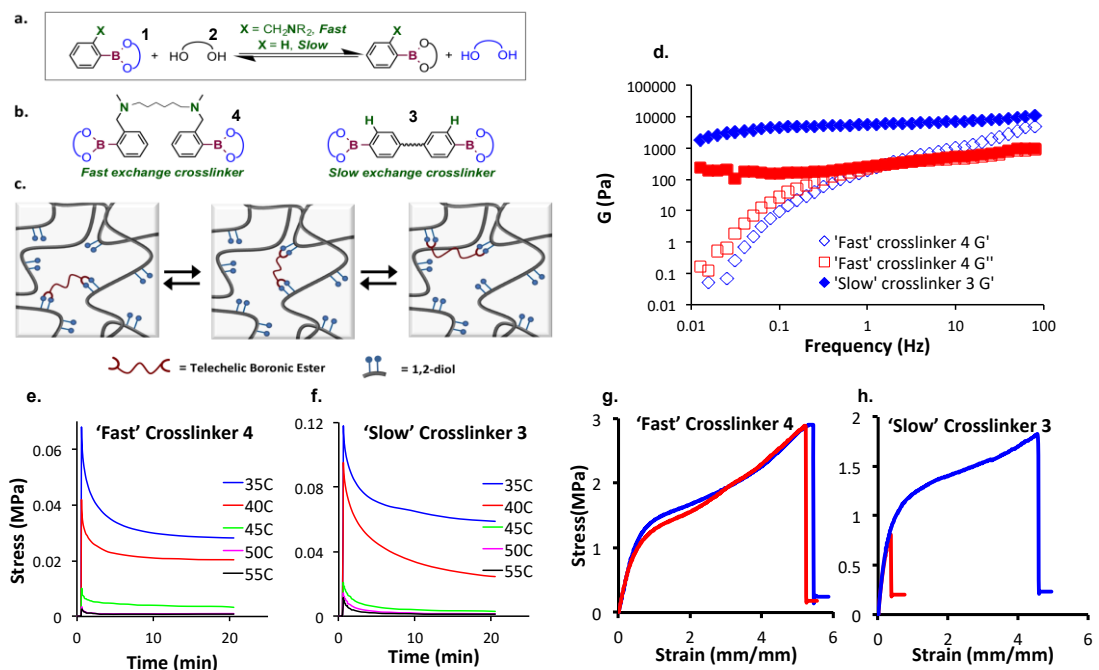


**Figure 1.** Boronic ester-based dynamic polymer network. **a-c:** Design concept and tunable crosslinkers; **d:** Tunable dynamic properties in gel form; **e-f:** Tunable dynamic properties in bulk; **g-h:** Tunable self-healing efficiency via molecular design.

## 2. Silicon-oxide as a New Dynamic Covalent Motif for Dynamic Polymer Design

Silicon-oxide bond is ubiquitous in natural and synthetic materials. The scope of material properties of Si-O based materials is vast, ranging from polydimethylsiloxanes (PDMS), among the softest of rubbers, to inorganic glass, an extremely strong and hard material. Furthermore, the high chemical and thermal stability of Si-O linkage also makes it a desirable motif for the design of robust dynamic materials. Despite these attractive features, Si-O bond has not been explored for the design of dynamic polymer materials.

Recently, we successfully demonstrated Si-O linkage as a new dynamic covalent motif for dynamic material design. Through minimal molecular perturbation, i.e., the introduction of a neighboring amino moiety, we show that the Si-O bond exchange rate can be accelerated by almost three orders of magnitude. By incorporating such Si-O linkage into covalently crosslinked polymer networks, we demonstrate dynamic covalent network polymers displaying both malleability and reprocessability. The malleability of the networks were studied by monitoring stress relaxation at varying temperature and their topology freezing temperatures ( $T_v$ ) were determined. Notably, this is thus far the only example of using autocatalysis to control the vitrimer topology freezing temperature ( $T_v$ ). Furthermore, this is the first experimental observation of a transition from Williams–Landel–Ferry (WLF) behavior to Arrhenius behavior for the temperature dependence of the viscosity for the networks because of a special case scenario of  $T_v$  (47 °C)  $\ll$   $T_g$  (125 °C), providing direct support to both the theory of topology freezing through molecular kinetic arrest of vitrimers, as well as the mechanism of fluidity of the system described in this paper. Finally, the tunable exchange dynamics coupled with the high thermal stability and reprocessability of Si-O based polymers should allow for broad applications for this family of materials. We are currently investigating the use of Si-O bond exchange for various other dynamic material designs.

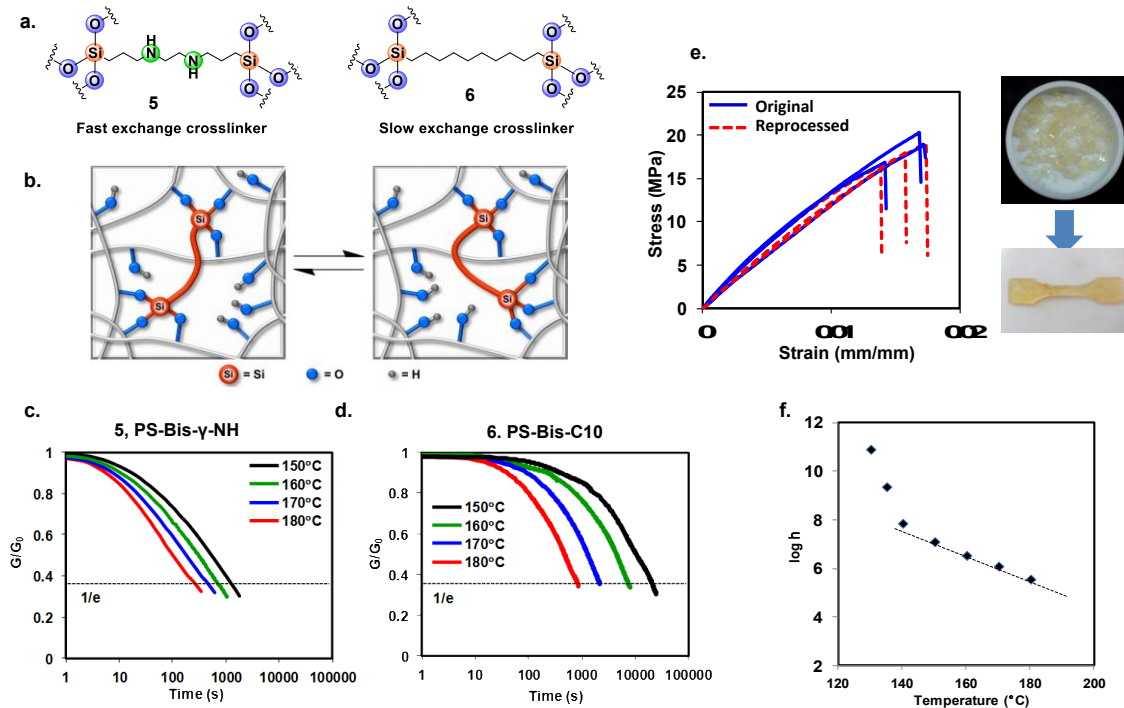


**Figure 2.** Si-O based vitrimer design. **a-b:** Design concept and tunable crosslinkers; **c:** Different stress relaxation for fast and slow dynamic networks; **e:** Reprocessability of the covalent network; **f:** Unique transition from WLF to Arrhenius behavior for the viscosity of the network.

### 3. Large Continuous Mechanical Gradient Formation via Metal-Ligand Interactions

Mechanical gradients are often employed in nature to prevent damage from large forces by creating a smooth transition from strong to weak biological materials. Synthetic mimics of these natural structures are highly desired to improve distribution of stresses at interfaces and reduce contact deformation in manmade materials. Current synthetic gradient materials commonly suffer from non-continuous transitions, relatively small gradients in mechanical properties, and difficult syntheses. Inspired by the polychaete worm jaw, we have developed a novel approach to generate stiffness gradients in polymeric materials via incorporation of monodentate, dynamic metal-ligand crosslinks. Through spatial control of metal ion content, we create a continuous mechanical gradient that spans over a 200-fold difference in stiffness, approaching the mechanical contrast observed in biological gradient materials.

The metal-ligand network demonstrated in this work represents the largest continuous gradient change in mechanical properties observed to date at over two orders of magnitude, representing a dramatic improvement in gradient materials. In addition, using only a two-step synthesis and a common laboratory syringe pump, the metal-ligand gradient materials can be reliably produced showing their broad appeal and ease of synthesis. We anticipate that introduction of these types of monodentate, metallopolymer gradients will spur further studies into the biomimetic, dissipative materials. With more rigorous engineering control (pull rate, temperature, metal added), materials with even much larger mechanical gradients could feasibly be obtained. In addition, the flexibility of this system will allow for a variety of different mechanical gradients to be studied using different metals, labile ligands, and counterions. Ongoing studies pursuing these goals, as well as gaining more mechanistic insight are currently being undertaken in our lab.

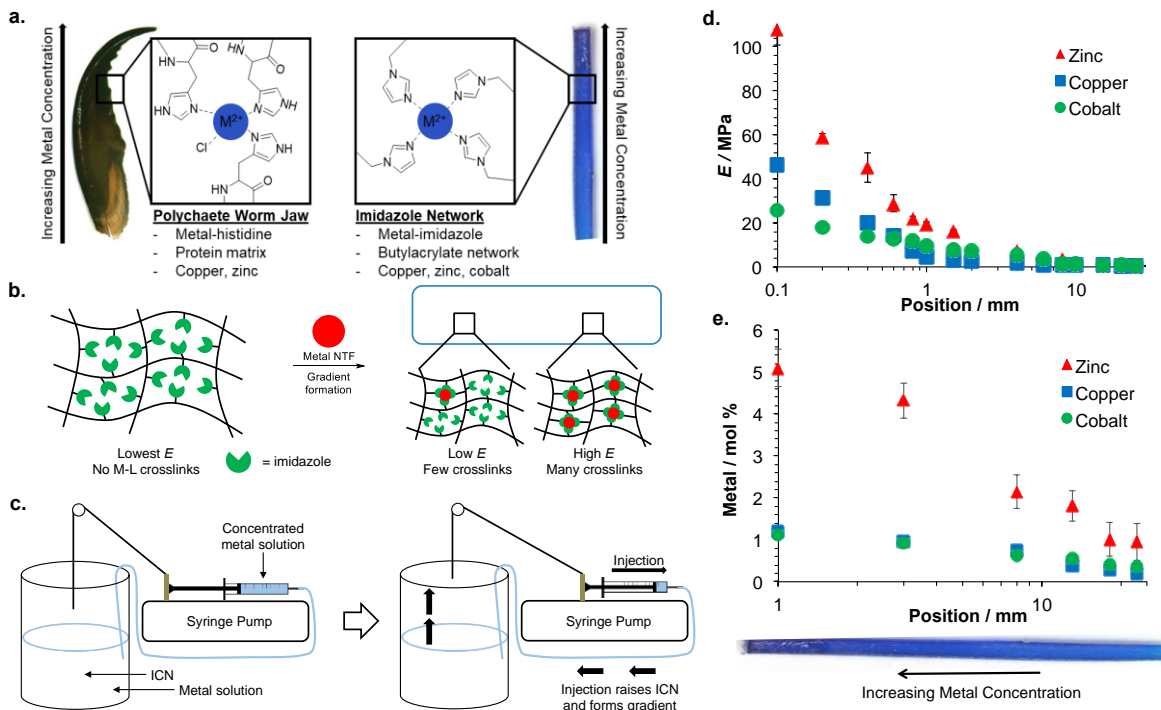


**Figure 3.** Bioinspired design of materials with large mechanical gradient. **a:** Bioinspired design concept; **b:** Cartoon depicting metal incorporation into the network to form gradient polymer; **c:** Schematics depicting the simple set up for fabricating the gradient sample; **d:** Gradient of Young's modulus ( $E$ ) along the lateral axis of the samples as determined by nanoindentation. **e:** Relative metal concentration along the lateral axis of the samples as determined by XPS.

## Future Plans

### (1) Further Investigation of Dynamic Materials Based on Dynamic B-O Bonds

We will continue tuning the dynamic B-O bonds for malleable and self-healing material design. Besides boronic ester exchange, we will expand to the study of other type of B-O linkages, such as boroxine motif for dynamic materials. We will also pursue "green" dynamic materials design by using renewable, biodegradable components.

### (2) Further Exploration of Metal-Ligand Dynamic Materials

We will further our investigation of using metal-ligand interaction for the design of self-healing and gradient materials. Various networks, metal ions, counter ions, will be investigated for expanding the dynamic window of the materials. For mechanical gradients, much larger gradients will be pursued.

### (3) Investigation of Dynamic Photo-responsive Materials

We will investigate several strategies for the development of dynamic photoresponsive materials. With precise temporal and spatial control of mechanical properties, such smart dynamic materials should be very useful for further development of actuators and robotics.

## Publications in year 2015-2017 (which acknowledge DOE support):

1. Nishimura, Y.; Chung, J.; Guan, Z. "Silicon-oxide as a New Dynamic Covalent Motif for Dynamic Polymer Design", *manuscript submitted*.

2. Neal, J. A.; Oldenhuis, N. J.; Novitsky, Al. L.; Samson, E. M.; and Guan, Z. “Large Continuous Mechanical Gradient Formation via Metal-Ligand Interactions”, *manuscript submitted*.
3. Ogden, W.; Guan, Z. “Recyclable and Malleable Boroxine Network Materials”, *manuscript in preparation*.
4. Jia, X.; Qin, C.; Friedberger, T.; Guan, Z.; Huang, Z. “Degradation of Polyethylenes into Liquid Fuels via Cross Alkane Metathesis” *Science Advances* **2016**, 2, 6.
5. Mozhdehi, D.; Neal, J. A.; Grindy, S. C.; Cordeau, Y.; Ayala, S.; Holten-Anderson, N.; and Guan, Z. “Tuning Mechanical Response in Self-Healing Metallopolymer Networks Through Metal-Ligand Complex Geometry and Exchange Dynamics” *Macromolecules* **2016**, 49, 6310.
6. Ishige, R.; Williams, G. A.; Higaki, Y.; Ohta, N.; Sato, M.; Takahara, A.; and Guan, Z. “In situ Ultra-Small-Angle X-ray Scattering Study Under Uniaxial Stretching of Colloidal Crystal Prepared by Silica Nanoparticles Bearing Hydrogen-Bonding Polymer Grafts” *IUCrJ* **2016**, 3, 211.
7. Grindy, S. C.; Learsch, R.; Mozhdehi, D.; Cheng, J.; Barrett, D. G.; Guan, Z.; Messersmith, P. B.; Holten-Andersen, N. “Control of hierarchical polymer mechanics with bioinspired metal-coordination dynamics” *Nature Materials* **2015**, 14, 1210.
8. Williams, G. A.; Ishige, R.; Chung, J.; Takahara, A.; Guan, Z. “Mechanically robust and self-healable superlattice nanocomposites by self-assembly of “sticky” nanoparticles” *Adv. Mater.* **2015**, 27, 3934.
9. Hashemi, A.; Jouault, N.; Williams, G. A.; Zhao, D.; Cheng, K.; Kaiser, J.; Guan, Z.; Kumar, S. K. “Enhanced Glassy State Mechanical Properties of Polymer Nanocomposites via Supramolecular Interactions” *Nano Lett.* **2015**, 15, 5465.
10. Chen, Y.; Guan, Z. “Self-healing thermoplastic elastomer brush copolymers having a glassy polymethylmeth-acrylate backbone and rubbery polyacrylate-amide brushes” *Polymer* **2015**, 69, 249.

## Development of Smart, Responsive Communicating and Motile Microcapsules

Daniel A. Hammer and Daeyeon Lee, Department of Chemical and Biomolecular Engineering, University of Pennsylvania, Philadelphia, PA 19104

### Program Scope

The scope of this project is to design motile systems using microcapsules that can respond to changes in environmental stimuli, and display smart behavior on length-scales well beyond the size of the capsule itself. Central to our design are vesicles of various designer chemistries, including polymersomes – vesicles whose membrane is assembled from block-copolymers – and protein vesicles. We can make large, uniform populations of polymersomes and engineer these capsules to encapsulate and release active agents such as nanoparticles or active molecules in response to stimuli such as light or small molecules. We can also use proteins to either assemble vesicles or incorporate bioactivity, such as protease cleavable domains, into vesicles. We can micro-contact print adhesion ligands on surfaces to immobilize vesicles, either in patterns or uniformly. Furthermore, we will use principles of self-propulsion from either thermal or biochemical interactions to make capsules that are motile on designer surfaces. The long-term impact of this work will be to develop autonomous motion of microcapsules that mimic biological cell motility and convert chemical energy to mechanical motion.

The specific objectives of this work are:

- 1. To use enzymatic activity to engineer release from capsules.** We will devise capsules that can be induced to release contents in response to enzymatic activity.
- 2. To use specific and weak adhesion and micro-contact printing to immobilize polymersomes and microparticles.** The key is have sufficient adhesion to immobilize particles, but weak enough adhesion to allow the particles to move, either by controlling the density of adhesive contacts or the strength of receptor-ligand interactions.
- 3. To demonstrate collective motion of micron-sized particles in response to external stimuli,** by adhering particles weakly on printed surfaces in specially designed micromachined chambers in which convection is minimized, and adding appropriate stimuli.
- 4. To synthesize spontaneously motile systems, based on floppy vesicles that interact with spatial arrays of proteins.** Through thermal fluctuation of vesicles and their interaction with a surface, and by tuning the adhesion to be weak, we endeavor to make spontaneously motile systems using engineered adhesion or enzymatic activity.

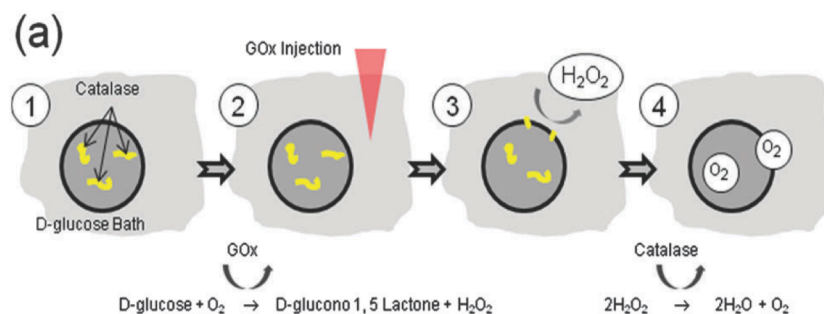
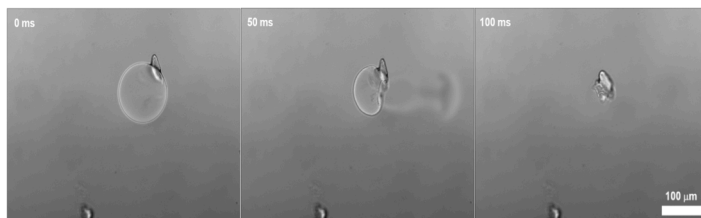


Figure 1. The design of capsules that release contents on cue, in response to addition of glucose oxidase to a surrounding media immersed in glucose, which produces H<sub>2</sub>O<sub>2</sub> that passes freely through the membrane. Entrapped-catalase in polymersomes generates O<sub>2</sub> which leads to vesicle failure. (Jang et al., 2016).

## Recent Progress

**Catalase-Driven Vesicle Release.** We can generate release from polymersomes enzymatically through external chemical control, using glucose as an active agent. We encapsulated the enzyme catalase in the interior of a polymersome. Catalase decomposes  $H_2O_2$  to water and oxygen ( $O_2$ ). To generate  $H_2O_2$ , we added glucose to the outer solution. Then, upon the addition of glucose oxidase (GOx) to the outer solution, glucose is converted to gluconic acid and hydrogen peroxide, and  $H_2O_2$  transverses the membrane,  $O_2$  is produced and the vesicle



**Figure 2.** Failure of catalase-loaded polymersomes. A catalase-loaded polymersome is dispersed in a 290 mOsm glucose solution. The catalase concentration of the inner phase is 0.2 wt. %. When 5 wt. % glucose oxidase solution is injected into the glucose solution,  $H_2O_2$  is generated, passes through the membrane, is reduced by the catalase to water and  $O_2$ , which leads to the failure of the vesicle.

bursts. **Figure 1** shows a schematic illustration of our experimental design. Sequential polymersome failure was captured by high speed videomicroscopy, as illustrated in **Figure 2**.  $S_v$ , the fraction of vesicles that survive, decreases with time at all glucose oxidase concentrations. The rate of release can be modulated by the concentration of enzymes inside and outside the vesicle. Thus, we have developed an effective

strategy for enzymatically driven release of materials from capsules through exogenous control (Jang et al. *Soft Matter*, 2016).

**Self-assembling recombinant proteins.** Our ultimate goal is to develop self-actuating

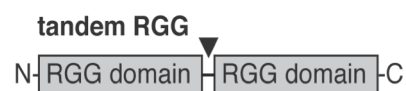


**Figure 3.** Construction of a tandem RGG protein, made through molecular biology.

synthetic cells that are controlled by enzymatic activity from within. This requires the generation of organelles that can be inserted or self-assembled within synthetic cells. Although one strategy is to make organelles that are surrounded by membranes, the insertion of channels and receptors into membranes is cumbersome, making control difficult. We have pursued an alternative approach to make membraneless organelles through the self-assembly of coacervating

proteins. We have developed a recombinant protein that can self-assemble into liquid droplets by making a coacervating phase; and we can reverse this self-assembly through the action of a protease. Our design is based on LAF-1, an intrinsically disordered protein that phase separates in solution (Elbaum-Garfinkle et al., 2015). The domain of LAF-1 responsible for phase separation is RGG (rich in arginines and glycines), and purified forms of RGG can also induce phase separation, albeit at a higher concentration. Motivated by this observation, we hypothesized that an engineered protein construct with two RGG domains in tandem (**Figure 3**) would phase separate more robustly (at lower concentrations), due to enhanced intermolecular interactions and multivalency, than monomeric RGG. Tandem RGG self-assembles into droplets robustly, as shown in **Figure 4**, and more robustly than single RGG at all concentrations (not shown). The phase separation is reversible, with turbidity appearing, disappearing, and then appearing again upon cooling, heating, and then cooling again.

Tandem RGG, and the ability to add functional domains to the protein through molecular

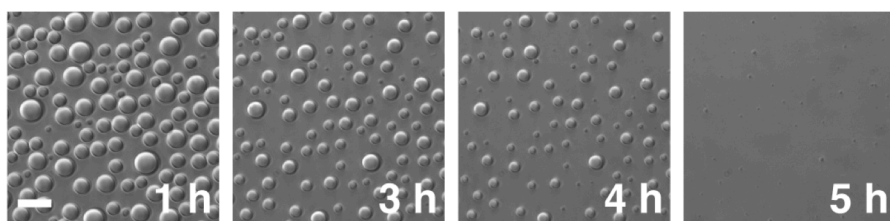


Figure 4. The dissolution of tandem RGG droplets containing a thrombin cleavable domain, by thrombin. Cleavage is specific to the sequence of the cleavable domain. Scale bar is 10 microns.

biology. provides us with enormous flexibility for developing designer functionality for membraneless organelles. One of many examples is that division of a tandem RGG into two single RGG domains would

reverse the phase separation. Accordingly, we produced a protein with two RGG domains separated by a domain that can specifically be cleaved by the protease thrombin, Leu-Val-Pro-Arg-Gly-Ser – that is RGG-LVPRGS-RGG. This intact tandem self assembles. However, when thrombin is added to the protein solution, the thrombin cleaves the tandem into monomers, leading to the gradual disappearance of the droplets (**Fig 4A-D**). Negative controls, in which we cloned a tandem RGG variant in which the LVPRGS thrombin recognition site was mutated to LVRPGS are sufficient to abolish thrombin cleavage at that site, as seen by SDS-PAGE and light microscopy.

The ability to make tandem RGG that phase separates opens up a number of possibilities for assembly specific chemistry into membrane-less organelles, some of which are illustrated in **Figure 5**, including the recruitment of an arbitrary number of active enzymes to the surface of the organelle using zipper proteins. The assemblies open the possibility of releasing interior active proteins upon the presentation of one (an “or” gate) or two (an “and” gate) proteases, among numerous other bioactive control strategies that can be coded by molecular biology.

**Generation of new Polyelectrolyte Capsules Using So-NICE.** We have developed a new method of making microcapsules, so called surfactant organized nanoscale interfacial complexation in emulsion (So-NICE). So-NICE microcapsules can withhold small molecules, such as protein surfatants, for an extended periods of time (several weeks). SO NICE microcapsules are salt responsive and thus can release encapsulated materials in response to an increase in the ionic strength, making them a powerful tool for ion mediated release (Duan et al., 2017). SO-NICE capsules were used to make motile capsular microswimmers using PT binding proteins (below).

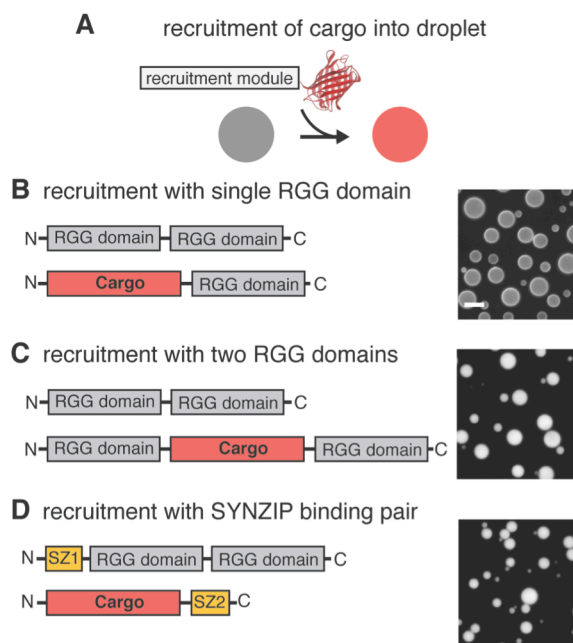


Figure 5. The ability to make tandem allows for specific sequestration of active components to membraneless organelles (A) by co-sequestration of single (B) or double (C) RGG modules, or zipper domains (D).

**Self Motile Capsules.** We incorporated Pt metal particles into the membrane of SO-NICE capsules made from branched poly(ethylenimine) (bPEI) and poly(acrylic acid) (PAA), two model cationic and anionic polyelectrolytes, respectively. A small amount of platinum (Pt) nanoparticles were dispersed in the bPEI solution. After complexation, partial dewetting leads to the formation of Pt a patch on the NICE capsule surface. Subsequently, catalysis by Pt generates oxygen from a solution of H<sub>2</sub>O<sub>2</sub> leading to the movement of NICE capsules. Pt-incorporating NICE capsules in 3.5 % H<sub>2</sub>O<sub>2</sub> solution exhibit a velocity of  $2.20 \pm 0.89$  micron/s while Pt-incorporating NICE capsules in deionized water show  $0.82 \pm 0.04$  micron/s. Currently, we are trying to increase the catalytic power and directionality of these capsules.

We are also building a motile synthetic cell in which protocell's mobility would be driven by an external chemical agent (see aim 1, above). We have incorporated the enzyme catalase into the lumen of polymersomes made by rehydration. These vesicles are floppy and display membrane fluctuation owing to thermal forces. However, because enzymatic activity is known to lead to the formation of a motive force (Dey and Sen, 2017), we argued that incorporation of catalase within a flaccid vesicle, and addition of its substrate, would lead to the formation of a more forcefully fluctuating membrane. We made catalase containing vesicles that had a small degree of biotinylation, to insure immobilization on a surface coated with a low density of avidin, and showed that these vesicles display enhanced diffusion (random motility) in the presence of hydrogen peroxide. The motility increased with increasing concentrations of H<sub>2</sub>O<sub>2</sub> (see **Figure 6**). Negative controls show the motility is not seen in the absence of H<sub>2</sub>O<sub>2</sub>, catalase or adhesive interactions. **Thus we have achieved the objective of making an autonomously motile synthetic cell.**

**Future Plans.** To **(1)** characterize the random motility of catalase containing vesicles as a function of adhesion strength, catalase concentration, and hydrogen peroxide concentration. **(2)** To demonstrate directional motion by placing catalase containing vesicles in a microfluidic gradient of H<sub>2</sub>O<sub>2</sub>. **(3)** To determine if the direct motion of vesicles can be extended to other enzymes than catalase. That is, does motion require the generation of singlet oxygen, or do other enzymatic reactions work. **(4)** To show that capsule motility can be driven by glucose and glucose oxidase added externally. **(5)** To incorporate membraneless organelles with enzymatic activity in protocells, and demonstrate that this activation can drive the motility of a model protocell. **(6)** To demonstrate the release of entrapped nanoparticles or analytes and the displacement of bound beads or vesicles on a substrate in the presence of an external stimulus.

## References

- Jang, W.S. ..., D. Lee, D. A. Hammer, (2016), *Soft Matter* **12**(4):1014-1020.  
 Elbaum-Garfinkle, S., Y. Kim, ..., and C. P. Brangwynne (2016) *PNAS* **112**(23):7189-7194.  
 Duan, G.... K. J. Stebe, D. Lee, in press, *Langmuir*, doi: 10.1021/acs.langmuir.7b01526.  
 Dey, K.K., and A. Sen. (2017) *JACS* **139**:7666-7676.

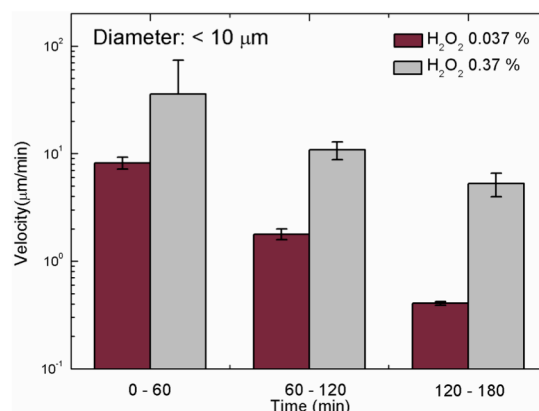


Figure 6. Velocity of polymersomes with entrapped catalase made by rehydration, illustrating the motility as a function of time, and that motility increases with hydrogen peroxide concentration.

## Two Year Publication List

Duan, G., M. F. Haase, K. J. Stebe, D. Lee "One-Step Generation Salt-Responsive Polyelectrolyte Microcapsules via Surfactant Organized Nanoscale Interfacial Complexation in Emulsions (SO NICE)", in press, Langmuir, doi: 10.1021/acs.langmuir.7b01526.

Wang, L.; Sloand, J.; Gaffey, A.; Venkataraman, C.; Wang, Z.; Trubelja, A.; Hammer, Daniel A.; Atluri, P.; Burdick, J. A. (2017) "Injectable, guest-host assembled polyethylenimine hydrogel for siRNA delivery," Biomacromolecules **18**(1):77-86; doi: 10.1021/acs.biomac.6b01378.

Xiao, Q., Rubien, J., Wang, Z., Reed, E., Hammer, D. A.; Sahoo, D., Heiney, P., Yadavalli, S., Goulian, M., Wilner, S., Baumgart, T., Vinogradov, S., Klein, M. & Percec, V., (2016). "Self-Sorting and Co-Assembly of Fluorinated, Hydrogenated, and Hybrid Janus Dendrimers into Dendrimersomes," JACS **138**: 1162-1167. doi: 10.1021/jacs.6b08069.

Qi X., Zhichun W., D. Williams, P. Leowanawat, M. Peterca, S. E. Sherman, S. Zhang, D.A. Hammer, P. A. Heiney, S. R. King, D. M. Markovitz, S. André, H.-J. Gabius, M. L. Klein and Vi. Percec, (2016.) "Why do some membranes of unhealthy cells adopt a cubic architecture?," ACS Central Science **2**(12): 943-953. doi: 10.1021/acscentsci.6b00284.

D. A. Hammer, Z. Wang, E. Reed, C. Gao, and K. B. Vargo, (2017). "Synthetic membranes from block co-polymers, recombinant proteins and dendrimers," to be published in the Handbook of Lipid Membranes, edited by Cyrus Safinya and Jachim Radler.

W.S. Jang, S. C. Park, K. P. Dooley, S. F. Wheeler, D. Lee, D. A. Hammer, (2016), "Enzymatic Reaction-Triggered Rupture of Polymersomes," Soft Matter **12**(4):1014-1020; doi:10.1039/c5sm01881a.

Y. Jang, .-S. Jang, C. Gao, T. Shim, J. C. Crocker, D. A. Hammer and D. Lee (2016), "Tuning the Mechanical Properties of Recombinant Protein-Stabilized Gas Bubbles Using Triblock Copolymers," ACS Macro Letters **5**(3):371-376. doi: 10.1021/acsmacrolett.6b00057.

Q. Xiao, S. Zhang, Z. Wang , S. E. Sherman , R.-O. Moussodia , M. Peterca , A. Muncan, D. Williams, D. A. Hammer, S. Vértesy, S. André, H.-J. Gabius, M. Klein and V. Percec (2015), "Onion-like glycodendrimersomes from sequence-defined Janus glycodendrimers and influence of architecture on reactivity to a lectin," PNAS USA. **113**(5):1162-1167. doi: 10.1073/pnas.1524976113.

Benjamin S. Schuster, Ranganath Parthasarathy, Ellen H. Reed, Matthew Good, and D.A. Hammer, (2017), "Assemblies of disordered proteins which can be dissolved by proteases," in preparation for Proceedings of the National Academy of Sciences, USA.

## Surface Mechanical Properties of Bio-Inspired Architectures

Anand Jagota\* (anj6@lehigh.edu) and Chung-Yuen Hui& (ch45@cornell.edu)

\*D331 Iacocca Hall, Chemical Engineering, Lehigh University, Bethlehem PA 18015.

&Sibley School of Mechanical and Aerospace Engineering, Cornell University, Ithaca, NY 14853

### Program Scope

The overall goal of our work is to design and study bioinspired architectures, and to understand the surface mechanical properties of compliant/soft materials. We draw inspiration from materials in nature that have evolved remarkable surface architectures with unique mechanical properties. Our interest is in the materials science of (a) obtaining and controlling surface mechanical properties, and (b) the role of surface stress in compliant materials. We are currently focused on two questions:

(a) *What is the role of surface stress in the mechanical behavior of soft biomaterials?*

Biomaterials and synthetic biomimetic materials are usually “soft” or compliant compared to conventional engineering materials (e.g., metals and ceramics). Until recently, the effect of the surface mechanical properties, such as the solid surface stress, on their mechanical behavior has generally been ignored. However, it has become apparent from recent findings, including those of our DOE-supported research, that surface stress plays a very significant and sometimes dominant role in a variety of mechanical phenomena in soft materials. We are studying several such phenomena, e.g., wetting of compliant surfaces, shape change due to surface tension, role of surface stress in cell development, contact mechanics, and fracture.

(b) *How does one endow a surface with highly selective adhesion and friction using shape complementarity?* There are many examples in nature, ranging from the molecular (shape and charge recognition between folded proteins) to millimeter-scale attachment devices (contacting and attachment surfaces in insects and lizards), of architectures that obtain highly selective and enhanced properties using shape-complementarity. We are studying how some simple designs of shape-complementary surfaces can strongly and selectively enhance adhesion and friction. In particular, we have discovered that interfacial dislocations appear spontaneously, permitting interlocking of regular arrays of complementary shapes even in the presence of misorientation.

### Recent Progress

#### 1. Droplets on Compliant Substrates: Spontaneous Motion and Interaction

The mechanics and physics of wetting of a solid surface is a fundamental problem of broad importance and interest; it has been studied nearly exclusively for stiff (nearly rigid) surfaces [1]. We are now finding that the static wetting of highly compliant substrates can be quite different because of the influence of surface stress[2, 3]. In addition, new aspects of wetting dynamics are emerging [4, 5]. Droplet motion arises in many natural phenomena, ranging from the familiar gravity-driven slip and arrest of raindrops on windows, to the directed transport of droplets for water harvesting by plants and animals. Deliberate transportation and manipulation of droplets is also important in many technological applications, including droplet-based microfluidic chemical reactors and heat exchangers for thermal management. Droplet motion usually requires gradients of surface energy or temperature, or external vibration to overcome contact angle hysteresis. We have discovered a new phenomenon in which a drying droplet placed on a periodically compliant surface undergoes spontaneous, erratic motion in the absence of surface energy gradients and

external stimuli such as vibration. Our model for this process shows that the system undergoes a set of mechanical instabilities (Fig. 1; [6]).

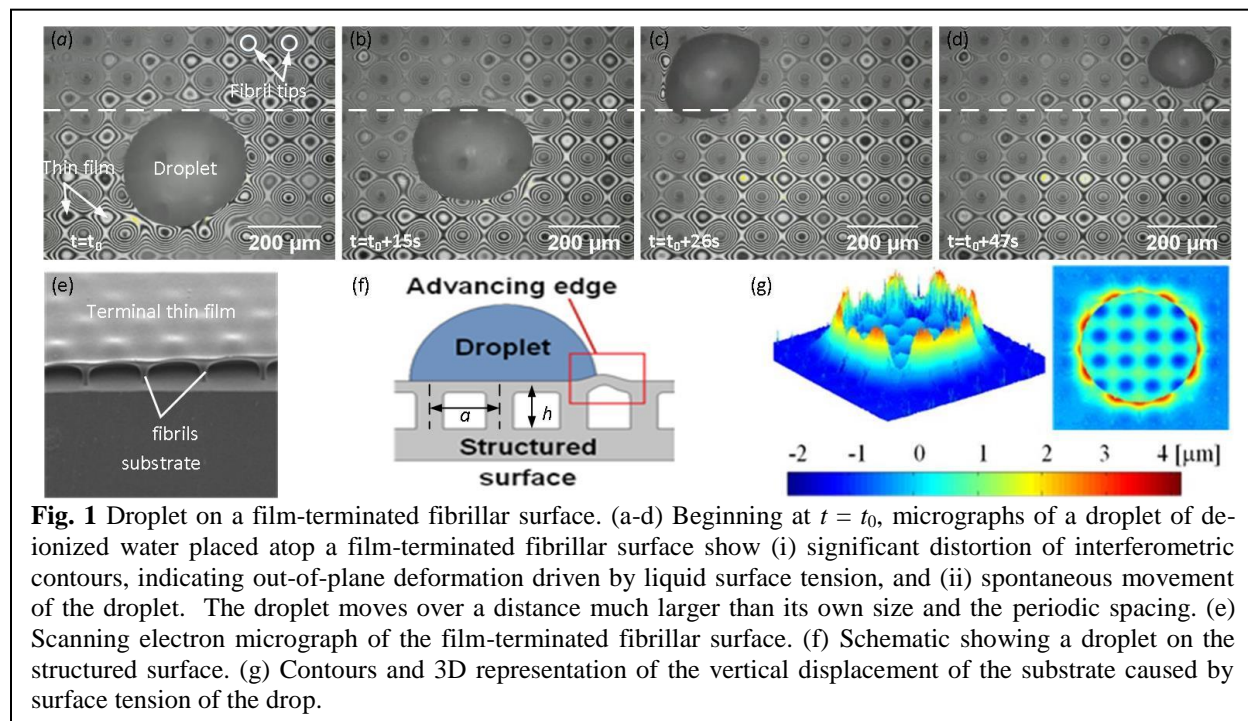


**Fig. 1** Droplet on a film-terminated fibrillar surface. (a-d) Beginning at  $t = t_0$ , micrographs of a droplet of de-ionized water placed atop a film-terminated fibrillar surface show (i) significant distortion of interferometric contours, indicating out-of-plane deformation driven by liquid surface tension, and (ii) spontaneous movement of the droplet. The droplet moves over a distance much larger than its own size and the periodic spacing. (e) Scanning electron micrograph of the film-terminated fibrillar surface. (f) Schematic showing a droplet on the structured surface. (g) Contours and 3D representation of the vertical displacement of the substrate caused by surface tension of the drop.

We previously discovered that the Laplace pressure of a droplet placed on one side of an elastic thin film can cause significant deformation in the form of a bulge on its opposite side [3]. We show that this deformation can be detected by other droplets suspended on the opposite side of the film, leading to interaction between droplets separated by the solid (but deformable) film [7]. The interaction is repulsive when the drops have a large overlap and attractive when they have a small overlap. This observation has been explained by analyzing the energy landscape of the droplets interacting via an elastically deformed film. This novel phenomenon involving wetting of compliant surfaces and can lead to techniques for directed motion of droplets confined to one side of a thin elastic membrane by manipulations on the other side.

## 2. Role of surface stress in cell fate and proliferation.

It has long been known that the modulus of extracellular matrix (ECM) regulates cell fate and morphogenesis [8]. Cells physically probe the modulus of the ECM using integrin based adhesion complexes. We have recently collaborated with Matthew Paszek's group at Cornell to show that cells on a soft surface sense its solid surface stress [9] through integrins and canonical mechano-transduction pathways. For soft materials with high surface energies, surface stresses can dominate over the elastic modulus in directing cell response. Our findings emphasize the importance of solid surface stress as a design parameter for soft biomaterial scaffolds.

## 3. Related studies on the role of surface stress in soft materials mechanics

The role of surface stress is pervasive in soft materials. It is important to explore its various manifestations, which we have undertaken by studying contact and wetting problems with large deformation, wetting of a partially immersed compliant rod, surface stress measurement by indentation of a thin film, and the role of surface stress in resisting fracture. We have also co-authored a review article on the role of surface stress that aims to summarize recent progress.

#### 4. Geometry of Defects at and Friction of Shape-Complementary Soft Interfaces

In nature, shape complementarity is often used to enhance adhesion selectively. Complementary arrays of surface structures, such as 1D ridges (Fig. 2a) or fibrils arranged in a 2D lattice (Fig. 2b), can inter-digitate to achieve adhesion and friction enhancement controlled by shape recognition. Relative misorientation and lattice parameter mismatch is accommodated by defects that are meso-scale dislocations with mixed screw and edge character. The arrangement of such dislocations plays a critical role in determining the mechanical properties of the interface. We are studying the geometric properties of one-dimensional (ridge/channel) and two-dimensional (arrays of pillars) shape-complementary interfaces in the presence of both relative misorientation (twist) and difference in lattice spacing. We further study how properties such as adhesion and friction depend on geometrical characteristics of the interface.

Fig 2(c) and (d) show patterns of dislocations that appear at interfaces [10]. We can accurately predict the geometry of these patterns in terms of misorientation, lattice parameter mismatch, and the underlying structure of the interface. Adhesion depends very sensitively on this geometry as we have shown previously. So does friction, as shown in Fig. 2(e).

#### Future Plans

- *Role of Surface Stress in the Surface Mechanical Behavior of Compliant Solids:* We will continue our work on understanding the role of surface stress in the surface mechanical properties of compliant materials and structures. We will focus on adhesive contact problems, wetting, and interfacial fracture. We will also explore whether more complex *solid* surface rheology is possible on gel surfaces using strongly surface-active molecules.

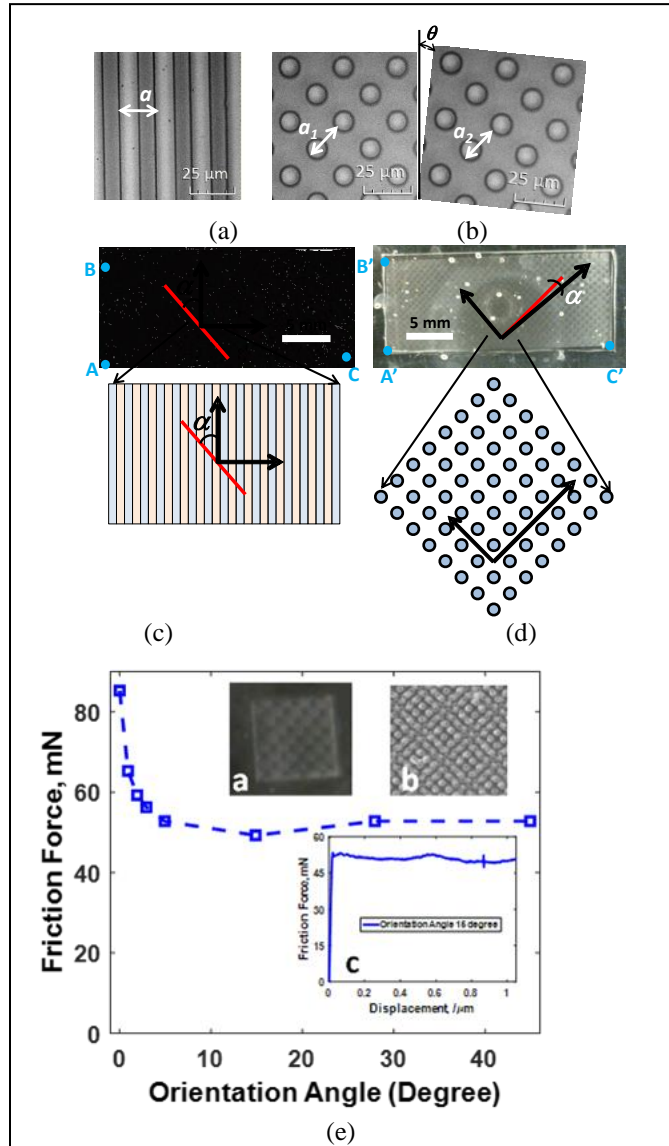


**Fig 2.** Optical micrographs of (a) ridge/channel samples, and (b) square arrangement of fibrils. Each sample consists of a pair of PDMS layers with some difference in lattice parameter (in this case, with ratio  $\lambda = 1.05$ ) and relative twist (in this case  $\theta = 6^\circ$ ). (c) Typical pattern of approximately parallel lines appears at the interface between two nominally complementary ridge/channel samples with a difference in lattice spacing and slight misorientation, (d) Typical pattern observed at the interface between two nominally complementary surfaces with a 2D array of micropillars. (e) Friction between two fibrillar interfaces depends on misorientation and is accommodated by motion of the dislocations (see also inset figure and optical micrographs.)

- *Shape Complementary Structures:* We will continue our study of shape complementary hetero-interfaces between elastomers and gels to include novel self-healing gels (in collaboration with Prof. Shu Yang, University of Pennsylvania), thus to use the shape-complementary mechanism to provide adhesion to otherwise “slippery” interfaces. We will continue our study of how the geometry of shape-complementary surfaces affects their adhesion and friction.

- *Role of surface stress in cell fate and proliferation:* We will continue our collaboration with Matthew Paszek’s group at Cornell to study how surface stress regulates cell functions. Recent experiments on very soft substrates have shown that cells can communicate with each other, presumably through surface stresses. A surprising result is that the mean square movements of cells moving on the surface of liquid-like gels were significantly higher than cells moving on surfaces of gels with higher elastic modulus. In addition, cell motion in liquid-like gels is highly correlated. We plan to develop models to understand this phenomenon.

- *Continue Work on Techniques.*

As we find important technique-related issues, whether experimental or theoretical, whose solution will aid the entire community, we will pursue them on a selective basis. Specifically, our work on the role of solid surface stress in soft materials is resulting in techniques for the measurement of solid surface stress. New numerical techniques are needed to study how surfaces of compliant substrates resist concentrated shear forces (e.g. near a contact line).

## References

1. deGennes, P.-G., F. Brochard-Wyart, and D. Quere, *Capillarity and Wetting Phenomena. Drops, Bubbles, Pearls, Waves*. 2002, New York: Springer Science+Business Media, Inc.
2. Jerison, E.R., et al., *Deformation of an Elastic Substrate by a Three-Phase Contact Line*. Physical Review Letters, 2011. **106**(18): p. 186103.
3. Nadermann, N., C.-Y. Hui, and A. Jagota, *Solid surface tension measured by a liquid drop under a solid film*. Proceedings of the National Academy of Sciences, 2013. **110**(26): p. 10541-10545.
4. Karpitschka, S., et al., *Liquid drops attract or repel by the inverted Cheerios effect*. Proceedings of the National Academy of Sciences, 2016. **113**(27): p. 7403-7407.
5. Jagota, A., *Role reversal: Liquid “Cheerios” on a solid sense each other*. Proceedings of the National Academy of Sciences, 2016. **113**(27): p. 7294-7295.
6. Liu, T., et al., *Spontaneous Droplet Motion on a Periodic Compliant Substrate*. Langmuir, 2017. **33**(20): p. 4942-4947.
7. Liu, T., et al., *Interaction of Droplets Separated by an Elastic Film*. Langmuir, 2016. **33**(1): p. 75-81.
8. Engler, A.J., et al., *Matrix elasticity directs stem cell lineage specification*. Cell, 2006. **126**(4): p. 677-689.
9. Cheng, Z., et al., *Solid Surface Stresses Direct Cellular Behaviors Through Integrin-Based Mechanotransduction*. Nature Materials, 2017(under revision).
10. Dillen, J., et al., *Geometry of defects at shape-complementary soft interfaces*. Extreme Mechanics Letters, 2016. **9**: p. 74-83.

## Publications

1. Hui, C.-Y. and A. Jagota, "Planar equilibrium shapes of a liquid drop on a membrane," *Soft Matter*, 2015 **11**(46) 8960-8967.
2. Jagota, A., "Role reversal: Liquid "Cheerios" on a solid sense each other," *Proceedings of the National Academy of Sciences*, 2016. **113**(27): p. 7294-7295.
3. Liu, T., et al., "Spontaneous Droplet Motion on a Periodic Compliant Substrate," *Langmuir*, 2017. **33**(20): p. 4942-4947.
4. Liu, T., et al., Interaction of Droplets Separated by an Elastic Film. *Langmuir*, 2016. **33**(1): p. 75-81.
5. Cheng, Z., et al., "Solid Surface Stresses Direct Cellular Behaviors through Integrin-Based Mechanotransduction," *Nature Materials*, 2017. Under revision.
6. Liu, T., A. Jagota, and C.-Y. Hui, "Effect of surface tension on the adhesion between a rigid flat punch and a semi-infinite neo-Hookean half-space." *Extreme Mechanics Letters*, 2016. **9**: p. 310-316.
7. Liu, T., A. Jagota, and C.-Y. Hui, "A closed form large deformation solution of plate bending with surface effects." *Soft Matter*, 2017. **13**(2): p. 386-393.
8. Hui, C.-Y. and A. Jagota, "Wetting of a partially immersed compliant rod." *Journal of Applied Physics*, 2016. **120**(19): p. 195301.
9. Xu, X., et al., "Surface tension measurement from the indentation of clamped thin films." *Soft matter*, 2016. **12**(23): p. 5121-5126.
10. Style, R.W., et al., "Elastocapillarity: Surface tension and the mechanics of soft solids." *Annual Review of Condensed Matter Physics*, 2017. **8**: p. 99-118.
11. Hui, C.-Y., T. Liu, and M.-E. Schwaab, "How does surface tension affect energy release rate of cracks loaded in Mode I?" *Extreme Mechanics Letters*, 2016. **6**: p. 31-36.
12. Dillen, J., et al., "Geometry of defects at shape-complementary soft interfaces." *Extreme Mechanics Letters*, 2016. **9**: p. 74-83.
13. C-Y. Hui, A. Jagota, "Effect of surface tension on the relaxation of a viscoelastic half-space perturbed by a point load," *Journal of Polymer Science Part B: Polymer Physics*. **54** 2 274-280 (2016).
14. Chung-Yuen Hui, Tianshu Liu, Thomas Salez, Elie Raphael, Anand Jagota, "Indentation of a rigid sphere into an elastic substrate with surface tension and adhesion," *Proceedings of the Royal Society A*, **471** 2175 p 20140727 (2015).
15. Chung-Yuen Hui, Anand Jagota, Nichole Nadermann, Xuejuan Xu, "Deformation of a Solid Film with Surface Tension by a Liquid Drop," *Procedia IUTAM*, **12** 116-123 (2015).
16. Tianshu Liu, Anand Jagota, Chung-Yuen Hui, "Adhesive contact of a rigid circular cylinder to a soft elastic substrate—the role of surface tension," *Soft Matter*, **11** [19] 3844-3851 (2015).

## Surface Mechanical Properties of Bio-Inspired Architectures

Anand Jagota\* (anj6@lehigh.edu) and Chung-Yuen Hui& (ch45@cornell.edu)

\*D331 Iacocca Hall, Chemical Engineering, Lehigh University, Bethlehem PA 18015.

&Sibley School of Mechanical and Aerospace Engineering, Cornell University, Ithaca, NY 14853

### Program Scope

The overall goal of our work is to design and study bioinspired architectures, and to understand the surface mechanical properties of compliant/soft materials. We draw inspiration from materials in nature that have evolved remarkable surface architectures with unique mechanical properties. Our interest is in the materials science of (a) obtaining and controlling surface mechanical properties, and (b) the role of surface stress in compliant materials. We are currently focused on two questions:

(a) *What is the role of surface stress in the mechanical behavior of soft biomaterials?*

Biomaterials and synthetic biomimetic materials are usually “soft” or compliant compared to conventional engineering materials (e.g., metals and ceramics). Until recently, the effect of the surface mechanical properties, such as the solid surface stress, on their mechanical behavior has generally been ignored. However, it has become apparent from recent findings, including those of our DOE-supported research, that surface stress plays a very significant and sometimes dominant role in a variety of mechanical phenomena in soft materials. We are studying several such phenomena, e.g., wetting of compliant surfaces, shape change due to surface tension, role of surface stress in cell development, contact mechanics, and fracture.

(b) *How does one endow a surface with highly selective adhesion and friction using shape complementarity?* There are many examples in nature, ranging from the molecular (shape and charge recognition between folded proteins) to millimeter-scale attachment devices (contacting and attachment surfaces in insects and lizards), of architectures that obtain highly selective and enhanced properties using shape-complementarity. We are studying how some simple designs of shape-complementary surfaces can strongly and selectively enhance adhesion and friction. In particular, we have discovered that interfacial dislocations appear spontaneously, permitting interlocking of regular arrays of complementary shapes even in the presence of misorientation.

### Recent Progress

#### 1. Droplets on Compliant Substrates: Spontaneous Motion and Interaction

The mechanics and physics of wetting of a solid surface is a fundamental problem of broad importance and interest; it has been studied nearly exclusively for stiff (nearly rigid) surfaces [1]. We are now finding that the static wetting of highly compliant substrates can be quite different because of the influence of surface stress[2, 3]. In addition, new aspects of wetting dynamics are emerging [4, 5]. Droplet motion arises in many natural phenomena, ranging from the familiar gravity-driven slip and arrest of raindrops on windows, to the directed transport of droplets for water harvesting by plants and animals. Deliberate transportation and manipulation of droplets is also important in many technological applications, including droplet-based microfluidic chemical reactors and heat exchangers for thermal management. Droplet motion usually requires gradients of surface energy or temperature, or external vibration to overcome contact angle hysteresis. We have discovered a new phenomenon in which a drying droplet placed on a periodically compliant surface undergoes spontaneous, erratic motion in the absence of surface energy gradients and

external stimuli such as vibration. Our model for this process shows that the system undergoes a set of mechanical instabilities (Fig. 1; [6]).

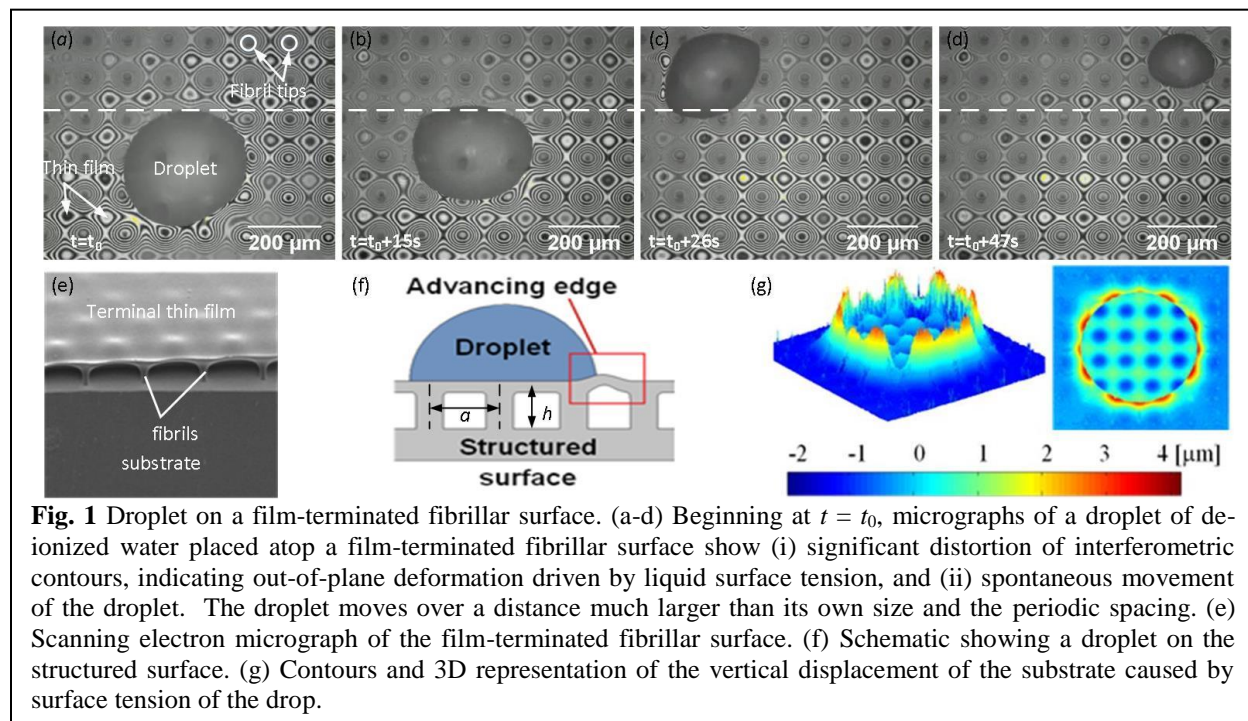


**Fig. 1** Droplet on a film-terminated fibrillar surface. (a-d) Beginning at  $t = t_0$ , micrographs of a droplet of de-ionized water placed atop a film-terminated fibrillar surface show (i) significant distortion of interferometric contours, indicating out-of-plane deformation driven by liquid surface tension, and (ii) spontaneous movement of the droplet. The droplet moves over a distance much larger than its own size and the periodic spacing. (e) Scanning electron micrograph of the film-terminated fibrillar surface. (f) Schematic showing a droplet on the structured surface. (g) Contours and 3D representation of the vertical displacement of the substrate caused by surface tension of the drop.

We previously discovered that the Laplace pressure of a droplet placed on one side of an elastic thin film can cause significant deformation in the form of a bulge on its opposite side [3]. We show that this deformation can be detected by other droplets suspended on the opposite side of the film, leading to interaction between droplets separated by the solid (but deformable) film [7]. The interaction is repulsive when the drops have a large overlap and attractive when they have a small overlap. This observation has been explained by analyzing the energy landscape of the droplets interacting via an elastically deformed film. This novel phenomenon involving wetting of compliant surfaces and can lead to techniques for directed motion of droplets confined to one side of a thin elastic membrane by manipulations on the other side.

## 2. Role of surface stress in cell fate and proliferation.

It has long been known that the modulus of extracellular matrix (ECM) regulates cell fate and morphogenesis [8]. Cells physically probe the modulus of the ECM using integrin based adhesion complexes. We have recently collaborated with Matthew Paszek's group at Cornell to show that cells on a soft surface sense its solid surface stress [9] through integrins and canonical mechano-transduction pathways. For soft materials with high surface energies, surface stresses can dominate over the elastic modulus in directing cell response. Our findings emphasize the importance of solid surface stress as a design parameter for soft biomaterial scaffolds.

## 3. Related studies on the role of surface stress in soft materials mechanics

The role of surface stress is pervasive in soft materials. It is important to explore its various manifestations, which we have undertaken by studying contact and wetting problems with large deformation, wetting of a partially immersed compliant rod, surface stress measurement by indentation of a thin film, and the role of surface stress in resisting fracture. We have also co-authored a review article on the role of surface stress that aims to summarize recent progress.

#### 4. Geometry of Defects at and Friction of Shape-Complementary Soft Interfaces

In nature, shape complementarity is often used to enhance adhesion selectively. Complementary arrays of surface structures, such as 1D ridges (Fig. 2a) or fibrils arranged in a 2D lattice (Fig. 2b), can inter-digitate to achieve adhesion and friction enhancement controlled by shape recognition. Relative misorientation and lattice parameter mismatch is accommodated by defects that are meso-scale dislocations with mixed screw and edge character. The arrangement of such dislocations plays a critical role in determining the mechanical properties of the interface. We are studying the geometric properties of one-dimensional (ridge/channel) and two-dimensional (arrays of pillars) shape-complementary interfaces in the presence of both relative misorientation (twist) and difference in lattice spacing. We further study how properties such as adhesion and friction depend on geometrical characteristics of the interface.

Fig 2(c) and (d) show patterns of dislocations that appear at interfaces [10]. We can accurately predict the geometry of these patterns in terms of misorientation, lattice parameter mismatch, and the underlying structure of the interface. Adhesion depends very sensitively on this geometry as we have shown previously. So does friction, as shown in Fig. 2(e).

#### Future Plans

- *Role of Surface Stress in the Surface Mechanical Behavior of Compliant Solids:* We will continue our work on understanding the role of surface stress in the surface mechanical properties of compliant materials and structures. We will focus on adhesive contact problems, wetting, and interfacial fracture. We will also explore whether more complex *solid* surface rheology is possible on gel surfaces using strongly surface-active molecules.

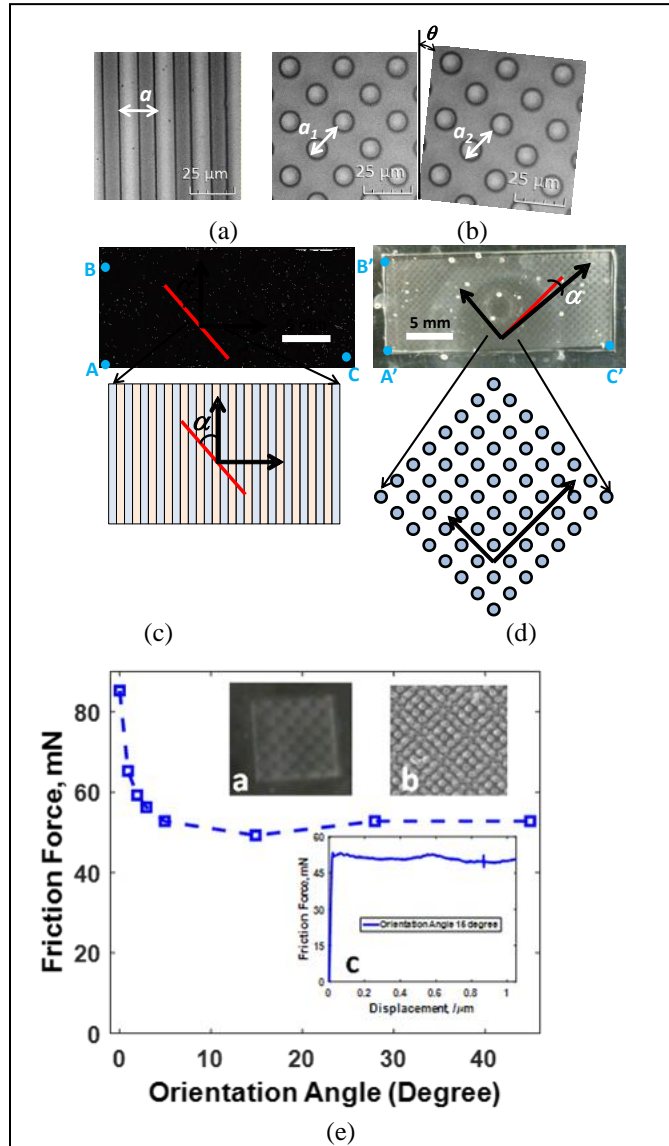


**Fig 2.** Optical micrographs of (a) ridge/channel samples, and (b) square arrangement of fibrils. Each sample consists of a pair of PDMS layers with some difference in lattice parameter (in this case, with ratio  $\lambda = 1.05$ ) and relative twist (in this case  $\theta = 6^\circ$ ). (c) Typical pattern of approximately parallel lines appears at the interface between two nominally complementary ridge/channel samples with a difference in lattice spacing and slight misorientation, (d) Typical pattern observed at the interface between two nominally complementary surfaces with a 2D array of micropillars. (e) Friction between two fibrillar interfaces depends on misorientation and is accommodated by motion of the dislocations (see also inset figure and optical micrographs.)

- *Shape Complementary Structures:* We will continue our study of shape complementary hetero-interfaces between elastomers and gels to include novel self-healing gels (in collaboration with Prof. Shu Yang, University of Pennsylvania), thus to use the shape-complementary mechanism to provide adhesion to otherwise “slippery” interfaces. We will continue our study of how the geometry of shape-complementary surfaces affects their adhesion and friction.

- *Role of surface stress in cell fate and proliferation:* We will continue our collaboration with Matthew Paszek’s group at Cornell to study how surface stress regulates cell functions. Recent experiments on very soft substrates have shown that cells can communicate with each other, presumably through surface stresses. A surprising result is that the mean square movements of cells moving on the surface of liquid-like gels were significantly higher than cells moving on surfaces of gels with higher elastic modulus. In addition, cell motion in liquid-like gels is highly correlated. We plan to develop models to understand this phenomenon.

- *Continue Work on Techniques.*

As we find important technique-related issues, whether experimental or theoretical, whose solution will aid the entire community, we will pursue them on a selective basis. Specifically, our work on the role of solid surface stress in soft materials is resulting in techniques for the measurement of solid surface stress. New numerical techniques are needed to study how surfaces of compliant substrates resist concentrated shear forces (e.g. near a contact line).

## References

1. deGennes, P.-G., F. Brochard-Wyart, and D. Quere, *Capillarity and Wetting Phenomena. Drops, Bubbles, Pearls, Waves*. 2002, New York: Springer Science+Business Media, Inc.
2. Jerison, E.R., et al., *Deformation of an Elastic Substrate by a Three-Phase Contact Line*. Physical Review Letters, 2011. **106**(18): p. 186103.
3. Nadermann, N., C.-Y. Hui, and A. Jagota, *Solid surface tension measured by a liquid drop under a solid film*. Proceedings of the National Academy of Sciences, 2013. **110**(26): p. 10541-10545.
4. Karpitschka, S., et al., *Liquid drops attract or repel by the inverted Cheerios effect*. Proceedings of the National Academy of Sciences, 2016. **113**(27): p. 7403-7407.
5. Jagota, A., *Role reversal: Liquid “Cheerios” on a solid sense each other*. Proceedings of the National Academy of Sciences, 2016. **113**(27): p. 7294-7295.
6. Liu, T., et al., *Spontaneous Droplet Motion on a Periodic Compliant Substrate*. Langmuir, 2017. **33**(20): p. 4942-4947.
7. Liu, T., et al., *Interaction of Droplets Separated by an Elastic Film*. Langmuir, 2016. **33**(1): p. 75-81.
8. Engler, A.J., et al., *Matrix elasticity directs stem cell lineage specification*. Cell, 2006. **126**(4): p. 677-689.
9. Cheng, Z., et al., *Solid Surface Stresses Direct Cellular Behaviors Through Integrin-Based Mechanotransduction*. Nature Materials, 2017(under revision).
10. Dillen, J., et al., *Geometry of defects at shape-complementary soft interfaces*. Extreme Mechanics Letters, 2016. **9**: p. 74-83.

## Publications

1. Hui, C.-Y. and A. Jagota, “Planar equilibrium shapes of a liquid drop on a membrane,” *Soft Matter*, 2015 **11**(46) 8960-8967.
2. Jagota, A., “Role reversal: Liquid “Cheerios” on a solid sense each other,” *Proceedings of the National Academy of Sciences*, 2016. **113**(27): p. 7294-7295.
3. Liu, T., et al., “Spontaneous Droplet Motion on a Periodic Compliant Substrate,” *Langmuir*, 2017. **33**(20): p. 4942-4947.
4. Liu, T., et al., Interaction of Droplets Separated by an Elastic Film. *Langmuir*, 2016. **33**(1): p. 75-81.
5. Cheng, Z., et al., “Solid Surface Stresses Direct Cellular Behaviors through Integrin-Based Mechanotransduction,” *Nature Materials*, 2017. Under revision.
6. Liu, T., A. Jagota, and C.-Y. Hui, “Effect of surface tension on the adhesion between a rigid flat punch and a semi-infinite neo-Hookean half-space.” *Extreme Mechanics Letters*, 2016. **9**: p. 310-316.
7. Liu, T., A. Jagota, and C.-Y. Hui, “A closed form large deformation solution of plate bending with surface effects.” *Soft Matter*, 2017. **13**(2): p. 386-393.
8. Hui, C.-Y. and A. Jagota, “Wetting of a partially immersed compliant rod.” *Journal of Applied Physics*, 2016. **120**(19): p. 195301.
9. Xu, X., et al., “Surface tension measurement from the indentation of clamped thin films.” *Soft matter*, 2016. **12**(23): p. 5121-5126.
10. Style, R.W., et al., “Elastocapillarity: Surface tension and the mechanics of soft solids.” *Annual Review of Condensed Matter Physics*, 2017. **8**: p. 99-118.
11. Hui, C.-Y., T. Liu, and M.-E. Schwaab, “How does surface tension affect energy release rate of cracks loaded in Mode I?” *Extreme Mechanics Letters*, 2016. **6**: p. 31-36.
12. Dillen, J., et al., “Geometry of defects at shape-complementary soft interfaces.” *Extreme Mechanics Letters*, 2016. **9**: p. 74-83.
13. C-Y. Hui, A. Jagota, “Effect of surface tension on the relaxation of a viscoelastic half-space perturbed by a point load,” *Journal of Polymer Science Part B: Polymer Physics*. **54** 2 274-280 (2016).
14. Chung-Yuen Hui, Tianshu Liu, Thomas Salez, Elie Raphael, Anand Jagota, “Indentation of a rigid sphere into an elastic substrate with surface tension and adhesion,” *Proceedings of the Royal Society A*, **471** 2175 p 20140727 (2015).
15. Chung-Yuen Hui, Anand Jagota, Nichole Nadermann, Xuejuan Xu, “Deformation of a Solid Film with Surface Tension by a Liquid Drop,” *Procedia IUTAM*, **12** 116-123 (2015).
16. Tianshu Liu, Anand Jagota, Chung-Yuen Hui, “Adhesive contact of a rigid circular cylinder to a soft elastic substrate—the role of surface tension,” *Soft Matter*, **11** [19] 3844-3851 (2015).

## **Bioinspired mineralizing microenvironments generated by liquid-liquid phase coexistence**

**Christine D. Keating, Department of Chemistry, Pennsylvania State University, University Park, PA 16802.**

### **Program Scope**

Understanding how Biology uses mineralizing microenvironments to control the process and outcome of materials synthesis is a grand challenge that promises to enable new routes to high-performance materials. This project exploits bioinspired microenvironments formed through liquid-liquid phase coexistence to understand and control mineral formation. Liquid-liquid phase coexistence has only recently been appreciated as a mechanism for subcellular compartmentalization. Intracellular aqueous droplet phases are increasingly appreciated to be key features of intracellular organization, providing distinct biochemical microenvironments where reactions can be controlled by local concentration of reagents and biocatalysts. Liquid-liquid phase separation thus appears to be an important and previously unappreciated tool in Biology's toolbox for materials synthesis.

This project's bioinspired mineralizing microenvironments are expected to: (1) enable gradients of organic and inorganic inclusions within minerals/crystals by tuning their local availability during their synthesis; and (2) produce distinct mineral compositions in adjacent compartments at the microscale, with control over their physical association, from noncontacting through Janus structures to core-shell geometries. These microenvironments further provide exciting opportunities to explore the impact of competing reactions and complex active media on materials synthesis. Although the goal is not to produce specific structures for applications but rather to understand and control the mineralization process in multiphase aqueous solutions, we anticipate that the insight gained will enable future applications. Key scientific questions to be addressed include: How does the local environment during mineral formation control the resulting material composition, structure, and properties? What is the impact of real-time modulations in this environment during the reaction?

### **Recent Progress**

After developing artificial mineralizing vesicles (AMVs) based on enzyme-loaded, liposome-stabilized all-aqueous emulsion droplets in the last funding cycle, we have expanded this platform to include one or more reactive subcompartments to further control the reaction microenvironment.<sup>1,2</sup> Our general approach is to include Ca<sup>2+</sup>-chelating polymers to form a Ca<sup>2+</sup>-rich aqueous phase, which serves as a polymer-induced liquid precursor (PILP) within the AMVs. Although local production of CO<sub>3</sub><sup>2-</sup> was sufficient to restrict CaCO<sub>3</sub>(s) formation to the interior of AMVs even without preconcentrating Ca<sup>2+</sup>,<sup>2,3</sup> incorporation of a Ca-rich phase provides greater control over the local mineralizing environment. Already this enables some control over the size, shape, and composition of the resulting hybrid organic/inorganic material. Recent effort has focused on characterizing this material and modulating its formation and properties as a function of the microenvironment in which it is formed.

*Mineralization in multiphase artificial mineralizing vesicles (AMVs).* Figure 1 illustrates mineralization in subcompartmentalized AMVs. The principal difference between these structures and the AMVs we have published previously is the presence of the polycarboxylic acid, polyaspartic acid (PAA, molecular weight range 2–11 kDa). When PAA is added to the

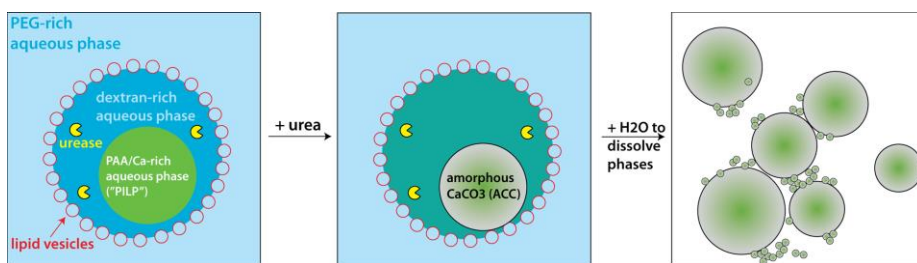


**Figure 1.** Mineralizing microenvironments formed by liquid-liquid phase separation. (left) Artificial mineralizing vesicle that contains a polymer-induced liquid precursor. Addition of urea induces calcium carbonate formation; carbonate ions are enzymatically produced in the dextran-rich phase and react with  $\text{Ca}^{2+}$  in the PILP. After mineralization, dilution of the AMV samples with water dissolves all of the phases and releases the mineral for analysis.

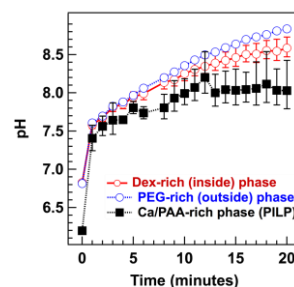


**Figure 2.** Difference in pH between adjacent microenvironments is maintained throughout the reaction.

PEG/dextran ATPS, it partitions into the dextran-rich phase, with a local concentration enrichment of 3x. In the presence of  $\text{Ca}^{2+}$ , it forms a third, PAA-rich phase in which the concentrations of  $\text{Ca}^{2+}$  and PAA are enriched 45x and 90x as compared to the PEG-rich phase. A notable feature of this system is that urease, the enzyme which catalyzes mineralization, is concentrated into a different phase than the  $\text{Ca}^{2+}$  (Dx-rich vs. PAA-rich phases). Upon addition of urea, carbonate and ammonia are produced. Mineralization occurs at the interface of the dextran-rich phase and the PAA/Ca-rich phase and ultimately throughout the PAA/Ca-rich phase. This reaction is accompanied by an increase in pH that we have found varies between the compartments, with a persistently lower pH maintained in the PAA/Ca-rich phase (Figure 2).

Mineral formed in these microenvironments has been characterized by electron microscopy, powder XRD, and vibrational spectroscopy. It is amorphous  $\text{CaCO}_3$  (ACC) with a relatively high water content and associated carboxylates (presumably from bound PAA). Micron-scale ACC spheres appear to correspond to entire PAA-rich phase compartments for some AMVs within the sample. Additional, smaller ACC particles are also present as well; these appear to arise from mineralization of larger compartments, for which PAA/Ca phase dissolution occurred before mineralization was complete. Literature examples exist for retention of overall shape during ACC conversion to crystalline forms when entrapped by a hard template such as polycarbonate membranes or the pores of colloidal crystals.<sup>4,5</sup> Living organisms generally use soft matter to constrain mineralization; we anticipate that local mineral growth in the PAA-rich phase can serve this function in our AMVs and thus far this appears to be the case.

#### *Effect of different polycarboxylates and combinations of polycarboxylates on mineral formation.*

In our multiphase system, organic components serve not only as traditional structure-directing agents but can also alter the phase properties (size, composition, pH, viscosity) and consequently the distribution of reagents between phases. We began our investigation into the consequences of varying the Ca-chelating polymer by changing only the length. Mineral formed in phases made using monodispersed PAA (MW = 1.4 and 14 kDa) are notably different than those formed with the polydisperse PAA used in the experiments described above. The low MW PAA does not form a Ca/PAA-rich phase, while the 14 kDa PAA forms PILPs that appear similar to those seen in the polydisperse PAA samples. After mineralization occurred in these systems, mineral was extracted and analyzed via SEM. The  $\text{CaCO}_3$  particles seen in the low MW PAA sample that lacked PILPs are small and appear amorphous but have an additional unexpected feature: small round impressions in the mineral, roughly 100 nm in diameter. These structures result from embedded lipid vesicles present during the formation of the ACC. In contrast, mineral formed in the 14 kDa PAA-containing AMV system takes on the overall shape and size of the phase within

which it forms, but exhibits a rough surface with cubic protrusions and contains a mixture of amorphous and crystalline material. When both long and short PAA is present, we see material similar to those seen for the polydisperse PAA described above, indicating that multiple PAA lengths serve important roles in during the mineralization process.

Slight changes to the chemical structure of the polymeric chelator also impact the mineral morphology. PAA and polyglutamic acid (PGA) differ only in one additional  $\text{CH}_2$  group between the amide backbone and the carboxylate moiety.

When PGA is substituted for PAA in the AMVs, a PGA/Ca phase still occurs, but the resulting mineral has a different overall morphology and is predominantly crystalline rather than amorphous. When both polycarboxylates are present, two concentric phases occur, presumably one rich in PGA/Ca and the other in PAA/Ca. The  $\text{CaCO}_3$  microspheres that form inside these structures have a smooth surface and are composed of predominantly ACC. These results are exciting because the ability to incorporate additional phases with differing structure-directing organic components provides an additional means of tuning the mineralizing microenvironment and is an important step towards forming different mineral compositions in adjacent compartments.

*Heat treatment of the mineral samples changes the crystal structure while maintaining the overall shape.* We were interested to learn whether the large, spherical ACC structures formed in AMVs could be converted to spherical calcite structures.  $\text{CaCO}_3$  formed inside a PAA-containing AMV was heated to facilitate conversion to calcite. The resulting particles were still roughly spherical, with signs of the core shell structure still intact (Figure 3). The IR spectrum for this heat-treated material indicates loss of water and conversion towards a more calcite-like structure (Figure 4), and optical microscopy indicated that the heat-treated samples were birefringent, as expected for calcite. We are excited to expand on this to convert  $\text{CaCO}_3$  formed under a variety of conditions with different overall shape and organic inclusions to calcite to evaluate the optical and mechanical properties of the resulting minerals.

*Internal structure of  $\text{CaCO}_3$  microspheres.* Scanning electron microscope images show signs of stress fractures, and sometimes holes, in some of the  $\text{CaCO}_3$  microspheres. This suggested that the microspheres may not be solid. To investigate the interior structure of the particles, cross-sections of single  $\text{CaCO}_3$  spheres formed in PAA-containing AMVs were obtained using focused ion beam milling (FIB, Figure 5, left) and by embedding the particles in epoxy for microtoming (Figure 5, right). SEM images of the center of the microspheres, exposed by

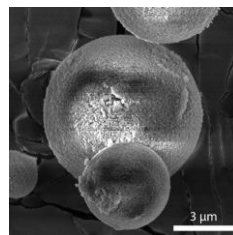


**Figure 3.** Scanning electron microscope image of  $\text{CaCO}_3$  mineral particles formed in PAA-containing AMVs after heat treatment.

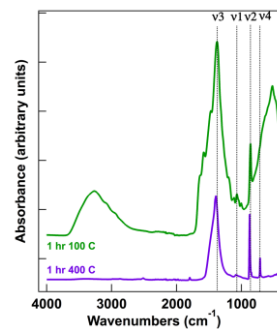


**Figure 4.** IR spectra for  $\text{CaCO}_3$  mineral particles formed in PAA-containing AMVs after heat treatment.

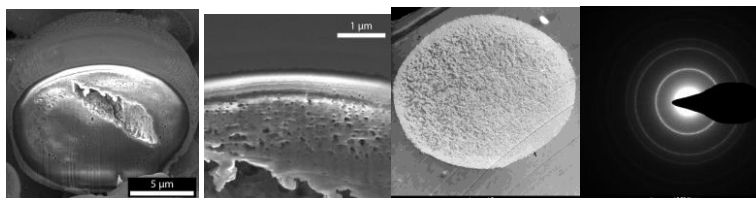


**Figure 5.** Viewing the inside of the  $\text{CaCO}_3$  spheres formed in PAA-containing AMVs by: (left 2 panels) Ion milling to reveal interior followed by SEM imaging; (right 2 panels) Microtome sectioning with TEM imaging and electron diffraction pattern indicating polycrystalline structure after heating. All data are for the polydisperse PAA systems.

FIB, show core-shell structures. The shell appears to be solid, while the core is porous. MicroRaman analysis also shows a core/shell structure with denser shells and indicates that PAA is incorporated throughout these CaCO<sub>3</sub> microspheres. TEM images of microtomed sections also indicate denser material in the shell region and a porous interior; in these (heated) samples, diffraction patterns show microcrystalline structure. Efforts are underway to further characterize these materials and to evaluate differences between microspheres formed in different phase systems. We hope to gain not only structural information but also to probe mechanical properties across these thin sections of organic/inorganic hybrid material and have begun atomic force microscopy studies.

### **Future Plans**

Our focus in the immediate future is to continue our efforts to understand how microenvironments produced by liquid-liquid phase separation within artificial mineralizing vesicles can be used to control the availability of mineral precursors, structure-directing agents, and potential organic and inorganic inclusions during mineralization. Our results thus far suggest that compositional gradients can occur due to reaction progression that in turn impact the reaction rates, locations, and products. We are also interested in taking advantage of our ability to form multiple adjacent mineralizing compartments to enable co-mineralization of multiple materials. By performing different mineral-forming reactions in different liquid phase compartments within the same artificial mineralizing vesicle, we will generate different minerals in close proximity to each other. The shape and association of the two solid products will be varied by controlling the relative interfacial tensions between their precursor phases. We will also explore competing enzymatic reactions that form distinct mineral products and that form/dissociate the microenvironments in which these minerals form, and look for emergent properties in these complex systems.

### **References**

1. Bioreactor droplets from liposome-stabilized all-aqueous emulsions. Dewey, D. C.; Strulson, C. A.; Cacace, D. N.; Bevilacqua, P. C.; Keating, C. D. *Nature Communications* **2014**, *5*, 4670.
2. Aqueous emulsion droplets stabilized by lipid vesicles as microcompartments for biomimetic mineralization. Cacace, D. N.; Rowland, A. T.; Stapleton, J. J.; Dewey, D. C. and Keating, C. D. *Langmuir* **2015**, *31*, 11329-11338.
3. Biocatalyzed mineralization in an aqueous two-phase system: Effect of background polymers and enzyme partitioning. Cacace, D. N.; Keating, C. D. *J. Mater. Chem. B* **2013**, *1*, 1794-1803.
4. Biomimetic model systems for investigating the amorphous precursor pathway and its role in biomineralization. Gower, L. B. *Chemical Reviews* **2008**, *108*, 4551-4627.
5. Synthesis of single crystals of calcite with complex morphologies. Park, R. J.; Meldrum, F. C. *Advanced Materials* **2002**, *14*, 1167-1169.

### **Publications**

1. Aqueous emulsion droplets stabilized by lipid vesicles as microcompartments for biomimetic mineralization. Cacace, D. N.; Rowland, A. T.; Stapleton, J. J.; Dewey, D. C. and Keating, C. D. *Langmuir* **2015**, *31*, 11329-11338.

## Guiding Nanoparticle Assemblies through the use of DNA Nanocages

Sanat K. Kumar, Oleg Gang

Columbia University, New York, NY

Shawn Douglas

University of California, San Francisco, CA.

### Program Scope

The major goal of this research is to use DNA frames to assist in the assembly of nanoparticles (NPs) or proteins into desired 3D arrays. We propose to entrap the NPs into the frames and then organize them through the assembly of the encoded frames. The work involves the assembly of DNA into frames (“origami”), assembling the frames into 3D superstructures and characterizing the resulting structures and modeling to complement, understand the interpret the experimental results. The work aims developing a general method for organizing inorganic and organic nano-components into designed 3D arrays.

### Recent Progress

#### Experiment

We have been actively developing a new approach for creating fully self-sustainable 3D DNA ordered frameworks, which lattice symmetry is determined by the spatially defined anisotropic bonds of DNA frames (cages). Such frameworks will be able to host practically any types of nanoparticles or bio-macromolecules through engaging them, thus provide a universal platform for building ordered 3D materials by design. The approach potentially allows to decouple the process of 3D material fabrication via self-assembly from the specific particle details, as result it promising for establishing a broadly applicable nano-assembly methodology. We have achieved a significant progress in this direction: (i) achieved for the first time the 3D crystallization of complex shaped DNA origami frames; (ii) demonstrated a new approach for building designed 3D arrays of inorganic particles (gold and cadmium selenide) using DNA framework; (iii) demonstrated for the first time an ability to organize proteins in complex, yet fully designed, 3D arrays; (iv) developed a methodology for probing and characterizing DNA frameworks using scattering and electron microscopy methods.

For our experimental realization 3D DNA crystalline frameworks, we designed polyhedral DNA cages, octahedron and cubes, which vertices can hybridize through single stranded (ss) DNA with complementary strands on other cages. Octahedral DNA origami frame consist of twelve edges with each edge composed of a 6-helix-bundle (6HB) with a length of 84 base pairs to maintain the 3D morphology in buffer solution. Assembly of octahedra was carried out by mixing M13mp18 DNA scaffold with designed staple strands, followed by annealing. DNA sticky ends (marked blue in Figure 1a) were encoded to each vertex of the octahedron (OB) as shown in Figure 1a for further assembly with a vertex of another octahedron (OR) by complementary DNA (marked red). Using SAXS probing we reveal that for appropriate binding motifs between vertices self-assembly of micro-sized 3D DNA crystals can be achieved.

A significant advantage of this assembly method is that, we can insert any nanomaterials on demand inside of the DNA cages to obtain various kinds of complex lattices, where the lattice symmetry is dictated by valence and shape of the frame and its composition by engaged host species. For example, as shown in Figure 2a, we insert quantum dots

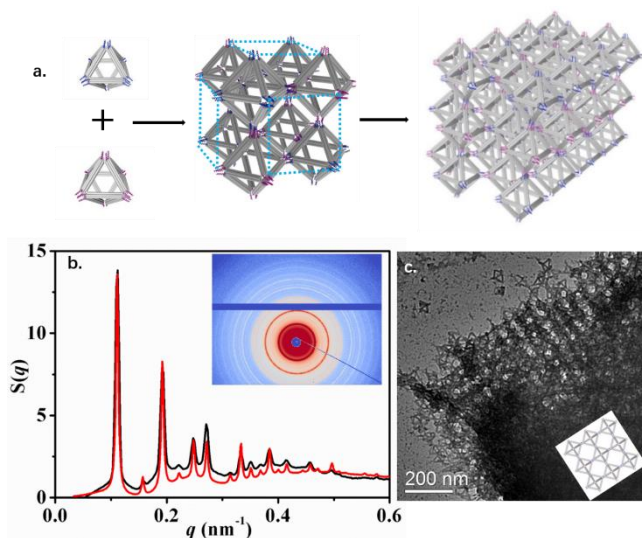


Figure 1. Assembly of octahedra into ordered DNA framework. (a). DNA octahedra frames with complementary sticky ends were mixed to form DNA lattice. The unit cell is shown in a middle (b). SAXS pattern and extracted structure factor  $S(q)$  for 3D DNA lattice (black curve for experimental data and red curve for fitting). (c). Representative negative stained TEM image for octahedral DNA lattice with the illustration showing corresponding orientation.

(QDs, 5nm core) into DNA frame. Figure 2b demonstrates a correct assembly of octahedron-QD complex. By mixing QDs and octahedral frames with complementary strands at vertices, followed by annealing, an ordered 3D array of QD was obtained. Figure 2c (black curve) illustrates structure factor obtained from the synchrotron small angle x-ray

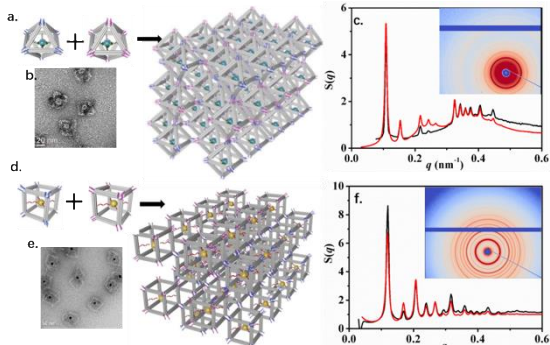


Figure 2. Designed assembly of 3D nanoparticle superlattices through caging particles in the DNA framework. (a). Assembly of QDs (blue sphere) arrays, where QDs are engaged by octahedra that are linked into 3D superlattice. (b). Representative negative stained TEM image for octahedron engaged QD. (c). SAXS image and the corresponding structure factor  $S(q)$  for QDs superlattice (black curve experimental data and red curve for fitting). (d). Assembly of 10nm gold nanoparticles, engaged by cubic frames, into 3D superlattice. (e). Representative negative stained TEM image for gold nanoparticle in a cube frame. (f). SAXS pattern and extracted  $S(q)$  for nanoparticle superlattice (black curve experimental data and red curve for fitting).

scattering SAXS measurements of this system. A high ordered structure with over ten peaks was observed and it matches well with the fitting curve (red line in Figure 2c) for the respective illustrated lattice formed by inter-vertex bindings. We then applied the demonstrated strategy for creation of other DNA framework symmetries, based on other frame geometries, such as cube. The designed cube DNA frame (Figure 2d) has dimensions similar to octahedron. The individual cubes are significantly skewed as demonstrated previously, which was resulted from intrinsic flexibility of cubic scaffold, but 10 gold particle hybridized inside cube allow for stabilization its shape, as shown by TEM imaging (Fig. 2e). Upon mixing and annealing of cubes with complementary strands at vertices 3D lattice of particle, arranged according to the DNA framework, is formed, as revealed by in-situ SAXS characterization. The 2D scattering patterns and the corresponding structural factor (Figure 2f) show the formation of body-centered-cubic (BCC) lattice. Each cube connects to eight other cubes by its hybridized vertices, that 8-fold directional valence promote the BCC arrangement. Remarkably, the theoretical findings (below) are in a full agreement with this observations for both octahedra and cubic frameworks.

Other than inorganic nanoparticles, DNA cages could also encapsulate other nano-size materials, for example, proteins. That potentially allow addressing challenges in protein structure determination, and to create highly dense protein arrays for catalytic, sensing and metabolic applications. We used streptavidin as model protein to demonstrate the feasibility of such approach. Figure 3a show the design of the frame with six streptavidins located at inner vertices. We first assembled such DNA-protein complex, as revealed by cryo-TEM 3D reconstruction (Fig. 3c). We then mixed and annealed complementary octahedra with encapsulated streptavidins to form 3D framework. We probed these assemblies for fluorescently labeled streptavidins by Confocal Fluorescence Microscopy (as shown in Figure 3d and observed  $\sim 5\mu\text{m}$  which matches well with the morphology and size of 3D DNA framework shown in Figure 1c). The internal structure of the streptavidin/protein assemblies was probed by SAXS (Figure 3e). While the peaks at the similar positions for empty and protein filled 3D DNA frameworks were observed, the intensity ratios of several peaks is different. Our detailed scattering modelling demonstrates that this difference is related to the presence proteins, and the results of the modelling are in excelnt agreement with the experimental observations. Thus, we have demonstrated for the first time, that well defined and fully designed DNA constructs can be utilized for building prescribed 3D frameworks. Such frameworks provide a universal scaffolding platform for organizing inorganic and bio-organic nano-objects into a 3D arrays.

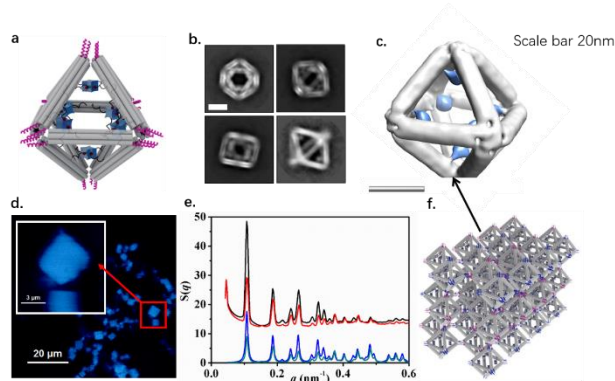


Figure 3. Encaging of 6 streptavidin inside DNA octahedron frame and the assembly of this DNA-protein blocks into 3D lattice. (a). An illustration of 6 streptavidin (green part) inserted octahedron. (b). Reference based 2D class average. (c). 3D density maps of 6 streptavidin engaged octahedron. (d). Representative confocal fluorescence microscopy images for assembled DNA-protein crystals. (e). Structure factor for empty and protein filled frameworks, data (top) and modelling (bottom). (f). An illustration of assembly of 6 streptavidin engaged octahedra into 3D DNA-protein superlattice.

## Theory

To gain additional insights into experimental observations, we seek to derive from first principles a theoretical model to understand molecular driving force governing the self-assembly of these DNA nanocages. Conventional theories for

DNA-mediated self-assembly build off of the idea proposed by Murray et al. which considers close contact as the driving force between interacting colloids and calculates a ground state free energy of formation for a given morphology. Many of the proposed theories are valid in the limit of both isotropic and dense distributions of interactions sites for all molecular species. These assumptions tend to be valid for traditional DNA-grafted colloidal/nanoparticle self-assembly as they reflect the high grafting densities employed. Our experimental system, however, operate in the opposite limit. Interactions sites are localized to small regions on the particles and the “patchy” sites tend to be sparse, reflecting a low DNA grafting density. For these reasons, conventional theories fail to properly capture the molecular driving forces governing DNA nanocage self-assembly. To properly account for these interactions, we extend the works proposed by Wertheim for associating fluids.

By definition, an associating fluid corresponds to a fluid composed of molecular species that interact with both a short-ranged and highly directional attractive potential, which aligns with the dominating interactions between DNA nanocages. To adapt Wertheim’s theory for our system, we must address one major assumption in the original derivation. Wertheim’s theory is a first order thermodynamic perturbation theory – that is, properties are calculated as an excess energy relative to some reference state. Wertheim employed a hard sphere fluid as the reference point of perturbation. Within this framework, interactions between associating “patches” can be viewed as a chemical reaction between two “unbonded” sites to form a “bonded” pair, allowing us to define the equilibrium constant as

$$K_l = n \int f_A(r) g_{HS}(r) d\vec{r} \quad (1)$$

where  $g_{HS}(r)$  is the radial distribution function of the reference hard sphere fluid and  $f_A(r)$  is the Mayer-f function defined as  $f_A(r) = \exp(-U(r)/kT) - 1$  where  $U(r)$  is the potential energy of interaction between the patches. The free energy change for the system can then be calculated as  $\Delta G = -kT \ln K_l$ .

The above expression for the equilibrium constant accurately describes bulk fluid self-assembly, but will fail for lattice predictions as the crystalline morphology deviates too far from that of a bulk fluid to be properly captured by a first order approximation. Here, we recast the reference state to that of any crystalline structure of interest and obtain an equivalent equilibrium rate constant

$$K_c = \frac{\rho_o^{n-1}}{(n-1)!} \int f_A^{\phi(m,n)}(r) g_{CR}(r) d\vec{r} \quad (2)$$

where  $\rho_o$  is the density,  $g_{CR}(r)$  is the radial distribution function of the reference crystalline structure, and  $\phi(m,n)$  is a coordination saturation parameter that depends on  $n$ , the number of patches, and  $m$ , the crystal coordination number associated with the reference structure.

$$\phi(m, n) = \begin{cases} n & m \geq n \\ m & m < n \end{cases} \quad (3)$$

While subtle, it is worth noting important differences between  $K_l$  and  $K_c$ . First, the reference state is in term of a hard sphere crystal lattice rather than that of a liquid hard sphere fluid.  $K_l$  describes the free energy change due to local perturbations about a homogeneous solution that results from patchy associations.  $K_c$ , on the other hand, probes how turning on association between particles already occupying lattice sites further stabilizes the reference crystal structure. Second, the power  $\phi(m,n)$  acting on  $f_A(r)$  accounts for association of a reference particle to its neighbors within the crystal lattice. In the limit where  $m \geq n$ , the reference particle possesses an excess number of patches than required by the crystal coordination number. Here, all attractions that stabilize the lattice are satisfied and  $\phi = n$ , indicating that there are  $n$  bonds formed per particle within the lattice. In the opposite limit where  $m < n$ , the reference crystal has a coordination number greater than that of the number of patchy sites available on the particle. In those situations, the energetic contribution from association is limit to the number of patches on the particle, thus  $\phi = m$ . The pre-factor  $\rho_o^{n-1}/n!$  accounts for both the indistinguishably and probability of finding  $n - 1$  particles within the cutoff interaction distance.

Utilizing  $K_c$ , we can now calculate the lattice free energy of formation for the observed experimental structures. Fig. 4a and 4b represent the patchy model used in free energy calculation for the cubic and octahedral frames. Briefly, the cube has 8 interactions sites (one at each corner) and the octahedron has 6 patchy sites at each vertex. The size of the patch site reflect the experimental design parameters that correspond to a 10% and 8% vertex truncation of the cube and octahedron, respectively. Here, we predict that the cubic system preferentially self assembles into a body-centered

cubic structure (BCC) whereas the octahedron packs into a simple cubic (SC) lattice (Fig. 1c). The transition between BCC and SC morphologies can be explained by decomposing the  $\Delta G$  into its enthalpic and entropic components,  $\Delta G = \Delta H - T\Delta S$ . By a standard binomial expansion, we can write  $f_A^\phi = \sum_{k=0}^{k=\phi} \binom{\phi}{k} (-1)^{\phi-k} \left[ \exp\left(-\frac{u(r)}{kT}\right) \right]^k$ . Applying the patchy particle requirement for strong and short-ranged binding results in,  $\Delta H \sim \frac{m}{n} \phi(m, n) u_o$  and  $\Delta S \sim \ln \left[ \frac{m \rho_o^{n-1}}{n!} \right]$  where  $u_o$  is the potential well of patch-patch attraction between the particles. By inspection,  $\Delta H \gg \Delta S$  and the total free energy becomes enthalpically dominated. For cubes within this enthalpically driven crystallization regime, BCC is favored for as it has enough interaction sites to fully saturate bonding within the lattice (BCC has a coordination number of 8). Along the same vein, SC (coordination number 6) is less favored since the extra two patchy sites are not satisfied, reducing the effective free energy gain for a cube within the SC lattice by 25%. Similarly, for the case of the octahedron, SC is favored over BCC because the octahedron lacks the two additional patchy sites to fully saturate an 8 coordination lattice. While we expect a deficit valency (relative to the crystal coordination number) to destabilize the lattice, our analysis indicates that an excess patch count also serves to reduce lattice stability as the net energy gain per particle is reduced due to the presence of “free” sites. These results emphasize that there exist a crucial interplay between patch count and the crystal coordination of the resulting lattice, suggesting that valency matching could provide a powerful design handle for DNA nanocage self-assembly.

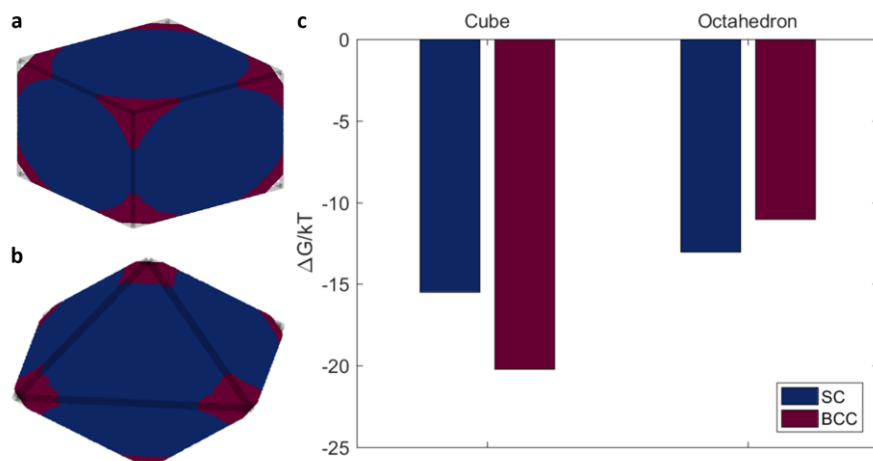


Figure 4. Free energy calculation. a). Patchy model of cubic nanocage. b). Patchy model of octahedral nanocage. Blue indicates non-interacting regions and magenta represents patchy association sites. Transparent lines included to as a visual guide to frame each polyhedron. c). Lattice free energy prediction per patchy particle. In agreement with experimental observations, the body-centered cubic (BCC) and simple cubic (SC) are the predicted equilibrium structures for cubes and octahedron, respectively.

## Future Work

Our future work is focused on designing the DNA origami (frames) structure so that we can a priori design the resulting crystalline structure of the nanoparticle arrays that result. This will involve a close collaboration between the theoretical works of Kumar and Douglas, and the experimental works of Gang and Douglas. In particular, we highlight the use of CAD Nano to design the DNA frames, while the use of the inverse design approach will greatly facilitate us to pinpoint the DNA structures that we need for the Douglas group to design.

## References

- [1]. Ye Tian, Tong Wang, Yugang Zhang, Huilin Li and Oleg Gang “Lattice Engineering via Nanoparticle-DNA Frameworks”, *Nature Materials*, doi:10.1038/nmat4571 (2016)
- [2]. W. Liu, J. Halverson, Y. Tian, A.V. Tkachenko, O. Gang, “Self-organized architectures from assorted DNA-framed nanoparticles”, *Nature Chemistry*, 8, 867–873 (2016)
- [3]. S. Ciarella, O. Gang, F. Sciortino Toward the observation of a liquid-liquid phase transition in patchy origami tetrahedra: a numerical study” *The European Physical Journal E*, 39, 131 (2016)
- [4]. Wenyang Liu, Nathan A. Mahynski, Oleg Gang, Athanassios Z. Panagiotopoulos, and Sanat K. Kumar “Self-Assembly of Directionally Interacting Spheres and Rods”, *ACS Nano*, 11, 4950 (2017)
- [5]. M. S. Wertheim “Fluids with highly directional attractive forces. ii. thermodynamic perturbation theory and integral equations”, *J. Stat. Phys.*, 35, 35 – 47 (1984).
- [5] M. S. Wertheim “Fluids with highly directional attractive forces. iii. multiple attraction sites”, *J. Stat. Phys.*

42, 459-476 (1986).

[6]. F. Sciortino, E. Bianchi, J. F. Douglas, P. Tartaglia, "Self-assembly of patchy particles into polymer chains: A parameter-free comparison between wertheim theory and monte carlo simulation", J. Chem. Phys, 126, 193903 (2007).

### **Publications**

[1]. Wenyan Liu, Nathan A. Mahynski, Oleg Gang, Athanassios Z. Panagiotopoulos, and Sanat K. Kumar "Self-Assembly of Directionally Interacting Spheres and Rods", ACS Nano, 11, 4950 (2017)

## **Controlled synthesis and ordered assembly of Co<sub>3</sub>O<sub>4</sub> nanowires using genetically engineered bacterial flagella as biotemplates**

**Principal Investigator: Chuanbin Mao, Department of Chemistry & Biochemistry,  
University of Oklahoma**

**Co-Investigator: Chunlong Chen, Physical Science Division, Pacific Northwest National  
Laboratory**

### **Program Scope**

Lithium-ion batteries have been widely used as power sources for portable electronic devices including mobile phones, laptops and tablets, digital cameras, as well as electric vehicles such as aircrafts and electric wheelchairs. To develop the next generation lithium-ion batteries, it is essential to improve the electrochemical performance of electrode materials. Co<sub>3</sub>O<sub>4</sub>, an important member of transition metal oxides, is a promising alternative anode material in lithium-ion batteries because its theoretical capacity (890 mAh/g) is almost three times higher than that of graphite (372 mAh/g), which is the commonly used anode material.<sup>1-2</sup> On the other hand, using nanosized materials as anode materials batteries can greatly improve the energy density and cycling stability of lithium-ion batteries due to their unique properties comparing to their bulk forms.<sup>3-5</sup> It has been demonstrated that Co<sub>3</sub>O<sub>4</sub> nanoparticles (NPs) can retain nearly 100% of the capacity for up to 100 cycles under high recharging rates, which can hardly be achieved by conventional anode materials.<sup>6-7</sup> Among the different morphologies of nanosized Co<sub>3</sub>O<sub>4</sub>, one-dimensional (1D) Co<sub>3</sub>O<sub>4</sub> nanostructures have exhibited superior electrochemical performance than others since they can give short pathways for electron transport and high kinetics for lithium ion insertion/extraction.<sup>1, 7-10</sup> Inspired from this, we will use the bioengineered bacterial flagella as a biotemplate to understand the rules that govern the nucleation and assembly of Co<sub>3</sub>O<sub>4</sub> NPs on flagella to form nanowires (NWs) with controllable length, and the assembly of the resultant NWs into 2D/3D Co<sub>3</sub>O<sub>4</sub>-flagella nanocomposites.

We aim to gain a fundamental understanding on the influence of the displayed peptides and other processing parameters on the flagella assembly and the resulting biomimetic control over the synthesis and assembly of Co<sub>3</sub>O<sub>4</sub> NPs and NWs. We will carry out two specific aims: **Aim 1: Understanding the self-assembly of genetically engineered flagella and its outcome for site-specific nucleation and growth of Co<sub>3</sub>O<sub>4</sub> NPs and NWs.** We will take advantage of our flagellar display technique to genetically insert peptides with different lengths and charges. Fundamental studies about the effect of these foreign peptides on flagella morphology, surface structure and chemistry, as well as in vitro assembly dynamics will be performed. After the primary study of in vitro assembled and genetically engineered flagella templates, Co<sub>3</sub>O<sub>4</sub> NPs will be synthesized or assembled all over the bionanofibers to form Co<sub>3</sub>O<sub>4</sub> NWs with various patterns and structures. The mechanism of Co<sub>3</sub>O<sub>4</sub> formation on flagella surface including the effects of different foreign

peptides on nanomaterial morphology will be investigated. **Aim 2: Understanding controllable alignment of 1D Co<sub>3</sub>O<sub>4</sub>-flagella NWs into highly-ordered 2D and 3D structures.** The organization of Co<sub>3</sub>O<sub>4</sub>-flagella NWs into highly ordered 2D and 3D complexes will decrease the gap between individual nanomaterials and practical application, and understanding the pathways leading to the organization will provide guidance for achieving different organizations. Due to the filamentous morphology, uniform size and magnetic property of these NWs, we aim to conduct fundamental studies on how different processing factors control the organization pathways in two fabrication methods, evaporation induced assembly and magnetic field-assisted assembly, which can lead to different organized structures, including radically aligned NWs films, single-orientation horizontally aligned NWs arrays, multi-orientation multilayered NWs assemblies and vertically aligned NWs arrays.

### Recent Progress

We mainly focused on the first aim in the past year. So far we have successfully displayed various foreign peptides containing different sequences, charges and length on the surface of flagella through genetic engineering (Table 1). The *in vitro* assembly of wild flagella and the engineered flagella displaying E10 peptide were studied through depolymerization and repolymerization (Figure 1). The reassembled flagella showed same morphology to the intact flagella which are directly purified from the bacteria body. This indicates the establishment of the *in vitro* assembly method of flagella. In addition, the Co<sub>3</sub>O<sub>4</sub> NPs with different sizes (3.5 nm, 6 nm and 11 nm) were synthesized (Figure 2). These NPs will be aligned on flagella templates displaying different foreign peptides to form Co<sub>3</sub>O<sub>4</sub> NWs with various patterns and structures through electrostatic interaction.

**Table 1.** Sequences to be displayed on the surface of flagella. E, glutamate; K, lysine; G, glycine.

Name	Sequence
E5	EEEEEE
E10	EEEEEEEEEE
E20	EEEEEEEEEEEEEEEEEEEE
G5	GGGGG
G10	GGGGGGGGGG
G20	GGGGGGGGGGGGGGGGGGGG
K5	KKKKK

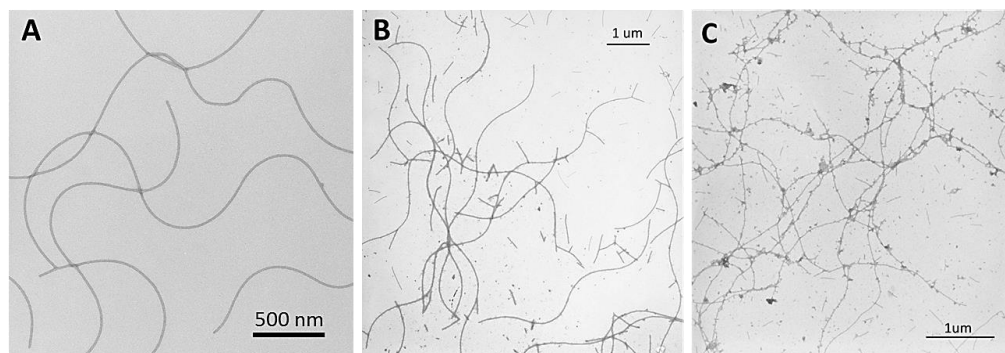


**Figure 1.** TEM images of intact wild type flagella purified from bacteria surface (A), *in vitro* reassembled wild type flagella (B), and *in vitro* reassembled engineered flagella displaying E10 peptide all over the bionanofibers (C).

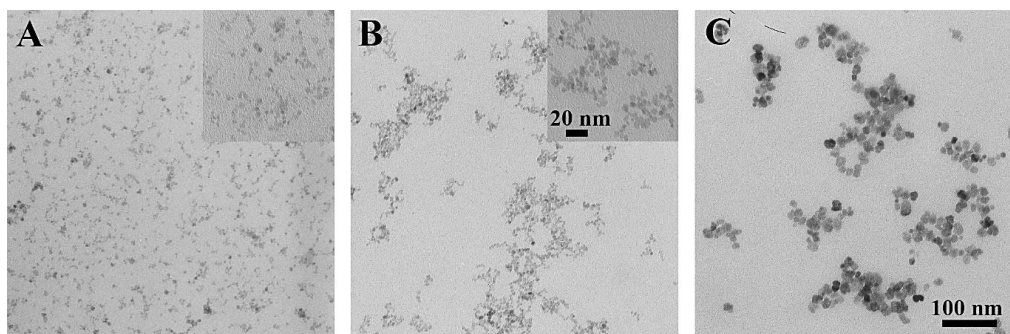


**Figure 2.** TEM images of  $\text{Co}_3\text{O}_4$  nanoparticles with different sizes. A, 3.5 nm; B, 6 nm; and C, 11 nm, respectively.

## Future Plans

We will collaborate with Dr. Chun-Long Chen at PNNL to investigate the effect of the foreign peptide for the morphology of natural and engineered flagella through Cryo-TEM. The dynamic study of flagellin polymerization, or in vitro flagella assembly, will be performed exploiting in situ AFM. After the primary study of in vitro assembled and genetically engineered flagella templates,  $\text{Co}_3\text{O}_4$  NPs will be synthesized or assembled all over the bionanofibers to form  $\text{Co}_3\text{O}_4$  NWs with various patterns and structures. In addition, the dynamic investigation of the mechanism of  $\text{Co}_3\text{O}_4$  formation on flagella surface including the effects of different foreign peptides on nanomaterial morphology will be performed.

## References

1. Yao, X. Y.; Xin, X.; Zhang, Y. M.; Wang, J.; Liu, Z. P.; Xu, X. X.,  $\text{Co}_3\text{O}_4$  nanowires as high capacity anode materials for lithium ion batteries. *J Alloy Compd* **2012**, *521*, 95-100.
2. Cabana, J.; Monconduit, L.; Larcher, D.; Palacin, M. R., Beyond Intercalation-Based Li-Ion Batteries: The State of the Art and Challenges of Electrode Materials Reacting Through Conversion Reactions. *Adv Mater* **2010**, *22* (35), E170-E192.
3. Wang, Y. G.; Li, H. Q.; He, P.; Hosono, E.; Zhou, H. S., Nano active materials for lithium-ion batteries. *Nanoscale* **2010**, *2* (8), 1294-1305.
4. Ji, L. W.; Lin, Z.; Alcoutlabi, M.; Zhang, X. W., Recent developments in nanostructured anode materials for rechargeable lithium-ion batteries. *Energ Environ Sci* **2011**, *4* (8), 2682-2699.
5. Poizot, P.; Laruelle, S.; Grugeon, S.; Dupont, L.; Beaudoin, B.; Tarascon, J. M., Electrochemical reactivity and reversibility of cobalt oxides towards lithium. *Cr Acad Sci li C* **2000**, *3* (8), 681-691.
6. Poizot, P.; Laruelle, S.; Grugeon, S.; Dupont, L.; Tarascon, J. M., Nano-sized transition-metal oxides as negative-electrode materials for lithium-ion batteries. *Nature* **2000**, *407* (6803), 496-499.
7. Shaju, K. M.; Jiao, F.; Debart, A.; Bruce, P. G., Mesoporous and nanowire  $\text{Co}_3\text{O}_4$  as negative electrodes for rechargeable lithium batteries. *Phys Chem Chem Phys* **2007**, *9* (15), 1837-1842.

8. Jiang, J. A.; Li, Y. Y.; Liu, J. P.; Huang, X. T., Building one-dimensional oxide nanostructure arrays on conductive metal substrates for lithium-ion battery anodes. *Nanoscale* **2011**, *3* (1), 45-58.
9. Reddy, M. V.; Rao, G. V. S.; Chowdari, B. V. R., Metal Oxides and Oxysalts as Anode Materials for Li Ion Batteries. *Chem Rev* **2013**, *113* (7), 5364-5457.
10. Nam, K. T.; Kim, D. W.; Yoo, P. J.; Chiang, C. Y.; Meethong, N.; Hammond, P. T.; Chiang, Y. M.; Belcher, A. M., Virus-enabled synthesis and assembly of nanowires for lithium ion battery electrodes. *Science* **2006**, *312* (5775), 885-888.

## Biomolecular assembly processes in the design of novel functional materials

Jeetain Mittal

Department of Chemical and Biomolecular Engineering, Lehigh University, Bethlehem, PA 18015.

Email: [jeetain@lehigh.edu](mailto:jeetain@lehigh.edu)

### Program Scope

The objective of our research program is to develop new computational models calibrated, aided, and validated by experimental measurements to understand and predict biomolecular assembly processes with a special emphasis on these happening in the presence of nanomaterials such as carbon nanotubes, gold, and polymer nanoparticles. The first focus area is the rational design of complex materials mediated by hybridization between DNA-functionalized particles (DFPs) (1). We have developed a multiflavoring approach to demonstrate the usefulness of DFP assembly for the design of binary superlattices. We are also contributing to the development of a new class of photoluminescent reporters consisting of single-walled carbon nanotubes (SWCNTs) noncovalently complexed with single-stranded DNA (ssDNA). The understanding of nucleic acid behavior at interfaces is relevant for a wide range of scientific and technological applications such as DNA-based nanomaterials, recognition and separation of carbon nanotubes (2), and DNA biosensors and microarrays (3). In addition, we are developing a computational model to understand the self-assembly behavior of intrinsically disordered proteins into liquid-like and hydrogel states. We are particularly interested in mapping out the sequence-dependent phase behavior of proteins that can be used as a guide for the design of protein-based materials.

### Recent Progress

**Binary superlattice design.** Most commonly used single-flavored DFPs are grafted with one type of DNA sequence that can only recognize and bind its complementary binding partner on another particle. The blending of different types of DNA sequences on the same particle can allow tunable control over inter-particle interactions, referred to here as multi-flavored DFPs (Figure 1). We have studied the role of this additional tuning parameter in the selection of stable crystalline structures in two-dimensional (2D) and three-dimensional (3D) assembly of micron-sized colloidal silica particles. We show that such a simple extension can be used to program diverse 2D lattices, e.g., non-closed packed square lattice, close-packed hexagonal lattice with compositional ordering in alternating-string (AS), honeycomb, and kagome structures (Figure 2). We note that the current approach for binary superlattice formation primarily relies on entropic packing effects to generate structures with desired lattice

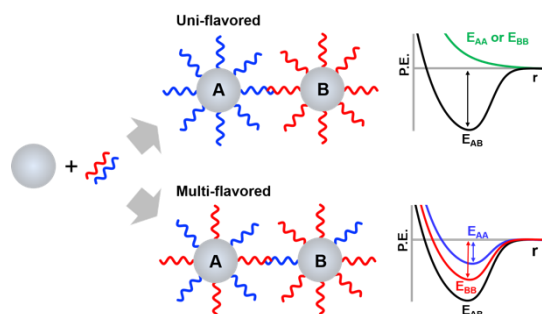


Figure 1. Multiflavoring design scheme to tune interparticle interactions.

symmetries. Our approach can be characterized as an enthalpic design strategy, which takes advantage of interparticle attractions between equally-sized, to guide assembly into compositionally ordered lattices.

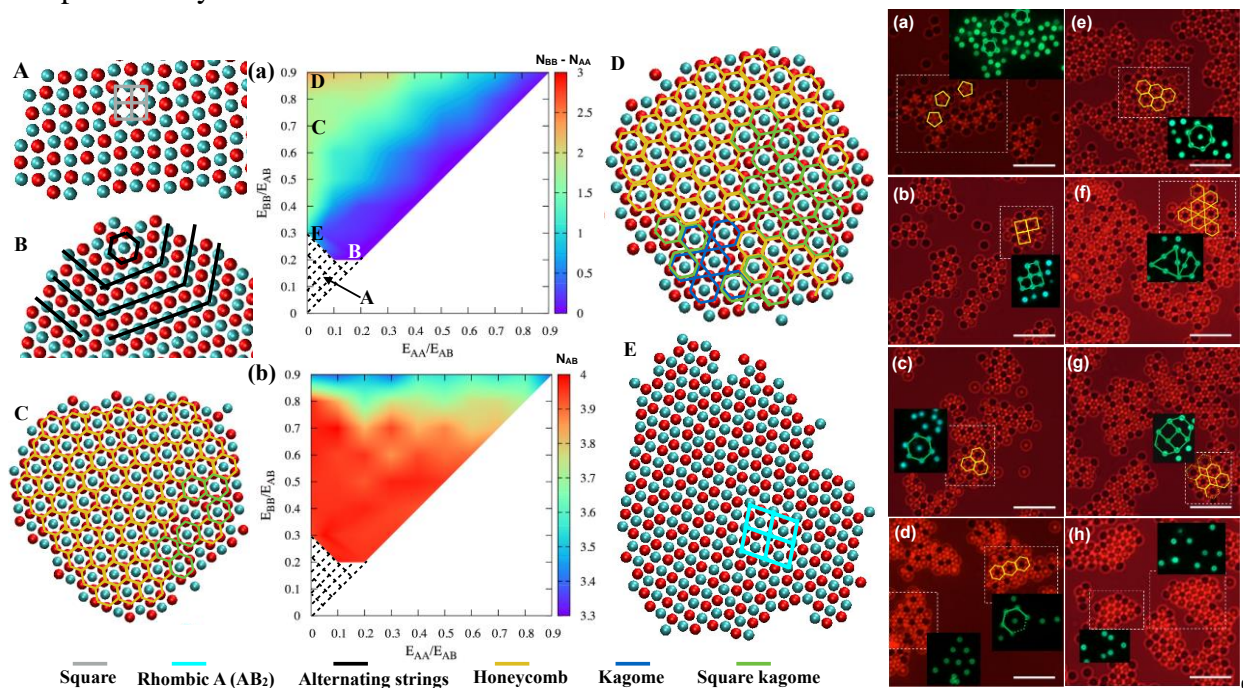


Figure 2. (Left) Computational order diagram for 2D assembly of DFPs using multiflavoring approach shown in Fig. 1. (Right) Experimental validation of simulation results using micron-sized silica particles.

In case of 3D binary superlattice design, we have applied the same strategy as above. As shown

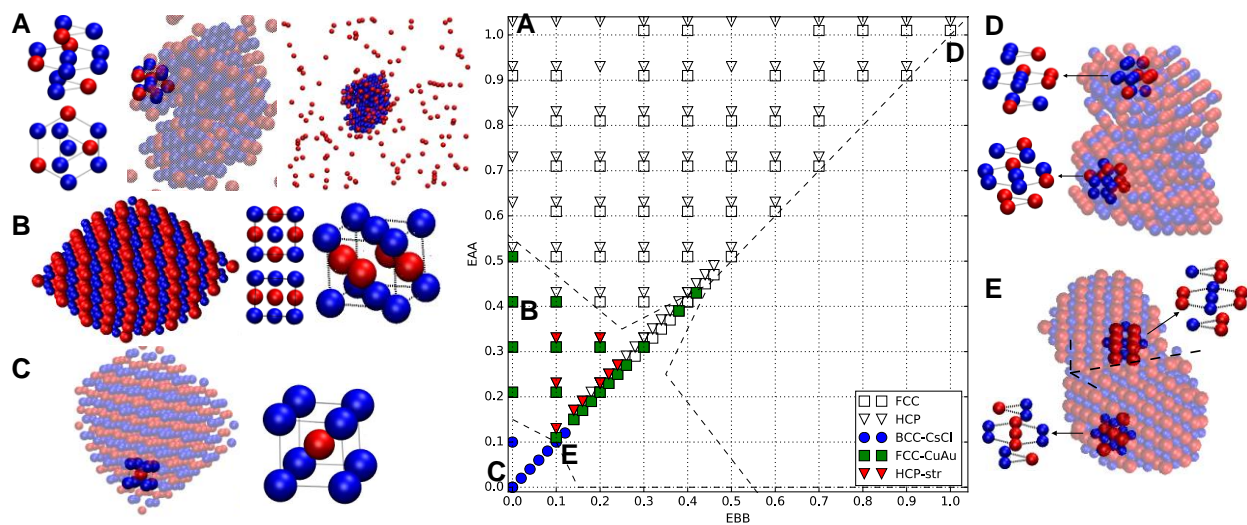


Figure 3. (Left) Computational order diagram for 3D assembly of DFPs using multiflavoring approach shown in Fig. 1. Representative snapshots from MD simulations are also shown highlighting various binary superlattices that can be formed with this approach.

in Figure 3, we can observe formation of non-closed packed BCC lattice for low values of interparticle interaction strengths between same type of particles, but these lattices transform to close-packed hexagonal lattices such as FCC and HCP at high values. We also check the compositional order in these cases and find that BCC, FCC, HCP lattices are of CsCl, CuAu, and Straight types, respectively. Most importantly, unlike 2D systems we do not observe the formation of high symmetry compositional lattices such as AB<sub>2</sub> or AB<sub>3</sub> type binary superlattices. Further analysis of the crystalline lattices along the vertical axis (zero x-axis value) suggests that the crystalline lattices are of higher stoichiometry, but the arrangement of A and B particles is not compositionally ordered. Work is under progress to better understand this and to find ways to promote compositional order. These studies should open the door for assembling complex nanostructured materials using a controllable synthesis strategy.

**Development of nanobiosensors.** In collaboration with Prof. Dan Heller's group at Memorial Sloan Kettering Cancer Center, we have studied the self-assembly of ssDNA molecules adsorbed on SWCNT and the response of SWCNT-DNA reporter to the presence of other macromolecules such as mRNA and lipids (Figure 4).

We used all-atom simulations to assess the stability of the partially hybridized DNA molecules adsorbed on the nanotube surface. We found that the hybridized DNA is stable in the vertically aligned configuration, which is consistent with experimental data.

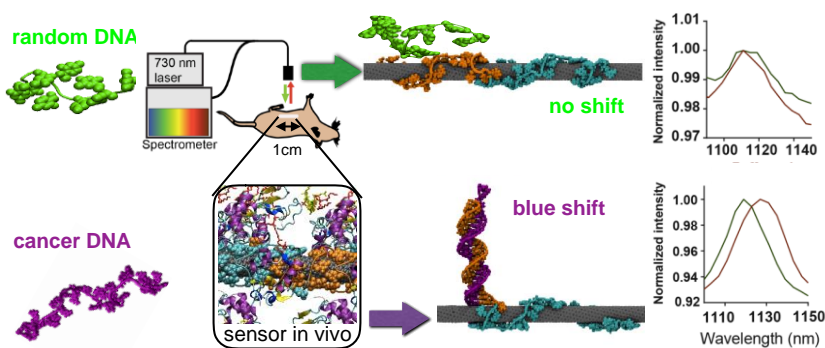


Figure 4. Schematic of the reporter which can distinguish between the spectral response to a disease biomarker from a random DNA sequence.

We used our simulation data further to understand spectral response upon hybridization. We found two competing effects, increase in water density near the nanotube but a decrease in anionic phosphate groups, that will give rise to blue shift as observed in experiment. Simulations also helped identifying empty patches on the nanotube surface that were experimentally saturated with SDBS surfactant to stabilize and enhance the reporter signal. In separate study, we also conducted simulations in the presence of lipid molecules such as cholesterol and sphingomyelin. The adsorption of lipid molecules especially cholesterol was found to reduce water density near the SWCNT-ssDNA reporter that will result in red shift as expected from experimental data. We also elucidated the structure of cholesterol adsorbed and assembled on the nanotube surface in the presence of ssDNA.

**Protein-based material design.** As part of this research program, we are developing a new coarse-grained model to study the phase separation of intrinsically disordered proteins (IDPs) into dense liquid-like and solid-like hydrogel states. Our primary aim is to have a model which is scale accurate and computationally efficient to perform large-scale assembly simulations that can

guide the advancement of better theoretical understanding of sequence-dependent phase behavior of proteins. So far, we have been successfully able to put together a working model which is

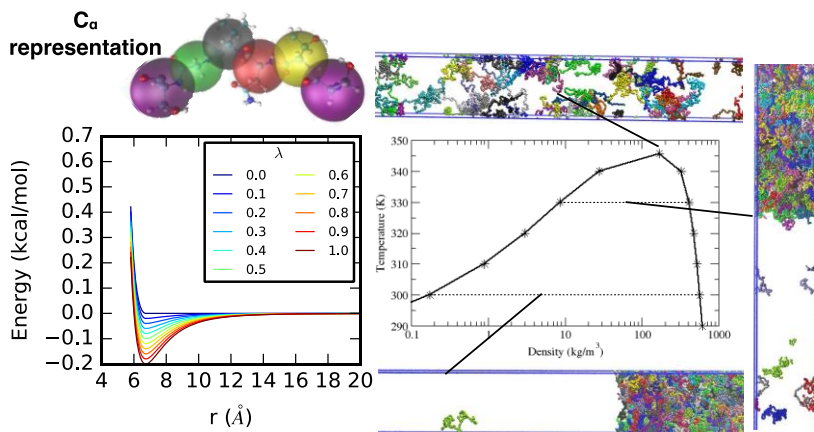


Figure 5. (Left) Coarse-grained model and inter-residue interactions modeled with an LJ-type potential for which potential well-depth is tuned based on amino-acid hydrophobicity. (Right) Representative phase diagram for an IDP showing coexistence between low-density and high-density liquid-like assemblies.

based on  $C\alpha$ -representation of each amino acid and inter-residue interactions are parameterized based on hydrophobicity scale. Some details and results obtained from this model are shown in Figure 5. Preliminary results show that the model is suitable for studying the effect of mutations on protein phase behavior, but further work is needed to make it suitable to study temperature and salt

dependent changes in the phase behavior.

## Future Plans

We plan to focus on the following research questions in near future: (i) *Large scale simulations of DFP assembly using graphics processing units (GPUs)*. To elucidate the molecular details of the assembly process, we have implemented our coarse-grained model to HOOMD, which can provide simulation speed-up by several orders of magnitude. (ii) *Calculations of thermodynamic phase diagrams*. To go beyond observations from MD simulations and to dissect the role of thermodynamic and kinetic factors in DFP assembly, we are currently developing new tools to generate thermodynamic phase diagrams efficiently. (iii) *Effect of DNA properties on the kinetics of particle assembly*. We intend to use our CG model to study kinetic processes underlying DNA-mediated interactions and how to tune these to help obtain thermodynamically most stable crystalline structures.

## References

1. Park, S. Y., Lytton-Jean, A. K., Lee, B., Weigand, S., Schatz, G. C., & Mirkin, C. A. (2008). DNA-programmable nanoparticle crystallization. *Nature*, 451(7178), 553.
2. Zheng, M., et al. "Structure-based carbon nanotube sorting by sequence-dependent DNA assembly." *Science* 302.5650 (2003): 1545-1548.
3. Jeng, E. S., Moll, A. E., Roy, A. C., Gastala, J. B., & Strano, M. S. (2006). Detection of DNA hybridization using the near-infrared band-gap fluorescence of single-walled carbon nanotubes. *Nano Letters*, 6(3), 371-375.

## Publications

1. H. Zerze, N. A. Mahynski, E. Pretti, V. K. Shen, and J. Mittal, “Three-dimensional assembly of multiflavored DNA-functionalized particles” *Soft Matter* (to be submitted).
2. M. Song, Y. Ding, H. Zerze, M. A. Snyder, and J. Mittal, “Binary superlattice design by controlling DNA-mediated interactions” *Langmuir* (submitted).
3. G.L. Dignon, G. Zerze, J. Mittal, Membrane Interactions Stabilize Helicity in Human Islet Amyloid Polypeptide. *J. Phys. Chem. B* (under review)
4. P. V. Jena, D. Roxbury, T. V. Galassi, L. Akkari, C. P. Horoszko, J. Budhathoki-Uprety, N. H. Pipalia, A. S. Haka, J. D. Harvey, J. Mittal, F. R. Maxfield, J. A. Joyce, and D. A. Heller “A carbon nanotube optical reporter maps endolysosomal lipid accumulation and heterogeneity” *ACS Nano* (under review).
5. Z. Monahan, V. H. Ryan, A. M. Janke, K. A. Burke, G. H. Zerze, R. O’Meally, G. L. Dignon, A. E. Conicella, W. Zheng, R. B. Best, R. N. Cole, J. Mittal, F. Shewmaker, and N. L. Fawzi, "Low complexity domain phosphorylation disrupts FUS phase separation, aggregation, and toxicity" *EMBO Journal* (in press).
6. N. A. Mahynski, H. Zerze, H. W. Hatch, V. K. Shen, and J. Mittal, “Assembly of multiflavored two-dimensional colloidal crystals” *Soft Matter* (in press).
7. J. D. Harvey, P. V. Jena, H. A. Baker, G. H. Zerze, R. M. Williams, T. V. Galassi, Roxbury, J. Mittal, and D. A. Heller ”A carbon nanotube reporter of microRNA hybridization events in vivo”. *Nature Biomedical Engineering*, 1, 0041 (2017).
8. M. Song, Y. Ding, M. A. Snyder, and J. Mittal, “Effect of nonionic surfactant on association/dissociation transition of DNA-functionalized colloids” *Langmuir* 32, 10017 (2016).
9. A. E. Conicella, G. Zerze, J. Mittal, and N. L. Fawzi, “ALS Mutations Disrupt Phase Separation Mediated by  $\alpha$ -Helical Structure in the TDP-43 Low-Complexity C-Terminal Domain” *Structure* 24, 1537 (2016).
10. H. W. Hatch, S. Y. Yang, J. Mittal, and V. K. Shen. “Self-assembly of trimer colloids: Effect of shape and interaction range”, *Soft Matter* 12, 4170 (2016).
11. Z. A. Levine, M. V. Rapp, W. Wei, R. G. Mullen, C. Wu, G. H. Zerze, J. Mittal, H. H. Waite, J. N. Israelachvili, and J.-E. Shea “Surface force measurements and simulations of mussel-derived peptide adhesives on wet organic surfaces” *Proceedings of the National Academy of Sciences USA* DOI: 10.1073/pnas.1603065113 (2016).
12. G. Zerze, J. Mittal, and R. B. Best “Diffusive dynamics of contact formation in disordered polypeptides”, *Physical Review Letters* 116, 068102 (2016).
13. G. Zerze and J. Mittal, “Effect of O-linked Glycosylation on the Equilibrium Structural Ensemble of Intrinsically Disordered Polypeptides”, *Journal of Physical Chemistry B* 119, 15583 (2015).
14. G. Zerze, R. G. Mullen, Z. A. Levine, J.-E. Shea, and J. Mittal, “To what extent does surface hydrophobicity dictate peptide folding and stability near surfaces?” *Langmuir* 31, 12223 (2015).
15. G. Zerze, R. B. Best, and J. Mittal, “Sequence and temperature-dependent properties of disordered proteins from atomistic simulations”, *J. Phys. Chem. B* 119, 14622 (2015).

# Neutralization of a Distributed Coulombic Switch Tunes Reflectin Assembly and Biophotonics

Daniel E. Morse (Principle Investigator) and Robert Levenson (co-Investigator)

Institute for Collaborative Biotechnologies

University of California, Santa Barbara, CA 93106-5100

## Program Scope

Fundamental mechanisms and structure-function relationships of signal-dependent, dynamically tunable reconfigurability of proteins and protein-inspired synthetic, photonically active materials.

## Recent Progress

We have discovered the molecular mechanism by which the block copolymeric reflectin proteins act as a molecular machine, driving an osmotic motor to dynamically tune the color of light reflected from specialized cells in squid skin.

Cephalopods (squids, octopuses and cuttlefish) use tunable coloration for communication and camouflage (1). In addition to their pigmented chromatophores, Loliginid squid possess tunably iridescent cells in their skin called iridocytes. In these cells, acetylcholine (ACh) governs changes in subcellular Bragg lamellae to dynamically tune the color and brightness of reflected light through a structural (non-pigmentary) mechanism (**Figure 1A-B**). These Bragg lamellae, formed by periodic invaginations of the cell membrane, are filled with the metastable and transparent reflectin proteins that we have shown mediate tunability (**Figure 1C-D**). ACh-triggered phosphorylation progressively neutralizes the cationic reflectins, triggering the condensation and hierarchical assembly of the unpigmented reflectins (2,3). As a result of this transition, the reflectins act as a molecular machine, controlling an osmotic motor that

reversibly and cyclably tunes dehydration and rehydration of the Bragg lamellae, simultaneously controlling their refractive index, thickness and spacing to tune their photonic properties (4). The reflectins are archetypically structured as block copolymers, with highly conserved, repeated peptide domains separated by positively charged linkers (**Figure 1E**). Their sequences indicate

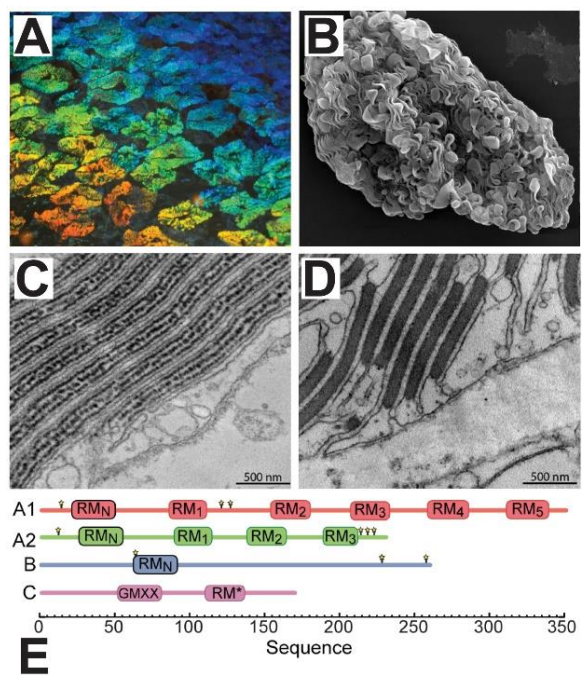


**Figure 1.** **A)** Dark-field image of iridescent *D. opalescens* iridocytes. **B)** SEM of an iridocyte, showing invaginations of cell membrane forming Bragg lamellae. **C-D)** Negatively stained TEM images of the tunable Bragg lamellae before (**C**) and after (**D**) ACh activation, showing induced condensation of reflectins. **(E)** Schematic of *D. opalescens* reflectin proteins.

that they are intrinsically disordered. Uniqueness of these sequences, with no known homologs, makes bioinformatic analyses challenging.

Codon-optimized recombinant *D. opalescens* reflectin proteins were expressed in *E. coli*, purified and analyzed for assembly after dilution in low ionic strength buffers, using titration with pH as an *in vitro* surrogate for the phosphorylation *in vivo*. Analyses by dynamic light scattering (DLS) and other biophysical methods revealed that charge neutralization generates

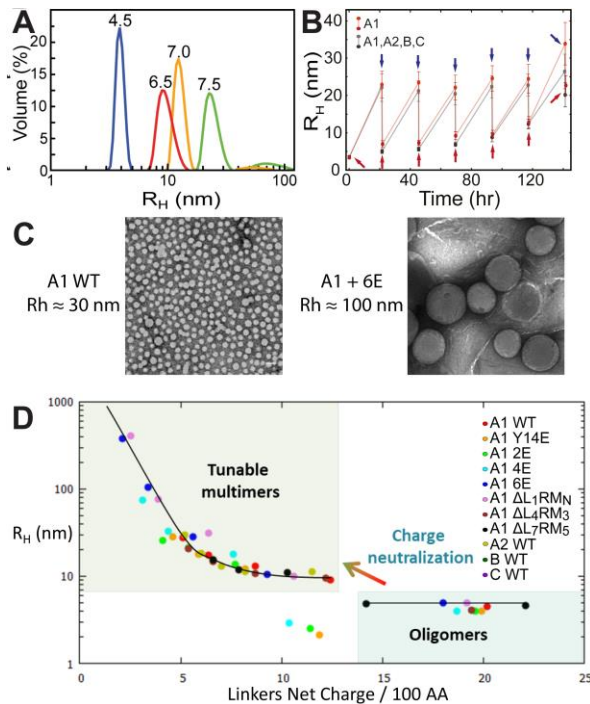


**Figure 2.** (A) Volume distribution of tunable *D. opalescens* reflectin A1 assemblies in buffers of increasing pH. (B) *In vitro* cyclability of reversible assembly (@ pH 7.5, blue arrows) and disassembly (pH 4.5, red arrows) of reflectin A1 and physiological mixture of all 4 reflectins. (C) Negatively stained TEM images of A1 WT and A1 mutant with six additional glutamates at sites of *in vivo* phosphorylation. (D) Size versus calculated linker net charge density for A1 WT and a library of mutants, plus A2, at various pH values, demonstrating the predictive relationship between these variables.

stable, low polydispersity spherical assemblies of reproducible size, with progressive neutralization (higher pH) producing larger particles (5) (Figure 2A). Assemblies varied from ~12 (oligomers) to thousands (multimers) of reflectin monomers. Assembly of reflectin A1 and of mixtures of the 4 different reflectins found in the iridocytes (Figure 1E) reversibly and cyclably formed particles of ca. 50-100 nm when neutralized by pH titration (Figure 2B), thus recapitulating the physiological process *in vitro*.

To identify the structural determinants of assembly, we characterized deletion and “phosphomimetic” (extra glutamate) mutants of A1. Purified phosphomimetic and deletion mutant reflectins formed monodisperse, reversible assemblies morphologically similar to those of the native (wild-type, WT) protein, as demonstrated by TEM (Figure 2C) and DLS. Most significantly, sizes of the assemblies of the different reflectin proteins varied as a function of sequence and pH in a manner best predicted by the calculated net charge density (Figure 2D). The expected pH-driven charge neutralization (through histidine deprotonation) occurs almost entirely in the cationic linkers, suggesting that these regions serve as a distributed electrostatic switch controlling assembly, with neutralization of their

intra- and inter-molecular Coulombic repulsion required for condensation and hierarchical assembly. In contrast, the calculated net charge density of the conserved motifs is not associated with assembly size, indicating their role in assembly may be structural, as supported by the findings below.

Changes in tryptophan fluorescence, ANS fluorescence, and tryptophan-ANS FRET reveal significant, progressive changes in A1 conformation as it transitions from the monomeric state (in H<sub>2</sub>O) to the oligomeric (pH 4.5) and multimeric (pH 6.5) assemblies. The progressive blue shift in tryptophan's emission wavelength indicates transition to less solvent exposure. Similarly, ANS fluorescence and tryptophan-ANS FRET increase greatly upon multimerization, indicating formation of hydrophobic surfaces close to the conserved motifs. The phosphomimetic mutants show identical blue shifts to A1 WT, suggesting that those factors tuning assembly size are independent of the structural changes that occur during assembly.

Computational analyses of potential secondary structures by calculation of hydrophobic moments show that the conserved motifs have a strong entropic potential to form phase-segregated amphiphilic secondary structures, especially  $\alpha$ -helices and  $\beta$ -sheets (**Figure 3A**) (6). The conserved N-terminal motif shows a 10°-shift in maximal hydrophobic moment from the potential  $\alpha$ -helix, indicating it might have a special role in assembly. Analysis of A1 assembly by circular dichroism spectroscopy confirms predictions that the H<sub>2</sub>O-solubilized A1 monomers are largely unstructured, while, charge neutralization-induced multimerization (at pH 7.5) drives the emergence of  $\beta$  secondary structure, as indicated by enlargement of the shoulder at ~218 nm. CD spectra of oligomeric assemblies (at pH 4.5) more closely resemble the less ordered monomers (**Figure 3B**).

Analyses of the recombinant tunable reflectins and their mutant derivatives *in vitro* revealed a direct relationship between the extent of charge neutralization of the positively charged linker peptides to progressively overcome their Coulombic repulsion, the resulting emergence of secondary folding and hydrophobicity, and the size of the resulting reflectin assemblies *in vitro*. These findings further elucidate the mechanistic origin of the synergistic effects of reflectin neutralization on the tunable color and brightness of reflectance *in vivo*. Analysis of deletion mutants reveals that the “switch” controlling the neutralization-dependent structural transitions underlying tunability is not localized, but instead is spatially distributed in the multiple linkers along the reflectin's length. These results help establish a framework for understanding the *in vivo* and *in vitro* assembly behavior of the reflectins and may help provide inspiration for new tunably reconfigurable and photonically useful materials.

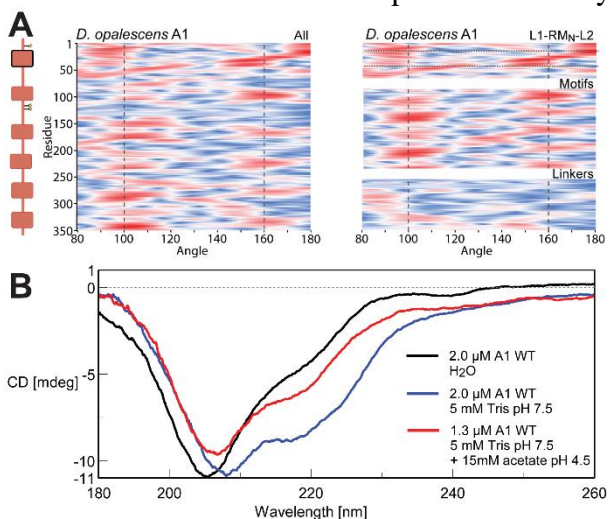


**Figure 3. A)** Calculated hydrophobic moments of *D. opalescens* A1, using an 18-residue scan window (*y*-axis) and successive side chain angles ranging from 80°-180°. Conserved motifs show a potential for highly amphiphilic secondary structure at angles corresponding to  $\alpha$ -helices and  $\beta$ -sheets. **B)** Circular dichroism spectroscopy of A1 reveals the progressive emergence of secondary structure upon oligomerization (pH 4.5) and multimerization (pH 7.5).

## Future Plans

We are genetically engineering the cloned recombinant reflectins to further probe the determinants of tunable assembly through the generation and analysis of additional truncations, site-specific mutants and analysis of reflectins from other species in which the reflectins are not tunable. These studies will be complemented by analyses of synthetic peptides in efforts to identify and analyze the functional roles of structures minimally required for tunability. We are extending our analyses to conditions of high ionic strength, in which our analyses indicate additional novel behaviors. Cryo-electron microscopy, x-ray scattering, circular dichroism and other biophysical tools are being used to help us further understand reflectin's ultrastructural and secondary structure changes controlling assembly and disassembly.

## References

1. Mähger LM, Denton EJ, Marshall NJ, Hanlon RT. Mechanisms and behavioural functions of structural coloration in cephalopods. J R Soc Interface. 2009 Apr 6;6(Suppl 2):S149–63.
2. Izumi M, Sweeney AM, DeMartini D, Weaver JC, Powers ML, Tao A, et al. Changes in reflectin protein phosphorylation are associated with dynamic iridescence in squid. J R Soc Interface. 2010 Mar 6;7(44):549–60.
3. DeMartini DG, Krogstad DV, Morse DE. Membrane invaginations facilitate reversible water flux driving tunable iridescence in a dynamic biophotonic system. Proc. Natl. Acad. Sci. USA. 2013 Feb 12;110(7):2552–6.
4. Tao AR, DeMartini DG, Izumi M, Sweeney AM, Holt AL, Morse DE. The role of protein assembly in dynamically tunable bio-optical tissues. Biomaterials. 2010 Feb;31(5):793–801.
5. Levenson R, Bracken C, Bush N, Morse DE. Cyclable Condensation and Hierarchical Assembly of Metastable Reflectin Proteins, the Drivers of Tunable Biophotonics. J Biol Chem. 2016 Feb 19;291(8):4058–68.
6. Eisenberg D, Weiss RM, Terwilliger TC. The hydrophobic moment detects periodicity in protein hydrophobicity. Proc Natl Acad Sci U S A. 1984 Jan;81(1):140–4.

## Publications (supported by BES over 13 months since start of grant 6/1/16)

Levenson, R., DeMartini, D.G., Morse, D.E. (2017) Molecular Mechanism of Reflectin's Tunable Biophotonic Control: Opportunities and Limitations for New Optoelectronics. APL Materials. (in press).

Levenson, R., Bracken, C., Sharma, C., Arata, C., Morse, D.E. (2017) Neutralization of a Distributed Coulombic Switch Tunes Reflectin Assembly. J. Biol. Chem. (submitted)

## Electrostatic Driven Self-Assembly Design of Functional Nanostructures

Monica Olvera de la Cruz, Northwestern University (PI) and Michael J. Bedzyk, Northwestern University (Co-PI)

### Program Scope

The aim of the program is to understand how biomolecular architecture, including charge, governs the molecular packing and the overall morphology of self-assembly. In our recent and future work, we focus on the coupling of intermolecular steric and electrostatic interactions as well as the overall elastic forces to systematically study the structure of charged flexible nanoribbon assemblies. This research direction is motivated by our current combined experimental and theoretical studies on peptide amphiphile (PA) self-assembly, described below.

### Recent progress

#### Electrostatics-Driven Hierarchical Buckling of Charged Flexible Ribbons

Thin ribbons can develop rich morphologies, including helical and twisted ribbons, which constitute the basis for realizing several biological functions and designing new structures in nanotechnology [1]. Controlling ribbon shape remains a challenging issue in the design of ribbonlike biomaterials. Here the coupling of electrostatic interactions and equilibrium shapes of charged ribbons is studied using numerical simulations in combination with analytical geometric analysis [2]. Long-range electrostatic repulsion is found to govern the hierarchical buckling of the ribbon from its initially flat shape to its undulated and out-of-plane twisted conformations. In this process, screening length is the key controlling parameter, suggesting that a convenient way to manipulate the ribbon morphology is simply to change the salt concentration. We find that these shapes originate from the geometric effect of the electrostatic interaction, which fundamentally changes the metric over the ribbon surface.



Fig 1. AFM image of dried  $C_{16}K_1$  nanofibers that were initially assembled in aqueous solutions at pH = 5 and with no added NaCl (left). Shapes of nanoribbons from simulation and theory as the salt concentration increases (right).

#### Electrostatic Control of Polymorphism in Charged Amphiphile Assemblies

Peptide amphiphile (PA) molecules in which a hydrophobic alkyl tail is covalently linked to an amino acid sequence provide a flexible and modular system for systematically analyzing the effects of steric and electrostatic interactions on molecular assembly [3,4]. This work focused on a PA with a palmitoyl tail coupled to two ionizable lysine groups ( $C_{16}-K_2$ ) [5]. The degree of ionization could be reconfigured in response to pH variations, as verified by pH titration curves and Monte-Carlo simulations (Fig. 2a). Based on the oft-applied packing parameter model [6], these “cone-shaped” PA molecules are expected to assemble into spherical micelles. However, SAXS/WAXS (Fig. 2b) and Cryo-TEM (Fig. 2b) experiments

demonstrate that the assembly of this PA transforms from spherical to cylindrical micelles to crystalline bilayers with high aspect ratio (nanoribbons) as the effective molecular charge is reduced by increasing the solution pH from 5 to 9. Detailed SAXS/WAXS analysis reveals that in bilayer membranes, the two leaflets are interdigitated with the tilted PA lipid tails crystallized on a rectangular lattice (Fig. 2c). This interdigitation overcomes the requirement (based on packing parameter model) that the molecules have to be cylindrically shaped in order to assemble into bilayers. Future work will test the generality of this packing motif.

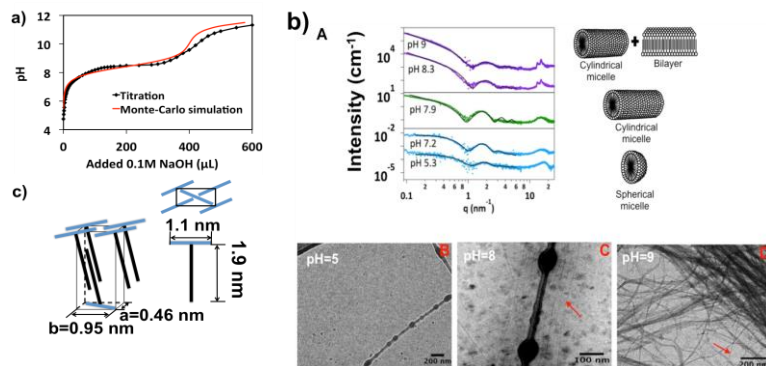


Fig 2. (a)  $C_{16}K_2$  titration curve (black) and Monte-Carlo simulation result (red) showing how pH changes as a function of the volume of NaOH added. (b) A: In situ SAXS/WAXS data for 4 mM  $C_{16}K_2$  solutions at pH=5. The solid black curves are the best fits for  $0.1 \text{ nm}^{-1} < q < 6 \text{ nm}^{-1}$  based on the assembly structures on the right panel. B-D: Cryo-TEM images at different pH showing assembly structures as indicated by SAXS/WAXS. (c) Molecular packing model of  $C_{16}K_2$  bilayer at pH = 9 derived from WAXS analysis, which combines molecular box model and powder averaging of Bragg rods from 2D crystal lattices [7].

counterions and diminishes the counterion translational entropy, while also reducing the total electrostatic potential. Interestingly, the competition between these effects leads to a fraction of condensed counterions independent of the fiber radius.

### Co-assembly of Peptide Amphiphiles and Lipids into Supramolecular Nanostructures Driven by Anion- $\pi$ Interactions

Co-assembly of binary systems driven by specific non-covalent interactions can greatly expand the structural and functional space of supramolecular nanostructures. Self-assembly of peptide amphiphiles and fatty acids driven primarily by anion- $\pi$  interactions is investigated [9] as a function of peptide sequences functionalized with a perfluorinated phenylalanine residue to promote anion- $\pi$  interactions with carboxylate headgroups in fatty acids. Positioning the aromatic units close to the N-terminus of the peptide backbone near the hydrophobic core of cylindrical nanofibers leads to strong anion- $\pi$  interactions between both components. As the aromatic units are moved along the peptide backbone away from the hydrophobic core, the interactions with dodecanoic acid transform the cylindrical supramolecular morphology into ribbon-like structures. Our findings reveal how co-assembly involving designed specific interactions can drastically change supramolecular morphology and even cross from nano to micro scales.

### Water Dynamics from the Surface to the Interior of a Supramolecular Nanostructure

Water within and surrounding the structure of a biological system adopts context-specific dynamics that mediate virtually all of the events involved in the inner workings of a cell. These events range from protein folding and molecular recognition to the formation of hierarchical structures. Water dynamics are mediated by the chemistry and geometry of interfaces where water and biomolecules meet. Here, we experimentally and computationally investigate the translational dynamics of vicinal water molecules within the volume of a supramolecular peptide nanofiber measuring 6.7 nm in diameter [10]. Using Overhauser dynamic nuclear polarization relaxometry (ODNP), we show that drastic differences exist in water motion within a distance of about one nanometer from the surface, with rapid diffusion in the hydrophobic interior and immobilized

### Ion Condensation onto Self-Assembled Nanofibers

Self-assembled peptide amphiphile (PA) nanofibers are a class of supramolecular materials with promising applications in nanotechnology. Alignment of nanofibers, which is essential for biomaterials applications, is achieved at low salt concentrations in the PA nanofiber suspensions. The effect of ion concentration on the properties of these nanostructures is analyzed using atomistic molecular dynamics simulations [8]. Simulations reveal that nanofibers with the highest cross-section density have expanded radii. This expansion decreases the accessible volume for sodium

water on the nanofiber surface (Fig. 3). These results demonstrate that water associated with materials designed at the nanoscale is not simply a solvent, but rather an integral part of their structure and potential functions.

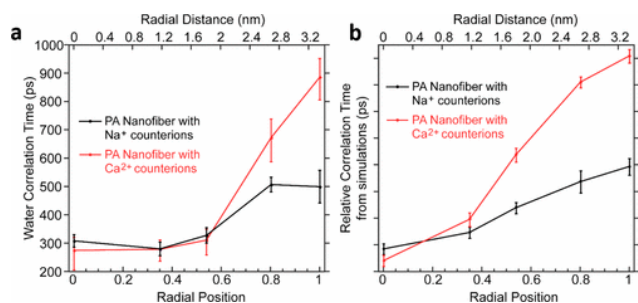


Fig. 3 Water dynamics through the nanofiber cross section. (a) Water-correlation times measured by ODNP and (b) by atomistic MD simulations as a function of radial position within the cross section of nanofibers. Water dynamics are much slower near the hydrophilic, charged residues at the nanofiber surface than at the core.

### Ion Transport Mechanisms in Liquid-Liquid Interface

Interfacial liquid-liquid ion transport is of crucial importance to biotechnology. In [11] a water-in-oil microemulsion is formulated with density and dimensions amenable to atomistic molecular dynamics simulation, facilitating convergent theoretical and experimental approaches to elucidate interfacial ion transport mechanisms. Lutetium(III) cations are transported from the 5 nm diameter water pools into the surrounding oil using an extractant (a lipophilic ligand). Changes in ion coordination sphere and interactions between the interfacial components are studied using a combination of synchrotron X-ray scattering, spectroscopy, and atomistic molecular dynamics simulations revealing no evidence of interfacial extractant monolayers, but rather ions are exchanged through water channels that penetrate the surfactant monolayer and connect to the oil-based extractant. Our results highlight the dynamic nature of the oil-water interface and show that lipophilic ion shuttles need not form flat monolayer structures to facilitate ion transport across the liquid-liquid interface.

### Future Plans

We will focus on charged nanoribbon bilayers, which have biological counterparts [1], and can exhibit periodic undulations, twists and helical turns that reduce the intermolecular repulsive interactions. Our recent MD simulations [2] have predicted such structural modulations. Furthermore, with the introduction of salt these nanoribbons can transform into large bilayer sheets of low aspect ratio, which can roll onto themselves (nanocochleate structures). Our preliminary experimental studies on the assembly of PA C<sub>16</sub>-K<sub>1</sub> show both these structural features: twisted crystalline nanoribbons are observed at low pH, when all the PA are expected to be in their ionized state. These nanoribbons transform into nanocochleates when the electrostatic repulsions are screened by addition of a few mM of NaCl (see Fig. 4). We

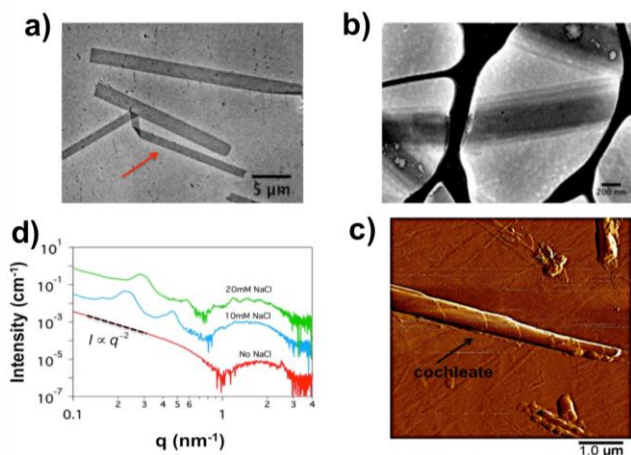


Fig. 4. Characterization of C<sub>16</sub>-K<sub>1</sub> assemblies at pH = 5. Cryo-TEM images: (a) in the absence of NaCl, (b) in a 10 mM NaCl solution and (c) in-situ tapping mode AFM image. (d) SAXS intensity profiles at pH =5 gives interbilayer separation of ~ 26 and ~ 21 nm in the cochleate structure.

will trace the transformation from twisted nanoribbons to large planar bilayers to nanocochleates in C<sub>16</sub>-K<sub>1</sub> assembly by varying salt concentration. Nanoribbon alignment will be induced by shearing methods such as flow-induced shear in nanoribbon solutions trapped in thin capillaries. We will study large disparity in head-tail size effects on the morphology.

Theoretical simulation will be performed to visualize the effects of salt condition on the equilibrium PA ribbon structures. The model used in [2] simplified the membrane with a triangulated surface composed of vertices connected by bonds with spring constant. Preliminary results show this model cannot explain the rolling-up mechanism of cochleate structures. We believe additional salt changes the bilayer structure in molecular level. When no salt is added, the electrostatic repulsion between the headgroups impeded the formation of bilayer, but the long hydrocarbon chain greatly favors bilayer (when the tail length > 12, a bilayer is favored). Therefore, PAs are forming a bilayer with interdigitation, with which the head-head distance is increased to minimize the repulsion. When salt is added, the head-head repulsion is weaker, so that the interdigitation is not required for the stable bilayer structure. Part of the membrane could transition from gel phase to liquid phase. When neutralized by Cl<sup>-</sup>, some C<sub>16</sub>K<sub>1</sub> slip along the normal direction, thereby increasing the bilayer thickness and curvature in the membrane becomes possible. MARTINI simulation will be performed to verify this assumption.

## References

1. Palmer, L.C.; Velichko, Y.S.; Olvera de la Cruz, M.; and Stupp, S.I., Supramolecular self-assembly codes for functional structures, *Phil. Trans. R. Soc. A* 365, 1417 (2007)
2. Yao, Z.W. and Olvera de la Cruz, M., Electrostatics-Driven Hierarchical Buckling of Charged Flexible Ribbons, *Phys. Rev. Lett.* 116, 148101 (2016)
3. Leung, C.Y.; Palmer, L.C.; Qiao, B.F.; Kewalramani, S.; Sknepnek, R.; Newcomb, C.J.; Greenfield, M.A.; Vernizzi, G.; Stupp, S.I.; Bedzyk, M.J.; and de la Cruz, M.O. Molecular Crystallization Controlled by pH Regulates Mesoscopic Membrane Morphology *ACS Nano* 6, 10901-10909 (2012)
4. Leung, C. Y., Palmer, L. C., Kewalramani, S., Qiao, B. F., Stupp, S. I., Olvera de la Cruz, M. O., and Bedzyk, M. J., Crystalline polymorphism induced by charge regulation in ionic membranes *Proc. Natl. Acad. Sci. USA* 110, 16309-16314 (2013)
5. Gao, C.; Li, H.; Li, Y.; Kewalramani, S.; Palmer, L.C.; Dravid, V.P.; Stupp, S.I.; Olvera de la Cruz, M.; Bedzyk, M.J., Electrostatic Control of Polymorphism in Charged Amphiphile Assemblies, *J. Phys. Chem. B* 121, 1623-1628 (2017)
6. Israelachvili, J. N. Intermolecular and Surface Forces, 3rd Edition 2011
7. Harutyunyan, B. D.; A.; Kewalramani, S.; Aytun, T.; Fairfield, D. J.; Stupp, S. I.; Bedzyk, M. J. Molecular Packing of Amphiphilic Nanosheets Resolved by X-ray Scattering. *J. Phys. Chem. C*, 2017, 121, 1047-1054 (2017)
8. Deiss-Yehiely, E.; Ortony, J.H.; Qiao, B.F.; Stupp, S.I.; de la Cruz, M.O., Ion Condensation onto Self-Assembled Nanofibers *J. Pol. Sci. Part B-Pol. Phys.* 55, 901-906 (2017)
9. Yu, Z.L.; Erbas, A.; Tantakitti, F.; Palmer, L.C.; Jackman, J.A.; de la Cruz, M.O.; Cho, N.J.; Stupp, S.I. Co-assembly of Peptide Amphiphiles and Lipids into Supramolecular Nanostructures Driven by Anion- $\pi$  Interactions *J. Am. Chem. Soc.* 139, 7823-7830 (2017)
10. Ortony, J.H.; Qiao, B.; Newcomb, C.J.; Keller, T.J.; Palmer, L.C.; Deiss-Yehiely, E.; Olvera de la Cruz, M.; Han, S.; Stupp, S.I., Water Dynamics from the Surface to the Interior of a Supramolecular Nanostructure *J. Am. Chem. Soc.* 139, 8915-8921 (2017)
11. Qiao, B.; Muntean, J.V.; Olvera de la Cruz, M.; Ellis, R.J.; Ion Transport Mechanisms in Liquid-Liquid Interface. *Langmuir* 33, 6135-6142 (2017)

## Publications

1. Yao, Z.W. and Olvera de la Cruz, M., Electrostatics-Driven Hierarchical Buckling of Charged Flexible Ribbons, *Phys. Rev. Lett.* 116, 148101 (2016)
2. Gao, C.; Li, H.; Li, Y.; Kewalramani, S.; Palmer, L.C.; Dravid, V.P.; Stupp, S.I.; Olvera de la Cruz, M.; Bedzyk, M.J., Electrostatic Control of Polymorphism in Charged Amphiphile Assemblies, *J. Phys. Chem. B* 121, 1623-1628 (2017)
3. Harutyunyan, B. D.; A.; Kewalramani, S.; Aytun, T.; Fairfield, D. J.; Stupp, S. I.; Bedzyk, M. J. Molecular Packing of Amphiphilic Nanosheets Resolved by X-ray Scattering. *J. Phys. Chem. C*, 2017, 121, 1047-1054 (2017)
4. Deiss-Yehiely, E.; Ortony, J.H.; Qiao, B.F.; Stupp, S.I.; de la Cruz, M.O., Ion Condensation onto Self-Assembled Nanofibers *J. Pol. Sci. Part B-Pol. Phys.* 55, 901-906 (2017)
5. Yu, Z.L.; Erbas, A.; Tantakitti, F.; Palmer, L.C.; Jackman, J.A.; de la Cruz, M.O.; Cho, N.J.; Stupp, S.I. Co-assembly of Peptide Amphiphiles and Lipids into Supramolecular Nanostructures Driven by Anion- $\pi$  Interactions *J. Am. Chem. Soc.* 139, 7823-7830 (2017)
6. Ortony, J.H.; Qiao, B.; Newcomb, C.J.; Keller, T.J.; Palmer, L.C.; Deiss-Yehiely, E.; Olvera de la Cruz, M.; Han, S.; Stupp, S.I., Water Dynamics from the Surface to the Interior of a Supramolecular Nanostructure *J. Am. Chem. Soc.* 139, 8915-8921 (2017)
7. Qiao, B.; Muntean, J.V.; Olvera de la Cruz, M.; Ellis, R.J.; Ion Transport Mechanisms in Liquid-Liquid Interface. *Langmuir* 33, 6135-6142 (2017)

## Exploration of Chemically-Tailored, Hierarchically-Patterned 3-D Biogenic and Biomimetic Structures for Control of Infrared Radiation

Joseph W. Perry (PI), School of Chemistry & Biochemistry, Georgia Institute of Technology  
Kenneth H. Sandhage (Co-PI), School of Materials Engineering, Purdue University

### Program Scope

The **objectives** are: i) To learn how to shift the optical transmission and reflection behaviors of biological structures from the visible into the infrared (IR) via shape-preserving chemical conversion of such structures into synthetic IR materials, and ii) To obtain fundamental understanding as to how biological structures may be mimicked and coupled with synthetic inorganic chemistries to enable a new generation of biomimetic materials for controlling IR radiation.

The proposed effort comprises 3 collaborative thrusts:

**Thrust I: Chemical conversion of bio-enabled SiO<sub>2</sub>-bearing structures into high-refractive index IR materials.** SiO<sub>2</sub>-based diatom frustules with particular overall frustule shapes and fine features will be chemically converted into 3-D replicas comprised of nanostructured materials with high IR refractive indices. Kinetic mechanisms and nanostructural evolution upon such reactive conversion will be evaluated to allow for high-fidelity replication.

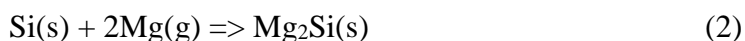
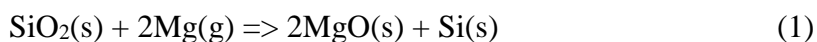
**Thrust II: Syntheses of structurally-tailorable biomimetic inorganic assemblies.** SiO<sub>2</sub> diatom-mimetic structures and multilayered oxide replicas of butterfly-mimetic structures will be synthesized via coating of patterned templates or patterning of coated templates. The influences of oxide precursors, coating conditions, and drying/pyrolysis kinetics on nanostructural evolution of coated structures will be examined. These structures will then be converted into IR replicas.

**Thrust III: Simulation and measurement of bio-enabled IR transmission and reflection.** Simulations and optical measurements will be used to evaluate: i) how the morphologies of high-index replicas of diatom frustules, and biomimetic analogues, affect IR transmission, and ii) how butterfly-mimetic structures comprised of high-index IR materials affect IR reflection. Modelling of IR behavior will be used to guide the design and syntheses of new lightweight bio-enabled structures with tailorable IR transmission and/or reflection.

### Recent Progress

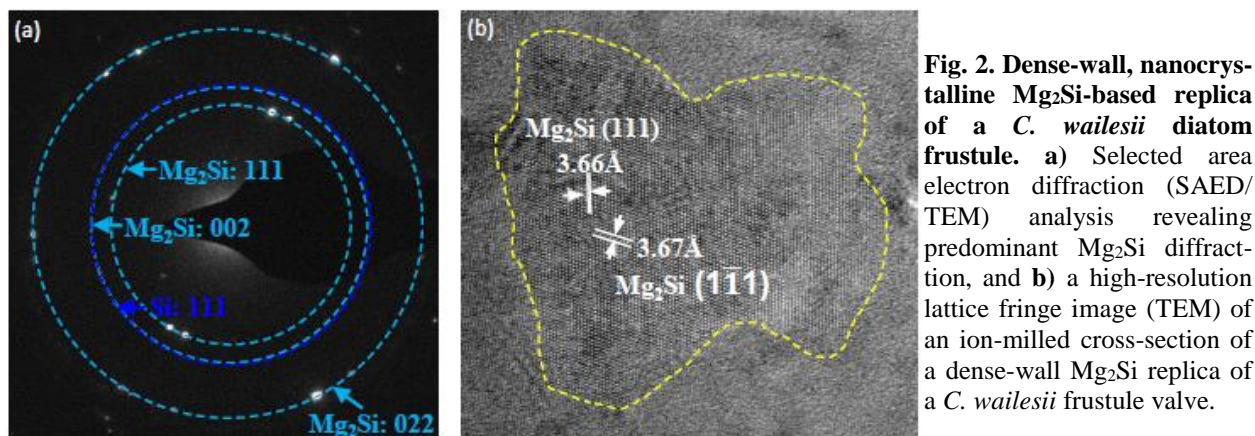
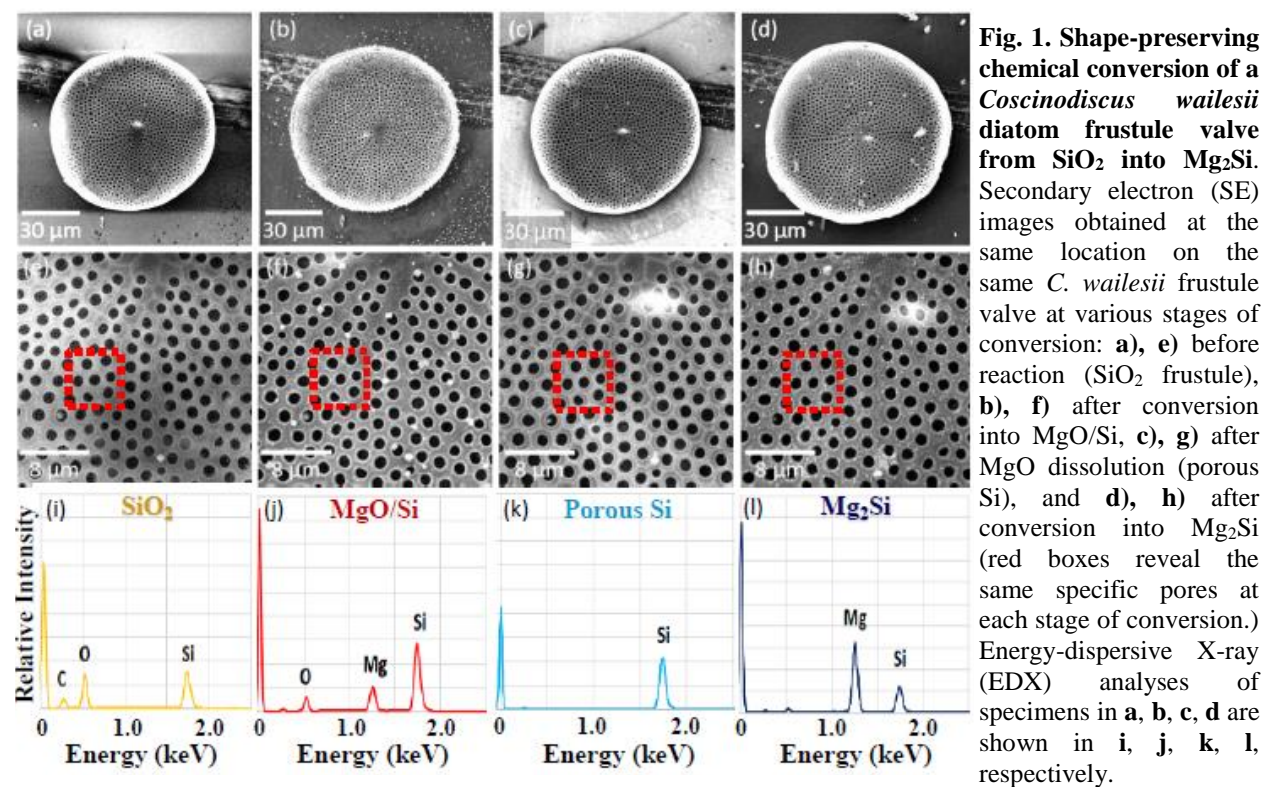
**Thrust I. Chemical conversion of bio-enabled SiO<sub>2</sub>-bearing structures into high-refractive index IR materials.**

A *Coscinodiscus wailesii* diatom strain (CCMP2513) was obtained from the Provasoli-Guillard National Center for Culture of Marine Phytoplankton (CCMP, Bigelow Laboratory for Ocean Sciences, West Boothbay Harbor, ME). The *C. wailesii* culture was grown in L1 medium<sup>1</sup> at 20°C with 13 h light/11 h dark cycles in a walk-in environmental growth chamber. The cultured diatom cells were harvested by centrifugation, washed with DI water (to remove precipitated salts from the growth media) and then heated in air to pyrolyze organic constituents to yield SiO<sub>2</sub> frustules. The *C. wailesii* SiO<sub>2</sub> frustules were dispersed with gentle stirring in ethanol and deposited via pipette onto thin (0.4 mm) polished sapphire substrates (note: sapphire exhibits modest optical absorption at near-infrared wavelengths<sup>2</sup> which allowed for the transmission measurements discussed in Thrust III below.) The frustules were then converted into Mg<sub>2</sub>Si replicas via the following two sequential gas/solid reactions:



Reaction (1) was first conducted using a Mg<sub>2</sub>Si source of Mg(g) to allow for the formation of *C. wailesii* frustule replicas comprised of only MgO and Si products (i.e., to avoid the formation of

Mg<sub>2</sub>Si in this first step). After selective acid dissolution of the MgO product, the resulting porous-wall Si frustule replicas were allowed to react with Mg(g) generated from pure solid Mg to generate Mg<sub>2</sub>Si via reaction (2). Secondary electron (SE) images and energy-dispersive X-ray analyses at various stages of conversion (from SiO<sub>2</sub> to MgO/Si to porous-wall Si to Mg<sub>2</sub>Si) of the same *C. wailesii* frustule valve are shown in Figure 1. The overall frustule valve morphology and pore pattern were retained with high fidelity at each stage of the conversion process. The well-preserved overall frustule morphology was also confirmed by quantitative analyses of the sizes of particular pores at each conversion stage. Transmission electron microscopy (TEM, Figure 2) of an ion-milled cross-section confirmed that the final frustule replicas were comprised of dense-wall, nano-crystalline Mg<sub>2</sub>Si. The *C. wailesii* SiO<sub>2</sub> frustules, and replicas comprised of MgO/Si and Mg<sub>2</sub>Si, were fixed to the sapphire substrates with Pt using a focused ion beam mill and shipped to the Perry group for analyses of IR transmission and focusing (Thrust III below).



### **Thrust II: Syntheses of structurally-tailorable biomimetic inorganic assemblies.**

The syntheses of SiO<sub>2</sub>-bearing films on sapphire, and conversion of the SiO<sub>2</sub> in such films into Mg<sub>2</sub>Si-bearing films, have been examined for the purpose of generating diatomimetic and butterfly-mimetic structures for control of IR transmission and reflection. SiO<sub>2</sub> films were prepared by spin coating of a methylcellulose-bearing tetraethyl orthosilicate (MC/TEOS) precursor solution onto polished sapphire substrates (ave. roughness, R<sub>a</sub>, of 0.2 nm), vacuum drying, and then firing at 700°C for 15 min in air. The resulting macrocrack-free SiO<sub>2</sub> films (ave. thickness of 570 nm) were then allowed to react with Mg(g) generated from Mg<sub>2</sub>Si to generate MgO/Si films. The MgO product was then removed by acid dissolution, followed by washing in DI water and drying in an Ar atmosphere. The resulting porous Si film was then allowed to react with Mg(g) from a solid Mg source to generate a macrocrack-free Mg<sub>2</sub>Si film. Atomic force microscopic analyses indicated that the average roughness value of the Mg<sub>2</sub>Si film was 10.8 nm. Pores were then patterned into the Mg<sub>2</sub>Si film via focused-ion-beam (FIB) milling. Top-down SEM images of these films at various stages of conversion, and EDX analyses of the porous Si and Mg<sub>2</sub>Si films, are shown in Figure 3. The FIB milling of *C. walesii* pore patterns, and modified version of such patterns, into the Mg<sub>2</sub>Si films are underway to allow for tailoring of the IR transmission/focusing behavior. Other activities in Thrust II have included: i) the syntheses of multilayer SiO<sub>2</sub>-bearing films of varied layer thickness via repeated spin coating/firing, and selective reaction of the SiO<sub>2</sub> layers into MgO/Si and then into Mg<sub>2</sub>Si (for evaluation of multiwavelength IR reflection, analogous to multiwavelength visible reflection of *Papilio sp.* butterfly scales), and ii) evaluation of the kinetics of Mg<sub>2</sub>Si formation via the direct reaction of Mg with Si.

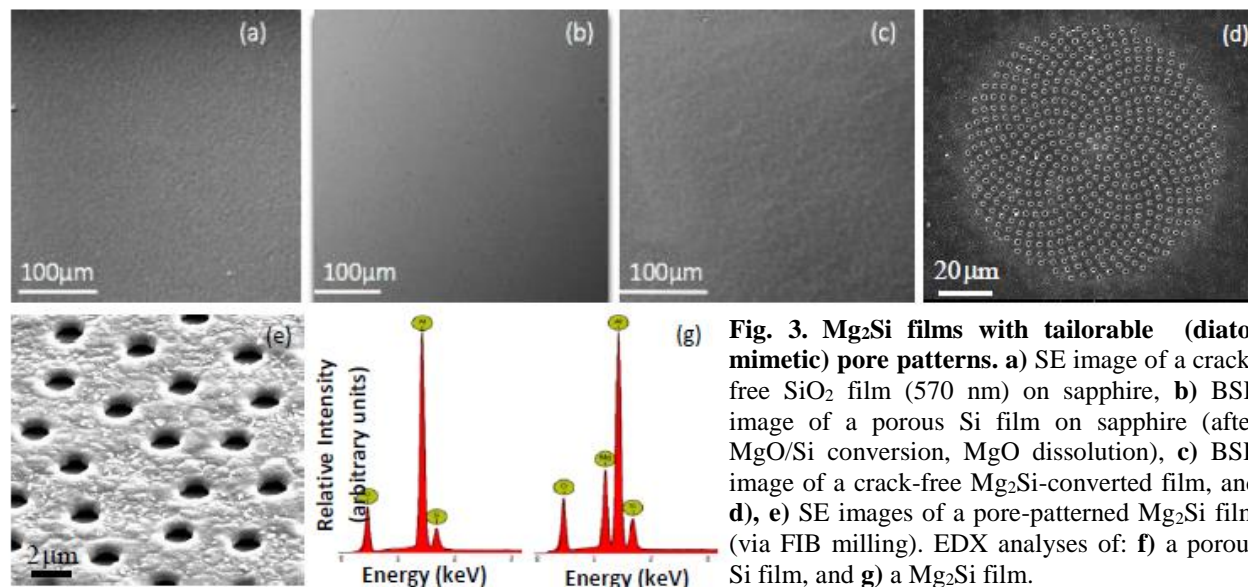


**Fig. 3. Mg<sub>2</sub>Si films with tailorable (diatomimetic) pore patterns.** a) SE image of a crack-free SiO<sub>2</sub> film (570 nm) on sapphire, b) BSE image of a porous Si film on sapphire (after MgO/Si conversion, MgO dissolution), c) BSE image of a crack-free Mg<sub>2</sub>Si-converted film, and d), e) SE images of a pore-patterned Mg<sub>2</sub>Si film (via FIB milling). EDX analyses of: f) a porous Si film, and g) a Mg<sub>2</sub>Si film.

### **Thrust III: Simulation and measurement of bio-enabled IR transmission and reflection.**

Simulations (Beamprop, RSoft software suite) of the optical transmission and focusing of *C. walesii* SiO<sub>2</sub> frustules, and of replicas comprised of MgO/Si and Mg<sub>2</sub>Si, have been conducted in the wavelength range of 550-2850 nm (note: simulations for Mg<sub>2</sub>Si were limited to  $\geq 1750$  nm where the Mg<sub>2</sub>Si refractive index is known<sup>4</sup>). Such simulations were conducted using *C. walesii* pore patterns imported directly from SEM images of the valves, with average pore diameters of 1.15 μm (for pores on the foramen layer of the valve) and 150 nm (for pores on the cribrum layer of the valve). For all compositions, multiple focal points were predicted where the focal length

(distance of the focal spot from the valve replicas) for any particular focal spot decreased as the wavelength increased. Additionally, the focal volume (the degree of light confinement) and intensity of a given spot were found to concomitantly increase with distance away from the plane of the valve, consistent with previous reports limited to visible and shorter NIR wavelengths<sup>1,2</sup>. Focal distances were predicted to be strongly dependent on the index of the valve material. While the most intense focusing of SiO<sub>2</sub> valves was predicted to be within 400 μm of the valve surface, intense spots out to 1-3 mm were predicted for MgO/Si and Mg<sub>2</sub>Si (higher index) valve replicas. Focal imaging and intensity profiling of single *C. walesii* SiO<sub>2</sub> valves, and single MgO/Si and Mg<sub>2</sub>Si valve replicas, were accomplished by flood illumination of the valves with femtosecond laser pulses while monitoring the transmitted intensity in the plane behind the valve using a CCD camera sensitive in the 550-1050 nm range. Depth profiling of the precise locations of discrete foci and intensity profile analysis were performed out to a distance of up to 1 mm for

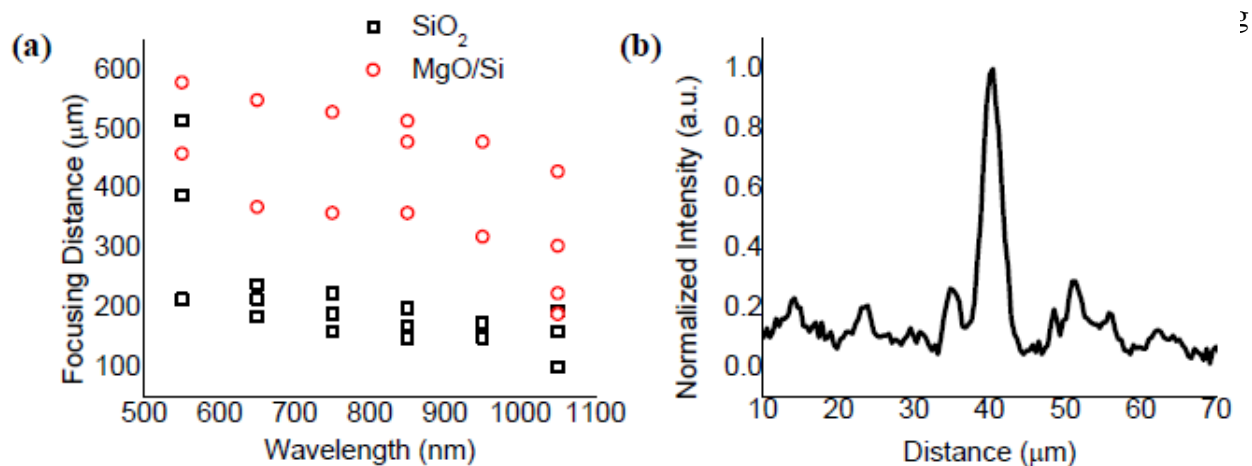


**Fig. 4. a)** Focal distances of focal spots generated by a SiO<sub>2</sub> *C. walesii* valve and a MgO/Si valve replica over wavelengths of 550-1050 nm, and **b)** intensity profile of a focal spot generated by a MgO/Si valve replica at 650 nm.

which was consistent with trends in the visible range from previous reports<sup>3</sup>. In agreement with our simulations, the measured depths of focal spots of high intensity for MgO/Si valve replicas tended to be greater than for SiO<sub>2</sub> valves. This work demonstrates that the focusing effect observed in the visible range for *C. walesii* valves can be transferred into the IR (a primary hypothesis of this effort), and over appreciably longer focal lengths, with higher index *C. walesii* valve replicas.

### Future Plans

Future work will include: i) Extensive measurement and simulation of the focal lengths and focal spot intensities of *C. walesii* SiO<sub>2</sub> valves and valve replicas comprised of MgO/Si and Mg<sub>2</sub>Si at IR wavelengths up to 3 μm; ii) Syntheses, and IR focusing measurements and simulations up to 3 μm, of MgO/Si and Mg<sub>2</sub>Si films with *C. walesii* pore patterns and modified pore patterns (to understand the roles of various aspects of the pore patterns on IR focal lengths and focal spot intensities); iii) Syntheses, and IR reflection measurements and simulations, of multilayer Mg<sub>2</sub>Si-bearing films with varied numbers of layers, layer thicknesses, and layer curvatures (to develop further understanding of the roles of such layer features on multiwavelength reflection, analogous to multiwavelength visible reflection of *Papilio sp.* butterfly scales).

## References

1. R. R. L. Guillard, P. E. Hargraves, *Phycologia*, **32**, 234-236 (1993).
2. E. D. Palik, *Handbook of Optical Constants of Solids*, Elsevier Publishers, 1997.
3. L. De Stefano, I. Rea, I. Rendina, M. De Stefano, L. Moretti, *Optics Express*, **15**, 18082-18088 (2007)
4. D. McWilliams, D. W. Lynch, *J. Opt. Soc. Am.*, **53**, 298-299 (1963).

## Publications

1. A. S. Gordin, B. M. deGlee, C. E. Alvarez, G. A. Cohoon, O. D. Herrera, P. D. Brooke, Y. Fang, S.-H. Hwang, N. Vogel, K. Meyers, M. Hildebrand, K. Kieu, J. Aizenberg, R. A. Norwood, K. H. Sandhage, "A Bio-Enabled Structure with a Large Three-Dimensional Photonic Bandgap," submitted.
2. A. S. Gordin, K. H. Sandhage, "*In situ* high-temperature X-ray diffraction analysis of Mg<sub>2</sub>Si film formation kinetics via reaction of Mg films with Si single crystal substrates," submitted.

The DoE/BES project has also provided support for the work associated with the following papers submitted over the past year, including:

3. Y. Zhang Ye Cai, S.H. Hwang, G. Wilk, F. DeAngelis, A. Henry, K. H. Sandhage, "Containment Materials for Liquid Tin at 1350°C as a Heat Transfer Fluid for High Temperature Concentrated Solar Power," submitted.
4. W. B. Goodwin, D. Shin, D. Sabo, S. Hwang, Z. J. Zhang, J. C. Meredith,\* K. H. Sandhage,\* "Tunable Multimodal Adhesion of Three-Dimensional, Nanocrystalline CoFe<sub>2</sub>O<sub>4</sub> Pollen Replicas," *Bioinspiration and Biomimetics*, accepted for publication.

## Invited Presentations

1. J. W. Perry, "Basics of Two-Photon Absorption," Foundations of Nonlinear Optics (FoNLO) Workshop, Lehigh Univ., Lehigh, PA, Aug. 27, 2015.
2. K. H. Sandhage, "Complex-Shaped, Chemically-Tailored, Three-Dimensional Functional Inorganic Materials," Presentation to Raytheon, Purdue University, W. Lafayette, IN, Oct. 16, 2015.
3. J. W. Perry, "Organic and Hybrid Materials for Photonics and Electronics," Humboldt Universität, Berlin, DE, Oct. 22, 2015.
4. J. W. Perry, "Organic and Hybrid Materials for Photonics and Electronics," Nano@Tech, Georgia Institute of Technology, Atlanta, GA, Sept. 22, 2015.
5. K. H. Sandhage, W. B. Goodwin, A. S. Gordin, J. P. Vernon, S. C. Davis, Y. Fang, Ye Cai, "Materials Alchemy: Changing the Chemistries but not Shapes of 3-D Biogenic and Synthetic Structures," Symposium E, Engineering and Application of BioInspired Materials, Materials Research Society Fall Meeting, Boston, MA, Dec. 1, 2015.
6. J. W. Perry, "Two-Photon Absorbing Materials for 3D Microfabrication & Materials for Energy Storage," Gwinnet School of Math, Science and Technology, Jan. 21, 2016.
7. K. H. Sandhage, "Bio-Enabled, Chemically-Tailored Hierarchically-Structured 3-D Materials," CIMTEC, Symposium O (Mining Smartness from Nature: From BioInspired Materials to Bionic Systems), Perugia, Italy, June 2, 2016.
8. K. H. Sandhage, "Biomaterials Alchemy: Changing the Chemistries, But Not Shapes, of Biogenic Structures," 1<sup>st</sup> NASA Biomimicry Summit and Education Forum, Cleveland, OH, Aug. 3, 2016.

9. K. H. Sandhage, "Fabrication of Complex-Shaped Advanced Materials," Presentation to Rolls-Royce Corporation, Indianapolis, IN, Aug. 16, 2016.
10. K. H. Sandhage, "Shape-Preserving Transformation of Biogenic and Synthetic Structures into Chemically-Tailored 3-D Microscopic and Macroscopic Materials," Colloquium Talk, Dept. Engineering Technology, Northern Kentucky University, Newport, KY, Nov. 2, 2016.
11. J. W. Perry, *et al.* "Biophotonics and plasmonics: potential sensing and Pollen based SERS," Novel Optical Materials and Applications Conference, Cetraro, Calabria, Italy, June 26, 2017
12. J. W. Perry, "Biophotonics and Plasmonics: Potential sensing and Pollen based SERS," MRS Symposium 2016, Phoenix, Arizona. March 30, 2016.

**Project Title: “Miniaturized Hybrid Materials Inspired by Nature: Directed Assembly in Dissipative Charged Biomolecular Materials Systems”**

**Principle Investigator (PI): C. R. Safinya**

**Co-PIs: Y. Li and K. Ewert**

**Materials Department, University of California at Santa Barbara**

**Santa Barbara, CA 93106**

**E-mail: safinya@mrl.ucsb.edu**

**Program Scope**

The objective of our research program is to develop a scientific understanding of directed assembly in charged biomolecular materials systems (protein- membrane- and nucleic acid-based). We design and study biomimetic systems based on our understanding of highly complex assemblies in cells. Our systems can result in functionally novel assemblies, either at equilibrium, in kinetically trapped states, or under dissipative conditions. Notably, the nanoscale assemblies may either be similar to, *or highly distinct* from, those occurring in vivo, owing to the complex nature of the systems. Examples include lipids assembled into membranes with distinct shapes [1], bundles of microtubules and networks of neurofilaments (NFs) [2-5].

Among the building blocks we use are microtubules (MTs) as model rigid polyelectrolytes [6,7], and charged biological membranes and vesicles as model sheets and spheres with *controllable* charge density [1]. A relatively simple group of “mediators of interactions” are multivalent ions (MVIs, e.g. metal ions  $Mg^{2+}$ ,  $Ca^{2+}$ ,  $Sr^{2+}$ ,  $Ba^{2+}$ , and transition metal ions  $Mn^{2+}$ ,  $Co^{2+}$ ,  $Zn^{2+}$ ) [8]. Their mechanisms of action significantly deviate from polyampholytic mediators; for example, truncated polypeptides derived from intrinsically disordered protein Tau (considered as polyvalent macromolecular counterions, PVMCIs, with charge ranging from  $Q = +4e$  to  $+30e$ ) [9].

Among the goals of the project is the characterization of biomolecular assemblies in the non-biological - strong electrostatic regime - where PVMCIs and MVIs are expected to form thin 2D layers near oppositely charged surfaces. These systems are expected to exhibit novel new types of attractions not present in the weak electrostatic regime (more typical of macromolecular assemblies in cells). Our recent study, describes the discovery of widely-spaced microtubule (MT)-Tau bundles with distinct architectures with hexagonal and one-dimensional string-like symmetry [9]. Remarkably, the bundle structures are not present at equilibrium [7] and only emerge under dissipative conditions [9]. Ongoing work with this system in the presence of MVIs, is allowing us to explore, for the first time, emergent behavior resulting from competing interactions mediated by MVIs and charged truncated Tau polypeptides. Aside from the inherent experimental interest in these systems from the perspective of bio-polyampholyte mediated assembly, the studies should also form the basis for new models where current ion- and charged macromolecular- mediated assembly models are for equilibrium systems.

The projects utilize the broad spectrum of expertise of the PI and the two co-PIs in biomolecular self-assembling methods, custom organic/polymer synthesis and purification of biological molecules, synchrotron x-ray scattering, electron and optical microscopy, and SAXS-osmotic pressure techniques for *in-situ* force measurements.

## Recent Progress

### (I) Protein Tau Mediated Electrostatic Interactions lead to Microtubule Bundles under Dissipative Conditions with Distinct 1D and 2D Architectures.

The current study was designed to elucidate the molecular mechanism of protein Tau-mediated microtubule assembly under dissipative out-of-equilibrium conditions (i.e. mimicking the cytoskeletal environment of cells with samples consuming the energy released by GTP hydrolysis) [9]. Tau is an intrinsically disordered protein and a polyampholyte (i.e. a charged polymer containing both positive and negative charges). Synchrotron SAXS and plastic embedded TEM enabled both angstrom-resolution ensemble-averaged structural information and nm-scale real-space local fine structure, respectively.

Our study revealed steady-state structures that are stable over time (> 24 hours, Fig. 1, Middle, Right). In-situ synchrotron SAXS under osmotic pressure allowed us to map out the energy landscape of Tau-mediated, GTP-dependent microtubule bundles. In the absence of applied pressure, the microtubule reaction mixture exhibits Tau-induced phase separation into microtubule bundles, demonstrating the presence of an attractive component to Tau-mediated interactions between microtubules. SAXS and TEM revealed widely-spaced bundles (energy minimum at microtubule wall-to-wall distance  $D_{w-w} \approx 26-41$  nm) with hexagonal (Fig. 1, Right) and string-like symmetry, the latter mimicking bundles found in the axon-initial-segment. The data suggests a mechanism where the sum of sub- $k_B T$  cationic/anionic charge-charge attractions, by weakly penetrating Tau projection domains (PDs) on opposing microtubules, stabilize bundles (see Fig. 1, Left). A second minimum ( $D_{w-w} \approx 16-23$  nm), indicative of antiparallel dipole-dipole interactions of interpenetrating Tau PDs, is revealed under osmotic pressure.

Significance. This highly unusual interaction between widely-spaced surfaces is made possible by the non-uniform charge distribution of the projection domain of Tau, where segments of the N-terminal tail (which shift the active zone to the mid-layer) contain shorter, cationic/anionic domains enabling attraction between Tau on opposing microtubule surfaces. This discovery should spur analytical and computer modeling efforts, which take into account the specific sequence of Tau, to more quantitatively describe the Tau-mediated interactions. Generalizable principles derived from this system could serve as inspiration for polyampholyte-directed assembling materials.

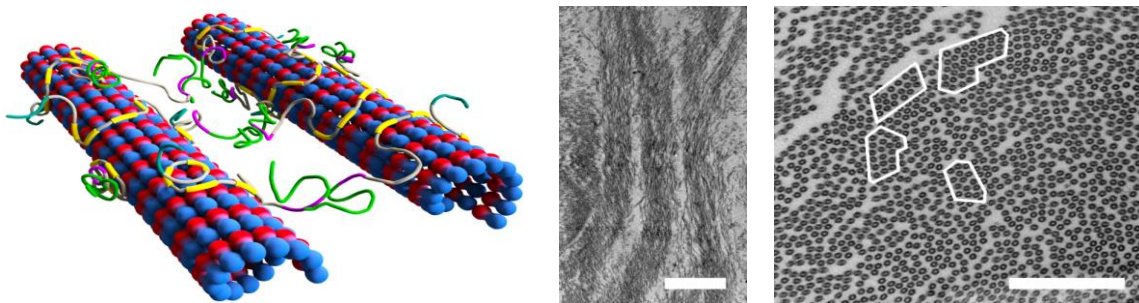


Fig. 1 LEFT: Cartoon of the widely-spaced energy minimum between neighboring microtubules with attached intrinsically disordered Tau. Here, Tau is seen to mediate microtubule bundles by transient charge-charge attractions between the cationic residues (purple/gray) and the anionic residues (green) in the amino-terminal tail. MIDDLE: Electron microscopy (side view) of microtubules assembled with Tau ( $\Phi_{3RM}=\text{tau/tubulin dimer molar ratio}=1/20$ ) at low magnification show distinct bundled domains, demonstrating phase separation. RIGHT: Top view of domains of hexagonally-ordered arrays of microtubules (identified in white outlines,  $\Phi_{3RL}=1/20$ ) with vacancies likely resulting from the suppressed (but still occurring) dynamic instability. Adapted from [9].

## (II) Neurofilament Networks Form Salt-Responsive Hydrogels with Distinct Sidearm-Dependent Isotropic and Anisotropic Phases.

Neurofilaments (NFs) – the neuron-specific intermediate filament proteins – are assembled into 10 nm wide filaments in a tightly controlled ratio of three different monomer types: NF-Low (NF-L), NF-Medium (NF-M), and NF-High (NF-H) (Fig. 2). Our previous work on reconstituted NF hydrogels has shown the dependence of network properties, including filament alignment and spacing, on the subunit composition. We used polarized optical microscopy and SAXS to explore the full salt-dependent phase behavior of reconstituted NF networks as a function of various binary and ternary subunit ratios [10]. We observed three salt-induced phases: the anisotropic (orientationally ordered)  $B_G$  (Blue Gel) and  $N_G$  (nematic gel) phases, and the isotropic  $I_G$  phase. We note the emergent sidearm roles, particularly that of NF-H in driving the parallel to cross-filament transition, and the counter-role of NF-M in suppressing the  $I_G$  phase. More specifically, in copolymers of NF-LH, NF-H shifts the  $I_G$  to  $N_G$  transition closer to the physiological salt concentrations, as compared to NF-M in copolymers of NF-LM.

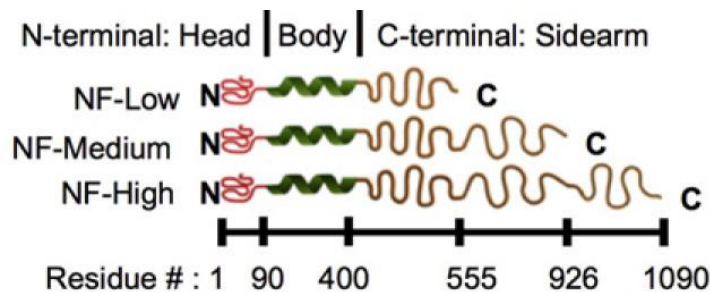


Fig. 2. : Schematic representation of NF-Low, NF-Medium, and NF-High subunits, with unstructured N- and C-termini (the head and tail domain, respectively) flanking an alpha-helical rod domain (the body). Their main distinction lies in the length and charge of their tail domains. The formation of coiled coils via the alpha-helical rod domains drives the multimerization of the NF subunits into

the mature NF — 10 nm in diameter. While the body domains form the core of the mature filament, the tail domains projecting radially outwards, enabling them to interact with those from neighboring filaments (mainly through electrostatic associations), thus driving network formation. Adapted from [10].

Significance. Understanding the role of individual subunits in regulating the filament network structure will enable us to understand the mechanisms that drive the anisotropic and isotropic networks with distinct viscoelastic mechanical properties and water retention behavior.

### **Future Plans**

Emerging structures in active microtubule-protein Tau bundles mediated by multivalent ions: Competition between Tau mediated versus multivalent ion mediated interactions. In the next series of experiments we will study the protein Tau (biological polyampholyte)/microtubule (MT) active system [9] in the presence of multivalent ions (MVIs), which under certain conditions is expected to transition the system into the electrostatic strong coupling regime. Our group has previously shown that in the absence of the electrostatic cross-linker Tau, solutions containing MTs and MVIs are driven into the strong coupling regime where short-range attractions between MTs, resulting in tightly spaced bundles, are mediated by correlations between the fluctuations of the MVIs bound to the surface of MTs. In contrast, Tau's highly charged projection domain (a polyampholyte containing a large anionic polypeptide section in the N-terminal region) shifts the MT-MT interaction regime to the mid-plane between widely spaced MTs and away from the region near MT surface. The experiments will bring together and explore, for the first time, these competing interactions (i.e. mediated by MVIs and charged polypeptide Tau) in an active matter system where we expect new emerging behavior. We

should note that although such competing interactions are present in the highly complex cellular environment the formation mechanisms and the resulting structures have not been elucidated.

## References

1. Safinya, C. R.; Raviv, U.; Needleman, D. J.; Zidovska, A.; et al.: Nanoscale Assembly in Biological Systems: From Neuronal Cytoskeletal Proteins to Curvature Stabilizing Lipids. *Advanced Materials* **2011**, *23*, 2260-2270.
2. Safinya, C. R.; Deek, J.; Beck, R.; Jones, J. B.; Li, Y.: Assembly of Biological Nanostructures: Isotropic and Liquid Crystalline Phases of Neurofilament Hydrogels. *Annual Review of Condensed Matter Physics* **2015**, *6*, 113-136.2
3. Ojeda-Lopez, M. A.; Needleman, D. J.; Song, C.; Ginsburg, A.; Kohl, P.; Li, Y.; Miller, H. P.; Wilson, L.; Raviv, U.; Choi, M. C.; Safinya, C. R.: Transformation of taxol-stabilized microtubules into inverted tubulin tubules triggered by a tubulin conformation switch. *Nature Materials* **2014**, *13*, 195-203.
4. Deek, J.; Chung, P. J.; Kayser, J.; Bausch, A. R.; Safinya, C. R.: Neurofilament sidearms modulate parallel and crossed-filament orientations inducing nematic to isotropic and re-entrant birefringent hydrogels. *Nature Communications* **2013**, *4*, 2224.
5. Beck, R.; Deek, J.; Jones, J. B.; Safinya, C. R.: Gel Expanded-Gel Condensed Transition in Neurofilament Networks Revealed by Direct Force Measurements. *Nature Materials*. **2010**, *9*, 40-46.
6. Chung, P. J.; Choi, M. C.; Miller, H. P.; Feinstein, H. E.; Raviv, U.; Li, Y.; Wilson, L.; Feinstein, S. L.; Safinya, C. R.: Direct force measurements reveal that protein Tau confers short-range attractions and isoform-dependent steric stabilization to microtubules. *Proc. Natl. Acad. Sci. U. S. A. (PNAS Plus)* **2015**, *112*, E6416-E6425.
7. Choi, M.C.; Raviv, U.; Miller, H.P.; Gaylord, M.R.; Kiris, E.; Ventimiglia, D.; Needleman, D.J.; Kim, M.W.; Wilson, L.; Feinstein, S.C.; Safinya, C.R.: Human Microtubule-Associated-Protein Tau Regulates the Number of Protofilaments in Microtubules: A Synchrotron X-ray Scattering Study. *Biophysical J.* **2009**, *97*, 519-527.
8. Needleman, D. J.; Ojeda-Lopez, M. A.; Raviv, U.; Miller, H. P.; Li, Y.; Song, C.; Feinstein, S. C.; Wilson, L.; Choi, M. C.; Safinya, C. R.: Ion specific effects in bundling and depolymerization of taxol-stabilized microtubules. *Faraday Discussions* **2013**, *166*, 31-45.
9. Chung, P. J.; Song, C.; Miller, H. P.; Li, Y.; Choi, M. C.; Wilson, L.; Feinstein, S. C.; Safinya, C. R.: Tau mediates microtubule bundle architectures mimicking fascicles of microtubules found in the axon initial segment. *Nature Communications* **2016**, *7*, 12278.
10. Deek, J.; Chung, P. J.; Safinya, C. R.: Neurofilament networks: Salt-responsive hydrogels with sidearm-dependent phase behavior. *Biochim. Biophys. Acta - General Subjects* **2016**, *1860*, 1560-1569.
11. Needleman, D. J.; Ojeda-Lopez, M. A.; Raviv, U.; Miller, H. P.; et al.: Higher-order assembly of microtubules by counterions: From hexagonal bundles to living necklaces. *Proc. Natl. Acad. Sci. U.S.A.* **2004**, *101*, 16099-16103.

**Publications (BES-supported, last 24 months, only in print and accepted papers)**

12. Chung, P. J.; Choi, M. C.; Miller, H. P.; Feinstein, H. E.; Raviv, U.; Li, Y.; Wilson, L.; Feinstein, S. L.; Safinya, C. R.: Direct force measurements reveal that protein Tau confers short-range attractions and isoform-dependent steric stabilization to microtubules. *Proc. Natl. Acad. Sci. U. S. A. (PNAS Plus)* **2015**, *112*, E6416-E6425. DOI: [10.1073/pnas.1513172112](https://doi.org/10.1073/pnas.1513172112) (featured in an [SSRL Highlight](#) in Feb. 2017).
13. Majzoub, R. N.; Ewert, K. K.; Jacovetty, E. L.; Carragher, B.; Potter, C. S.; Li, Y.; Safinya, C. R.: Patterned Threadlike Micelles and DNA-Tethered Nanoparticles: A Structural Study of PEGylated Cationic Liposome–DNA Assemblies. *Langmuir* **2015**, *31*, 7073-7083. DOI: [10.1021/acs.langmuir.5b00993](https://doi.org/10.1021/acs.langmuir.5b00993).
14. Safinya, C. R.; Chung, P. J.; Song, C.; Li, Y.; Ewert, K. K.; Choi, M. C.: The effect of multivalent cations and Tau on paclitaxel-stabilized microtubule assembly, disassembly, and structure. *Adv. Colloid Interf. Sci.* **2016**, *232*, 9-16. DOI: [10.1016/j.cis.2015.11.002](https://doi.org/10.1016/j.cis.2015.11.002); PMID: [4864139](https://pubmed.ncbi.nlm.nih.gov/27041399/).
15. Deek, J.; Chung, P. J.; Safinya, C. R.: Neurofilament networks: Salt-responsive hydrogels with sidearm-dependent phase behavior. *Biochim. Biophys. Acta - General Subjects* **2016**, *1860*, 1560-1569. DOI: [10.1016/j.bbagen.2016.03.018](https://doi.org/10.1016/j.bbagen.2016.03.018).
16. Chung, P. J.; Song, C.; Miller, H. P.; Li, Y.; Choi, M. C.; Wilson, L.; Feinstein, S. C.; Safinya, C. R.: Tau mediates microtubule bundle architectures mimicking fascicles of microtubules found in the axon initial segment. *Nature Communications* **2016**, *7*, 12278. DOI: [10.1038/ncomms12278](https://doi.org/10.1038/ncomms12278) (featured in an [SSRL Highlight](#) in Feb. 2017).
17. Choi, M. C.; Chung, P. J.; Song, C.; Miller, H. P.; Kiris, E.; Li, Y.; Wilson, L.; Feinstein, S. C.; Safinya, C. R.: Paclitaxel suppresses Tau-mediated microtubule bundling in a concentration-dependent manner. *Biochim. Biophys. Acta - General Subjects* **2017**, *1861*, 3456-3463. DOI: [10.1016/j.bbagen.2016.09.011](https://doi.org/10.1016/j.bbagen.2016.09.011).
18. Chung, P. J.; Song, C.; Miller, H. P.; Li, Y.; Raviv, U.; Choi, M. C.; Wilson, L.; Feinstein, S. C.; Safinya, C. R.: Synchrotron small-angle X-ray scattering and electron microscopy characterization of structures and forces in microtubule/Tau mixtures. *Meth. Cell Biol.*, in press.

## Measuring transport characteristics of water confined in biological materials

**PI: Ozgur Sahin**

**Department of Biology Sciences and of Physics, Columbia University**

### Program Scope

Our program aims to understand limits of water-driven energy conversion in biological materials. Current efforts focus on measurements and modeling of the transport behavior of water confined in nanoscale pores of biological materials, which will provide an understanding of the limits of power density of these materials. We are using spores of *Bacillus* as a model system due to their highly reversible water absorption and release characteristics. We have previously built an experimental setup to probe nanoscale water dynamics with millisecond time resolution using nanomechanical cantilever sensors. We now use this setup to gather transport kinetics data under various environmental conditions and with spores whose structure is modified by genetic alterations so that the measured transport kinetics can be attributed to individual spores and their sub-structures. We are developing and testing theoretical models to interpret water transport measurements and obtain quantitative information about viscosity of the biologically-nanoconfined water and its associated activation energy. Together, these quantities will allow characterizing the behavior of water confined in biological materials and relate it to energy conversion performance.

### Recent Progress

We have developed an experiment that allows detailed characterization of the transport behavior of nanoconfined water in bacterial spores. Our previous work has shown that spores of *Bacillus* respond strongly to changes in relative humidity by expanding and contracting reversibly, acting as a highly effective muscle generating force as water goes in and out of spores (Fig. 1b) [1,2]. The resulting forces facilitate detailed probing of water transport kinetics via nanomechanical cantilever sensors, which are formed by coating cantilevers with spores (Fig. 1c).

Spores contain a dehydrated genomic core that is surrounded by a loosely cross-linked peptidoglycan cortex and a proteinaceous coat. Biophysical and chemical studies have shown that small molecules like glucose and amino acids can permeate through the coat and the cortex, whereas larger molecules such as lysozyme are blocked [3]. Dimensions of these molecules suggest that cortex and coat layers contain pores with dimensions around 1 to 2 nm in fully hydrated spores. However, pore dimensions must gradually become smaller when spores contract at low relative humidity. Because hydraulic resistance of pores depends strongly on pore dimensions, we probed hydration-dehydration kinetics of spores by varying relative humidity. After setting the relative humidity to a predetermined value, brief photo-thermal pulses from a light emitting diode (LED) weakly perturb the equilibrium of spores by modulating their temperature (Fig. 1d). Forces generated during the transient water exchange allow determination

of spore response time from the deflection signals. Furthermore, by adjusting the set-point relative humidity, this setup facilitates probing the effects of spore nanopore dimensions on water transport (Fig. 1e).

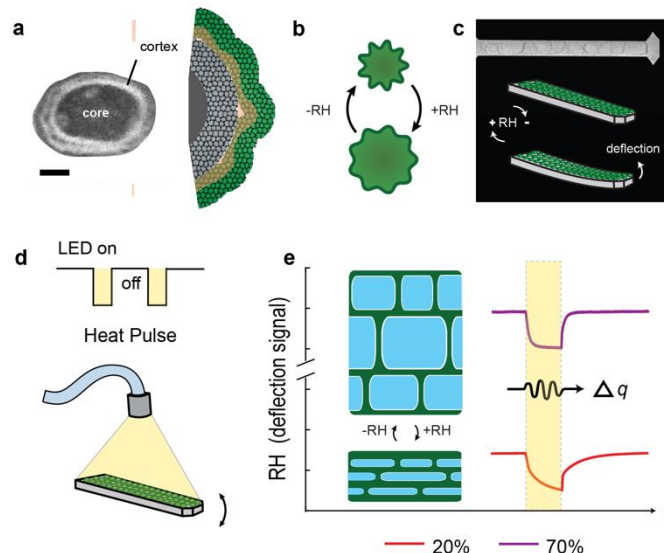


**Figure 1 | Probing transport kinetics of nanoconfined water with photothermally-driven nanomechanical cantilever sensors.** **a**, Electron microscopy image of a spore with depiction of porous hygroscopic cortex and coat layers. **b**, Relative humidity dependent spore expansion and contraction. **c**, Spores are spray-coated onto one side of an AFM cantilever that bends in proportion to hydration-dehydration cycling. **d**, Fiber-optic LED provides a local photothermal pulse to perturb spore-water equilibrium. **e**, The effect of changing pore dimensions with relative humidity on water transport kinetics is probed by monitoring the cantilever deflections.

Using this setup, we measured the transient response of the spore-cantilever system at different set-point relative humidities (Fig. 2a,b). We found that time constant measurements did not correlate with the quantity of spores deposited on cantilevers. However, spores that lack a majority of the coat layer due to mutations in *cotE* and *gerE* genes revealed significantly faster response times. Therefore, the transient deflection signals are governed by the transport kinetics within individual spores. This critical result shows that although we deposit large quantities of spores on a cantilever, the measured response times reflect average characteristics of spores.

To interpret the transport measurements, we used poroelastic theory. According to poroelastic theory, pressure of the pore fluid obeys a diffusion equation, such that the time it takes pressure to reach equilibrium after a photo-thermal pulse,  $\tau \sim \alpha L^2 / D_p$ , depends on poroelastic diffusivity,  $D_p$ , the thickness of the region over which pressure spreads,  $L$ , and  $\alpha$ , which is a prefactor that depends on the geometry of the system.  $D_p$  is related to the properties of the porous material and the pore fluid:  $D_p \sim Ed^2 / \eta$ , where  $E$  is the longitudinal elastic modulus of the poroelastic material,  $d$  is the effective pore diameter, and  $\eta$  is the viscosity of the fluid.

To quantify the viscosity of nanoconfined water, we estimated  $L$  with the thickness of coat and cortex layers as determined from electron microscopy images of spore cross sections, while taking into account gradual changes in spore dimensions with relative humidity (Fig. 2c). We estimated  $d$  to vary approximately linearly with relative humidity, starting from nearly zero for vacuum dried spores and reaching  $1.5 \pm 0.5$  nm nominally when fully hydrated, where the upper limit reflects sieving properties of spore coat and cortex. We estimated  $E$  as a function of relative humidity from changes in spore dimensions. The resulting estimates are given in Fig. 2d. These preliminary estimates depend on a number of approximations that could be refined further.

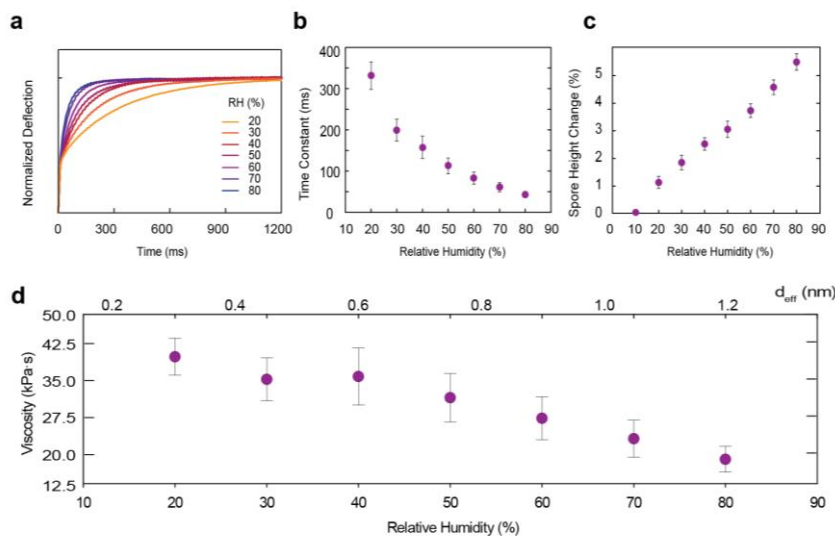


**Figure 2 | Humidity dependent confinement effects on water transport.** **a**, Cantilever deflection signals following photo-thermal pulses shown for a range of relative humidity levels at constant temperature. **b**, Relaxation time constants derived from deflection signals. Error bars are standard error of five measurements. **c**, The spore’s relative height change is shown as a function of relative humidity. Error bars are standard error of five measurements for twenty spores. **d**, Preliminary estimates of effective spore water viscosity versus relative humidity (bottom) and the corresponding effective confinement length (top).

The same experimental setup also allows determining the activation energy of water transport. By relying on a simple Arrhenius type exponential relationship for viscosity, we obtained activation energies from temperature dependent measurements of transport kinetics (Fig. 3a, b). Measurements in the range of 15% to 70% relative humidity show activation energy to increase substantially (Fig. 3c). Furthermore, the data show that the spore water undergoes a steep transition around 20% relative humidity, where activation energy rises from about 6 kCal/mol, which is close to the activation energy of liquid water, and exceeds 9 kCal/mol at 25% relative humidity. By 70%, the activation energy value reaches 12 kCal/mol. The sharp transition near 20% relative humidity could indicate a significant change in overall water structure, as the nominal diameter of pores at this relative humidity is close to the dimensions of a water molecule. The narrow diameter of pores might prevent formation of short-range order in water structure, which requires a larger spacing due to the three-dimensional structure of hydrogen-bonded networks of water molecules.

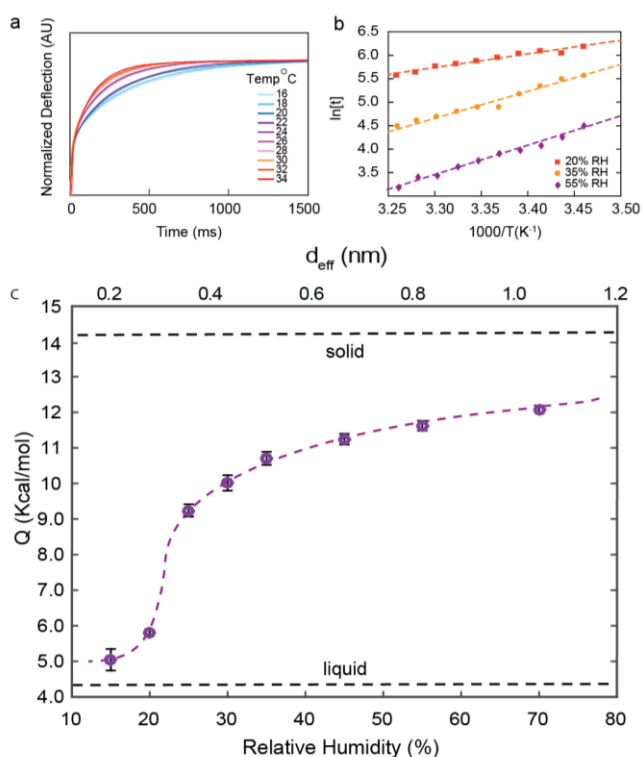


**Figure 3 | Activation energy water transport under nanoconfinement.** **a**, Temperature dependent transient deflection curves recorded following photo-thermal pulses at constant relative humidity. **b**, Inverse temperature versus natural log of time constants. **c**, Activation energies, denoted as  $Q$ , derived from the slopes of linear fits are plotted for a range of humidities and corresponding effective pore dimensions ( $d_{\text{eff}}$ ). For comparison, activation energies of water transport in liquid and solid phases are marked with dashed lines. Error bars are standard error reflecting three separate spore-coated cantilevers.

## Future Plans

We plan to investigate potential effects of dissolved ions on the transport characteristics of biologically-nanoconfined water. The present experimental setup does not allow us to introduce ions to spores, however, we plan to develop an atomic force microscopy based experiment that probes spores' frequency dependent dynamic stiffness in response to changing buffer conditions.

## References

- 1- Chen, X., Mahadevan, L., Driks, A. & Sahin, O. Bacillus spores as building blocks for stimuli-responsive materials and nanogenerators. *Nat. Nanotechnol.* **9**, 137-141, (2014)
- 2- Chen, X. *et al.* Scaling up nanoscale water-driven energy conversion into evaporation-driven engines and generators. *Nat. Commun.* **6**, 7346, (2015).
- 3- He, L. M. & Tebo, B. M. Surface charge properties of and Cu(II) adsorption by spores of the marine Bacillus sp. strain SG-1. *Appl. Environ. Microb.* **64**, 1123-1129 (1998).

## Publications (supported by the DOE grant)

- 1- Cavusoglu, A-H., Chen, X., Gentine, P. and Sahin, O. "Potential for natural evaporation as a reliable renewable energy resource." *Nat. Commun.*, in press.

## Strain distributions and structural changes in motor-driven gels

Omar A. Saleh (PI), Deborah K. Fygenson (co-PI), and Robert M. McMeeking (co-PI)  
UC Santa Barbara

### Program Scope

The overarching goal of this project is to study the effects of molecular motor proteins on the structure and dynamics of a biopolymer hydrogel. Motor proteins are nanoscale transducers, converting chemical energy embedded in the solution into local mechanical work on hydrogel strands, and thus potentially driving structural changes and/or non-equilibrium dynamics within the gel material. Our long term goals are to understand mechanical aspects of motor-driven strain within the hydrogel, and to create systems that restructure in response to motor activity.

To accomplish these goals, we are performing experimental studies of condensed DNA systems acted upon by DNA motors, in concert with theoretical studies of hydrogel mechanics. Our experimental approach focuses on two types of systems: 1) Stably crosslinked DNA hydrogels that respond to motor-derived forces by deforming, then snapping back elastically to the initial shape (Fig. 1), and 2) Transiently crosslinked DNA liquids that can be driven to flow and form alternate structures through motor activity (Fig. 2). In this abstract, and the accompanying talk, we will focus on system 2, DNA liquids, for which there are more recent results.

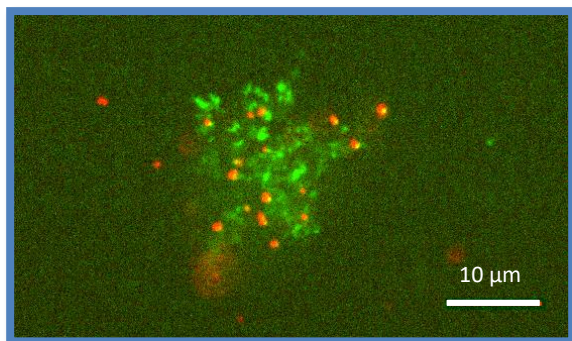


**Figure 1.** Fluorescent image of a DNA hydrogel. DNA is labeled green; red indicates embedded fluorescent particles. High-speed tracking of the bright red particles reveals gel deformations due to motor protein activity.

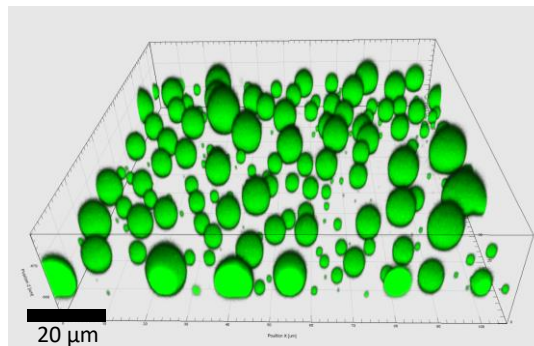


**Figure 2.** Perspective rendering of 3-D confocal image of fluorescently-labeled liquid DNA droplets that have sedimented onto a glass coverslip.

---

### Recent Progress

Our DNA liquids are based on a multi-arm geometry termed a DNA nanostar (1). Each nanostar has four arms that join at a central junction (see schematic, top of Fig. 3) and whose distal ends terminate in a palindromic single-stranded sequence ('sticky end'). As a result of those sticky ends, a solution of nanostars will, at low temperature, bind each other and form a condensed phase. We have recently shown (2) that the nature of this condensed phase is sensitive

to the precise design of the nanostar: particularly, the presence of an unpaired base (pink dots in Figure 3) adjacent to the sticky end causes the nanostars to form liquid-like droplets.

The liquid nature of these droplets is attested by their spherical shape owing to surface tension (see Fig. 2 and Fig. 3), the ability of droplets to coalesce upon collision, and by rheological studies that show low-frequency dominance of the loss

over the storage modulus (Fig. 4). Analysis of the rheological and coalescence behavior leads to estimates of 50 Pa s for DNA droplet viscosity (compared to  $10^{-3}$  for water), and 0.01 dyne/cm for DNA droplet surface tension (compared to 70 dyne/cm for water); both values hold at room temperature. The high viscosity and low surface tension can be attributed to the large size of the molecules and the kinetics of binding between the sticky ends; roughly comparable values can be found for other macromolecular liquids (e.g. coacervates).

An intriguing feature of the system is that miscibility of two types of nanostars is controlled by the sequence of the sticky ends. For example, when quenching a solution containing red-dyed nanostars with a CGATCG sticky end and blue-dyed nanostars with a GAGCTC sticky end, the result is immiscible behavior (separate red and blue droplets; Fig. 5). Remnant weak attractions cause the droplets to adhere, though this adhesion is so weak as to not perturb the spherical droplet shape. This adhesion can be engineered, for example by including crosslinking ‘surfactant’ nanostars that have two sticky ends binding to the red phase, and two that bind the blue phase (Fig. 5); introduction of this species leads to strong adhesion and droplet deformation.

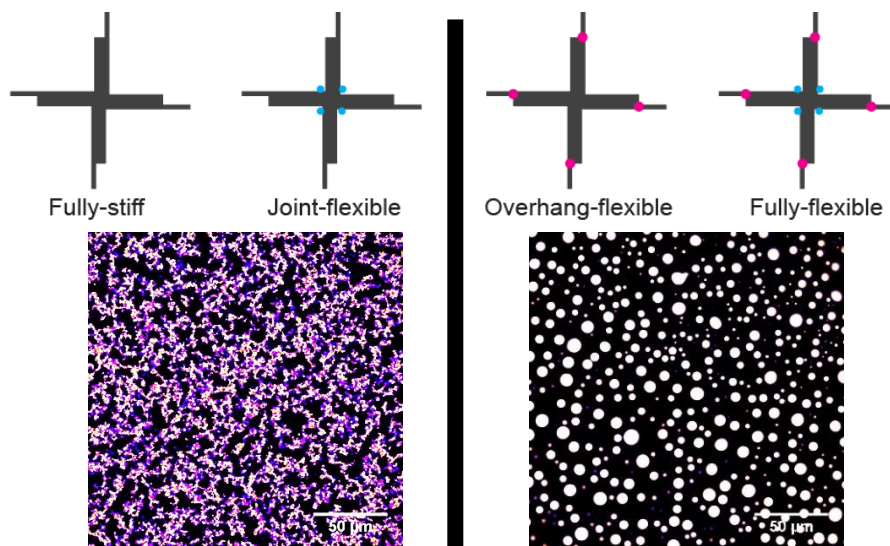


**Figure 3:** Illustration of the effect of nanostar design on nanostar phase. Top: Schematic of four different nanostar designs, each with 20 bp double-stranded DNA arms terminating in a 6 or 7 base single-stranded ‘sticky end’. Extra bases near the sticky end (pink dots) cause maturation into liquid droplets (right image). Nanostars lacking those bases form fractal-aggregate gels (left image). The presence of extra bases near the junction (blue dots) does not impact phase.

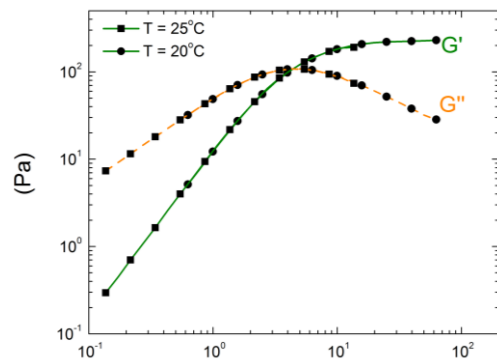


**Figure 4:** Rheology of a DNA nanostar liquid, showing classic viscoelastic liquid behavior, with the loss modulus ( $G''$ , orange) dominating over the storage modulus ( $G'$ , green) at low frequencies.

We have begun to investigate the effects of interfacing motor proteins with the DNA droplets, using the T7 RNA polymerase (RNAP). T7 RNAP is a phage protein with a robust transcription activity *in vitro*. Using this motor requires the presence of a gene under control of a T7 promoter. We have found that creating a gene with sticky ends complementary to the nanostars permits their segregation into the DNA liquid phase (Fig. 6). Further, the segregated genes still retain transcriptional activity, though at a lesser level than when free in solution, or integrated into fractal-aggregate gels, presumably due to accessibility differences (Fig. 6). Finally, and most intriguingly, we have found that transcription from genes within the nanostar liquids leads to structure changes, particularly clustering of the genetic DNA strands within the droplet (Fig. 6). The resulting structures are reminiscent of ‘hotspots’ observed within cell nuclei, in which active genes are segregated away from other genetic material (3). In our system, we tentatively ascribe this structure formation to interactions created by the RNA transcripts, though we note that activity-induced phase segregation in polymer systems has recently been shown to be feasible theoretically (4).

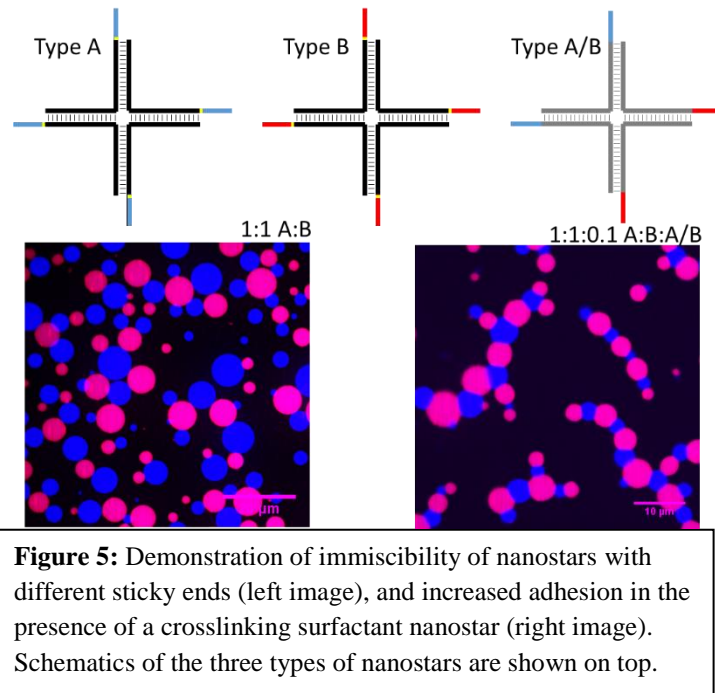


**Figure 5:** Demonstration of immiscibility of nanostars with different sticky ends (left image), and increased adhesion in the presence of a crosslinking surfactant nanostar (right image). Schematics of the three types of nanostars are shown on top.

transcription from genes within the nanostar liquids leads to structure changes, particularly clustering of the genetic DNA strands within the droplet (Fig. 6). The resulting structures are reminiscent of ‘hotspots’ observed within cell nuclei, in which active genes are segregated away from other genetic material (3). In our system, we tentatively ascribe this structure formation to interactions created by the RNA transcripts, though we note that activity-induced phase segregation in polymer systems has recently been shown to be feasible theoretically (4).

### Future Plans

Our future plans are organized into three thrusts. First, we continue to work on the elastic DNA hydrogel systems driven by motors; that work was not extensively discussed in this abstract. We have extensive data in that system; future efforts will focus on modeling, including analytical approaches and finite-element simulations using newly-developed constitutive models (5).

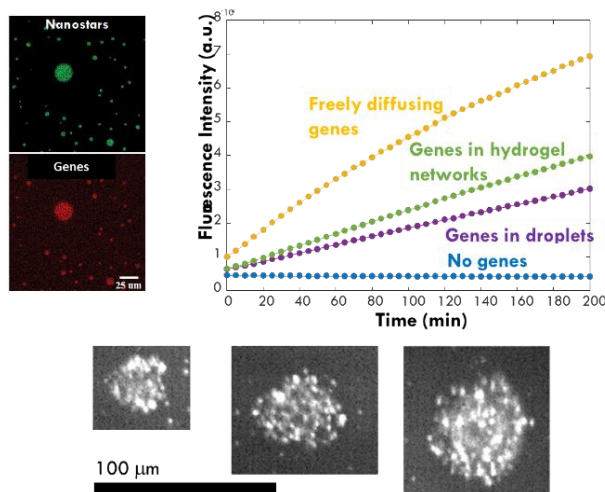


**Figure 6:** Preliminary data on nanostar liquids containing genes. Genes with complementary sticky ends segregate into DNA droplets (top left), and can be transcribed, though with reduced efficiency compared to genes free in solution (top right). Transcription induces a clustering phenomenon, in which fluorescently labeled genes form discrete spots within the droplet (three example droplets shown on bottom).

A second thrust is to understand and exploit the meso-scale droplet structures created from heterogeneous nanostar solutions, as shown in Fig. 5. This system permits localization of specific DNA components both to separate compartments (i.e. separate droplets), and to the droplet interface. DNA structure and sequence controls protein interactions—thus we posit that the meso-scale structures can be exploited to controllably target motor proteins to specific locations, leading to novel and dramatic active-material behaviors. We will also investigate this system using theoretical approaches; this system is particularly ripe for such approaches due to the expected complex interplay of transient motor forces, mesoscale structure, interfacial energies, and viscoelastic behavior.

Our third thrust will focus on the artificial nucleus concept depicted in Fig. 6: our preliminary data show that genes can be partitioned into liquid DNA droplets, and that their transcription leads to structural changes akin to those seen in living systems. This finding needs to be rigorously verified and checked for generality; we will do so by varying the various system parameters, including the identity (sequence) of the gene and the type of polymerase.

## References

- (1) Biffi, S. *et al.* Phase behavior and critical activated dynamics of limited-valence DNA nanostars. *Proceedings of the National Academy of Sciences* **110**, 15633-15637, (2013). doi:10.1073/pnas.1304632110
- (2) Nguyen, D.T. & Saleh, O. A. Tuning phase and aging of DNA hydrogels through molecular design. *Soft Matter* (2017). doi: 10.1039/c7sm00557a.
- (3) Sutherland, H. & Bickmore, W. A. Transcription factories: gene expression in unions? *Nat Rev Genet* **10**, 457-466 (2009). doi: 10.1038/nrg2592
- (4) Smrek, J. and Kremer, K.. Small Activity Differences Drive Phase Separation in Active-Passive Polymer Mixtures. *Physical Review Letters* **118**, 098002, (2017). doi:10.1103/PhysRevLett.118.098002
- (5) Bacca, M. & McMeeking, R.M. A viscoelastic constitutive law for hydrogels. *Meccanica* (2017). doi:10.1007/s11012-017-0636-y

## Publications

1. Park, C.-Y., Fygenon, D. K. & Saleh, O. A. Electrostatics and depletion determine competition between 2D nematic and 3D bundled phases of rod-like DNA nanotubes. *Soft Matter* **12**, 5089-5095, (2016). doi:10.1039/C6SM00222F
2. Noselli, G., Lucantonio A., McMeeking R.M. & DeSimone, A. Poroelastic toughening in polymer gels: A theoretical and numerical study. *J. Mech. Phy. Solids* **94**, 33-46 (2016). doi: 10.1016/j.jmps.2016.04.017
3. Bacca, M. & McMeeking, R.M. A viscoelastic constitutive law for hydrogels. *Meccanica* (2017). doi:10.1007/s11012-017-0636-y
4. Nguyen, D.T. & Saleh, O. A. Tuning phase and aging of DNA hydrogels through molecular design. *Soft Matter* (2017). doi: 10.1039/c7sm00557a.

## **Programmable Dynamic Self-Assembly of DNA Nanostructures**

**Rebecca Schulman, Johns Hopkins University (collaborative project with Elisa Franco, University of California Riverside)**

### **Program Scope**

The synthesis of novel materials with self-regulation properties akin to those of biological cells is a central challenge in biomolecular materials research. In biological systems, behaviors such as growth, division, and self-repair emerge because molecular self-assembly processes are coupled to and directed by signal transduction and gene expression networks. The goal of this project is to construct synthetic materials with similarly complex structure, where the capacity for adaptive, dynamic responses within materials is achieved by coordinating synthetic self-assembly processes with synthetic molecular circuits and control systems.

To do so, we are creating modular, programmable biosystems composed of nucleic acid nanostructures and signal processing systems, where the simplicity and modularity of Watson-Crick hybridization by DNA and RNA is key to their development and the precise control that can be achieved. As part of this project, we previously developed a toolkit where assembly and disassembly of nucleic acid structures can be directed by nucleic acid circuits that can in turn take different chemical stimuli, such as proteins or small molecules, as inputs. Our current goal is to build more complex architectures and structures that can undergo complex forms of reorganization through the direction of molecular circuits that orchestrate the assembly and disassembly of multiple types of components in multiple temporal stages. We are developing mechanisms to allow materials to exhibit sustained dynamical behaviors and show how molecular circuits can orchestrate complex adaptive responses including self-repair and motility.

The biological inspiration for the materials in this study is the cytoskeleton, in which a small set of one-dimensional fibers assembled from a small set of monomers are organized into a variety of different structures such as spindles, sarcomeres, cilia or filopodia by molecules that branch, crosslink, stabilize or destabilize the fibers and in turn the genetic circuits that control the spatiotemporal abundance and activity of these molecular components<sup>Ref1</sup>. We are studying DAE-E DNA tile nanotubes as a model fiber<sup>Ref2</sup> and dynamic genelet<sup>Ref3</sup> and strand-displacement nucleic acid circuits<sup>Ref4</sup> which can be coupled using short nucleic acid message strands that serve as inputs and outputs from both these circuits and these structures.

### **Recent Progress**

*Self-assembly of DNA nanotube architectures with programmable control over shape and flexibility.* To build micron-scale 2- and 3-dimensional architectures that self-organize in response to cues from the environment, we constructed junctions that direct the growth of DNA nanotubes into architectures. Building on our prior work developing seeds for DNA nanotube growth, DNA origami structures that act as templates for nanotube nucleation<sup>Ref5</sup>, we have synthesized flexible DNA nanotube nunchuck structures<sup>Pub3</sup>, flexible two-nanotube architectures

and rigid multi-armed structures where the geometry between the architecture can be precisely controlled<sup>Pub2</sup>. We have also developed nanotube caps that can attach to growing ends, preventing further elongation.

*Responsiveness of assembly to the geometry of the environment.* The formation of reconfigurable architectures requires a system to respond to both the type and location of chemical cues. In the cytoskeleton, architectures form in particular regions and are anchored to cell membranes or the nuclear envelope. We have developed a model system for this type of response in which DNA tile nanotubes grow to connect molecular landmarks that adapt to the geometry of the landmarks presented<sup>Pub1</sup>. Landmarks may be separated by distances of 1-10 microns and are connected with yields of at least 80%. To form connections, nanotubes nucleate at landmarks, grow, and their ends diffuse. When the ends from complementary landmarks meet, they can join to form a stable connection. This process demonstrates how self-assembly

processes can adapt in complex, functional ways to the geometry of the assembly environment, and could be used as a primitive for the assembly of complex architectures. To understand the assembly process, we also developed quantitative molecular dynamics simulations of the growth, diffusion and joining processes that create connections.

*Molecular circuits for controlling assembly mode and timing.* Molecular circuits that control the timing of assembly events

could coordinate assembly processes requiring sequential events. We have developed a simple mechanism to control assembly timing in which an output molecule is slowly released but is rapidly consumed by a reservoir of delay species. After the delay species is depleted, the output begins to accumulate. This tunable DNA strand displacement system can delay the release of a DNA signal for 3-70 hours and release different signals at different times and rates<sup>Pub4</sup>.

Dynamic switching programs could allow a system to assembly one structure, then disassemble it and produce another. A fundamental motif for the control of cell state is the bistable switch, where a transient input triggers a permanent change in gene expression. We have

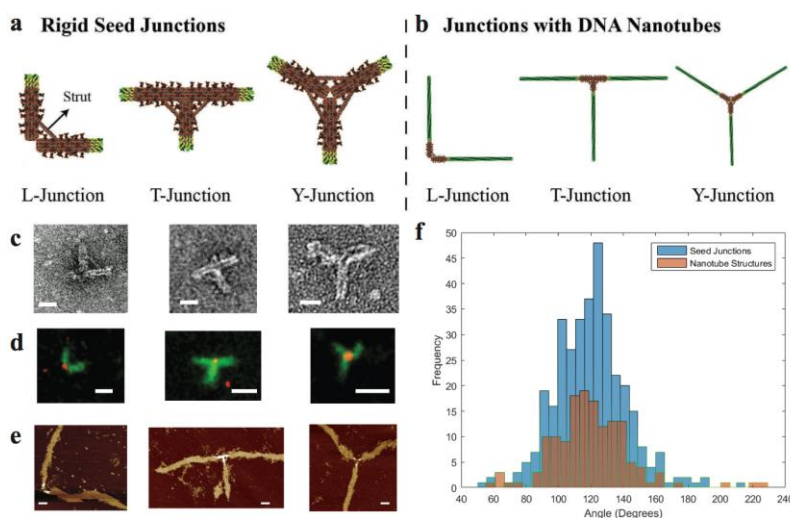


Figure 1: Rigid nanotube architectures [p2]. (a-b) Schematics for seeds and resulting architectures that grow from them (c) TEM images of seeds. Scale bars 25 nm. Fluorescence micrographs (d) and AFM images (e) of nanotube architectures grown from L, T and Y seeds. Scale bars 5  $\mu\text{m}$  and 50 nm. (f) Frequency histogram of angles between the components of the Y junction taken from TEM images for seeds (blue) and from fluorescence micrographs for nanotube architectures (brown), suggesting that the origami seed structures orient nanotube seeds at the angles prescribed by the seed structures.

been developing genelet circuits<sup>Ref3</sup> that act as inducible bistable switches *in vitro* that allow DNA self-assembly processes to switch between modes. Transient introduction of an RNA signal can switch the system into one state and switching can occur multiple times. We are developing models to understand coupled genelet and DNA nanostructure assembly dynamics and techniques to prevent undesired interactions between genelet circuit components and the components needed for assembly.

## **Future Plans**

*Self-regulation of biomolecular assembly kinetics using controlled monomer activation.* Controlling the concentration of the components of a self-assembly process over time could allow assembly processes to occur much more robustly or determine what type of structures is assembled. For example, within the actin cytoskeleton, chemical factors that sequester or release actin monomers control how actin fibers and network assemble<sup>Ref6</sup>. We are developing a system for controlling the activation and de-activation of DNA tile monomers over time in order to stabilize concentrations during assembly. This “homeostasis” system will maintain constant monomer concentrations over long times, enabling assembly to occur at constant rates and to store large concentrations of monomers in a “reservoir” that are released slowly as a complex dynamic assembly and organization program unfolds.

*Model-driven assembly of programmed 2- and 3-dimensional architectures consisting of one-dimensional polymeric fibers.* The formation of architectures within the cytoskeleton is also increasingly understood to require complex control over the spatial and temporal variation of the concentrations of the components involved in assembly. To develop control over architecture formation in synthetic systems, we are developing models that predict how the concentrations of assembly components, such as monomers and junctions determine the types of 3-dimensional architectures that form. These models will be used to design specific architectures and direct their formation in response to certain cues. We are building upon the molecular dynamics models that were developed to understand point-to-point assembly by integrating techniques for characterizing hierarchical self-assembly processes.

*Metamorphosis.* Models of self-assembly that predict what structures form under what conditions will make it possible to design metamorphic processes for architectures, where changes in the components of concentrations lead to a transition of one type of shape to another. We are identifying classes of architectures, such as branched networks and specific junctions or shapes, that can form and developing ways to direct rapid transitions between them using specific control over assembly kinetics. Our goal is to develop systems in which bistable circuit switches enable switching between two or more complex architectures in response to external chemical cues.

*Closed-loop and context-dependent control of self-assembly processes.* While open-loop dynamic control of assembly (such as control mediated by timing) can direct multistage

assembly processes and transitions between different architectures, more complex control mechanisms will be needed to develop a) robust architectures that can respond to perturbations of the environment during assembly or self-heal and b) dynamic architectures that treadmill or move processively. We are developing mechanisms that enable damaged or malformed nanostructures to produce signals that alter the self-assembly process by directing the destruction and reformation, thus enabling damaged structures to regenerate. To build dynamic architectures, we are investigating ways to enable assembled structures to likewise signal to destroy themselves in certain locations. By making disassembly process context-dependent, *i.e.* faster at one end of a one-dimensional nanostructure than another, it may be possible to develop structures that treadmill, a foundation for processive motion in cells.

## References

1. D. A. Fletcher and R. D. Mullins. Cell mechanics and the cytoskeleton. *Nature*, 463:485–492, 2010.
2. P.W.K. Rothmund, A. Ekani-Nkodo, N. Papadakis, A.Kumar, D. K. Fygenona and E. Winfree. Design and Characterization of Programmable DNA Nanotubes. *J. Am. Chem. Soc.* 126(50):16344–16353, 2004.
3. J. Kim and E. Winfree. Synthetic in vitro transcriptional oscillators. *Mol. Sys. Bio.* 7:465, 2011.
4. D. Y. Zhang and G. Seelig. Dynamic DNA nanotechnology using strand displacement reactions. *Nat. Chem.*, 3:103--113, 2011.
5. A. M. Mohammed and R. Schulman. Directing self-assembly of DNA nanotubes using programmable seeds. *Nano Let.*, 13:4006–4013, 2013.
6. M. F. Carrier and S. Shekhar. Global treading coordinates actin turnover and controls the size of actin networks. *Nat. Rev. Mol. Cell Biol.* 18:389-401, 2017.

## Publications

1. A. Mohammed, J. Zenk, P. Šulc and R. Schulman. "Self-assembling DNA nanotubes to connect molecular landmarks." *Nature Nanotechnology*, 12: 312-316, 2017.
2. T. Jorgenson, A. Mohammed, D. Agrawal and R. Schulman. "Self-Assembly of Hierarchical DNA Nanotube Architectures with Well-Defined Geometries." *ACS Nano* 17 (2): 1927-1936, 2017.
3. A. Mohammed, A. Chisenhall, D. Schiffels, L. Velazquez, D. Fygenon, R. Schulman. "Self-assembly of precisely defined DNA nanotube superstructures using DNA origami seeds." *Nanoscale* 9 (2): 522-526, 2017.
4. J. Fern, D. Scalise, A. Cangialosi, D. Howie, L. Potter, and R. Schulman. DNA Strand-Displacement Timer Circuits." *ACS Synthetic Biology* 6 (2): 190-193, 2016.
5. D. K. Agrawal, E. Franco and R. Schulman. "A Self-Regulating Biomolecular Comparator for Processing Oscillatory Signals", *Journal of the Royal Society Interface* 12 (111): 20150586, 2015.

## **Resilient Hydrogels from the nanoscale to the macroscale**

**Rebecca Schulman, Johns Hopkins University**

### **Program Scope**

Biological systems illustrate how a material composed of fragile molecular components can collectively be highly resilient. While the average protein, cell or even tissue may not last more than a few weeks, many animals and plants have lifetimes of a century or more. Continual component regeneration and multiple systems to resist mechanical and chemical damage together make this capacity possible. The goal of this project is to develop biomimetic methods to enable a material, specifically a DNA-crosslinked hydrogel, to resist damage to different features and across multiple scales using distinct, modular damage protection mechanisms.

Our current work focuses on two questions. First, how can a hydrogel material sense mechanical forces that could indicate the onset of a yield stress and resist them by becoming stronger? This question is inspired by the observation that living tissues can not only repair themselves if damaged, but can also adapt to stress by reconfiguring in order to avoid damage in the first place. Such a mechanism could make materials lightweight and flexible but still resistant to damage, and enable them to dynamically use limited resources to maximize their functionality. Second, how can a material with a particular spatial pattern recover that pattern autonomously if the pattern is damaged? The response to damage within skin or other organs cannot only return a material's microscopic properties to their original form but also repair their mesoscale organization. Such a feature is required if we are to not only build self-healing materials with homogeneous organization, but self-healing material devices with multiple layers or regions that each contribute to the functionality of the whole.

Our strategy for addressing these questions focuses on the use of simple materials with dynamic chemistries, specifically DNA hybridization, in which the mechanical, physical and chemical properties are well understood and tools exist for designing synthetic signal transduction cascades to mediate response, so that we can focus on complex responsiveness instead of material design.

### **Recent Progress**

To design materials that sense force and can respond by undergoing large-scale changes in material architecture, we have been developing molecular force sensors and signal transduction cascades that can transduce the desired outputs of these force sensors, nucleic acid signals, into the release of much large concentrations of molecular outputs. The goal of coupling these systems to develop a general mechanism to program material reorganization at the molecular level in response to forces presented at the macroscale; the molecular outputs produced most abundantly will direct material reorganization by interacting directly with the material.

To strengthen materials, we will couple the force sensors to molecular outputs that act to increase the number of crosslinks within a DNA-crosslinked hydrogel, because increasing the concentration of crosslinks is known to increase the elastic modulus of these materials<sup>1</sup>.

*Detecting tensile stress on a material at the macroscale with designed DNA sensors.* Our system for material toughening will be initiated by the molecular reactions that are triggered by applied force to the material as a whole. To detect these forces we are developing molecular sensors made from DNA complexes that crosslink polymer fibers within a hydrogel. The idea is that these sensors, upon experiencing force, will expose DNA sequence domains that can react with freely diffusing DNA species to produce species that then initiate material change. To detect the exposure of domains within a force sensor, we have developed a fluorescence assay: a working force sensor will cause the gel to fluoresce when stress is applied to the material that exposes the relevant domains. In collaboration with the Frechette laboratory at Johns Hopkins, we are using a custom force microscopy instrument to stretch or compress materials with force sensors by a controlled amount and then observe the fluorescence response with a fluorescence microscope. The design of such force-sensing systems requires that the range of expected material strains induce the range of strains on the molecules required to induce the desired conformational changes. Achieving this translation from the nanoscale to the macroscale is a research challenge: while the conformational changes of DNA molecules in response to applied force on the complex have been well-studied<sup>2</sup>, frameworks for understanding how forces on a hydrogel (a polymer network) will exert forces on the molecules within them are lacking. We have been collaborating with Thao Ngyuen at Johns Hopkins to predict this relationship for different hydrogel materials using the Arruda-Boyce polymer model<sup>3</sup>, which relates continuum tensile and compressive material strain to the force experienced at individual crosslinks. This theoretical work has led us to the choice of specific hydrogels, including the type of polymer and polymer and polymer crosslinks, and DNA force sensors. Preliminary results indicate that DNA force sensors can detect strains within hydrogels before yield.

*Transducing low-concentration nucleic acid signals into large-scale material alteration.* An effective system for material reorganization in response to force will be tunable, such that signals from force sensors can produce the amount of output needed for the effective remodeling of the material in which it is embedded. In particular, the output signals from force sensors will probably need to be amplified, because many crosslinks will need to be added or modified in order to significantly increase the material's modulus. We have been using techniques from dynamic DNA nanotechnology<sup>4</sup> to amplify the output signals from force sensors, *i.e.* short nucleic acid domains. We have shown that short nucleic acid signals present at low concentrations can be amplified by a DNA strand displacement process *in situ* such that a stimulus presented at concentrations of 100 nM or below can alter the conformations of crosslinks that are present at the millimolar concentrations within the hydrogel.

The second part of this proposal deals with the question of designing not just homogeneous materials but heterogeneous structure that can be resilient to damage. To address

this problem we are focusing on the example question of how to design a simple pattern within a material in which the domains are spatial regions of high or low concentrations of specific short single-stranded DNA molecules. A programmed, dissipative reaction-diffusion process drives the system to form a particular pattern at steady state. The design of the system is such that this pattern should reform if it is perturbed<sup>5</sup>. Further, we can design a variety of complex patterns using more complex reaction networks, such that the resulting patterns should still reform. In the first year of this project we have focused on the ability to design specific spatial patterns by designing the spatial structure of the material and the reaction-diffusion network.

*Autonomous formation of programmed millimeter-scale patterns within materials via programmed DNA reaction-diffusion processes.* We have developed reaction-diffusion systems that generate stable patterns of DNA oligonucleotide concentrations within agarose gels, including linear and “hill” (*i.e.* increasing then decreasing) shapes in one and two dimensions. The reaction networks that produce these patterns are driven by enzyme-free DNA strand-displacement reactions, in which reactant DNA complexes continuously release and recapture target strands of DNA in the gel; a balance of these reactions produces stable patterns. The reactant complexes are maintained at high concentrations by liquid reservoirs along the gel boundary. We monitored the patterns using time-lapse fluorescence microscopy and showed that the shape of our patterns can be easily tuned by manipulating the boundary reservoirs. To show that this system is programmable, we constructed two overlapping, stable gradients produced by two sets of non-interacting release and recapture reactions with DNA strand-displacement systems.

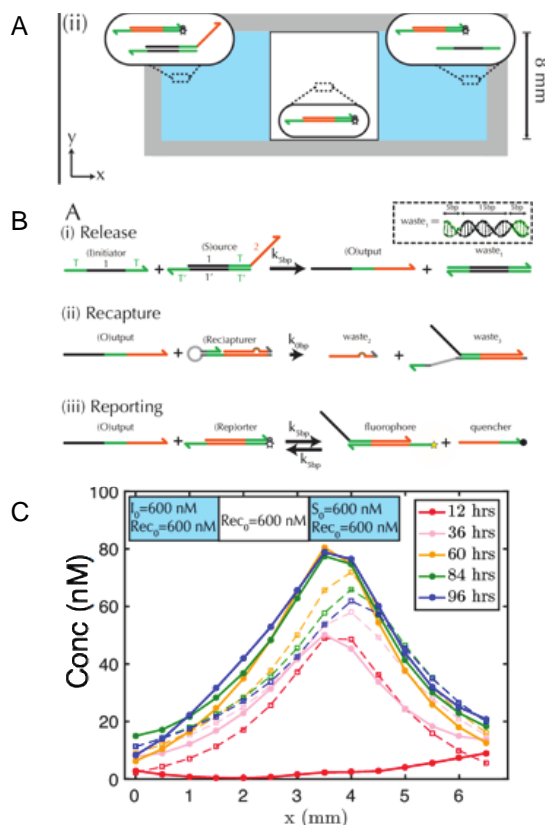


Figure 1: A designed reaction-diffusion process that forms a stable “hill” pattern. The energy to produce the pattern is provided by external fluid reservoirs (A) in which high-energy reactants are provided. These reservoirs provide input energy and act to form specific boundary conditions for the system. A cycle of output strand release and recapture (B) within the material produces the gradient. Gradients form and persist (solid lines C) in shapes and over time scales consistent with the predictions of 0-parameter fit simulations (dashed lines).

## Future Plans

*Transducing signals from DNA force sensors into nucleic acid signals that can initiate chemical cascades.* Once we have developed a system for exposing particular DNA sequence domains within a hydrogel in response to force, our next step will be to use this exposed domain to initiate a chemical reaction to show that the conformational change of the sensors can be used to initiate the signal transduction cascades for material reorganization we have been designing. To investigate this question, we have designed a simple reaction in which the force sensor can react with a DNA complex that is freely diffusing in solution and release a fluorescence signal. We can also alter this this response cascade to introduce amplification to increase the intensity of the signal.

*Self-healing DNA reaction-diffusion patterns.* In principle, the spatial patterns of DNA concentrations that we demonstrated should heal when perturbed. To demonstrate that this is the case, we have been developing a system for forming these gradients and perturbing them precisely by either adding or removing the output molecule that forms the gradient at certain locations. We will use this system to characterize the healing response. We are building a system in which gradients form within PEG hydrogels within a microfluidic device. Either inactivated output molecules or inactivated complexes that could capture the output molecules in their active form will be distributed throughout the PEG gel. These molecules will be activated using photouncaging chemistry, producing a precise perturbation.

## References

1. Lin D. C., Yurke B., and Langrana, N. A. Mechanical Properties of a Reversible, DNA-Crosslinked Polyacrylamide Hydrogel. *J. of Biomech. Eng.*, 126(1):104--110, 2004.
2. Bustamante, C., Bryant, Z., and Smith, S. B. Ten years of tension: single-molecule DNA mechanics. *Nature*, 421:423--427, 2003.
3. Arruda, E. M. and Boyce, M. C., 1993, A three-dimensional model for the large stretch behavior of rubber elastic materials. *J. Mech. Phys. Solids*, 41(2):389--412, 1003.
4. Zhang, D. Y. and Seelig, G. Dynamic DNA nanotechnology using strand displacement reactions. *Nature Chem.*, 3:103--113, 2011.
5. Scalise, D. and Schulman, R. Designing Modular Reaction-Diffusion Programs for Complex Pattern Formation. *Technology* 02:55--66, 2014.

## Publications

1. J. Zenk, D. Scalise, K. Wang, P. Dorsey, J. Fern, A. Cruz and R. Schulman. "Stable DNA-based Reaction-Diffusion Patterns", *RSC Advances* 7 18032-18040, 2017.

## Fabrication and Assembly of Robust, Water-Soluble Molecular Interconnects via Encoded Hybridization

Timothy F. Scott, University of Michigan, Department of Chemical Engineering

### Program Scope

This project involves the dynamic covalent self-assembly of sequence-specific oligomers to mediate the deterministic fabrication of thermally, chemically, and mechanically robust molecular interconnects and nanostructures. In contrast to Watson-Crick base pairing, which is mediated by hydrogen bonds, dynamic covalent reactant pairs are utilized whose dimerization reactions are orthogonal and reversible, specifically the boronic acid/vicinal diol and amine/aldehyde condensation reactions. Owing to their synthetic accessibility, model peptoids (i.e., poly-*N*-substituted glycines) bearing chiral pendant functional groups are synthesized using conventional solid phase synthesis. Upon selective protecting group deprotection and cleavage from the solid support, mixtures of oligomers bearing the reversible functional groups remain single strands until being subject to Lewis acid-mediated *in situ* acetal and acetonide deprotection to reveal aldehyde and vicinal diol functionalities, whereupon the oligomers self-assemble *via* hybridization between strands with complementary sequences. Under carefully controlled reaction conditions, nuclear magnetic resonance spectroscopy, liquid chromatography, and mass spectrometry are performed to examine the reaction kinetics and thermodynamic equilibrium of the reactant pair condensation and oligomer hybridization reactions.

### Recent Progress

(i) *Concurrent dynamic covalent assembly of >2 oligomeric strands.* Initial work on this project focused on Vernier templating to confirm the capability for the concurrent dynamic covalent assembly of greater than two oligomeric precursor strands. This is a recently-described self-assembly approach employing the co-reaction of oligomeric precursors with unequal numbers of complementary functional groups such that, whereas each component precursor only participates in as many interactions as its number of reactive functional groups allows, the total number of interaction sites on the Vernier complex is equal to the lowest common multiple of the functionality on the respective precursors.<sup>1</sup> Here, aldehyde- and amine-functionalized peptoid oligomers were added to chloroform such that the stoichiometric ratio of dynamic covalent reactants was 1:1; however, in this case, the functionalities of the peptoids E<sup>3</sup>A-Al<sub>*m*</sub> and E<sup>3</sup>A-Am<sub>*n*</sub> in the reaction mixture were not commensurate (i.e.,  $m \neq n$ , see Figure 1A). In the presence of a catalytic amount of scandium(III) triflate, the self-assembly of four different oligomer combinations were examined: VA-Al<sub>3</sub>Am<sub>4</sub> (i.e., trialdehyde/tetraamine), VA-Al<sub>4</sub>Am<sub>3</sub> (tetraaldehyde/triamine), VA-Al<sub>4</sub>Am<sub>6</sub> (tetraaldehyde/hexaamine), and VA-Al<sub>6</sub>Am<sub>4</sub> (hexaaldehyde/tetra-amine). These combinations were selected as each reaction was anticipated to yield 12-rung molecular ladder products, based on the lowest common multiple of both 3×4 and 4×6 (Figure 1B). MALDI mass spectra of the reaction

mixtures demonstrate major peaks assignable to the desired 12-rung ladder structures with observed molecular weights equivalent to the expected values (Figure 1C), demonstrating the success of this dynamic covalent approach to Vernier-templated self-assembly.

(ii) *Ultimate length and kinetics of dynamic covalent molecular ladder assembly.* Subsequently, to determine the ultimate attainable molecular ladder length, the assembly of complementary  $n \times n$  peptoids into  $n$ -rung molecular ladders was performed using aldehyde- and amine-functionalized peptoid sequences Al $_n$  and Am $_n$  ( $n = 8, 10, 12$  and  $16$ ).<sup>2</sup> In these mass spectra, the observed molecular weights of each dominant peak correspond to the expected values of desired molecular ladder structures Im $_8$ , **10**, **12**, and **16** respectively, indicating the successful formation of desired ladder structures (Figure 2A). Unreacted single peptoid strands were not observed in any of these mass spectra,

indicating that the dimerization reaction reached completion. However, in addition to the desired  $n$ -rung molecular ladders, a small amount of out-of-registry molecular ladders with  $(n-1)$  rungs, anticipated to arise at  $m/z$  values of  $+18$  (i.e., the H<sub>2</sub>O condensation product molecular weight) for each unreacted amine/aldehyde pair, was also detected in the reaction mixtures of Im $_8$ , **10**, and **12**.

Hybridization kinetics of molecular ladders with different numbers of rungs were examined by mass spectrometry. The evolution of molecular ladder Im $_8$  formation over the course of 7 days as captured by MALDI mass spectrometry is presented in Figure 2B. The desired ladder structure with 8 rungs was not initially observed in the mass spectra whereas a distribution of peaks corresponding to intermediate, out-of-registry ladders with different numbers of rungs ( $\leq 6$ ) were present as soon as hybridization started. These peaks were evenly spaced with an interval of 18, corresponding to the H<sub>2</sub>O condensation product molecular weight

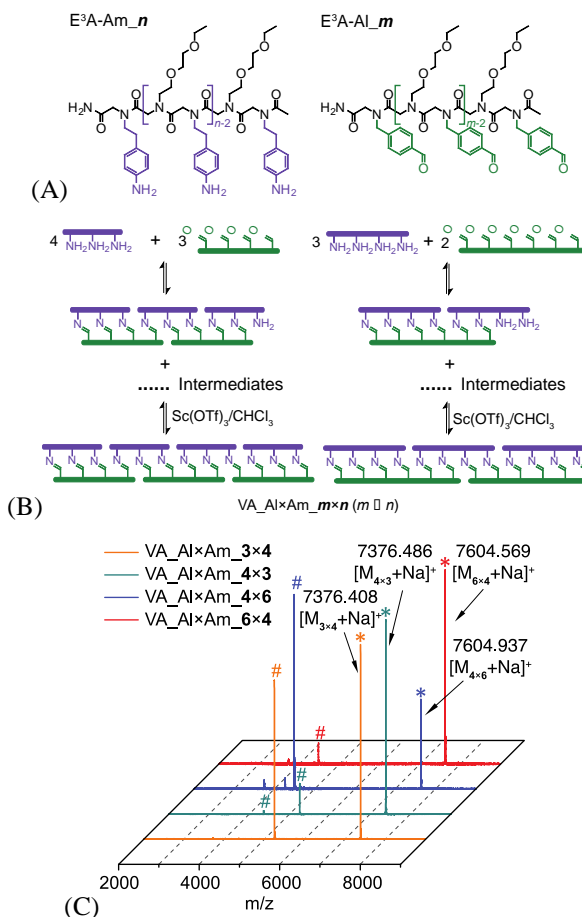


**Figure 1. Vernier-templated assembly of molecular ladders.** (A) Vernier-templated assembly of complementary oligopeptoids with non-commensurate functionalities into molecular ladders with  $m \times n$  rungs (VA $_n$ Al $_m$ Am $_n$ , where VA is ‘Vernier assembly’). (B) MALDI mass spectra of Vernier-templated molecular ladders. The target ladder structures are labeled with \* symbols and the intermediates are labeled with #. Calculated molecular weights for the target ladders:  $[M_{3 \times 4} + Na]^+ = [M_{4 \times 3} + Na]^+ = 7376.810$  g/mol;  $[M_{4 \times 6} + Na]^+ = [M_{6 \times 4} + Na]^+ = 7604.946$  g/mol. Intermediates are identified as (E<sup>3</sup>A-Al $_3$ )<sub>3</sub>(E<sup>3</sup>A-Am $_4$ )<sub>2</sub>; (E<sup>3</sup>A-Al $_4$ )<sub>2</sub>(E<sup>3</sup>A-Am $_3$ )<sub>3</sub>, (E<sup>3</sup>A-Al $_4$ )<sub>2</sub>(E<sup>3</sup>A-Am $_3$ )<sub>2</sub>; (E<sup>3</sup>A-Al $_4$ )<sub>2</sub>(E<sup>3</sup>A-Am $_6$ )<sub>1</sub>; (E<sup>3</sup>A-Al $_6$ )<sub>1</sub>(E<sup>3</sup>A-Am $_4$ )<sub>2</sub>.

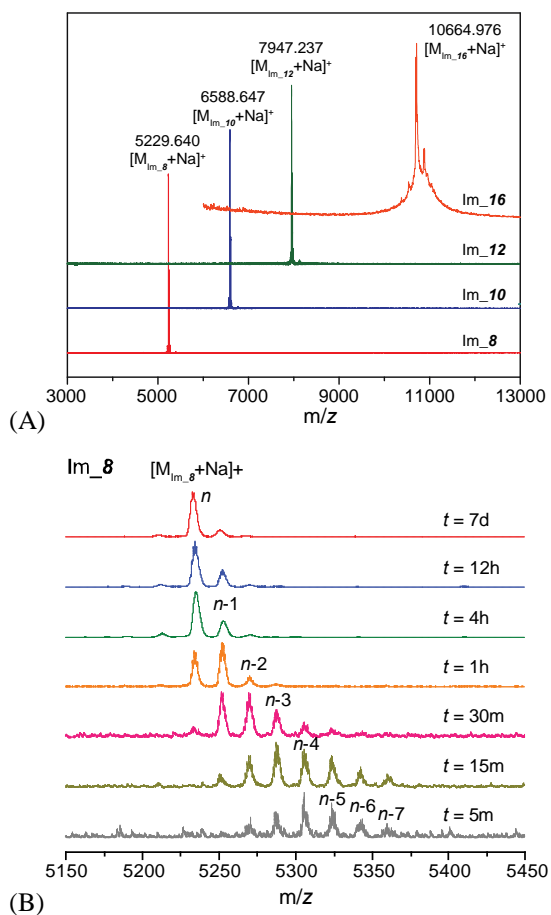


**Figure 2. Dynamic covalent assembly of peptoid-based molecular ladders.** (A) Dimerization of complementary peptoid oligomers with commensurate functionalities (HB<sub>*n*</sub>, where HB is ‘hybrid’). (B) Kinetics of the formation of molecular ladder with *n* = 8 rungs (IM<sub>8</sub>) over the course of 7 days by MALDI mass spectra of the reaction mixture at increasing time intervals.

for each unreacted amine/ aldehyde pair. As the reaction proceeded, the distribution of these intermediate out-of-registry molecular ladders shifted towards lower molecular weight as more out-of-registry ladders with fewer rungs continuously underwent inter-strand bond rearrangement to generate more imine linkages. As a result, intermediate ladder structures with more rungs, approaching the desired ladder structure, progressively increased with the disappearance of transient ladder species with fewer rungs.

(iii) *In situ* deprotection and sequence-specific hybridization. This project involves the synthesis and self-assembly oligomeric precursors bearing multiple, covalently co-reactive functional group types, necessitating the utilization of protecting groups to eliminate side reactions owing to premature reaction of the dynamic covalent reactive groups. Moreover, the premature

deprotection of these functionalities would result in the generation of cross-linked, intractable material, impeding both purification and, if kinetically-trapped, subsequent self-assembly of the precursor molecules. Thus, as utilization of molecular species bearing multiple coreactive functional groups necessitates performing deprotection of at least one of the protecting groups *in situ*, we developed an approach for *in situ* acetal deprotection using a

rare earth metal(III) triflate Lewis acid which, as it also catalyzes imine exchange reactions, acts in this context as a dual-role catalyst (see Figure 3A). Here, ethylene acetals in combination with allyloxycarbonyl (Alloc)-protected amines offered a viable and elegant system for orthogonal deprotection and self-assembly whereby, after the Alloc groups were selectively deprotected, the acetals were cleaved *in situ* using Sc(III) which would also serve to catalyze exchange of the imine groups resulting from the subsequent condensation reactions between the amine and revealed aldehyde groups.<sup>3</sup> After optimizing the catalyst concentration, water content, and reaction temperature, an octafunctional peptoid sequence bearing a block of four ethylene acetal and a block of four amine groups (i.e., Act-Al<sub>4</sub>-Am<sub>4</sub>) successfully underwent quantitative *in*

*situ* deprotection and self-assembly by anti-parallel self-hybridization to afford an 8-rung molecular ladder (Im\_8, see Figure 3B).

## Future Plans

Optimized pendant groups and reaction conditions as determined using model peptoid oligomers will be implemented in sequence-specific oligo(phenylene-ethynylene) strands, synthesized using conventional solid-phase synthesis. Oligomeric peptoid and phenylene-ethynylene sequences will be designed and synthesized such that, upon *in situ* deprotection, they will self-assemble into branched nanostructures, and mass spectrometry and atomic force microscopy will be utilized to characterize the identity and morphology, respectively, of these assemblies. Finally,  $\beta$ -peptoid sequences will be employed as template oligomers for a model replication approach *via* radical-mediated, vinyl ether/maleate alternating copolymerization. Reaction conditions necessary for monomer positioning and release of the daughter oligomer will subsequently be utilized in conjunction with Sonogashira coupling to afford sequence-specific phenylene-ethynylene oligomers as semi-conservative replicates of synthetically-accessible templates.

## Publications

- [1] Wei, T., Jung, J. H., & Scott, T. F., "Dynamic Covalent Assembly of Peptoid-Based Ladder Oligomers by Vernier Templating." *J. Am. Chem. Soc.* 137, 16196–16202 (2015).
- [2] Wei, T., Furgal, J. C., Jung, J. H., & Scott, T. F., "Long, self-assembled molecular ladders by cooperative dynamic covalent reactions." *Polym. Chem.* 8, 520–527 (2017).
- [3] Wei, T., Furgal, J. C., & Scott, T. F., "In Situ Deprotection and Dynamic Covalent Assembly using a Dual Role Catalyst," *Chem. Commun.*, 53, 3874–3877, (2017).

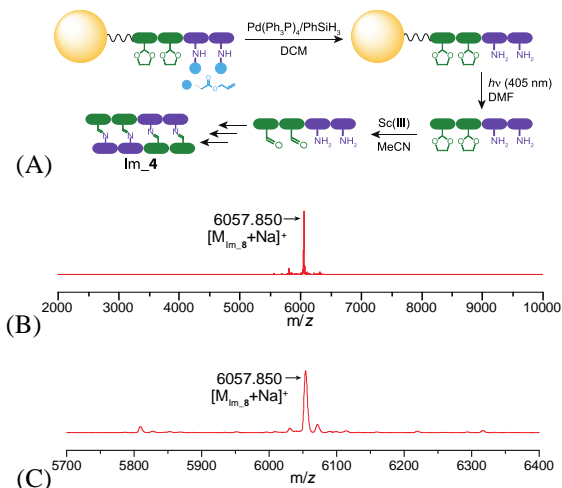


**Figure 3. *In situ* deprotection and molecular ladder dynamic covalent assembly.** (A) Upon Pd(0)-catalyzed Alloc deprotection, amine- and acetal-bearing oligomers generated by solid phase peptoid synthesis are photocleaved from resin, purified, and treated with Sc(OTf)<sub>3</sub> to effect *in situ* acetal deprotection and oligomer self-assembly. (B) The octa-functional peptoid Act-Al<sub>4</sub>-Am<sub>4</sub> (expected mass: [M<sub>Act-Al<sub>4</sub>-Am<sub>4</sub></sub>+Na]<sup>+</sup> = 3287.609 g/mol) treated with 0.2 eq. Sc(OTf)<sub>3</sub> in 2 v/v% water in acetonitrile for 4 days at 70°C. Im<sub>8</sub> (expected mass: [M<sub>Im<sub>8</sub></sub>+Na]<sup>+</sup> = 6056.097 g/mol) is the desired in-registry, 8-rung molecular ladder. (C) Magnification of the mass range near Im<sub>8</sub>.

## **Self-assembly for colloidal crystallization and biomimetic structural color**

**Michael J. Solomon (PI) and Sharon C. Glotzer (co-PI), University of Michigan Ann Arbor**

### **Program Scope**

The focus of this research program is to understand the self- and field-assisted assembly of anisotropic particles into colloidal crystals with iridescent structural color by measuring their phase behavior, assembled unit cell symmetry, defect structure, and spectral response due to diffraction. Colloidal crystals produce structural color because their periodic physical structure diffracts light at Bragg resonances. The complex structural color response of living systems is linked to the presence of structural morphologies more complex than simple close-packed arrays; we seek these more complex symmetries by assembly of anisotropic building blocks. The objectives of our work are to: (1) Describe the fundamental relationship between colloidal particle anisotropy, in both shape and pair potential interactions, and the symmetry of unit cells that can assemble at high volume fraction and under the effect of applied fields; (2) Understand how colloidal building block anisotropy and the characteristics of applied fields mediate the crystal quality of assembled structures, as quantified by measures such as crystal fraction, crystal size, and dislocation density; (3) Measure the spectral and light diffraction response of colloidal crystals of anisotropic particles and model the response in terms of the project's real space characterization and simulation of phase diagrams, unit cell symmetries, and crystal quality.

## Recent Progress

In the recent period, we have: (i) discovered new dense phases of Janus ellipsoids whose self-assembly mechanisms are being investigated by computer simulation; (ii) varied crystal quality to uncover the role of building block anisotropy, defect density, and crystal thickness on the functional properties of self-assembly, including structural color response; (iii) identified fundamental mechanisms of colloidal self-assembly in direct current (DC) electric fields.

### *Dense phases of Janus ellipsoids*

We pursued sedimentation-based densification of metallodielectric Janus ellipsoids, and produced dense arrays (Fig 1a) in which the Janus features exhibit long-range order (in addition to the positional order of the ellipsoids themselves). These structures display a kind of Janus-feature induced registry that assists packing, as shown by the proposed unit cell of the self-assembly (Fig. 1b). This study shows how the introduction of interaction anisotropy in ellipsoids affects the quality of order with in the range of colloid volume fraction that can lead to structural color. We are investigating the self-assembly of such Janus ellipsoids by computer simulation using the HOOMD-blue code [1]. We find that the ellipsoids self-assemble into a striped phase at densities  $\phi \leq 0.55$  due to the Janus particle attractions, cf. Fig 1c using a potential (cf. Fig 1d) developed as part of our previous collaboration [2]. The phase resembles the experimental result, however, even after a long equilibration period of over  $10^7$  molecular dynamics time steps, the ellipsoids still rotate around their long axis, while their particle centers practically do not move anymore. Therefore, the densely packed ellipsoids are frustrated with respect to their nearest-neighbor bonding based on the patch potential, precluding the long-range order. We rationalize this in the sense that the attractive tail of the anisotropically modulated simulation potential is too long-ranged, making it appear isotropic.

### *Role of building block anisotropy, defect density, and crystal thickness*

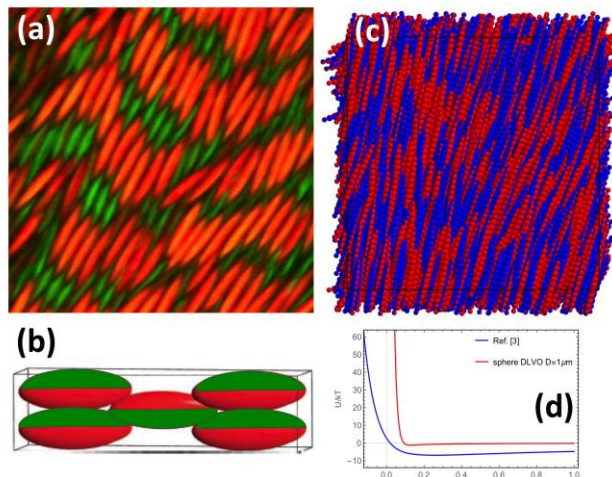


Figure 1. (a) Self-assembled, dense equilibrium phase of metallodielectric Janus ellipsoids. The red channel is the latex half of the particle; the green channel is the metallic half; (b) hypothesized unit cell; (c) self-assembled phase from 4096 Janus ellipsoids at  $\phi \approx 0.55$ ; (d) pair potential used in the simulation (blue) compared to DLVO potential for metallic particles (red). The simulations are for ellipsoids produced from overlapping spheres.

The self-assembled phases produced as part of this project (c.f. Figure 1) are test beds for understanding the role of defects in the functional properties of self-assembled structures. Janus particle suspensions assembled by densification through low-angle sample cell tilt were

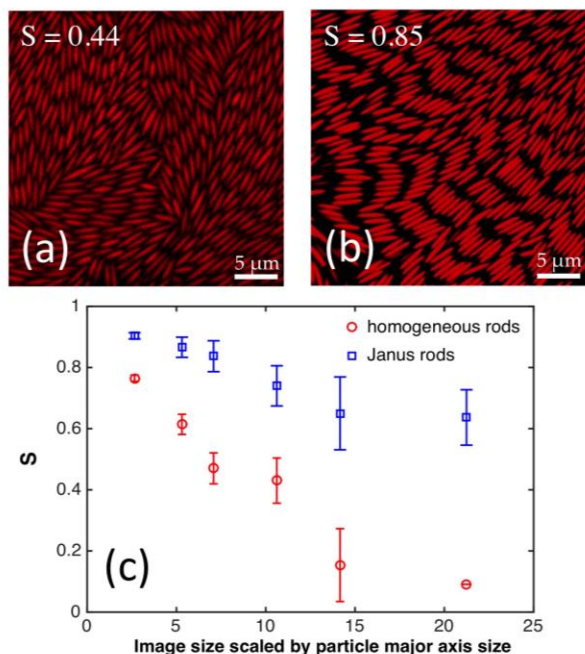


Figure 2. (a, b) Self-assembled phases of homogeneous and Janus ellipsoids, respectively, produced under equivalent conditions; (c) comparison of order quality as a function of domain size for the two kinds of particles.

characterized using confocal laser-scanning microscopy (CLSM). The disordered particle suspension gradually evolved into an ordered structure with nematic domains, which later displayed positional alignment as time elapsed. We investigated the quality of orientation by carrying out image analysis over a range of domain sizes and assessed the impact of Janus character through comparison to homogeneous ellipsoids assembled under comparable conditions (c.f. Fig 2a,b). Quality of order is assessed through a commonly used 2D order parameter (alignment factor), with  $S=0$  indicating random orientation and  $S=1$  full alignment. We find that the ordering extends to larger length scales in assemblies of Janus particles; homogenous particles exhibit low alignment at similar scales (c.f. Fig. 2c). The results indicate the *beneficial* effect that Janus character can have on the quality of ordering.

To further assess the quality of ordering, we developed a small-angle light scattering device (SALS) that can probe the kinetics of positional and orientational order in anisotropic suspensions. Figure 3 shows the CLSM images and SALS responses of colloidal ellipsoids assembled under AC-electric field conditions in which phases of low ordering ( $S = 0.63$ , Fig 3a,b), high orientational ordering ( $S = 0.88$ , Fig 3c,d), and high orientational and positional ordering ( $S = 0.9$ , Fig 3 d,e) are generated. In Fig 3d,e a stretched six-fold diffraction pattern is observed.

Such diffraction peaks are an indicator of sufficient crystallinity for structural color and iridescence; however, the relationship between microscopic ordering and structural color response is unknown. As a first step in

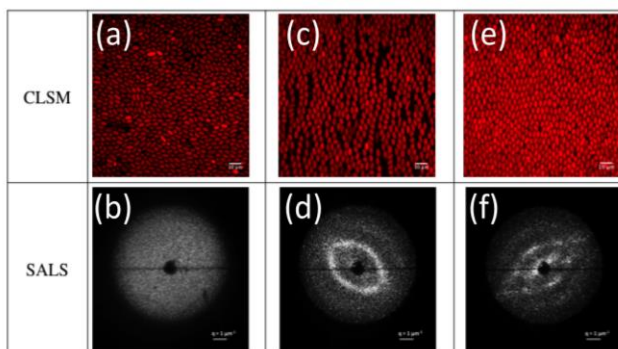


Figure 3. CLSM and SALS observations of colloidal ellipsoids assembled under different degrees of orientational and positional ordering (a,b:  $S = 0.63$ ; c,d:  $S = 0.88$ ; d,e:  $S = 0.9$ ). Scale bar is 10  $\mu\text{m}$  for CLSM

exploring this relationship, we asked how the thickness of a colloidal crystal affects structural color response. Colloidal crystals of different thickness were produced by evaporative deposition of polystyrene colloids (Fig 4a). Crystal thickness was measured with SEM cross-sectional imaging (Fig 4b) and the reflection spectrum was characterized by spectrophotometry (Fig 4c). This fundamental understanding of the spectral response (Fig 4d) has utility for applications.

### *Fundamental mechanisms of colloidal assembly in DC electric fields*

We studied dynamical interactions during electrophoresis in a suspension of poly(methyl methacrylate) colloids to better understand the retardation of colloidal mobility with volume fraction at high concentrations; this retardation is a significant determinant of the potential for using applied DC fields to generate reconfigurable structural color. We found a significant effect of colloidal electrokinetic properties on this retardation. When measurements of this kind were undertaken for Janus colloids, we discovered large-scale colloidal levitation that we hypothesize arises because of electro-diffusiophoresis.

### **Future Plans**

In the next period, we plan to combine experimental structural characterization and computer simulation to identify the mechanism by which Janus particles yield high quality self-assembled

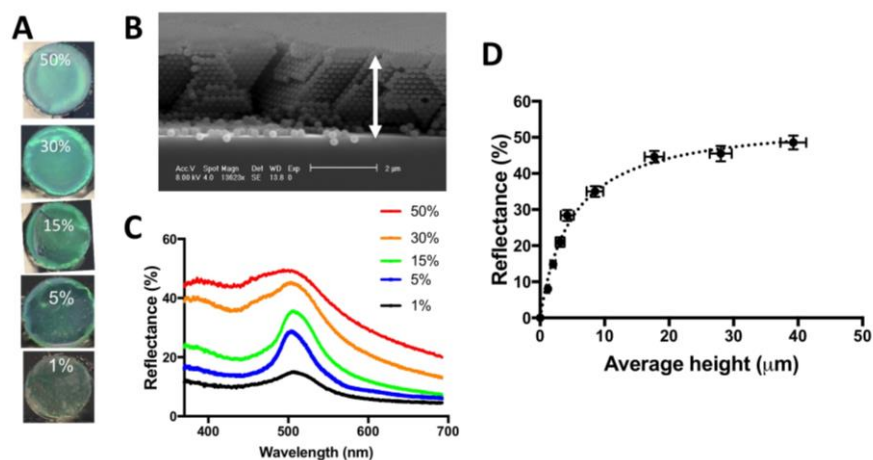


Figure 4. (A) Images of colloidal crystals produced by evaporation from polystyrene colloidal solutions of different initial  $\phi$ ; (B) SEM cross-section of crystal thickness; (C) Reflection spectrum of the series of crystals in (A); (D) reflection peak intensity as a function of crystal thickness.

structures relative to homogeneous particles; understanding the mechanism could potentially have broad utility for producing ordering in colloids. To explore the mechanism we will parameterize the Janus ellipsoid pair potential using a shorter-ranged attraction, such as the DLVO potential for a gold/polymer multilayer system [3]. The structural characterization will involve unit cell symmetry identification, order parameter analysis, and exploration of the intensity and width of diffraction peaks generated in the assemblies by SALS. We will use light scattering simulation tools to understand the effect of crystal size and defect density on the measured structural color response, as characterized by spectrophotometry. We will further characterize and understand the complex role of colloidal

electrokinetics on electric-field induced deposition, which will provide better fundamental understanding of our primary self-assembly tool for generating the dense assemblies of anisotropic colloids [4].

## References

1. Anderson, J. A. and Glotzer, S. C. “The Development and Expansion of HOOMD-Blue through Six Years of GPU Proliferation” <http://arxiv.org/abs/1308.5587>
2. Shah, A. A., Schultz, B., Zhang, W., Glotzer, S. C., and Solomon, M. J. “Actuation of Shape-Memory Colloidal Fibres of Janus Ellipsoids.” *Nature materials* 14, no. 1 (2015): 117–24,
3. Shemi, O. and Solomon, M. J. “Effect of Surface Chemistry and Metallic Layer Thickness on the Clustering of Metallodielectric Janus Spheres.” *Langmuir : the ACS journal of surfaces and colloids* 30, no. 51 (2014): 15408–15.
4. This research was conducted by Dr. Sepideh Razavi, Dr. Jens Gaser, Peng-Kai Kao, Tianyu Liu, Dr. Carlos Silvera Batista, Yanliang Liu, and the PIs.

## Publications support by BES in last two years

1. Ganesan, M. and Solomon, M. J. “High-Density Equilibrium Phases of Colloidal Ellipsoids by Application of Optically Enhanced, Direct Current Electric Fields” *Soft Matter* 6 (2017): 557.
2. Solomon, M. J. “Tools and Functions of Reconfigurable Colloidal Assembly” *submitted*.
3. Silvera Batista, C. A., Rezvantalab, H., Larson, R. G., and Solomon, M. J. “Controlled Levitation of Colloids through Direct Current Electric Fields” *Langmuir* (2017): doi:10.1021/acs.langmuir.7b00835.

## **Self-Assembly and Self-Repair of Novel Photovoltaic Complexes: Synthetic Analogs to Natural Processes**

**Michael S. Strano**  
**Carbon P. Dubbs Professor of Chemical Engineering**  
**Massachusetts Institute of Technology**  
**77 Massachusetts Avenue, 66-570**  
**Cambridge, MA 02139**  
[strano@mit.edu](mailto:strano@mit.edu)  
**617-324-4323**

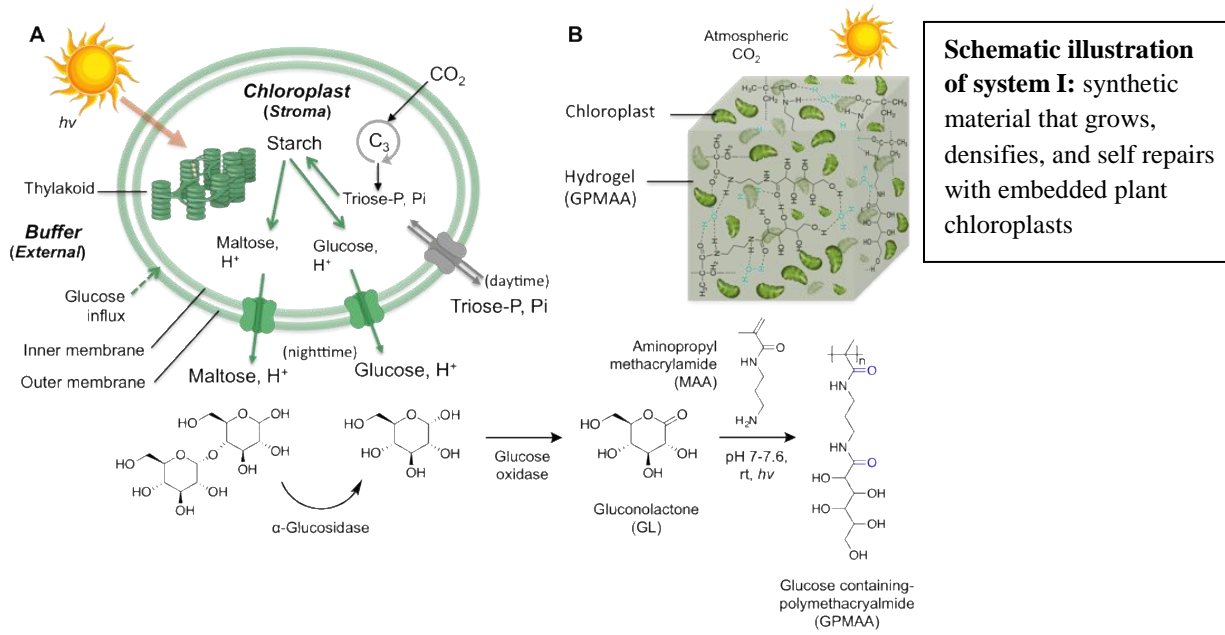
### **Program Scope**

Our laboratory at MIT has been interested in how we can learn from the mechanisms of self-assembly and self-repair displayed particularly in living plant systems to create human-synthesized analogs that benefit from these higher functions operating under non-biological conditions. This program in our laboratory is supported exclusively by the Department of Energy and has led to several important and novel areas of inquiry and technology.

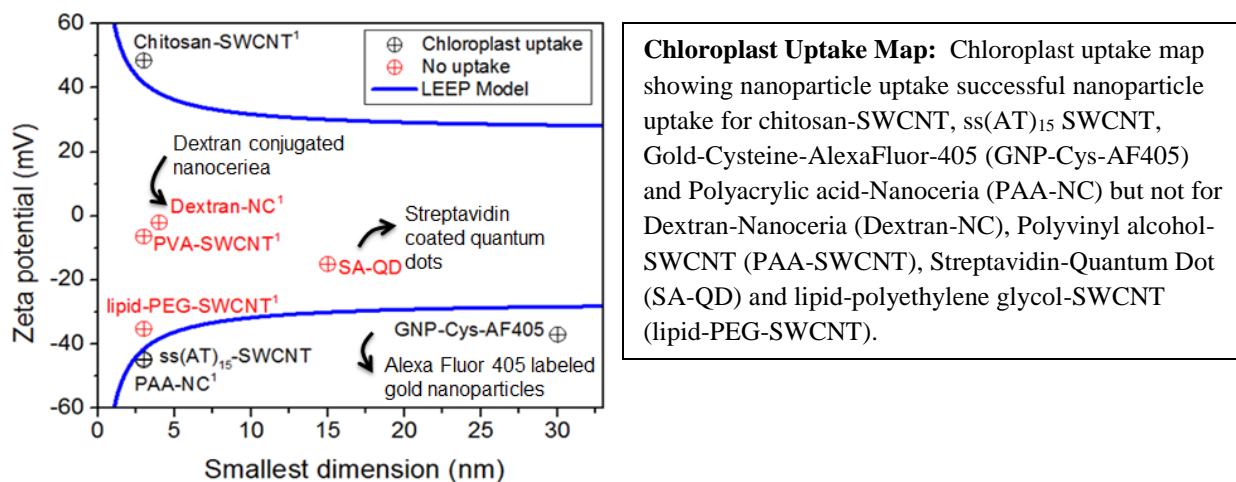
### **Recent Progress**

Materials exhibiting biomimetic carbon fixation and self-repair: Theory and experimental synthesis

We highlight our recent efforts in engineering biomimetic systems that exploit ambient solar energy harvesting and carbon dioxide reduction to high-energy products such as glucose and its polymeric derivatives. By performing these reactions within material compartments, we assert that it is possible to create materials that grow and self-repair using carbon dioxide as a carbon source. Such materials would significantly benefit transportation and construct costs, and exhibit self-healing and densification over time. We have made significant progress to date on two systems to date. The first involves the extraction of functional plant chloroplasts from biomass and their use as embedded, functional photocatalysts for the production of glucose and starches from ambient solar energy and carbon dioxide. Glucose can be converted to gluconolactone by glucose oxidase, which can readily react with nucleophiles, such as the primary amine group (-NH<sub>2</sub>) to generate a growing polymer matrix. We have investigated the importance of inorganic phosphate (Pi) concentration, glucose equilibrium across the chloroplast membrane, and the concentration of photo-generated reactive oxygen species (ROS) towards glucose export efficiency. We have enhanced glucose export from the isolated chloroplasts to gain quantifiable molecules to build self-growing material. Isolated chloroplasts are placed on the glucose oxidase immobilized-graphene oxide film in buffer containing co-monomer, 6-aminopropyl methacrylamide (MAA). In the presence of light and exposure to atmospheric carbon dioxide for 18 h at room temperature, the formation of hydrogel-like material was observed around the chloroplast membrane as confirmed by Raman spectroscopy 3D mapping.

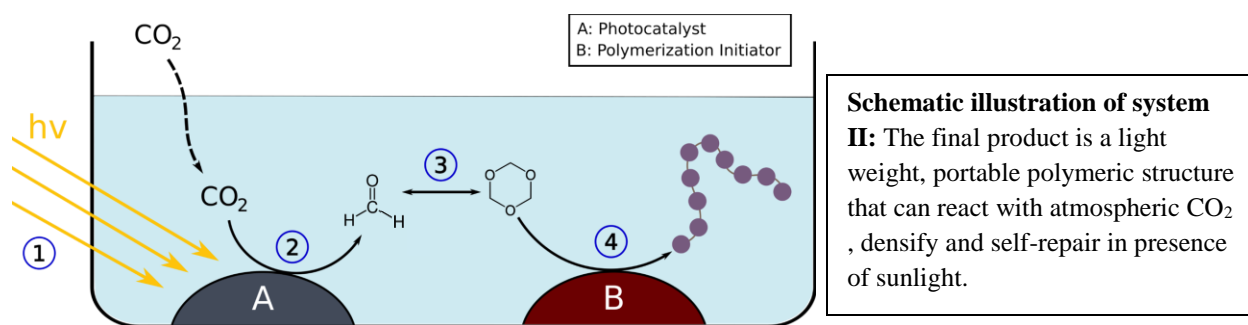


These efforts have benefited from a new technique, Lipid Exchange Envelope Penetration (LEEP) developed at MIT for the incorporation of nanoparticles into living plants, protoplasts and chloroplasts in-vivo.



Chemo-protective, stabilizing and photoactive nanoparticles can be incorporated into the chloroplast to preserve and extend its catalytic function. As a next generation material system, we replace the function of the chloroplast with a semiconducting photocatalyst,  $\text{TiO}_2$  or separately, graphitic  $\text{C}_3\text{N}_4$  for the direct  $\text{CO}_2$  reduction to formaldehyde. Domains performing this chemistry under ambient conditions can be coupled into a material with differing pH to generate 1,3,5-trioxane and polymerize to linear polyoxymethylene with a boron trifluoride

(BF<sub>3</sub>) or boron trifluoride diethyl etherate (BF<sub>3</sub>OEt<sub>2</sub>) as an initiator. This system uses the atmospheric CO<sub>2</sub> and converts it immediately, so it does not need to deal with storage of CO<sub>2</sub> and the energy required for that. The final product is a lightweight, portable polymeric structure that can react with atmospheric CO<sub>2</sub>, densify, and self-repair in presence of sunlight. Synthetic efforts going forward will examine hierarchical integration and self-healing of both systems, coupled to a theoretical framework within which we understand these fundamentally new types of materials.



## Future Plans

1. Spatial and temporal mathematical modeling of compartmental reactions in system 1 and 2, optimization of size and tessellation to best couple mass transfer, reaction rates and emerging mechanical properties
2. System I focus on hyper-stability of chloroplast extracts using nanobionics, extending catalytic function. Analogy with cell-free biosynthesis-pure synthetic (non-living) product formation from biologically derived precursors
3. System II catalytic screening, examining TiO<sub>2</sub> and photo-physical variants, Graphitic Carbon Nitride (g-C<sub>3</sub>N<sub>4</sub>), combination with carbon quantum dots, nitrogen-doping of carbon nanotubes, and graphene
4. Exploration of other biomimetic concepts to debottleneck growth rate and efficiency: coupled and cascading growth/repair chemistries, parallel use of the entire product distribution (i.e. maltose, formic acid, etc.), plastid engineering using nanobionics, examination of photonics

## References

1. Giraldo JP, Landry MP, Faltermeier SM, McNicholas TP, Iverson NM, Boghossian AA, Reuel NF, Hilmer AJ, Sen F, Brew JA, Strano MS, Plant Nanobionics Approach to Augment Photosynthesis and Biochemical Sensing, *Nature Materials*, 13, 400-408 (2014)

2. Boghossian AA, Sen F, Gibbons B, Sen S, Faltermeier SM, Giraldo JP, Zhang CT, Zhang JQ, Heller DA, Strano MS, Application of Nanoparticle Antioxidants to Enable Hyperstable Chloroplasts for Solar Energy Harvesting, *Advanced Energy Materials*, 3, 881-893 (2013)
3. Wong MH, Misra R, Giraldo JP, Kwak S, Son Y, Landry MP, Strano MS, “Lipid Exchange Envelope Penetration for Plant Engineering: a Universal Localization Mechanism”, *Nano Letters*, 16, 1161-1172 (2016)
4. Weise SE, Weber APM, Sharkey TD, Maltose is the major form of carbon exported from the chloroplast at night, *Planta*, 218, 474-482 (2004)
5. Koci K, Obalova L, Solcova O, Kinetic study of photocatalytic reduction of CO<sub>2</sub> over TiO<sub>2</sub>, *Chemical and Process Engineering*, 31, 395-407 (2010)
6. Chandrashekara MN, Desai D, Chanda M, Kinetics of solution polymerization of trioxane, *European Polymer Journal*, 21, 833-840 (1985)

## Publications

### Journal publications

1. Giraldo JP, Landry MP, Kwak S, Jain R, Wong MH, Iverson NN, Strano MS, “A Ratiometric Sensor from Single Chirality NIR Fluorescent Carbon Nanotubes: Application to in vivo Monitoring”, *Small*, 11, 3973-3984 (2015)
2. Wong MH, Misra R, Giraldo JP, Kwak S, Son Y, Landry MP, Strano MS, “Lipid Exchange Envelope Penetration for Plant Engineering: a Universal Localization Mechanism”, *Nano Letters*, 16, 1161-1172 (2016)
3. Wong MH, Giraldo JP, Kwak S, Koman V, Liu P, Sinclair R, Strano MS, “Nitroaromatic Detection and Infrared Communication using Wild Type Plants”, *Nature Materials*, 16, 264-272 (2017)
4. Kwak S, Wong MH, Salim Lew TT, Bisker G, Lee MA, Kaplan A, Dong J, Liu AT, Koman VB, Sinclair R, Hamann C, Strano MS, “Nanosensor Technology Applied to Living Plant Systems”, *Annual Review of Analytical Chemistry*, 10, 113-140 (2017)
5. Kwak S, Giraldo JP, Wong MH, Ell J, Weidman MC, Sinclair RM, Landry MP, Tisdale WA, Strano MS, A nanobionic light emitting plant (*under revision*)

### Patent Applications

1. Kwak S, Giraldo JP, Wong MS, Strano MS, Nanobionic light emitting plants, US Patent App 62/251,071 (2016)
2. Wong MH, Giraldo JP, Kwak S, Strano MS, Method for the self powered detection of nitroaromatics using a wild type plant. US Patent App 62/262,892 (2016)

## **New Functions Emerging from Dynamics in Supramolecular Biomolecular Materials**

**Principal Investigator: Samuel I. Stupp**

**Departments of Chemistry and Materials Science and Engineering, Northwestern University, 2220 Campus Drive, Evanston, IL 60208-3108**

### **Program Scope**

Our interest in self-assembly and templating as fundamental phenomena is based on the notion that the sophisticated function of materials found in biology requires organization at multiple length scales. The goal of this program is to use supramolecular chemistry integrated with other forces in order to learn how to program molecules for self-assembly of soft matter across scales, especially hierarchical structures.

### **Recent Progress**

#### *Water Dynamics*

It is well known that water within and surrounding the structure of biological systems adopts context-specific dynamics that mediate virtually all events involved in the inner workings of a cell, ranging from protein folding to molecular recognition, and the formation of hierarchical structures. Motivated by our previous work in which we measured rotational diffusion at different molecular sites within filamentous nanostructures,<sup>1</sup> we recently explored water dynamics in peptide amphiphile (PA) supramolecular nanostructures using the technique known as Overhauser dynamic nuclear polarization (ODNP) relaxometry.<sup>2</sup> ODNP combines electron paramagnetic resonance (EPR) and <sup>1</sup>H nuclear magnetic resonance (NMR) spectroscopies to capture events of translational diffusion of a water molecule as it passes by a radical electron spin label and is well suited to measure hydration dynamics at sub-nanometer length scales because this technique provides access to a broad range of water correlation times. We explored the water dynamics around a nanofiber composed of the PA molecule co-assembled with the same PA containing nitroxyl free radical spin labels covalently positioned at specific sites of the molecules in order to gain information on water dynamics at five distinct locations of the nanofiber cross-section.<sup>1</sup> We performed ODNP measurements at each spin label site of the PA supramolecular nanofibers. By this technique, we were surprised to find water molecules in the hydrophobic core and to observe that water dynamics in this region were insensitive to gelation of nanofiber solutions with added calcium salts, which either raised viscosity or caused gelation. Moving away from the core, water motion was observed to slow down and differences in water dynamics between the nanofiber in solutions and gels become apparent. Interestingly, at the surface of nanofibers, water dynamics slowed down dramatically and very large differences were detected in solutions versus gels. In the gelled state, water at the nanofiber surface reached correlation times characteristic of nearly solid water or water that is physically confined in a protein cavity. In the systems studied here, remarkable variation in water dynamics was detected between the fast-moving water at the core, and the slow, solid-like water at the surface, just 1.5 nm away. These results indicate that water dynamics can be an integral part of structure and function in hydrated materials.

### *Adaptive Properties in Supramolecular Materials*

We previously reported rapid exchange dynamics of molecular clusters in supramolecular nanofibers using stochastic optical reconstruction microscopy (STORM), which allows a resolution of ~20 nm.<sup>3</sup> Using STORM, we studied the exchange of molecules in PA nanofibers by mixing solutions of nanofibers that were labeled with different fluorescent cyanine dyes Cy3 and Cy5, which were chosen for their suitable photo-physical properties for STORM imaging. Our observations are consistent with an exchange mechanism involving monomers or small clusters of molecules inserting randomly into a fiber. The fundamental significance of this observation is the fact that strong interactions within supramolecular nanostructures lead to exchange of clustered molecules, thus generating a large diversity of structures. This result has implications for future strategies to search in supramolecular libraries for materials with optimal functions, including capacity to bind specific molecules or even catalytic activity.

We also recently investigated supramolecular glycopeptide nanostructures that display trisulfated monosaccharides on their surfaces for their ability to bind proteins known to contain polysaccharide-binding domains.<sup>4</sup> We found that binding does not disrupt the filamentous shape of the nanostructures or their internal peptide  $\beta$ -sheet backbone, but must involve accessible adaptive configurations to be able to interact with such different proteins. Our hypothesis is that rearrangement of water molecules is part of the adaptive behavior that enables these supramolecular materials to interact with very different proteins. Based on our study involving water dynamics in similar materials, displacement of water molecules harbored between  $\beta$ -sheets would expose different surfaces for interaction with proteins, thus enabling adaptive binding of molecules to these materials.

### *Dynamic Signaling and Reversibility of Hierarchical Structure*

We recently initiated research incorporating oligonucleotides and peptides with the objective of exploring the development of dynamic materials that could reversibly change properties or specific functions in response to chemistry in their environment (presence of specific molecules, pH). The Watson–Crick pairing of nucleotides offers the possibility of reversible changes in duplex structure via energetically competitive binding among different DNA sequences. Hence DNA is a good platform to encode dynamic behavior into synthetic materials. Our long-term vision is that experimental work with nucleotides present in molecular components of soft materials may offer clues on how to develop synthetic chemistry for self-assembly and dynamic behavior comparable to Watson–Crick pairing (“non-DNA DNA”).

We have developed the chemistries to synthesize peptide-DNA (P-DNA) which involved reacting single-stranded DNA bearing an amine moiety with dibenzocyclooctyne-sulfo-N-hydroxysuccinimide ester (DIBAC-sulfo-NHS) to install a cyclooctyne for subsequent copper-free click coupling to an azide containing peptide.<sup>5</sup> The conjugates were purified using reverse-phase HPLC, and their purity was verified by electrospray mass spectrometry. We then covalently grafted to alginate surfaces single stranded oligonucleotides that were complementary to sequences present in the P-DNAs and can therefore form duplex structures. Placing a peptide signal to cells in the P-DNA conjugate, we created surfaces that were potentially bioactive. We then explored dynamic changes in signaling using the concept of competitive binding displacement of the P-DNA in order to remove the signal from the surface and then re-introduce the P-DNA to renew the bioactivity (see Figure 1a). When we used the peptide RGDS as the biological signal, we could reversibly instruct fibroblasts cells to spread and retract over multiple cycles (Figure 1b). A key aspect of this platform is the ability to modify the surface with different DNA sequences, each complementary to a different P-DNA. Since each signal could be independently controlled it allowed us to study various combinations of cues. Our work offers a model system for dynamic materials that can switch the display of information on their surfaces reversibly.

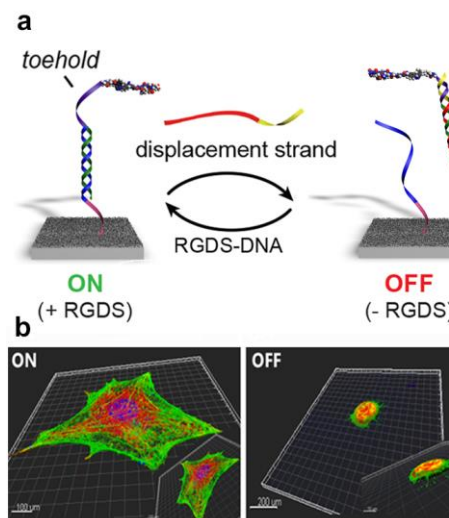


**Figure 1.** (a) Schematic representation of toehold-mediated strand displacement system. Engineering a toehold into the bioactive strand allows its removal by a fully complementary displacement strand, thus switching bioactivity OFF; this process regenerates the surface strand, allowing for a second addition of the RGDS-DNA to turn bioactivity back ON. This process can be repeated for multiple cycles. (b) Three-dimensional shadow projection image of confocal sections of fibroblasts on surfaces where RGDS was displayed (ON state after 2 h), and then removed using strand displacement (OFF state after 3 h).

Motivated by our work on dynamic surface signaling, we proceeded to integrate oligonucleotides in peptide amphiphiles. We decorated the peptide amphiphiles with single-stranded DNA or peptide nucleic acid (PNA) using two synthetic approaches. The first approach, similar to the P-DNA conjugates shown above, involves copper-free click coupling to an azide-containing peptide amphiphile. In a second approach, we synthesized a PA-PNA entirely on solid phase and purified as a single molecular species. PA-DNAs and PA-PNAs can be co-assembled with “filler” PAs that lack the nucleotides but have the same sequence in the PA segment, leading to nanofibers that display oligonucleotides.

We expected that mixing solutions containing supramolecular filaments with complimentary DNA sequences would lead to the formation of gels as a result of duplex-mediated crosslinking. A major goal of this work is to establish the reversibility of hierarchical structures taking advantage of competitive binding among DNA or PNA strands and correlating such dynamics to mechanical properties. We used the oligonucleotides in PA-DNAs to “glue” reversibly neighboring nanofibers, resulting in the assembly of hierarchical structures in the form of bundled fibers (Figure 2). We found these assemblies to be reversible upon “melting” the DNA crosslinks either by elevated temperature or competitive DNA binding. We were able to dissect

the key effects that control the nature of the assemblies and reversibility, for example the density of DNA strands and nanofiber dimensions. Especially exciting is that the investigation of these structures led us to test non-DNA chemistry to achieve programming of hierarchical structures that are possibly dynamic in nature (by changing pH for example).

## Future Plans

We are working to dissect the key effects that control the nature of the assemblies and reversibility, for example the density of DNA strands and nanofiber dimensions. We hope to be able to derive self-assembly design rules and test non-DNA chemistry to achieve programming of hierarchical structures that are possibly dynamic in nature (by changing pH for example). We are currently preparing to submit this work for publication. We will explore dynamics before and after Watson–Crick pairing with complementary strands. Generally, the experiments would probe water dynamics on the surface as a result of the presence of the signal, and also the fate of water dynamics when the complementary DNA strands or other molecules are added to solutions of the nanostructures. Another interesting direction for us to pursue is to identify physical properties of the nanostructures or the gel state they form that might be controlled by water dynamics. We will also consider peptide sequences that are known to interact with proteins on the surface of bacteria. It is expected that the complex water dynamics around our supramolecular nanostructures will also play an important role in recognition events at the bacterial membrane. The ability to understand and control can have important implications in quorum sensing for optimizing devices, such as microbial fuel production and CO<sub>2</sub> fixation.

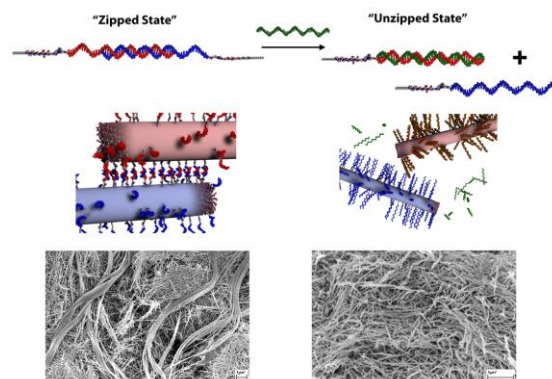


**Figure 2.** Hierarchical assembly of hybrid nucleic-acids peptide amphiphiles. DNA hybridization mediates the binding of peptide amphiphiles allowing them to reversibly transform from a gel (zipped state) to a solution (unzipped state) using toehold-mediated strand displacement. SEM micrographs show two populations within the “zipped state” consisting of hierarchical twisted bundles ( $d=1-3$  mm) and single fibers ( $d=10-15$  nm).

## References

1. Ortony, J. H.; Newcomb, C. J.; Matson, J. B.; Palmer, L. C.; Doan, P. E.; Hoffman, B. M.; Stupp, S. I., *Nat. Mater.* **2014**, *13* (8), 812-816.
2. Ortony, J. H.; Qiao, B.; Newcomb, C. J.; Keller, T. J.; Palmer, L. C.; Deiss-Yehiely, E.; Olvera de la Cruz, M.; Han, S.; Stupp, S. I., *J. Am. Chem. Soc.* **2017**, *139* (26), 8915-8921.
3. da Silva, R. M. P.; van der Zwaag, D.; Albertazzi, L.; Lee, S. S.; Meijer, E. W.; Stupp, S. I., *Nat. Commun.* **2016**, *7*, 11561.
4. Lee, S. S.; Fyrner, T.; Chen, F.; Álvarez, Z.; Sleep, E.; Chun, D. S.; Weiner, J. A.; Cook, R. W.; Freshman, R. D.; Schallmo, M. S.; Katchko, K. M.; Schneider, A. D.; Smith, J. T.; Yun, C.; Singh, G.; Hashmi, S. Z.; McClendon, M. T.; Yu, Z.; Stock, S. R.; Hsu, W. K.; Hsu, E. L.; Stupp, S. I., *Nat Nano* **2017**, *advance online publication*.
5. Freeman, R.; Stephanopoulos, N.; Álvarez, Z.; Lewis, J. A.; Sur, S.; Serrano, C. M.; Boekhoven, J.; Lee, S. S.; Stupp, S. I., *Nat. Commun.* **2017**, *8*, 15982.

### Publications Supported by BES (2015–2017)

1. Freeman, R.; Boekhoven, J.; Dickerson, M. B.; Naik, R. R.; Stupp, S. I. “Biopolymers and Supramolecular Polymers as Biomaterials for Biomedical Applications” *MRS Bull.* **2015**, 40, 1089-1101.
2. Yu, Z.; Tantakitti, F.; Yu, T.; Palmer, L. C.; Schatz, G. C.; Stupp, S. I. “Simultaneous Covalent and Non-Covalent Hybrid Polymerizations” *Science* **2016**, 351, 497-502.
3. Zha, R. H.; Velichko, Y. S.; Bitton, R.; Stupp, S. I. “Molecular Design for Growth of Supramolecular Membranes with Hierarchical Structure” *Soft Matter* **2016**, 12, 1401-1410.
4. Aytun, T.; Santos, P. J.; Bruns, C. J.; Huang, D.; Koltonow, A. R.; Olvera de la Cruz, M.; Stupp, S. I. “Self-Assembling Tripodal Small-Molecule Donors for Bulk Heterojunction Solar Cells” *J. Phys. Chem. C* **2016**, 120, 3602-3611.
5. Pazos, E.; Sleep, E.; Rubert Pérez, C. M.; Lee, S. S.; Tantakitti, F.; Stupp, S. I. “Nucleation and Growth of Ordered Arrays of Silver Nanoparticles on Peptide Nanofibers: Hybrid Nanostructures with Antimicrobial Properties” *J. Am. Chem. Soc.* **2016**, 138, 5507-5510.
6. da Silva, R. M. P.; Van der Zwaag, D.; Albertazzi, L.; Lee, S. S.; Meijer, E. W.; Stupp, S. I.; “Super-Resolution Microscopy Reveals Structural Diversity in Molecular Exchange Among Peptide Amphiphile Nanofibers” *Nat. Commun.* **2016**, 7, 11561. doi:10.1038/ncomms11561.
7. Yu, Z.; Tantakitti, F.; Palmer, L. C.; Stupp, S. I. “Asymmetric Peptide Nanoribbons” *Nano Lett.* **2016**, 16(11), 6967-6974.
8. Deiss-Yehiely, E.; Ortony, J. H.; Qiao, B.; Stupp, S. I.; Olvera de la Cruz, M. “Ion Condensation onto Self-Assembled Nanofibers” *J. Polym. Sci. B* **2017**, 55, 901-906.
9. Kazantsev, R. V.; Dannenhoffer, A. J.; Weingarten, A. S.; Phelan, B. T.; Harutyunyan, B.; Aytun, T.; Narayanan, A.; Fairfield, D. J.; Boekhoven, J.; Sai, H.; Senesi, A.; O'Dogherty, P. I.; Palmer, L. C.; Bedzyk, M. J.; Wasielewski, M. R.; Stupp, S. I. “Crystal Phase Transitions and Photocatalysis in Supramolecular Scaffolds” *J. Am. Chem. Soc.* **2017**, 139, 6120-6127.
10. Lee, S. S.; Fyrner, T.; Chen, F.; Alvarez, Z.; Sleep, E.; Chun, D. S.; Weiner, J. A.; Cook, R. W.; Freshman, R. D.; Schallmo, M. S.; Katchko, K. M.; Schneider, A. D.; Smith, J. T.; Yun, C.; Singh, G.; Hashmi, S. Z.; McClendon, M. T.; Yu, Z.; Stock, S. R.; Hsu, W. K.; Hsu, E. L.; Stupp, S. I. “Sulfated Glycopeptide Nanostructures for Multipotent Protein Activation” *Nat. Nanotechnol.* **2017**, in press DOI: 10.1038/nnano.2017.109
11. Ortony, J. H.; Qiao, B.; Newcomb, C. J.; Keller, T. J.; Palmer, L. C.; Deiss-Yehiely, E.; Olvera de la Cruz, M.; Han, S.; Stupp, S. I. “Water Dynamics from the Surface to the Interior of a Supramolecular Nanostructure” *J. Am. Chem. Soc.* **2017**, 139, 8915-8921.
12. Narayanan, A.; Cao, D.; Frazer, L.; Tayi, A. S.; Blackburn, A. K.; Sue, A. C-H.; Ketterson, J. B.; Stoddart, J. F.; Stupp, S. I. “Ferroelectric Polarization and Second Harmonic Generation in Supramolecular Co-Crystals with Two Axes of Charge-Transfer” *J. Am. Chem. Soc.* **2017**, 139, 9186–9191.
13. Freeman, R.; Stephanopoulos, N.; Alvarez, Z.; Lewis, J. A.; Sur, S.; Serrano, C. M.; Boekhoven, J.; Lee, S. S.; Stupp, S. I. “Instructing Cells with Programmable Peptide-DNA Hybrids” *Nat. Commun.* **2017**, 8:15982 doi:10.1038/ncomms15982

## Protein Self-Assembly by Rational Chemical Design

### F. Akif Tezcan, University of California, San Diego

#### Program Scope

Our research aims to develop chemical design strategies to control protein self-assembly and to construct protein-based materials new/emergent chemical and physical properties. Proteins represent the most versatile building blocks available to living organisms for constructing functional materials and molecular devices. Underlying this versatility is an immense structural and chemical heterogeneity that renders the programmable self-assembly of protein an extremely challenging design task. To circumvent the challenge of designing extensive non-covalent interfaces for controlling protein self-assembly, we have endeavored to develop a large toolkit of interactions (metal coordination, disulfide linkages, DNA hybridization, etc.) inspired by synthetic supramolecular chemistry to control protein self-assembly. Under our DOE-funded program, we established design strategies that led to the construction of a diverse array of discrete (*i.e.*, closed) or 0-, 1-, 2- and 3D (*i.e.*, infinite) protein assemblies with crystalline order over the entire nm to  $\mu\text{m}$  range. These novel protein-based materials possess emergent physical and functional properties such as maximal auxeticity and extreme negative thermal expansion. At the same time, the process of bottom-up protein design resulted in the development of new experimental platforms, allowing us to study and provide insights into the self-assembly of natural protein assemblies.

#### Recent Progress

Synthetic Modularity of Protein-Metal-Organic Frameworks: While some protein design approaches are intended to be inherently modular and allow design flexibility, they still require substantial adjustment of the protein building blocks or the self-assembly procedures on a case-by-case basis. In contrast, the field of supramolecular chemistry has benefitted from synthetic access to a large library of molecular building blocks and bonding strategies, which can be “mixed and matched” to create structural and functional diversity with relative ease. This synthetic versatility is aptly highlighted by metal organic frameworks (MOFs), which are a vast class of porous, crystalline materials composed metal-based hubs and organic linkers that can be combined in a modular fashion. We have recently adopted the design principles of MOFs to create 3D protein lattices in which spherical ferritin molecules decorated on their outer surfaces with metal coordination sites were linked together via bi-functional linkers with metal chelating head groups (**Figure 1**). Despite the remarkable size-mismatch between the linkers (196 g/mol) and the ferritin nodes (510,000 g/mol), the metal-linker interactions were sufficiently strong to dictate the arrangement of ferritin molecules into the desired body-centered-cubic (bcc) lattices. This system thus introduced a new class of tripartite hybrid materials whose self-assembly is dependent on each of its three separate components (protein-metal-organic linker).

In this period, we sought to follow up on our proof-of-principle study by examining if the modularity that is inherent in conventional MOFs also applies to protein-based MOFs. This modularity can be achieved by changing the metal ions anchored on the ferritin surface or by changing the synthetic linker.

With this in mind, we prepared: 1) three ferritin variants that possess  $Zn^{II}$ ,  $Ni^{II}$ , and  $Co^{II}$  centers in their  $C_3$ -symmetric pores anchored by the His 122 sidechains; these ions have different preferences for coordination geometry ( $Zn^{II}$ –tetrahedral;  $Ni^{II}$ –octahedral;  $Co^{II}$ –octahedral or tetrahedral) (**Figure 1a**). 2) five ditopic linkers with hydroxamate head groups that vary in their length and their geometry (linear or bent, with respect to the relative orientation of the hydroxamate headgroups) (**Figure 1b**). We found that all fifteen combinations ( $H^{122}$ ferritin-metal + linker) led to the

self-assembly of crystalline materials at room temperature in the parent body-centered geometry, as monitored by small-angle X-ray scattering (SAXS) at Argonne National Labs (**Figure 1c**). Importantly, we observed a clear structural relationship between metal coordination and the linker geometry that dictated the symmetry of the ferritin lattice. For example, with linear linker (e.g., p-bdh, linker 1 in **Figure 1b**) the tetrahedral  $Zn^{II}$  and  $Co^{II}$  yielded a bcc lattice due to the head-on attachment of the hydroxamate head groups, whereas the opposite trend was observed with  $Ni^{II}$ , which cannot bind the hydroxamate groups in a head-on fashion due to its octahedral geometry: linear ligands yield bct lattices and bent ligands produce bcc lattices. We obtained single-crystal X-ray diffraction data for the bct lattices of Zn-ferritin mediated by the long and flexible linker p-xbdh (linker 5 in **Figure 1b**). The resulting crystal structure clearly shows the p-xbdh linker bridging the Zn centers of neighboring ferritin nodes, as well as the off- $C_3$ -axis alignment of the ferritin molecules, giving rise to the cubic-to-tetragonal distortion (**Figure 1d**). Interestingly, for some metal-ferritin and linker combinations, we observed the simultaneous presence of multiple lattices, suggesting dynamic behavior. In fact, in one case, the unit cell dimensions of a cubic Ni-ferritin lattice decrease dramatically with increasing temperature, yielding a thermal expansion coefficient of  $\sim -900 \text{ ppm.K}^{-1}$  (over 50-80 °C), which is one of the most negative values observed for a crystalline material. Our results combined demonstrate that a) crystalline protein lattices can be synthetically modulated and b) they can display coherent, dynamic behavior, giving rise to unprecedented materials properties owing to their unique, tripartite composition.

***Self-Assembly of Coherently Dynamic 2D Protein Lattices:*** The rational design of 2D crystalline materials remains a considerable challenge and a very active area of development. We demonstrated that the  $C_4$  symmetric protein RhuA can be readily engineered with Cys residues (or metal-chelating bis-His motifs) at its corners to assemble into well-ordered, nearly defect-free

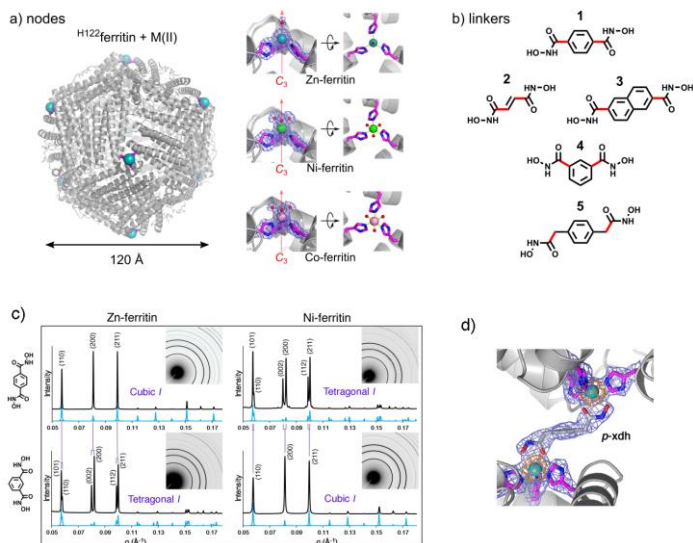


**Figure 1.** (a) and (b) Modular components of Protein-Metal-Organic Frameworks (PMOFs). (c) Representative SAXS patterns for PMOFs. (d) Close-up view of the linker 5-mediated ferritin-ferritin interface.

2D crystal lattices via disulfide bonding (**Figure 2a**).  $C^{98}$ RhuA crystals represent a unique example for any class of material (biological or abiological, natural or designed) coherently dynamic 2D lattice obtained by self-assembly. We determined that these lattices are auxetic, possessing a Poisson's ratio of  $-1$ , the lowest thermodynamically allowed value for an isotropic material. These properties make the  $C^{98}$ RhuA lattices potentially well-suited for mechanically or chemically actuated membranes and filters, molecular displays, as well as light-weight impact resistant materials. What's more,  $C^{98}$ RhuA lattices provide an ideal molecular scaffold for fabrication of functional 2D materials and for studying protein self-assembly and crystallization.

With the latter goal in mind, we have begun collaborating with Dr. Jim De Yoreo's group at PNNL for characterizing  $C^{98}$ RhuA self-assembly by in situ-liquid AFM. In initial experiments, we have observed the formation and growth of  $C^{98}$ RhuA crystals on poly-lysine treated mica (PL-mica) surfaces. Owing to the strong negative charge on one face of the  $C^{98}$ RhuA protein, protein binding was greatly enhanced for the positively charged PL-mica (**Figure 2b**). Single and multi-layer crystals were observed, with heights and calculated unit cells consistent with the values previously described from  $C^{98}$ RhuA studies in our lab. Thus far, we have observed at least two mechanisms: layer-by-layer growth, where proteins bind either laterally or vertically stack on top of existing crystals, and screw-dislocation/spiral growth, in which a small dislocation in a lower layer of the crystal merges with upper layers, which is more commonly observed in inorganic mineralization processes. We are currently aiming to build upon these observations to further characterize  $C^{98}$ RhuA crystallization kinetics and mechanisms (ideally to observe the nucleation events), as well as the self-healing processes enabled by disulfide bond reversibility,

In terms of using RhuA lattices as scaffolds for constructing functional nanomaterials, we decided to take a novel approach inspired by the enzymatic tailoring of cell surfaces. To this end, we genetically appended an amino acid sequence termed ybbR (DSLEFIASKA) to the N-terminus of  $C^{98}$ RhuA (which points to the surface of the 2D lattice). The ybbR sequence is a specific recognition motif for 4'-phosphopantetheinyl transferase (PPTase) enzymes which subsequently attach Coenzyme A-modified substrates to this motif. We showed that ybbR-modified  $C^{98}$ RhuA still forms the same 2D lattices as the parent protein, which are then conveniently labeled with different functional groups (e.g., fluorophores, **Figure 2c**) attached to CoA. Our next target is to demonstrate that such enzymatically functionalized protein lattice surfaces can be "reset" (or "recycled") by a complementary enzyme, AcpH, which specifically cleaves functional groups attached to ybbR sequences. Being able to specifically label and unlabel 2D protein surfaces in a reversible fashion would open up new avenues for many applications in bio/nanotechnology (sensing, catalysis, mechanics).

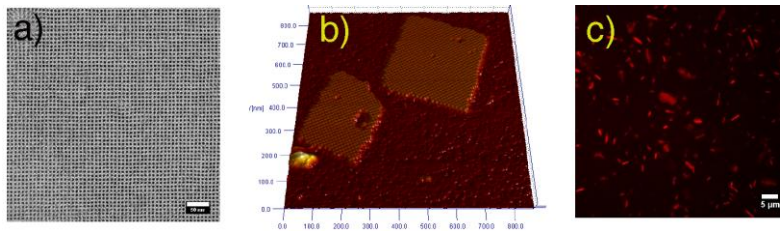


**Figure 2.** (a) Representative, TEM image of a  $C^{98}$ RhuA lattice. (b) High-resolution solution-AFM image of  $C^{98}$ RhuA crystals on PL-mica. (c) Fluorescence micrographs of  $C^{98}$ RhuA-ybbR lattices enzymatically labeled with rhodamine.

Computational Modeling of 2D Protein Lattice Dynamics: In the meantime, we also started investigating the molecular basis of what governs the lattice dynamics of  $C^{98}$ RhuA crystals. Toward understanding the stabilization of the closed state observed for  $C^{98}$ RhuA crystals, we have carried out umbrella sampling simulations of disulfide-linked  $C^{98}$ RhuA proteins in explicit solvent at constant temperature and pressure. The difference in lengths of the two axes (“A” and “B”) between opposing disulfide bonds in the pore was chosen as a representative reaction coordinate ( $\xi$ ). After system equilibration, >12 ns of simulations produced a well-converged potential of mean force (**Figure 3a**). Consistent with experimental observations, we observed a small energetic barrier separating the fully open state from a smooth, continuous energy funnel which reaches a thermodynamic minimum ( $\sim 12$  kcal/mol of stabilization) near the fully-closed state. Our subsequent Grid Inhomogeneous Solvation Theory analyses indicated that the stabilization of the closed conformation is entirely accounted for by solvent extrusion from the interfaces, meaning that dynamics of  $C^{98}$ RhuA lattices are entropically driven. Finally, we have also started engineering charged patches onto the  $C^{98}$ RhuA surfaces in order to investigate whether enthalpic contributions can be built in. Indeed, upon incorporation of repulsive negative charges (Glu57 and Glu66 mutations) into the lattice interfaces, we observed that the equilibrium state of  $E^{57}/E^{66}/C^{98}$ RhuA lattices was considerably more open compared to those of  $C^{98}$ RhuA (**Figure 3b**), which was also borne out by accompanying umbrella sampling calculations (**Figure 3a**). These results indicate that the structural dynamics of  $C^{98}$ RhuA lattices can be predictably modulated by rational design.

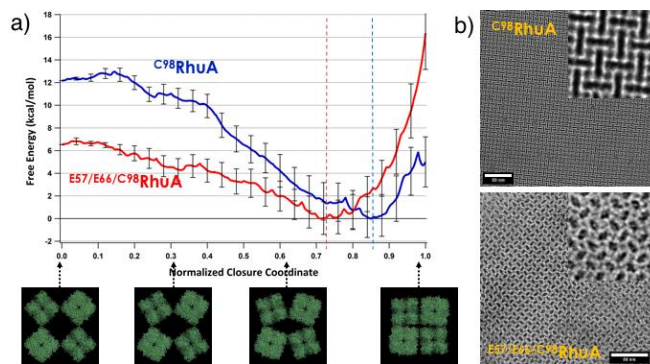


**Figure 3.** (a) Computed potential mean force profiles (i.e., free energy landscapes) of  $C^{98}$ RhuA (blue) and  $E^{57}/E^{66}/C^{98}$ RhuA lattices. (b) TEM images of equilibrated  $C^{98}$ RhuA (top) and  $E^{57}/E^{66}/C^{98}$ RhuA lattices (bottom).

### Future Plans

Our continuing goal is to develop new chemical design approaches to fabricate increasingly more complex, functional protein materials that not only emulate but also extend what natural evolution has produced. Our immediate objectives are: 1) development of a library of functional linkers to direct the formation of tunable, stimuli-responsive 3D protein lattices; 2) development of inorganic chemical strategies for the assembly of heteromeric protein assemblies consisting of multiple different building blocks; 3) to fabricate scalable, functionalized, patterned 2D protein crystals and to explore their mechanical/functional properties; 4) to elucidate the molecular basis of defect-free self-assembly of 2D RhuA crystals through computation and advanced imaging techniques; 5) to understand and exploit the molecular basis of the coherent dynamicity of 2D RhuA crystals toward the generation of responsive/adaptable protein devices.

## Publications

- 1) J. D. Brodin, S. J. Smith, J. R. Carr, F. A. Tezcan, “Designed, Helical Protein Nanotubes with Variable Diameters from a Single Building Block”, **J. Am. Chem. Soc.**, *137*, 10468-10471 (2015).
- 2) P. A. Sontz, J. B. Bailey, S. Ahn, F. A. Tezcan, “A Metal Organic Framework with Spherical Protein Nodes: Rational Chemical Design of 3D Protein Crystals”, **J. Am. Chem. Soc.**, *137*, 11598-11601 (2015).
- 3) J. B. Bailey, R. H. Subramanian, L. A. Churchfield, F. A. Tezcan, “Metal-Directed Design of Supramolecular Protein Assemblies”, **Methods in Enzymology**, *580*, 223-250 (2016)
- 4) S. J. Smith, R. J. Radford, F. A. Tezcan, “Tunable Helicity, Stability and DNA-Binding Properties of Short Peptides with Hybrid Metal Coordination Motifs”, **Chem. Sci.**, *7*, 5453–5461 (2016).
- 5) Y. Suzuki, G. Cardone, D. Restrepo, P. Zavattieri, T. S. Baker, F. A. Tezcan, “Self-Assembly of Coherently Dynamic, Auxetic, 2-Dimensional Protein Crystals”, **Nature**, *533*, 369–373 (2016).
- 6) L. A. Churchfield, A. George, F. A. Tezcan, “Repurposing Proteins for New Bioinorganic Functions”, **Essays in Biochemistry**, *61*, 245-258 (2017).
- 7) J. B. Bailey, L. Zhang, J. Chiong, S. Ahn, F. A. Tezcan, “Synthetic Modularity of Protein–Metal–Organic Frameworks”, **J. Am. Chem. Soc.**, *139*, 8160–8166 (2017).

**Dynamic, Adaptive, Systems and Materials: Complex, Simple, and Emergent Behaviors**  
**George M. Whitesides**  
**Department of Chemistry and Chemical Biology**  
**Harvard University**  
**Cambridge MA 02138**

### **Program Scope**

This program includes three major components, all related to functional, dissipative, adaptive systems, and soft-matter science.

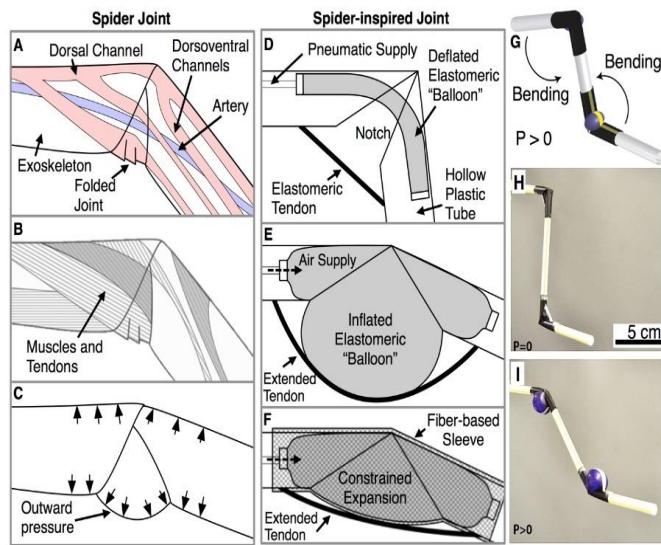
**a. Soft Actuators.** This program will extend an on-going—and productive—program, directed to the use of pneumatically actuated devices fabricated in organic soft matter (elastomers). It will demonstrate prototypes of a range of devices for gripping and moving objects that use either positive or negative pressure (e.g., vacuum) for actuation, or combinations of the two. One key scientific component of the program is the exploitation of mechanical instabilities, such as buckling and pop-through, to achieve useful work. The program will also develop materials and structures appropriate for new types of dissipative, soft systems (ultra-soft elastomers and gels; very tough elastomers; systems adapted for extreme conditions), and develop new uses of 3D printing in making new structures.

**b. Flames.** Flames are prototypical adaptive, dissipative systems. They are also enormously important practically, both from the vantage of energy production, and from that of damage done in accidental fires. The focus of this program is on collective behaviors of flames of multiple small flames, and on the lessons these behaviors can teach concerning complex, dissipative systems.

### **Recent Progress**

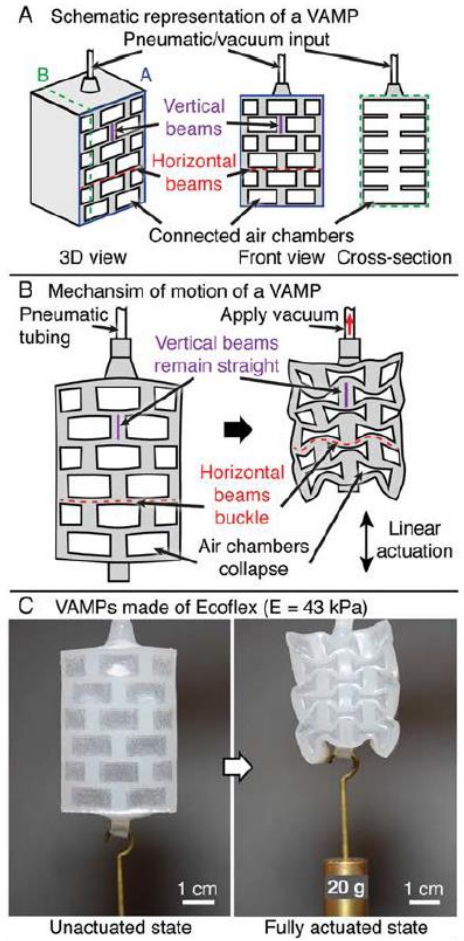
**Soft Actuators.** Our work has produced several themes. i) The development of a new soft structure that use a meso- or macro-scale elastic instability to generate a shape-memory effect. We have demonstrated that these systems are capable of phase transitions, from a parent phase to a ferro-elastic phase by a change in environmental pressure. In the ferroelastic phase, this material exhibits two variants of spontaneous strain, and one variant can be switched to the other variant under an external mechanical force. These mechanisms are conceptually the same as those in a one-way shape memory alloy. ii) The development of soft pneumatic actuators powered by negative pressure (vacuum) rather than positive pressure, known as vacuum-actuated machines (VAMs). We first used this principle to demonstrate a *rotary*-VAM, that provides a torque, by reversible, cooperative torsion, and collapse (*i.e.*, buckling) of a set of elastomeric beams. We then demonstrated vacuum-actuated muscle inspired pneumatic structures (VAMPs,

Figure 1), which are *linear-VAMs* that use this concept of reversible buckling in assemblies of elastomeric beams to generate linear motions, similar to those of skeletal muscles. Finally, this principle led to the development of *shear-VAMs*, a new design of a soft linear actuator that generates a tunable mechanical advantage. iii) This work has developed the use of multi-material three-dimensional (3D) printing to fabricate soft robots. First, a combustion-powered robot was fabricated whose body transitions from a rigid core to a soft exterior, and enables reliable interfacing between rigid driving components (controller, battery, etc.) and the primarily soft body. Powered by the combustion of butane and oxygen, this robot performs autonomous, untethered jumping. We then applied multi-material embedded 3D printing to create a soft robot with microfluidic logic, to allow autonomous movement. This fabrication method allowed pneumatic networks within a moulded, elastomeric robot body.



**Figure 2:** Cross-sectional sketches comparing the anatomy of spider joint to that of a spider-inspired joint and fabricated joints (A) Vasculature and (B) Musculature of a typical spiderjoint. (C) Sketch detailing the expansion of the artery by the hemolymph (the circulatory fluid) (D) Sketch of spider-inspired joint formed from a plastic tube with a notch, an elastomeric “balloon”, and a passive elastomeric tendon. (E) Sketch detailing the extension of the spider-inspired joint (F) Sketch detailing the extension of a spider-inspired joint where pneumatic expansion is constrained by a fiber-based sleeve that is flexible but inextensible. (G) Schematic of a limb with two identical actuators. Images of a limb with both actuators are unpressurized (H) and pressurized to  $\Delta P_0 = 70 \text{ kPa}$  (I).

actuation using materials in which stretching is limited, but that also provide significant



**Figure 1.** A vacuum-actuated muscle inspired pneumatic structure (VAMPs) lifting a 20 g weight

**“Intermediate”/Soft Structures:** Flexible but inextensible. Many biological systems that involve stretching and releasing tensile structures (e.g. tendons) do not dissipate as heat all of the work done in stretching the tendon, but recover some fraction of it during the release of strain. Taking stimuli from biology, this work led to the fabrication of intermediate hard-soft structures (Figure 2) using a polypropylene drinking straw (that can bend, but not stretch) and a pneumatically inflatable bladder (PDMS) as the elastic element. We have two interests in these systems. i) They allow the study of

structural strength. ii) They provide a model system with which to explore some of the characteristics of designs when used in fingers, legs, and other elements of our soft robotics systems. A variety of robots constructed from these structural elements demonstrate (i) crawling with one or two limbs, (ii) walking with four or six limbs (including an insect-like triangular gait), (iii) walking with eight limbs, or (iv) floating and rowing on the surface of water.

**Flames.** We have explored in detail – as a model system for small, intense, flames – the burning of a strip of nitrocellulose. The behavior of this system is quite remarkable. A single strip can undergo a transition between two states, one characterized by steady, low intensity combustion, and the second by unstable high intensity combustion (Figure 3 shows a bistable combustion system. (A) A 1-cm inverted “V” composed of three folds and two sides, each 1 cm in length. (B) Sequential high-speed images of a flame propagating along a strip of nitrocellulose. A slowly moving, “structured flame” (top) encounters the inverted “V” from (A) (middle) and transitions to a rapidly moving, “unstructured flame” (bottom)). We have considered this system as using the conceptual framework of a folded bifurcation, and identified the key feature leading to the transition as the nonlinear coupling between the chemical processes involved in combustion, and the “wind” – that is, convective flow of air reflecting the motion of hot gases-- and the flame. We have argued that this system provides a distant but instructive model for naturally occurring, high – intensity flames such as crown fires in forest fires. The utility of the model for this purpose remains to be seen, but it already provides one of the best – defined models for combustion that is available.

### Future Plans

**Soft Actuators.** Our future work in soft actuators will continue our progress in this field by developing new materials, design principles, and fabrication techniques, for soft actuators. We will continue to investigate other systems that exploit large nonlinearities in mechanical behavior of ‘soft’ materials for new mechanisms of actuation. We will extend work that we have already begun on elastomeric composites, to new soft, and semi-soft, materials, or combinations of materials, to identify new functions and capabilities in soft actuation. The major focus will continue to be on looking for nonlinear phenomena (buckling, “snap through”, and others) that have the potential to be the basis for new mechanisms of actuation, new types of soft actuators, and the implementation of logic and autonomy into soft devices. As we proceed with this work, we will demonstrate mechanical (and in principle other) functions, but applications are not the primary focus of the work at this point. We are more interested in exploring the possible space of new types of actuation, and new methods of coupling the properties of materials-- especially nonlinear properties under stress-- to potentially useful-- and necessarily relatively simple-- mechanical work.

**Flames.** Our future work will involve nitrocellulose-based systems as a model for “Forest Fires.” Nitrocellulose sheets are commercially available, burn exothermically, and are easily cut into

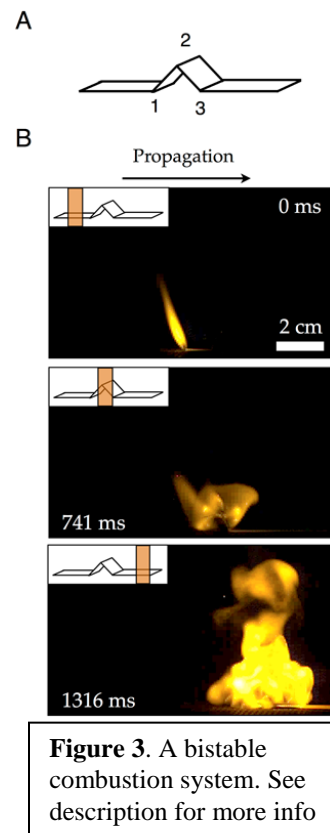


**Figure 3.** A bistable combustion system. See description for more info

strips (or other shapes), or punched into disks. We will use (i) tape-based experiments (burning tapes) to establish the fundamental of propagation of combustion of this system. How much heat is generated, and radiated from one burning tape to a parallel, adjacent one? What types of simple perturbations trigger instabilities in the stable, quiet type of flame, and what types trigger transitions between quiet and turbulent flames? How do flames propagating along parallel strips interact?, and (ii) disk-based systems (more versatile, but more complicated system: that of a flame propagating across a field of nitrocellulose discs supported on paper. We might be able to build an analog model of a forest or woodlands using these discs. In such a model, the slow-burning undergrowth or dry grass would be modeled by filter paper (which burns slowly); the trees (pine trees, for a model of a crown fire) would be represented by nitrocellulose discs (or other shapes) positioned on the filter paper. We also want to explore systems of individual flamelets (all of the parameters of each flame could be controlled individually). We have just begun to study this system, and it exhibits a remarkable range of dynamic behaviors; it is not, however, “reproducible” (at least not yet); the patterns of propagation vary with time, rather than repeating cyclically. We will either have to develop a statistical measure of behavior, or develop the system further to give better reproducibility.

#### **Publications Acknowledging This DoE BES Grant (2016 – 2017)**

"Tilted Magnetic Levitation Enables Measurement of the Complete Range of Densities of Materials with Low Magnetic Permeability", Nemiroski, A., Soh, S., Kwok, S. W., Yu, H.-D. and Whitesides, G. M. *J. Amer. Chem. Soc.*, 2016, 138, 1252-1257.

"Exploiting Non-Equilibrium Phase Separation for Self-Assembly", Grunwald, M., Tricard, S., Whitesides, G. M. and Geissler, P. L. *Soft Matter*, 2016, 12, 1517-1524.

"Phase-Transforming and Switchable Metamaterials", Yang, D., Jin, L., Martinez, R. V., Bertoldi, K., Whitesides, G. M. and Suo, Z. *Extreme Mechanics Letters*, 2016, 6, 1-9.

"Buckling Pneumatic Linear Actuators Inspired by Muscle", Yang, D., Verma, M. S., So, J.-H., Mosadegh, B., Keplinger, C., Lee, B., Khashai, F., Lossner, E., Suo, Z. and Whitesides, G. M. *Adv. Mater. Technol.*, 2016, 1, 1600055.

"Negative-Pressure Soft Linear Actuator with a Mechanical Advantage", Yang, D., Verma, M. S., Lossner, E., Stothers, D. and Whitesides, G. M. *Adv. Mater. Technol.*, 2016, 1, 1600164 1-6.

"Coated and Uncoated Cellophane as Materials for Microplates and Open-Channel Microfluidics Devices", Hamedi, M. M., Unal, B., Kerr, E., Glavan, A., Fernandez-Abedul, M. T. and Whitesides, G. M. *Lab on a Chip*, 2016, 16, 3885-3897.

"Soft, Rotating Pneumatic Actuator", Ainla, A., Verma, M. S., Yang, D. and Whitesides, G. M. *Soft Robotics*, in press 2017

## Exploring Fundamental Properties of Dynamic DNA Origami –Nanoparticle Composites

Jessica Winter (PI), Chemical and Biomolecular Engineering, Biomedical Engineering;  
Carlos Castro (co-PI), Mechanical and Aerospace Engineering; Michael Poirier (co-PI),  
Ezekiel Johnston-Halperin (co-PI), Department of Physics, The Ohio State University

### Program Scope

This research addresses fundamental needs for the development of deoxyribonucleic acid (DNA)-based energy materials by increasing understanding of: (1) the role of nanomaterial sterics and binding interactions on the equilibrium and kinetic properties of dynamic DNA origami structures, (2) mechanical potential energy storage via NP and DNA origami interactions, (3) energy exchange between the bulk solution and DNA-NP composite materials, and (4) nanoscale heat transfer on DNA de/hybridization kinetics in heterogeneous nanoscale environments. This research involves 3 objectives investigating energy harvesting by gold nanoparticles (AuNPs) or magnetic superparamagnetic iron oxide nanoparticles (SPIONs) and transfer of that energy with DNA origami “hinge” and “accordion” templates (i.e., hinge arrays) (**Figure 1**). DNA nanostructures are ideal materials for these studies since their geometry, stiffness, and motion can be precisely designed and controlled [1-3].

### Recent Progress

**Objective 1: Evaluate the ability of DNA-nanoparticle composites to store mechanical energy.**

The main goals of Objective 1 are to: (1) understand the influence of nanoparticles (NP) on the free energy landscapes of DNA origami nanodevices; (2) quantify how stored energy alters kinetics and thermodynamics of DNA binding; and (3) explore whether stored energy and sterics designed into DNA devices can generate emergent behaviors in DNA origami – NP

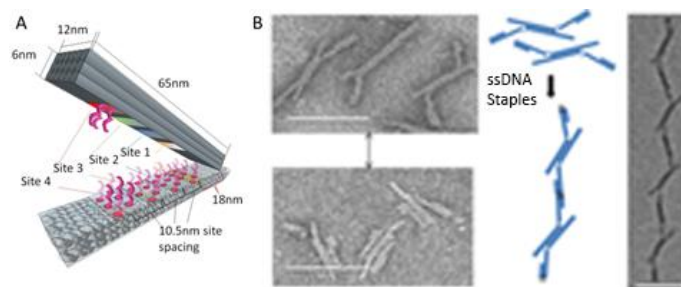


**Figure 1.** DNA Origami Structures. Hinges (A) can polymerize to form accordions (B). Scale bars = 50nm.

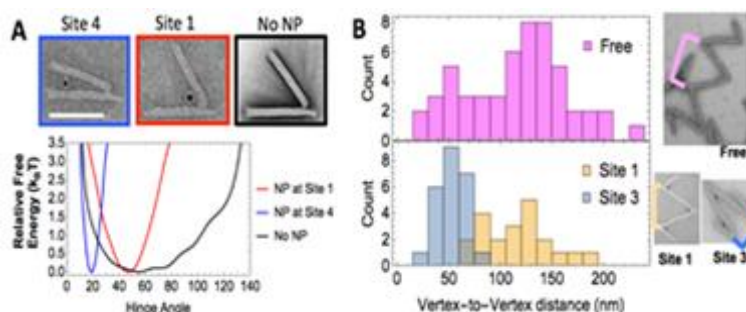


**Figure 2:** DNA origami–NP composite free energy landscapes. (A) Attaching NPs at different hinge sites constrained free energy landscapes relative to the free hinge. (Normalized to zero for comparison). Scale bar = 50 nm. (B) Functionalizing accordions with NPs at different sites altered vertex-vertex distance, as seen in TEM.

composites. We have made advances on two of these goals in the first 4 months of this project.

*(Obj. 1.1: Free Energy Landscapes)* We have successfully attached NPs to hinge and accordion structures at multiple locations (**Figure 2**). Hinges with NPs bound at two different locations demonstrate constraint in available hinge angle states compared to the free hinge, illustrating altered energy landscapes. Accordions (hinge array) with NPs bound at different locations demonstrated different vertex-to-vertex differences compared to free accordions. We are currently improving assembly efficiency for the accordion system and collecting more images and measurements. Nevertheless, the ability to make and image these systems is a crucial step to enabling further studies of energy landscapes. Further, accordion data show proof-of-concept toward the polymerization of these systems to useful sizes.

*(Obj. 1.2 Actuation Kinetics)* Using hinge-NP composite structures, we have begun to quantify thermodynamics and kinetics of binding and thermal actuation. Initial measurements were performed with the NP bound at site 4 (**Figure 1A**), closing the hinge to a small angle. Binding kinetics were quantified using fluorescence quenching assays (**Figure 3A**, right). TideFluor5 fluorophore (red) located on the hinge is directly adjacent to the NP binding site, so that NP binding (yellow) quenches fluorescence. The hinge is also functionalized with an Alexa488 fluorophore (blue) and a corresponding quencher (Blackhole Quencher 1, black) so that closing of the hinge results in Alexa488 quenching. The Alexa488 quenching curve closely follows the Tidefluor5 quenching curve (**Figure 3A**), illustrating that NPs bind on the minute timescale, with the hinge closing rapidly thereafter. In addition, equilibrium thermal actuation curves reveal that the length of the hybridization ssDNA (8, 9, or 10 bps) can alter actuation temperature (**Figure 3B**). Lastly, applying bulk heating or cooling, we find that thermal actuation can be accelerated to the time scale of a few seconds (**Figure 3C**). This is likely limited by the time required for bulk heating of the solution.

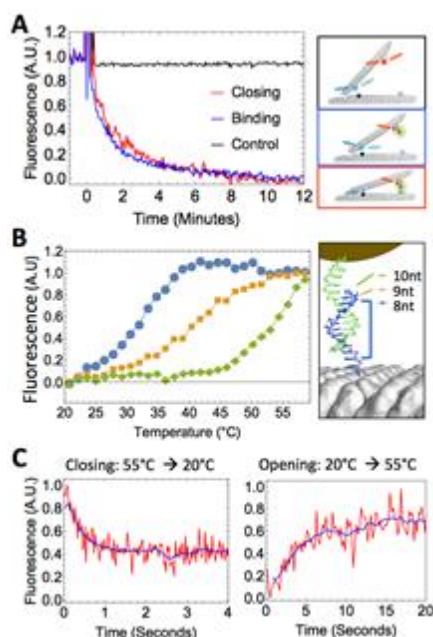


**Figure 3:** Hinge-NP composite kinetics and thermodynamics. (A) NP binding proceeds on the timescale of minutes and closing occurs very rapidly after binding. (B) Equilibrium thermal actuation curves with varying lengths of DNA-NP binding sites. (C) Thermally driven opening.

We have also made progress in developing experimental single molecule assays to measure DNA hinge actuation kinetics (**Figure 4A**). Hinges labeled with Cy3 (green) and Cy5 (red) fluorophores are immobilized on a coverslip coated with polyethylene glycol (PEG). A fraction of the PEG (~1%) is biotinylated to allow anchoring of hinges via a biotin-streptavidin-biotin linkage. Initial data was collected for hinges for which closing was mediated by weak transient base pairing directly across the hinge arms (in the absence of a NP). Thus, opening and closing were driven by thermal fluctuations, monitored by single molecular Förster Resonance Energy Transfer

(smFRET) (**Figure 4B**, donor (left) and acceptor signals (right), and **Figure 4C** sample trace of a single hinge.

**Objective 2: Explore localized delivery and transfer of heat to DNA origami-NP composites**

The main goals of objective 2 are to: (1) evaluate how mechanical potential energy and sterics influence DNA duplex actuation thermodynamics and kinetics, (2) determine the heat transport properties of DNA origami structures, and (3) discover whether local heat transfer in a heterogeneous nanoscale environment follows bulk heating models.

(Obj 2.1 Thermal Actuation Kinetics) To study bulk kinetics of DNA-NP composites requires ability to simultaneously measure fluorescence and actuate AuNPs. Therefore, a laser (actuation) was integrated with an existing fluorimeter, perpendicular to the emission photodiode and opposite the excitation beam to minimize unwanted scattering.

**Objective 3: Explore localized delivery of mechanical work to DNA origami-NP composites**

The main goals of objective 3 are to determine the impact of (1) DNA origami structures and (2) bulky NP cargoes on dsDNA interactions, and to (3) evaluate ability of DNA-NP composites to store and release energy from external fields.

(Obj 3.1, 3.2 Steric Influences on dsDNA Binding Strength) Single molecule force spectroscopy (i.e., magnetic tweezers) will be used for these first two objectives. During the first 4 months of this grant period, procedures were developed for DNA attachment to the hinges and for hinge attachment to the glass surface. Briefly, the DNA tether is a linearized pUC19 plasmid that has been modified to contain a 30 base pair ssDNA overhang that will be attached to the origami through a complimentary 30 base pair ssDNA overhang. The other end of the DNA tether contains a digoxigenin molecule that attaches to an antibody-coated glass surface that binds digoxigenin. The origami is biotin labeled so that it will attach to a streptavidin coated magnetic bead. Fitting the force response to the worm-like chain model showed that a majority of magnetic beads were attached to the surface through a single DNA molecule (**Figure 5**).

**Future Plans**

(Obj. 1.3 Emergent Behaviors) Dr. Gil Gallegos at New Mexico Highlands University will perform computation modeling of hinges with AuNPs bound at 2 sites for surface plasmon resonance (SPR)

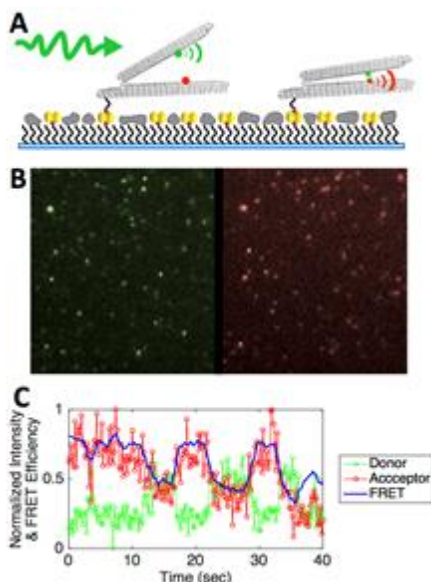


**Figure 4:** Single molecule DNA hinge kinetics. (A) Cy3 (green) and Cy5 (red) fluorophore-labeled hinges immobilized on a coverslip. (B) Sample images of Cy3 (left) donor and Cy5 (right) acceptor signals. (C) Sample trace of hinge actuation driven by weak transient base-pairing.

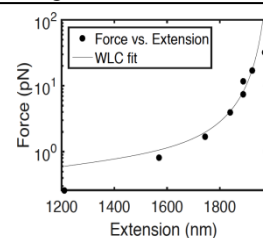


**Figure 5:** Force-extension curve for pUC19 DNA tether that will attach magnetic beads to single DNA hinges.

studies. Expected interactions will be evaluated as a function of distance, and compared to experimental results.

(Obj. 2.2 DNA Origami Thermal Properties, 2.3 Nanoscale Heat Transport) These objectives will be explored in the Y2 and Y3, respectively. We are currently building the instrumentation and DNA–NP composites necessary to perform this work.

(Obj 3.1, 3.2 Steric Influences on dsDNA Binding Strength) Magnetic tweezer experiments will be performed with hinges closed by DNA base pairing within a single hairpin. The average force required for actuating the device and dwell times will be measured. These studies will be compared to a hairpin without the hinge. We expect to explore hinges containing NPs thereafter.

(Obj 3.3 Electromagnetic Energy Exchange) SPION attachment provides for remote actuation and energy storage in DNA origami constructs. Whereas isolated SPIONs have no preferred magnetization orientation (**Figure 6, Left**), the symmetry breaking found in dimers leads to a preference for tip-to-tail alignment with an energy scale that depends inversely on the cube of their spacing and an attractive force that scales as the inverse fourth power (**Figure 6, Center**). An external magnetic field introduces an additional energy scale given by the Zeeman energy ( $E_Z = \mu \cdot H$ ) that lowers the overall energy of the latched and horizontal conformation (**Figure 6, Right**). Although these *static* effects are well described by existing models, a more careful modeling of the hinge structure *dynamics* and interaction with dynamic fluctuations of SPION magnetization is required. The hinge rotational correlation time is on the order of milli-seconds ( $\tau_1$ ), whereas magnetization fluctuations can range from milli- to nano-seconds depending on the strength of the applied field ( $\tau_2$ ). These models will be developed in parallel with experiment, starting with ensemble measurements and moving on to single molecule measurements.

DNA conjugation methods are being developed for this application. Commercial SPIONs are coated with ligands that are either organic (e.g. oleic acids) or are too large for the proposed studies (e.g., ~ 4nm amphiphilic polymers). Thus, we will perform ligand exchange followed by DNA conjugation via “click” chemistry [4] or permanently embed DNA strands in the NP by growing a thin silica shell (i.e. silica) around the SPION core.

## References

1. Castro, C.E., et al., *Nanoscale*, 2015: p. 5913-21.
2. Marras, A.E., et al., *PNAS*, 2015: p. 713-8.
3. Zhou, L., et al., *ACS nano*, 2014: p. 27-34.
4. Bishop, L.M., et al., *Langmuir*, 2012: p. 1322-1329.

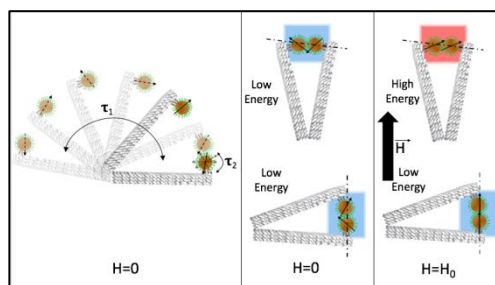


**Figure 6:** Example states of hinge-SPION conjugates at zero field ( $\tau_1$ = Time constant for hinge thermal fluctuations,  $\tau_2$ = Time constant for dipole moment flip at room temperature, arrows= direction of dipole orientation). Selected hinge conformations in zero (center) and non-zero (left) applied field. Latched and horizontal conformation has the lowest magnetostatic energy in a finite field.

## **Publications**

### *Conference Presentations (Speakers Underlined)*

J. Johnson, A. Dehankar, J. Winter and C. Castro. “Control of DNA Origami Mechanisms Via Gold Nanoparticles.” 17th IEEE International Conference on Nanotechnology, Pittsburgh, PA, (Jul 25-28, 2017).

J. Johnson, A. Dehankar, J. Winter and C. Castro. “Control of DNA Origami Mechanisms via Gold Nanoparticles,” Foundations of Nanoscience (FNANO), Snowbird, UT, (April 10-13, 2017).

A. Dehankar, J. Johnson, C. Castro, J.O. Winter, “Actuatable DNA origami-nanoparticle composites for energy harvesting and storage,” 253rd ACS National Meeting, San Francisco, CA (April 3, 2017).

## DNA nanostructure directed designer excitonic networks

Hao Yan, Arizona State University (Principal Investigator)

Neal Woodbury, Arizona State University (Co-Investigator), Yan Liu, Arizona State University (Co-Investigator), Mark Bathe, Massachusetts Institute of Technology (Co-investigator), David Whitten, University of New Mexico (Co-investigator)

### Program Scope

A fundamental limitation in the development of artificial molecular light harvesting structures is that generally if one places pigment molecules close enough to achieve very high energy transfer efficiency and absorbance cross section, the dyes interact in such a way that self-quenching occurs. This limits both the optical cross section and the overall efficiency of light capture in such systems. Nature overcomes this problem and achieves efficient energy transfer without self-quenching by controlling the environment, vibration characteristics, orientation and dynamics of the pigments involved in light harvesting. Natural light harvesting systems have evolved highly intricate chromophore architectures of protein-bound organic molecules that absorb and funnel solar energy with high efficiency and fast transfer rates using elegant excitonic circuitries<sup>1</sup>. Nature achieves this precise control over the properties of pigment complexes by using specific proteins as templates to guide the formation of very well defined pigment aggregates, groups of pigment molecules that are in close enough contact to undergo excitonic interactions resulting in new electronic properties that were not present in the monomer. In synthetic systems,

pigment aggregates are well known, and J-aggregates and H-aggregates have been long studied for their unique properties. In Nature, the chlorosomes of green bacteria form what appear to be classical J-aggregates and the light harvesting complexes of purple nonsulfur bacteria form ring structures that have many of the properties of J-aggregates such as a red-shifted absorbance spectrum and excited states that are delocalized over multiple pigment molecules<sup>2</sup>. These

photosynthetic systems leverage the spectral and enhanced transport properties of J-like aggregates to achieve fast exciton transport within the antenna and thus high light-harvesting efficiency<sup>3</sup>. (Figure 1A). The close interaction of the pigments results in substantial electronic coupling that lifts the degeneracy of excitonic states and therefore modifies the absorption and emission spectra of the monomer. In the case of J-aggregation, lower energy excitonic states acquire significant oscillator strength, resulting in a characteristic bathochromic shift of the absorption and fluorescence and often superradiant delocalized exciton states. The programmability of structural DNA nanotechnology<sup>4</sup> offers a unique opportunity to organize DNA-templated dye aggregates into rationally designed patterns that would enable numerous fundamental insights into the nature of how molecular organization (i.e., geometry, distance, etc.) of these photonic elements impacts their energy transfer mechanisms. The objective of the project is to create a new class of photonic materials that mimic biological light harvesting systems but with more robust components. The

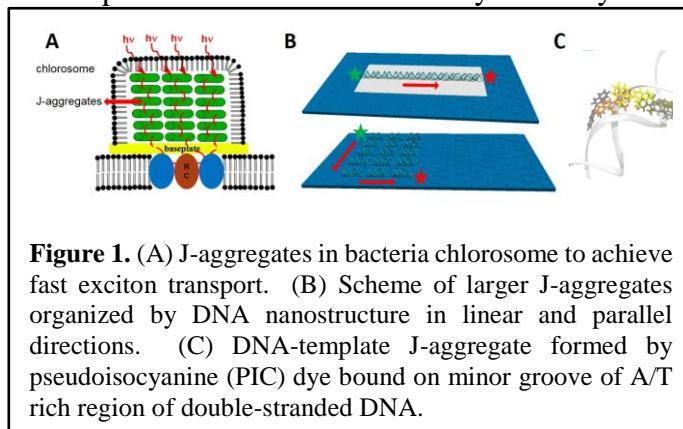


**Figure 1.** (A) J-aggregates in bacteria chlorosome to achieve fast exciton transport. (B) Scheme of larger J-aggregates organized by DNA nanostructure in linear and parallel directions. (C) DNA-template J-aggregate formed by pseudoisocyanine (PIC) dye bound on minor groove of A/T rich region of double-stranded DNA.

DNA template provides sufficient control over orientation and geometry of closely packed dyes to facilitate both a high absorbance cross section and efficient energy transfer without self-quenching. The overarching goal of the project is to be able to perform computational design and molecular assembly generating nanostructured excitonic systems with predictable properties and in the process better understand the fundamental underlying mechanisms of energy transfer and pigment coupling in closely packed systems similar to those created in Nature.

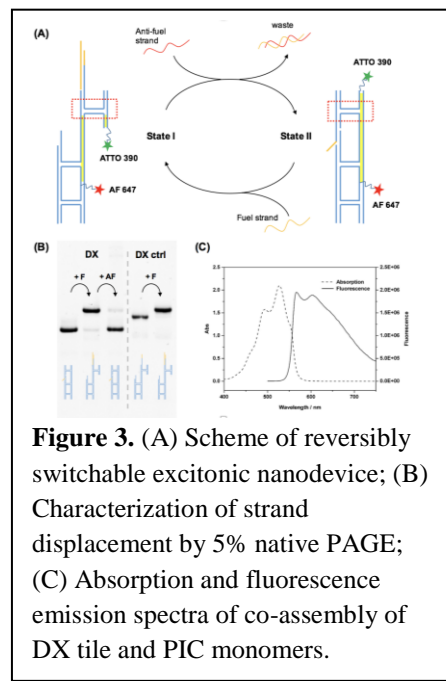
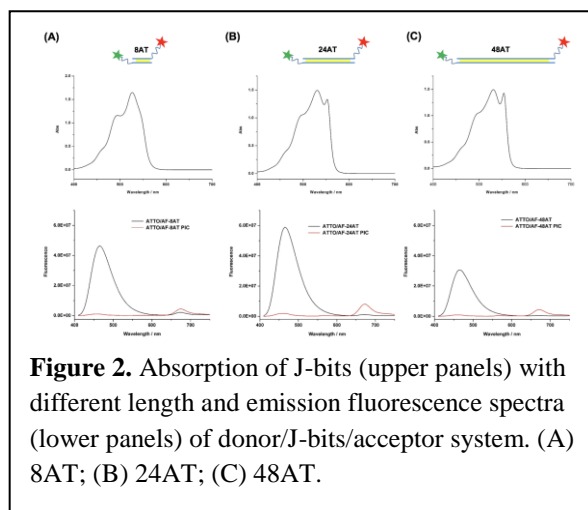
## Recent Progress

### 1. Simple donor-acceptor systems based on J-bits

The broad absorption spectrum generated in J-aggregates, combined with the increased fluorescence lifetime, increased natural radiative rate constant and broad fluorescence emission spectrum, which make J-bits attractive candidates as energy transfer elements. In the preliminary experiment, our collaborative effort with the Bathe group has demonstrated that pseudoisocyanine (PIC) dye can non-covalently but specifically bind with double-stranded A/T DNA segments to form J-like aggregates (J-bits)<sup>5</sup>. Here, we use double-stranded DNA (dsDNA) with different length and sequence as scaffold to construct J-bits and characterize the ability of a J-bit to accept energy from a donor and pass the energy to an acceptor. The dsDNAs containing various number of continuous A/T base pairs (8 bp, 24 bp and 48 bp) are used as templates, meanwhile the donor (green star, ATTO 390) and acceptor (red star, Alex Fluor 647) are modified and attached to the two ends of dsDNA respectively (**Figure 2**). The absorption spectra showed that the J-like aggregates form better in 24 bp and 48 bp dsDNA than those in 8 bp dsDNA judging from the intensity of the sharp red-shifted J-aggregates peak near 555nm. The steady state fluorescence emission spectra showed the emission of donors (ATTO390, 480 nm band) are remarkably quenched and emission of acceptors (AF647, 675 nm) are enhanced in all three systems. Comparing with the 8 bp J-bits system, we observed a better enhancement of emission fluorescence from acceptor in 24 bp and 48 bp systems, which is attributed to a better formed J-like aggregates on 24 bp and 48 bp dsDNA.

### 2. Switchable photonic nanodevice

Natural biological devices are designed to operate in dynamic conditions, responding to subtle biological cues that modulate their functions. The structural properties of DNA that allow it to serve as a versatile construction material have been exploited to create dynamic nanodevices. Here, we designed a reversibly switchable DNA nanodevice based on isomerization of Holiday junction manipulated by toehold mediated DNA strand displacement.



The switching would change the alignment of PIC monomers on the DNA nanostructure and consequently modulate energy transfer behavior of the complex. As shown in **Figure 3A**, a double crossover (DX) DNA tile is used as switchable scaffold. In the state II, Holiday junction (shown in the red box) with an unfavorable conformation is fixed on the scaffold. After adding fuel strand (orange strand), the hybridized sticky end would be displaced and the Holiday junction would re-fold to its favorable conformation (state I). And then, the anti-fuel strand (red strand) could displace the fuel stand and the DX tile would switch to state II powered by hybridization of sticky ends. PIC monomers would bind with the continuous A/T segment (yellow part) to form J-like aggregates as a switchable energy transfer pathway. We used native polyacrylamide gel electrophoresis (PAGE) to verify the switching process (**Figure 3B**). The absorption and emission fluorescence spectra showed that PIC monomers could bind with A/T segment to form J-like aggregate (**Figure 3C**).

### 3. Covalent linkage and seeded growth for J-aggregates formation

To create a new class of excitonic materials, we focus on the self-assembly of J- or J-like aggregates on DNA nanostructures using PIC dyes. However, the nonspecific binding between PIC monomers and DNA presents a challenge for the high efficiency energy transfer of J-aggregate, hence decreasing the concentration of free PIC monomers in solution is a big concern. For this purpose, we decided to covalently attach PIC monomers onto DNA strands via a click reaction between an azide functionalized pseudoisocyanine derivative **6** and an oligonucleotide containing an alkyne side chain **10**. (**Figure 4A**) The pseudoisocyanine linker **6** was synthesized by reaction of two heterocyclic quaternary salts **4** and **5**. Alkylation of quinolone **1** with 1-bromo-3-chloropropane afforded *N*-(3-chloropropyl) quinolone **2**. Reaction of compound **2** with sodium azide in DMF gave the *N*-(3-azidopropyl) quinolone **3**. The reactive chloroquinolium salt **4** was obtained by reaction of quinolone **3** with phosphoryl oxychloride. The alkyne group is introduced on the phosphate backbone via a phosphotriester linkage, which allows for the introduction of the pendant PIC groups at any chosen position(s). Next, we attempted the azide-alkyne cycloaddition reaction, and obtained PIC-modified oligonucleotides containing up to 8 covalently linked PIC monomers. We characterized the optical properties the co-assembly of the free PIC onto the dye-modified dsDNA. (**Figure 4B**) The absorption spectra showed that PIC could not bind with PIC-modified dsDNA to form a good J-like aggregate s. The possible reason is that the variations in the orientation of two isomers of phosphate group introduced by alkylation reaction would distort the close alignment of PIC monomers. Experiments are underway to solve this problem.

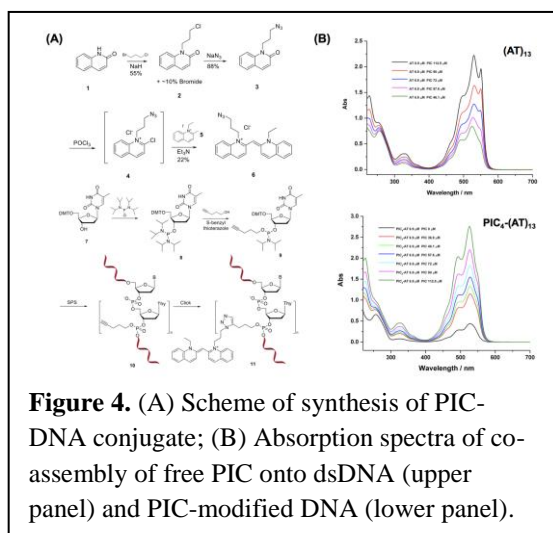


**Figure 4.** (A) Scheme of synthesis of PIC-DNA conjugate; (B) Absorption spectra of co-assembly of free PIC onto dsDNA (upper panel) and PIC-modified DNA (lower panel).

### 4. DNA-scaffolded conductive polymer routing

DNA nanotechnology offers precise geometrical control of the positioning of materials. Gothelf and co-workers recently reported<sup>6</sup> that a conductive polymer backbone modified with many short oligonucleotides can be aligned onto the DNA origami with well-defined geometries by DNA hybridization. The polymer wire can be used as a good channel for long-length energy transfer

with a defined or reconfigurable direction. Here, we designed a rectangular DNA origami (**Figure 5A**) as a scaffold and two rows of 9 nt ssDNA probes were placed on the right side of origami (blue box) for polymer routing. A donor (green star) and an acceptor (red star) are placed on the two edges of DNA origami by DNA hybridization. When the polymer is aligned onto the origami, the energy from donor will be transferred to the acceptor via the polymer. The rectangular DNA origami can be formed in a high yield and characterized by AFM (**Figure 5B**). We then confirmed poly(APPV-DNA) (provided by Dr. Gothelf) could be immobilized onto rectangular DNA origami by AFM.

### Future Plans

#### 1. Simple donor-acceptor systems based on J-bits

We will use time-resolved fluorescence spectra to characterize the fluorescent decay kinetics and efficiency of energy transfer on the donor/J-bits/acceptor system. In addition, we will design more complex donor-acceptor system by construct multi-element J-bits with controlled pattern and variable length.

#### 2. Switchable excitonic nanodevice

We will compare the energy transfer of the donor/J-bits/acceptor under two states and characterize the reversible switching process by steady-state and time-resolved fluorescence spectroscopy. Single molecule imaging will also be used to measure the switching process.

#### 3. Covalent linkage and seeded growth for J-aggregates formation

An alternative synthesis scheme will be used to obtain two isomers of alkyne-modified oligonucleotide respectively. We will characterize the optical properties the co-assembly of the free PIC onto the new dye-modified dsDNA.

#### 4. DNA-scaffolded conductive polymer routing

The ZnCdSSe/ZnS core/shell quantum dots (QDs) will be used as a donor in this design to overcome the broad absorption spectra and high extinction coefficient of the polymers, allowing more selective excitation of the donor. The DNA-functionalized QDs will be immobilized onto specific position based on specific DNA hybridization. We will characterize the energy transfer in the donor/polymer/acceptor system.

### References

- Şener, M. K., Olsen, J. D., Hunter, C. N. & Schulten, K. Atomic-level structural and functional model of a bacterial photosynthetic membrane vesicle. *Proceedings of the National Academy of Sciences* **104**, 15723-15728 (2007);
- Orf, G. S. & Blankenship, R. E. Chlorosome antenna complexes from green photosynthetic bacteria. *Photosynthesis Research* **116**, 315-331(2013);
- Prokhorenko, V. I., Holzwarth, A. R., Nowak, F. R. & Aartsma, T. J. Growing-in of optical coherence in the FMO antenna complexes. *Journal of Physical Chemistry B* **106**, 9923-9933 (2002);
- Seeman, N. C. DNA in a material world. *Nature* **421**, 427-431 (2003);
- E. Boulais, N.Sawaya, R. Veneziano, A. Andreoni, S. Lin, N. Woodbury, H. Yan, M. Bathe Programmed coherent coupling in a DNA-based excitonic circuit, *Nature Materials*, in revision (2017);
- J. B. Knudsen, Routing of individual polymers in designed patterns, *Nature Nanotechnology*, 10, 892-898 (2015).

**Publications:** None.

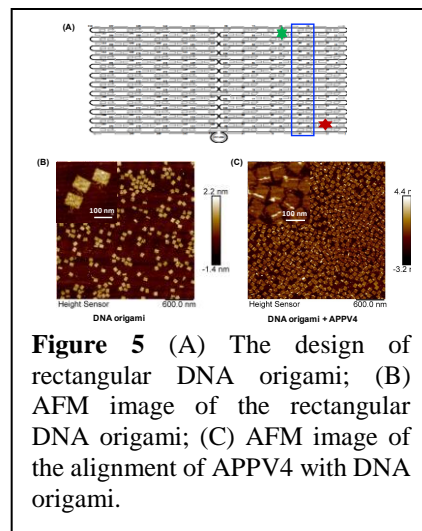


**Figure 5** (A) The design of rectangular DNA origami; (B) AFM image of the rectangular DNA origami; (C) AFM image of the alignment of APPV4 with DNA origami.

***POSTER  
SESSIONS***



## **Biomolecular Materials Principal Investigators' Meeting**

### **POSTER SESSION I**

*Tuesday, August 15, 2017*

1. **Joanna Aizenberg (Harvard University)**  
Energy Transductions in Multimodal Stimuli-Responsive Reconfigurable Systems with Information Encoding Capabilities
2. **Zvonimir Dogic (Brandeis University)**  
Large-Scale Self-Organization and Spontaneous Flows in Microtubule Based Soft Active Matter
3. **George Bachand (Sandia National Laboratories)**  
Active Assembly of Nanomaterials: Artificial Microtubules
4. **Erik Spoerke (Sandia National Laboratories)**  
Active Assembly of Nanomaterials: Artificial Microtubules
5. **Elisa Franco (University of California, Riverside)**  
Programmable Dynamic Self-Assembly of DNA Nanostructures
6. **Rebecca Schulman (Johns Hopkins University)**  
Programmable Dynamic Self-Assembly of DNA Nanostructures
7. **Anna Balazs (University of Pittsburgh)**  
Design and Synthesis of Structurally Tailored and Engineered Macromolecular (STEM) Gels
8. **Dan Morse (University of California, Santa Barbara)**  
Neutralization of a Distributed Coulombic Switch Tunes Reflectin Assembly and Biophotonics
9. **Monica Olvera de la Cruz (Northwestern University)**  
Electrostatic Driven Self-Assembly Design of Functional Nanostructures
10. **Anand Jagota (Lehigh University)**  
Surface Mechanical Properties of Bio-Inspired Architectures
11. **Chung-Yuen Hui (Cornell University)**  
Surface Mechanical Properties of Bio-Inspired Architectures
12. **Todd Emrick (University of Massachusetts-Amherst)**  
Functional Droplets and Particles: Recognition, Repair, and Transport
13. **Alexey Snezhko (Argonne National Laboratory)**  
Emergent Dynamics of Active Colloids

14. **Michael Solomon (University of Michigan)**  
Phoretically-Induced Deposition for Efficient Self-Assembly of Anisotropic Colloids at High Density
15. **Omar Saleh (University of California, Santa Barbara)**  
DNA Droplets: Design, Characterization and Manipulation
16. **George Whitesides (Harvard University)**  
Slit Tubes for Semi-Soft Pneumatic Actuators
17. **Jessica Winter (Ohio State University)**  
Exploring Fundamental Properties of Dynamic DNA Origami-Nanoparticle Composites

## **Biomolecular Materials Principal Investigators' Meeting**

### **POSTER SESSION II**

*Wednesday, August 16, 2017*

18. **Cyrus Safinya (University of California, Santa Barbara)**  
Miniaturized Hybrid Materials Inspired by Nature
19. **Juan de Pablo (Argonne National Laboratory)**  
Precision Synthesis and Assembly of Ionic and Liquid Crystalline Polymers
20. **Sam Stupp (Northwestern University)**  
New Functions Emerging from Dynamics in Supramolecular Biomolecular Materials
21. **Alfredo Alexander-Katz (MIT)**  
Biomimetic Templated Self-Assembly of Light Harvesting Nanostructures
22. **Padma Gopalan (University of Wisconsin-Madison)**  
Optical and Electro-optic Modulation of Biomimetically-Functionalized Nanocarbon Materials
23. **Chris Keating (Penn State University)**  
Bioinspired Mineralizing Microenvironments Generated by Liquid-Liquid Phase Coexistence
24. **Alex Noy (Lawrence Livermore National Laboratory)**  
Directed Organization of Functional Materials at Inorganic-Macromolecular Interfaces
25. **Jim De Yoreo (Pacific Northwest National Laboratory)**  
Directed Organization of Functional Materials at Inorganic-Macromolecular Interfaces
26. **Ozgur Sahin (Columbia University)**  
Measuring Transport Characteristics of Water Confined in Biological Materials
27. **Woo-Sik Jang, Daeyeon Lee and Daniel A. Hammer (University of Pennsylvania)**  
Enzymatic Reaction Powered Polymersome Protocells
28. **Nick Abbott (University of Wisconsin-Madison)**  
Bioinspired Hierarchical Design of Chiral Mesoscale Liquid Crystalline Assemblies
29. **Joe Perry (Georgia Tech)**  
Exploration of Chemically-Tailored, Hierarchically-Patterned 3-D Biogenic and Biomimetic Structures for Control of Infrared Radiation
30. **Gordana Dukovic (University of Colorado)**  
Control of Charge Transfer and Light-Driven Reactions in Nanocrystal-Enzyme Complexes

31. **Chuanbin Mao (University of Oklahoma)**  
Controlled Synthesis and Ordered Assembly of  $\text{Co}_3\text{O}_4$  Nanowires using Genetically Engineered Bacterial Flagella as Biotemplates
32. **Trevor Douglas (Indiana University)**  
Assembly of Virus Particle Nanoreactors Across Multiple Lengthscales

***AUTHOR  
INDEX***



Abbott, Nicholas L.....	41	Matyjaszewski, Krzysztof.....	54
Aizenberg, Joanna.....	46	McMeeking, Robert M.....	161
Alexander-Katz, Alfredo.....	50	Mittal, Jeetain.....	132
Aranson, Igor.....	34	Morse, Daniel E. ....	137
Ashby, Paul.....	29	Nealey, Paul.....	7
Bachand, George D. ....	3	Nilsen-Hamilton, Marit.....	18
Balazs, Anna C.....	46, 54, 60	Noy, Aleksandr.....	24
Bathe, Mark.....	205	Olvera de la Cruz, Monica.....	141
Bayer, Marcel.....	24	Perry, Joseph W. ....	146
Bedzyk, Michael J.....	141	Pine, David.....	64
Castro, Carlos.....	200	Poirier, Michael.....	200
Chaikin, Paul M. ....	64	Prozorov, Tanya.....	18
Chen, Chun-Long.....	24, 128	Russell, Thomas P.....	29
Chen, Wei.....	7	Safinya, C. R. ....	152
Darling, Seth.....	7	Sahin, Ozgur.....	157
de Pablo, Juan J.....	7, 41	Saleh, Omar A.....	161
De Yoreo, James J.....	24	Sandhage, Kenneth H.....	146
Dogic, Zvonimir.....	69	Sasaki, Darryl.....	3
Douglas, Shawn.....	123	Schulman, Rebecca.....	165, 169
Douglas, Trevor.....	73	Scott, Timothy F. ....	173
Dukovic, Gordana.....	77	Seeman, Nadrian C.....	64
Emrick, Todd.....	81	Snezhko, Alexey.....	34
Estroff, Lara A. ....	85	Sokolov, Andrey.....	34
Evans, John Spencer.....	90	Solomon, Michael J.....	177
Ewert, K. ....	152	Spoerke, Erik.....	3
Franco, Elisa.....	95	Stevens, Mark.....	3
Fygenson, Deborah K.....	161	Strano, Michael S.....	182
Gang, Oleg.....	123	Stupp, Samuel I. ....	186
Geissler, Philip.....	29	Tezcan, F. Akif.....	191
Glatz, Andreas.....	34	Tirrell, Matthew.....	7
Glotzer, Sharon C. ....	177	Travesset, Alex.....	18
Guan, Zhibin.....	99	Vaknin, David.....	18
Hammer, Daniel A. ....	104	van Burren, Anthony.....	24
Helms, Brett.....	29	Wang, Wenjie.....	18
Hillier, Andrew.....	18	Weck, Marcus.....	64
Hui, Chung-Yuen.....	109, 114	Whitesides, George M.....	196
Jagota, Anand.....	109, 114	Whitten, David.....	205
Johnston-Halperin, Ezekiel.....	200	Wiesner, Ulrich.....	85
Keating, Christine D.....	119	Winter, Jessica.....	200
Kumar, Sanat K.....	123	Woodbury, Neal.....	205
Lee, Daeyeon.....	104	Yan, Hao.....	205
Levenson, Robert.....	137	Zettl, Alex.....	29
Li, Y. ....	152		
Liu, Yan.....	205		
Mallapragada, Surya.....	18		
Mao, Chuanbin.....	128		



***PARTICIPANT  
LIST***



<b>Name</b>	<b>Organization</b>	<b>E-mail Address</b>
Abbott, Nicholas	University of Wisconsin, Madison	abbott@engr.wisc.edu
Aizenberg, Joanna	Harvard University	jaiz@seas.harvard.edu
Aizenberg, Michael	Harvard University	michael.aizenberg@wyss.harvard.edu
Alexander-Katz, Alfredo	Massachusetts Institute of Technology	aalexand@mit.edu
Allen, Taylor	Georgia Institute of Technology	tallen49@gatech.edu
Bathe, Mark	Massachusetts Institute of Technology	mbathe@mit.edu
Belding, Lee	Harvard University	lbelding@gmwgroup.harvard.edu
Chaikin, Paul	New York University	chaikin@nyu.edu
Chen, Chun-Long	Pacific Northwest National Laboratory	Chunlong.Chen@pnl.gov
de Pablo, Juan	University of Chicago	smarijan@uchicago.edu
Douglas, Trevor	Indiana University	trevdoug@indiana.edu
Dukovic, Gordana	University of Colorado, Boulder	gordana.dukovic@colorado.edu
Emrick, Todd	University of Massachusetts, Amherst	tsemrick@mail.pse.umass.edu
Evans, John	New York University	jse1@nyu.edu
Gang, Oleg	Columbia University	og2226@columbia.edu
Gharbi, Mohamed Amine	Brandeis University	magharbi@brandeis.edu
Guan, Zhibin	University of California, Irvine	zguan@uci.edu
Hammer, Daniel	University of Pennsylvania	hammer@seas.upenn.edu
Hui, chung yuen	Cornell University	ch45@cornell.edu
Jagota, Anand	Lehigh University	anj6@lehigh.edu
Jang, Woo-Sik	University of Pennsylvania	jangw@seas.upenn.edu
Keating, Christine	Pennsylvania State University	keating@chem.psu.edu
Kumar, Sanat	Columbia University	sk2794@columbia.edu
Kwak, Seonyeong	Massachusetts Institute of Technology	kwaksy14@mit.edu
Lee, Daeyeon	University of Pennsylvania	daeyeon@seas.upenn.edu
Levenson, Robert	University of California, Santa Barbara	robert.levenson@lifesci.ucsb.edu
Mallapragada, Surya	AMES Laboratory	suryakm@iastate.edu
Mao, Chuanbin	University of Oklahoma	cbmao@ou.edu
Maracas, George	US Department of Energy	george.maracas@science.doe.gov
Markowitz, Michael	US Department of Energy	mike.markowitz@science.doe.gov
McGee, David	The College of New Jersey	mcgeed@tcnj.edu
Mittal, Jeetain	Lehigh University	jeetain@lehigh.edu
Noy, Aleksandr	Lawrence Livermore National Laboratory	noy1@llnl.gov
Olvera de la Cruz, Monica	Northwestern University	m-olvera@northwestern.edu
Oshri, Oz	University of Pittsburgh	ozo2@pitt.edu

Peden, Charles	US Department of Energy	charles.peden@science.doe.gov
Perry, Joseph	Georgia Institute of Technology	joe.perry@gatech.edu
Razavi, Sepideh	University of Michigan	srazavi@umich.edu
Russell, Thomas	Lawrence Berkeley National Laboratory/University of Massachusetts	tom.p.russell@gmail.com
Safinya, Cyrus	University of California, Santa Barbara	safinya@mrl.ucsb.edu
Sahin, Ozgur	Columbia University	os2246@columbia.edu
Saleh, Omar	University of California, Santa Barbara	saleh@engineering.ucsb.edu
Salim Lew, Tedrick	Massachusetts Institute of Technology	tedrick@mit.edu
Sandhage, Kenneth	Purdue University	sandhage@purdue.edu
Sasaki, Darryl	Sandia National Laboratories	dysasak@sandia.gov
Schulman, Rebecca	Johns Hopkins University	rschulm3@jhu.edu
Scott, Timothy	University of Michigan	tfscott@umich.edu
Seeman, Nadrian	New York University	ned.seeman@nyu.edu
Snezhko, Alexey	Argonne National Laboratory	snezhko@anl.gov
Sokolov, Andrey	Argonne National Laboratory	sokolov@anl.gov
Solomon, Michael	University of Michigan	mjsolo@umich.edu
Spoeke, Erik	Sandia National Laboratories	edspeoer@sandia.gov
Strano, Michael	Massachusetts Institute of Technology	strano@mit.edu
Subramanian, Hari	University of California, Riverside	hkswamy@gmail.com
Thiyagarajan, Pappannan	US Department of Energy	p.thiyagarajan@science.doe.gov
Tirrell, Matthew	Argonne National Laboratory	mtirrell@anl.gov
Uchida, Masaki	Indiana University	muchida@indiana.edu
Vo, Thi	Columbia University	tdv2101@columbia.edu
Whitesides, George	Harvard University	mlegrand@gmwgroup.harvard.edu
Whitten, David	University of New Mexico	whitten@unm.edu
Wiesner, Ulrich	Cornell University	ubw1@cornell.edu
Winter, Jessica	The Ohio State University	winter.63@osu.edu
Woodbury, Neal	Arizona State University	laserweb@asurite.asu.edu
Yan, Hao	Arizona State University	Hao.Yan@asu.edu